DEPARTAMENT DE ASTRONOMÍA I ASTROFÍSICA

EVOLUTION FORMALISMS OF EINSTEIN EQUATIONS: NUMERICAL AND GEOMETRICAL ISSUES.

ISABEL CORDERO CARRIÓN

UNIVERSITAT DE VALÈNCIA
Servei de Publicacions
2009

Aquesta Tesi Doctoral va ser presentada a València el dia 2 de novembre de 2009 davant un tribunal format per:

- Dr. Antonio Marquina Vila
- Dr. Ewald Müller
- Dr. Eric Gourgoulhon
- Dr. Carles Bona García
- Dr. José Antonio Font Roda

Va ser dirigida per:
Dr. José Mª Ibáñez Cabanell

Dipòsit legal: V-955-2011
I.S.B.N.: 978-84-370-7722-2
Edita: Universitat de València
Servei de Publicacions
C/ Arts Gràfiques, 13 baix
46010 València
Spain
Telèfon:(0034)963864115

VNIVERSITAT DE VALÈNCIA
Departamento de Astronomía y Astrofísica

Evolution Formalisms of Einstein equations: Numerical and Geometrical Issues

TESIS DOCTORAL PRESENTADA POR

Isabel Cordero Carrión

Burjassot (Valencia), 15 de septiembre de 2009

Dr. José María Ibáñez Cabanell, catedrático de la Universidad de Valencia,

CERTIFICA:

Que la presente memoria, "Evolution Formalisms of Einstein equations: Numerical and Geometrical Issues", ha sido realizada bajo su dirección, por Isabel Cordero Carrión, y que constituye su tesis doctoral para optar al grado de Doctor en Física.

Y para que quede constancia y tenga los efectos que corresponda, firma el presente certificado en Burjassot, a 15 de septiembre de 2009.

Firmado: José María Ibáñez Cabanell

Más vale haber llegado a tocar el cielo con las manos por un instante
que anhelar hacerlo toda una vida.
No temas sentir,
no temas llorar, no temas gritar...
no temas arriesgarte a decidir.

Agradecimientos

Todo camino comienza con un paso, pero ese paso no siempre conoce el camino que le sigue. Las decisiones importantes no acostumbran a ser fáciles, aunque la posibilidad de escoger tu propia dirección puede llenar más que el vacío de la melancolía. Normalmente tienes que soltar algo para poder tomar otra cosa, un intercambio de momentos que permanecerán en la memoria.

Cuando apoyan tus iniciativas, te ofrecen conocimientos y ayuda, valoran tu trabajo y respetan tu forma de ser, puedes sentirte privilegiado; nada de esto he echado en falta de mi director de tesis. El comienzo de un buen día puede ser simplemente un saludo amable o una risa contagiosa. A los que hacen más de lo que muchos ven, gracias Manel y Feli por hacer que el papeleo de la tesis no pudiera con ninguno de los tres. Será difícil olvidar los aplausos entre las paredes de un antiguo monasterio, las normas de domesticación de los gatos de ciertos pueblos, calcetines bicolores en paseos por algún barranco, los sobres de azúcar del café sin café de las mañanas, las reuniones del astro-club y el poder de convocatoria de las galletitas, el eco de sonoras risas al principio del pasillo, el microclima del despacho con el aparatejo que echaba humo... de mi cabeza! Nunca un sargento dio mejor una alternativa, ni descubrió lo completos que pueden llegar a ser los niños, Juan Antonio. Sólo puedo agradecer los saludos de aquellos que formaron parte de la experiencia de verme al otro lado del pupitre, espero que para ellos también sea un buen recuerdo. No podría olvidarme de alguien que ha hecho que estar trabajando pueda hacerte llorar de risa, sea más que compañera de despacho una buena amiga, además de temible rival en campo contrario, Susana.

Han sido cuatro años, y los que venían de antes, de muchos viajes, figurada y no figuradamente, y de muy buenas experiencias. Muchas personas que te cuentan cómo se ve el mundo desde otro mundo o con otra mirada. Este híbrido, que ni hace matemáticas para los matemáticos (nunca perderé la rigurosidad...), que ni hace física para los físicos (particulitas y cuántica ya no dais tanto miedo...), y que para mí misma más que trabajar disfruto con la posibilidad

de hacer lo que quiero. Sigo pensando que los años de universidad fueron tan buenos por la magia y curiosidad de lo que pude aprender, y por la buena gente que estaba a mi lado, no importara el lugar: Conchita, Bea, Mariela, Dani, Jose, Jorge, Rebeca, Elena, Marta, Paula, Rober, Diego, Víctor, Joserra, Pascual, Dioni, Jota, Pili, Bea, Rosaura, Pablo, Raúl, Mario, Alberto... muchos nombres para escribirlos todos aquí pero un millón de imágenes para no olvidarlos, entre topología, análisis, cálculo, playitas, paellas, viajes en coche a Teatinos y Burjassot, afición al OBM por siempre.

No se quedó ahí todo. El calor de un sol que no aparece en cuarenta días puede suplirse con amistades profundas que se entrelazan para toda una vida, y que pueden volver a encontrarse a los pies de la Torre Eiffel o en el mirador de San Nicolás al otro lado de la Alhambra; Arancha, Rocío, Olga, Mar, Leti, Jose Luis, Paco, y los demás, *merci* por las cenitas de tortilla y de fondues, las velas, las celebraciones en los Campos Elíseos contando, y todos los abrazos.

Dicen que la nieve de los Alpes puede llegar a helar unos pies no demasiado abrigados al pasear por el castillo más mágico de un rey loco, que miedo es ver cómo tus pies se sostienen sobre la capa de un lago resquebrajándose, o que se puede organizar una cenita asiática deliciosa mezclando japonés, español, inglés y alemán, y Pablo, Laura, Harry, Pedro, Claudia, lo sabéis bien (Pablo te toca traducir al alemán). Hay ciudades que resultan acogedoras aún con grados bajo cero para una andaluza, donde es raro descubrir una cara morena, de pelo oscuro y ojos marrones, pero donde la amabilidad te permite descubrir la vida de sus gentes y formar parte de algunas, que no tienen nada que ver con la ciencia incluso. Pintar una casa bávara viendo partidos de España durante la Eurocopa y encontrarse a saltos durante la noche larga de la música, sólo Markus y Stefi podían conseguirlo (Markus ahora te toca a ti traducir). Una de esas vidas, puede empezar a conocerse incluso antes de que empiece... una amistad no entiende de costumbres ni de lenguas, entiende de confianza, de ayuda desinteresada, de saber hacer sonreir con poco; Thomas gracias por lo mucho que das sin esperar nada. En Munich pueden invitarte a fiestas antes de que se cumpla tu primer día de visita o pasear por el Isar durante una barbacoa con una ambulancia y unos cuantos amigos cerca, Andreas, Payel, Paula, Laura, Manolo, Marco, Margarita, Sebastián, Cecilia, Andrés, Fede, Michi...

Después de estos cuatro años, y mirando hacia atrás, es fácil descubrir a muchos amigos con los que has tenido el placer de trabajar, que son amigos

antes que otra cosa. Jérôme no olvido tu invitación a las playas de Eslovenia ni la copa que tenemos que tomar un día de agosto del 2013. José Luis tampoco me olvido del jamoncito de bienvenida en el barrio de Montparnasse. Eric y Ewald gracias por la ayuda, y el buen recibimiento que siempre tengo.

No podría dejar atrás al grupo de futboleros jueveros de Burjassot, para los que *"El fútbol es nuestra vida"*, como ellos bien saben: Susana, Avelino, Arnau, Paco, Carlos, Mer, Pancho, Tito, Abel, Javis, Ricardo, Salvatore, Pablo (medio alemán ya y además aún sin zapatillas), Joan, Teresa, Paquito, Celia y todos los que ahora mismo olvido sin querer... Por esos partiditos que animan cualquier semanita de trabajo en un día nublado, por los calurosos últimos partidos de la temporada a 40 grados pero sin perder las ganas, por esas risas y cervecitas de después. Seguiré dejando los balones a los pies de la mesa del despacho y buscando las zapatillas de tacos para poder jugar en césped. Espero poder encontrar tan buena gente como estos deportistas natos, y mejores fiesteros, y sobretodo poder seguir viniendo, de vez en cuando aunque sea, para recibir unos saludos. Junto con ellos a todos los que me he encontrado por la universidad en general, ya fuera para comer, para tomar un cafelito, para ir a recoger unos cuchillos a una sucursal bancaria... Vicente, Raúl, Neus, Felipe, Emilio, Héctor, algunos químicos, electrónicos, matemáticos, y muchos que ya he nombrado antes. Y otros tantos que me han hecho reír y disfrutar de pequeños detalles como la música, tocando, bailando o escuchando.

Este último año sobretodo, he tenido el placer de conocer a gente con intereses muy diversos, pero que tienen en común la curiosidad de mirar al cielo. Pasar de agua a nieve, reirse moviendo la Luna dentro de un planetario, cazar estrellas fugaces, discutir entre singularidades, replantearse la definición de rotonda, hacer turismo rural con telescopios en los maleteros, pintar un twister con sabor a chocolate, jugar al trivial en un submarino, y aún quedarán otras mil cosas más por hacer. Gracias Javis, Alberto, Pak, Kevin, Pepe, Gaetan, Susana, Alzina, Ale, Francesc, Jorge, Delfín, Carlos, Celia (algunos ya estáis repetidos por otro lado).

Puede que olvide algún nombre, o que esté presente sin llegar a mencionarlo explícitamente. Hay dos personas que han supuesto un apoyo incondicional tanto a nivel personal como profesional, unas confidentes del día a día, de los de las buenas noticias y de los momentos más duros, que algunas veces me conocen mejor de lo que yo misma creo conocerme. Son de este tipo de personas que te demuestran que la distancia no es excusa. Gracias Myriam y

Davi, vaya donde vaya, seguirá sin ser excusa la distancia que pueda separarnos, físicamente, pero nada más.

Aún queda un huequecito por rellenar en estos párrafos, para los que sin duda han estado a mi lado desde hace más tiempo. Esos a los que necesito ver algunos días de vez en cuando para poder cargarme de energía, esos de los que más abrazos recibo siempre, mi familia. A los que estuvieron tan orgullosos de tenerme cerca y que sé que el día de la lectura también estarán con el resto de gente escuchándome; tendré siempre en mi recuerdo al único que soportaba las notas agudas de la flauta sentado a los pies de la cama en silencio, y al que me llevaba en coche a todos los lados donde tenía que recoger algún papel y estaba deseando verme en el campo comiendo la paellita que preparaba. Gracias yaya por cuidarme siempre tan bien y ofrecerme lo mejor que tienes, pues no importa lo que reciba. Gracias Sacra y María José por estar tan cerca desde hace tanto tiempo, por poder contar con vosotras siempre que he necesitado ayuda y otros estaban más lejos.

El gracias más enorme y el abrazo más sincero debo dárselo a mis padres, mis hermanos Paco y Lucas, a Rocío y Marina, porque vosotros tenéis gran parte de la culpa de que yo pueda estar escribiendo esto. Sé que algunos estaréis calculando los 45 minutos de música en el mp3 para no dormirse en mitad de la defensa mientras una friki dice cosas raras sobre ondas gravitatorias, lo entiendo (aunque conseguiré que os leáis el resumen en español de la tesis... la tenacidad es una de mis virtudes, sí virtudes). Pero me bastará mirar hacia delante ese día, en mitad de todos los nervios del momento, para saber que no quisierais estar, a pesar de todo, en otro sitio. Ahora mismo no sé por donde me moveré dentro de un par de años, y mucho menos si seguiré con la investigación o me dará por llevar a cabo alguna de las ideas que tengo en mi inquieta cabeza. Pero de lo que no tengo ninguna duda es de que siempre os tendré a vosotros cerca.

Deseadme suerte...

PUBLICATIONS

The articles published during this thesis are the following ones:

J.L. Jaramillo, E. Gourgoulhon, I. Cordero-Carrión and J.M. Ibáñez, *Phys. Rev. D*, **77**, 047501 (2008).
Section 5.2 makes reference to this article.

I. Cordero-Carrión, J.M. Ibáñez, E. Gourgoulhon, J.L. Jaramillo and J. Novak, *Phys. Rev. D*, **77**, 084007 (2008).
Sections 4.3.1 to 4.3.3 made reference to this article.

I. Cordero-Carrión, P. Cerdá-Durán, H. Dimmelmeier, J.L. Jaramillo, J. Novak and E. Gourgoulhon, *Phys. Rev. D*, **79**, 024017 (2009).
Sections 4.2 and 4.3.5 made reference to this article.

CONTENTS

1. INTRODUCCIÓN, RESUMEN DE LAS PRINCIPALES IDEAS Y CONCLUSIONES

1.1 Introducción

El tema tratado a lo largo de la presente tesis es el estudio teórico y numérico de los formalismos de las ecuaciones de Einstein, con el propósito final de aplicar dicho estudio a la formación de agujeros negros y generación de ondas gravitatorias. Tanto las matemáticas como la física juegan un papel fundamental, complementándose la una a la otra, ya sea con respecto a las herramientas utilizadas, ya sea con respecto a los resultados presentados en este trabajo. La comunicación entre diferentes ramas específicas del conocimiento y de la ciencia pueden conducir a importantes avances, y algunas veces proporciona otro punto de vista original a la hora de plantear la estrategia para resolver un determinado problema.

El concepto de agujero negro fue introducido por John Michell en el año 1783 en un artículo enviado a la Royal Society: "Si el semi-diámetro de una esfera de la misma densidad que el Sol superase la del Sol en proporción de quinientos a uno, un cuerpo cayendo desde una altura infinita hacia él, habría adquirido en su superficie una velocidad mayor que la de la luz, y consecuentemente suponiendo que la luz es atraída por la misma fuerza en proporción a su masa, con otros cuerpos, toda luz emitida desde un objeto así retrocedería hacia él por su propia gravedad". Michell introdujo este concepto en el sentido de un objeto que tenía una atracción gravitatoria tal que incluso la luz no podría escapar de él. En 1796, el matemático francés Pierre-Simon Laplace explicó la misma idea en su libro *Exposition du Système du Monde*: "Un astro luminoso de la misma densidad que la Tierra, y cuyo diámetro sea doscientas cincuenta veces mayor que el del Sol, no dejaría en virtud de su atracción, que nos llegara ninguno de sus rayos hasta nosotros; es por tanto posible que los cuerpos más grandes del

universo, sean por sí mismos, invisibles...". La teoría de la Relatividad General presentada por Albert Einstein en 1915 postulaba que la luz y las trayectorias de todas las partículas son curvadas por la geometría del espacio-tiempo. Justo unos meses después, Karl Schwarzschild encontró una solución de las ecuaciones de Einstein que describía un agujero negro sin rotación, aunque en aquella época fue interpretada como una simple solución matemática sin mayor interés. Fue en 1967 cuando John Wheeler introdujo el término de *agujero negro* durante una conferencia en Nueva York.

Desde un punto de vista geométrico, un agujero negro puede ser considerado como una solución de las ecuaciones de Einstein que contiene una singularidad (curvatura infinita) en la métrica del espacio-tiempo. Desde un punto de vista astrofísico, un agujero negro es el resultado final de algunos tipos de colapso de un objeto estelar en concreto. Sin embargo, no está claro si después del colapso se forma una singularidad; en primer lugar, porque estas regiones del espacio-tiempo no son accesibles y, en segundo lugar, porque los efectos cuánticos necesitan un cuidadoso análisis en el contexto de una teoría consistente de gravedad cuántica.

Uno de los observables predichos por la Relatividad General, aún no detectados, son las ondas gravitatorias. Enormes esfuerzos experimentales, teóricos y numéricos se han llevado a cabo en los últimos cuarenta años, con el objetivo de detectar, predecir y estudiar las ondas gravitatorias emitidas desde diferentes escenarios astrofísicos y cosmológicos. Será una manera completamente nueva de mirar (y descubrir) el universo, incluso se convertirá en una posibilidad para desvelar la presencia de objetos ocultos, como los agujeros negros.

Para profundizar en el conocimiento de todos estos escenarios y objetos interesantes se necesita un formalismo de las ecuaciones de Einstein. Las diferentes formulaciones, las propiedades matemáticas del conjunto resultante de ecuaciones en derivadas parciales (problema bien puesto, unicidad local, etc.), pueden tener una importancia enorme y no siempre tienen la merecida atención. Un trabajo teórico difícil se ha llevado a cabo en este campo por parte de destacados investigadores matemáticos y físicos. Hay que reconocer la capacidad de las formulaciones más usadas, como la llamada BSSN (más detalles en el Capítulo 4), crucial en las recientes simulaciones de binarias de agujeros negros. Pero no debemos olvidar los nuevos formalismos introducidos en los últimos años, como el FCF, que será objeto de estudio en esta tesis, porque pueden ofrecer nuevas ideas y permitir comparaciones más realistas

entre diferentes resultados numéricos.

Finalmente, las herramientas numéricas disponibles hoy en día han hecho posible un importante progreso. Por ejemplo, los supercomputadores son capaces de mostrarnos cómo el universo evoluciona hacia una estructura homogénea macroscópica, que a pequeña escala presenta una estructura filamentosa; sin los ordenadores, es casi imposible imaginar las simulaciones de la evolución de sistemas de ecuaciones no lineales que gobiernan procesos complejos como la evolución de las estrellas, la dinámica de binarias de objetos compactos, chorros asociados a galaxias... y un largo etcétera.

1.2 Agujeros negros astrofísicos

En el Capítulo 3 se expone un análisis de los agujeros negros desde un punto de vista astrofísico, una clasificación de los mismos según su origen y masa, y algunos métodos de detección.

Desde un punto de vista clásico un agujero negro es un objeto compacto cuyo potencial gravitatorio en la superficie se aproxima a la mitad del cuadrado de la velocidad de la luz. Un agujero negro es un objeto suficientemente compacto que no permite a la luz escapar de él. La herramienta teórica para describir matemáticamente un agujero negro es la Relatividad General. El horizonte de un agujero negro es una superficie que delimita la región del espacio-tiempo del agujero negro desde la que no podemos recibir ningún tipo de señal.

La clasificación de agujeros negros estático y en rotación viene dada por las soluciones de Schwarzschild [1, 2] y Kerr [3], respectivamente, que puede presentarse en diferentes sistemas de coordenadas (ver Capítulo 3 para más detalles). Desde el punto de vista astrofísico, los agujeros negros pueden clasificarse, según su origen, en: aquellos procedentes del colapso estelar (agujeros negros estelares), aquellos procedentes de la fusión y procesos de acreción (agujeros negros supermasivos), y aquellos que pudieran ser reliquias del medio inhomogéneo altamente denso en el universo primitivo (agujeros negros primordiales). También se pueden clasificar, de acuerdo con su masa, en: poco masivos (como los estelares), de masa intermedia (de los que las evidencias observaciones existentes son muy pobres), supermasivos, y de muy baja masa (los primordiales). La Vía Láctea tiene en su centro un agujero negro supermasivo situado en SgrA*. La acreción de materia situada en un disco que rodea un agujero negro supermasivo es el mecanismo más eficiente de generación de

energía. No hay confirmación observacional de la existencia de agujeros negros primordiales; podrían ser las semillas de futuros agujeros negros supermasivos.

Para detectar observacionalmente un agujero negro existen varios métodos [4]. Los métodos cinemáticos usan la dinámica de los objetos cercanos al agujero negro para derivar propiedades de éste como su masa o spin, como en el caso del agujero negro central en nuestra propia galaxia; por ejemplo, la ley de Magorrian [5], obtenida empíricamente, relaciona la masa del agujero negro central de una galaxia con la velocidad estelar de dispersión. Otros métodos están basados en el estudio del espectro observado, como el análisis de ciertas líneas del hierro [6]. La presencia de chorros asociados a los agujeros negros supermasivos rodeados por un toro de acreción, en el escenario astrofísico de los núcleos activos de galaxia, puede ser usada como huella de la presencia de este tipo de agujeros negros. Las erupciones de rayos gamma (ERG) son eventos asociados a la presencia de agujeros negros de origen estelar. Atendiendo a su curva de luz, las ERG pueden clasificarse en dos grupos: por un lado, las de corta duración [7], situadas en galaxias elípticas viejas en zonas de formación estelar, que parecen estar asociadas con una pequeña parte de las fusiones de estrellas de neutrones y/o agujeros negros; y por otro lado, las de larga duración [8], situadas en zonas de formación estelar de galaxias de baja metalicidad, que parecen estar asociadas con una pequeña parte de las supernovas. La ausencia de luz procedente del interior de un agujero negro puede usarse, en principio, para detectarlo; el flujo decrece siguiendo una ley de potencias (con exponentes elevados) de la función horizonte (ver la descripción del agujero negro de Kerr en el Capítulo 3) que se anula en el horizonte, y depende en mucha medida del ángulo de inclinación del observador [9]. Otro de los métodos importantes de detección de los agujeros negros, en particular, son las lentes gravitatorias. Usando métodos fotométricos se observa la luz amplificada, observándose además múltiples imágenes de un mismo objeto, procedente de fuentes en las que un agujero negro juega el papel de lente gravitatoria [10]; con esta luz se puede medir la masa y otras propiedades del agujero negro.

Además de todos los métodos indirectos citados anteriormente, el único método directo para detectar los agujeros negros son las ondas gravitatorias. Las ondas gravitatorias son familiarmente consideradas como arrugas en la curvatura del espacio-tiempo, provocadas por aceleraciones de materia que no presentan simetría esférica. Se propagan a la velocidad de la luz. La emisión de ondas gravitatorias implica la emisión de energía. La primera detección

indirecta de ondas gravitatorias fue llevada a cabo en 1974 por Hulse y Taylor, estudiando el púlsar binario PSR B1913+16. Este descubrimiento les valió el Nobel en Física, al detectar que el período orbital decaía justo tal y como estaba predicho por la Relatividad General, para un sistema que estuviera perdiendo energía por la radiación de ondas gravitatorias. La amplitud de las ondas disminuye proporcionalmente con la distancia a la fuente. La estrategia para detectar ondas gravitatorias descansa en la idea básica de que, en su paso a través del detector, las distancias entre los objetos aumentan y se reducen rítmicamente; la magnitud de este efecto, para fuentes muy importantes, medido desde la Tierra es realmente pequeño, los cambios relativos son de a lo sumo 1 sobre 10^{20}, y de ahí la dificultad de medirlas.

Las ondas gravitatorias no han sido observadas aún de manera directa. Enormes esfuerzos experimentales están actualmente llevándose a cabo en este campo. El primer intento fue debido a Weber con su barra resonante; sistemas tipo barra más modernos están operativos, pero sólo son suficientemente sensibles para detectar ondas gravitatorias extremadamente potentes [11]. Unos detectores más sensibles son los interferómetros láser terrestres, como VIRGO [12], GEO600 [13], TAMA300 [14] o LIGO [15], y sus versiones avanzadas. Interferómetros en el espacio, como LISA [16], están siendo desarrollados. La comunidad científica espera que los observatorios de ondas gravitatorias detectarán señales en un futuro próximo. Una nueva ventana de información se abrirá permitiéndonos ver cosas inobservables con otro tipo de mensajeros (fotones, neutrinos...). Las binarias de objetos compactos (enanas blancas, estrellas de neutrones, y/o agujeros negros), las explosiones de supernovas, la acreción de materia en un agujero negro, y pulsaciones no esféricas de objetos son fuentes de radiación gravitatoria [17]. Las simulaciones numéricas proporcionan modelos muy útiles para el análisis de los datos que registran los observatorios de ondas gravitatorias. En los últimos años, el campo de la relatividad numérica ha avanzado enormemente, y es un ejemplo de sinergia entre observaciones y simulaciones numéricas.

1.3 Formalismos de las ecuaciones de Einstein

Dentro de los formalismos de las ecuaciones de Einstein caben destacar el formalismo 2+2 o formalismo nulo, y el formalismo 3+1. En el Capítulo 4 se explican más detalladamente estos formalismos.

El formalismo 2+2 se basa en hipersuperficies nulas. Dado un espacio-tiempo con una curvatura general, las hipersuperficies nulas son las superficies características del campo gravitatorio definidas a partir de un parámetro u = constante. En un sistema de coordenadas nulas, $u = x^0$ recibe el nombre de tiempo retardado, y es una de las funciones coordenadas. Una vez que una familia de hipersuperficies nulas ha sido establecida conteniendo a la coordenada previa, dos coordenadas adicionales, x^A, $A = 2, 3$, son elegidas como parámetros constantes a lo largo de cada rayo; estas coordenadas pueden visualizarse como ángulos ópticos y normalmente se denotan como $\theta = x^2$ y $\phi = x^3$. Esta elección de coordenadas implica que se anulen varias componentes de la métrica del espacio-tiempo, $g^{\mu\nu}$: $g^{uu} = g^{uA} = g_{11} = g_{1A} = 0$. La única coordenada que varía a lo largo de un rayo de luz dado es x^1. Normalmente se escoge como coordenada x^1 la distancia luminosidad desde la fuente, r. Véanse más detalles en [18, 19].

Bondi fue el primero en usar este tipo de coordenadas nulas para describir campos radiativos. Su trabajo fue seguido por un rápido desarrollo de otros formalismos nulos, que se distribuyeron en dos grupos: aquellos basados en aproximaciones de la métrica, como el desarrollado en el caso axisimétrico por Bondi, Metzner y van den Burg [20], y generalizado por Sachs [18], y aquellos basados en una tétrada nula en los que las identidades de Bianchi aparecen como parte del conjunto de ecuaciones, como es el caso del desarrollado por Newman y Penrose [21].

En el formalismo nulo las ecuaciones de Einstein se separan en cuatro grupos (ver más detalles en el Capítulo 4): cuatro ecuaciones de hipersuperficie, dos ecuaciones de propagación, cuatro ecuaciones de conservación y una ecuación que se satisface trivialmente (la contracción a través de la métrica de la propia ecuación tensorial de Einstein). Tras resolver las ecuaciones de propagación, de manera jerárquica, el resto de ecuaciones se satisfacen inmediatamente debido a que están conectadas a las demás a través de las identidades de Bianchi.

Con este formalismo, las ecuaciones de Einstein pueden ser resueltas de manera jerárquica. Numéricamente, la radiación gravitatoria en el infinito puede ser extraída directamente, ya que el infinito nulo puede estar contenido en la malla numérica compactificando la distancia luminosidad (que es una de las coordenadas del formalismo). Un problema de esta formulación es la formación de cáusticas, puntos donde dos o más rayos de luz se intersectan, en donde la causalidad se rompe. Cáusticas pueden darse, por ejemplo, en las

simulaciones de binarias de agujeros negros.

Vamos a fijarnos ahora en el formalismo 3+1. Este formalismo fue introducido en los trabajos de Lichnerowicz (1944) [22], Choquet-Bruhat (1952) [23], Arnowitt, Deser and Misner (1962) [24]. Véanse [25, 26, 27, 28] para una introducción y recientes aplicaciones en relatividad numérica. Para una función t de gradiente temporal, las hipersuperficies espaciales donde esta función es constante definen una foliación del espacio-tiempo. El campo vectorial ∂_t puede descomponerse en una parte proporcional al vector normal a la foliación, que está relacionada con la función paso, o tiempo propio entre hipersuperficies, y en otra parte tangente a la hipersuperficie, que está relacionada con el vector desplazamiento entre las curvas integrales del vector normal y del campo vectorial ∂_t. La métrica del espacio-tiempo puede escribirse en función de la función paso, del vector de desplazamiento y de la métrica espacial restringida a las hipersuperficies espaciales. Se puede definir la curvatura extrínseca de las hipersuperficies en función del vector normal a éstas y la métrica espacial.

Tanto las ecuaciones de Einstein como el tensor energía-momento pueden escribirse en términos de esta descomposición, dando lugar a un conjunto de ecuaciones de ligadura y un conjunto de ecuaciones de evolución. Gracias a las identidades de Bianchi, si las ecuaciones de ligadura se satisfacen en la hipersuperficie inicial, entonces también son satisfechas a lo largo de la evolución. Una vez escritas las ecuaciones, aparece una libertad (de gauge) de elección de la foliación y del campo a través del cual evolucionamos las ecuaciones, es decir, la libertad de elegir la función paso y el vector desplazamiento. Las variables dinámicas son las componentes de la métrica espacial de las hipersuperficies y las componentes de la curvatura extrínseca. En el caso de foliaciones tales que la traza de la curvatura extrínseca es constante, las ecuaciones para la función paso y el vector desplazamiento se desacoplan. Hay maneras indirectas de elegir estas variables, imponiendo condiciones sobre la traza de la curvatura extrínseca o sobre el tensor de distorsión. Ver más detalles de las ecuaciones en el Capítulo 4.

El sistema de las ecuaciones de Einstein en el formalismo 3+1 no está escrito en la forma más conveniente para la implementación numérica de dichas ecuaciones, ya que se desarrollan inestabilidades muy rápidamente (ver, por ejemplo, [29]). Kojima, Ooahara y Nakamura [30] presentaron en 1987 una reformulación conforme, sin traza, del sistema de ecuaciones del formalismo 3+1; en esta reformulación la traza de la curvatura extrínseca evoluciona por sepa-

rado, y la introducción de variables auxiliares elimina las derivadas segundas cruzadas en el tensor de Ricci.

La versión más utilizada del formalismo 3+1 es la conocida como BSSN (de Baumgarte, Shapiro [31], Shibata y Nakamura [32]). La robustez de este formalismo ha sido comparada con otros formalismos (véase el proyecto 'Apples with Apples') y presenta algunos inconvenientes, aunque su robustez ha podido observarse en implementaciones numéricas basadas en elecciones particulares de gauges y foliaciones (ver, por ejemplo, [33, 34]). Se han podido llevar a cabo simulaciones numéricas de larga duración, incluso en espacios-tiempo que tienen intensos campos gravitatorios, como aquellos que contienen agujeros negros y estrellas de neutrones (más detalles en el Capítulo 4). Gracias a las buenas propiedades de estabilidad de estas ecuaciones, el uso de esta reformulación, con las apropiadas elecciones, conforme, sin traza, está muy extendido en relatividad numérica. Por ejemplo, su robustez ha sido demostrada en las recientes simulaciones de la fusión de binarias de estrellas de neutrones [35], evolución de uno o dos agujeros negros (ver Sección 7.2), evolución de larga duración de estrellas de neutrones [34], y colapso gravitacional de estrellas de neutrones a agujeros negros [36].

Dentro del formalismo 3+1, el grupo de Meudon ha desarrollado una formulación completamente ligada llamada FCF (de Fully Constrained Formalism). En esta formulación se introduce una métrica plana invariante de una hipersuperficie a otra y que recoge el comportamiento asintótico de la métrica espacial de las hipersuperficies. Esta métrica se reescribe en términos de una conforme, que a su vez se descompone en términos de la métrica plana y la diferencia de ambas métricas. En cuanto a la libertad de elección de gauge, se impone que la traza de la curvatura extrínseca se anule y el gauge de Dirac generalizado, a lo largo de todas las hojas de la foliación. Poniendo en común todos estos elementos, las ecuaciones de Einstein se escriben como un conjunto de ecuaciones elípticas para la función paso, el vector desplazamiento y el factor conforme, junto con un sistema de evolución para la diferencia de las métricas plana y conforme (ver más detalles de las ecuaciones en el Capítulo 4). Este esquema está completamente ligado, ya que todas las ecuaciones de ligadura se resuelven en cada paso de tiempo; esto no sucede con las formulaciones de evolución libre, como BSSN, o parcialmente ligadas. La principal motivación de esta formulación FCF es obtener el máximo número posible de ecuaciones elípticas, que en principio son más estables que las ecuaciones hiperbólicas evi-

tando la violación de las ligaduras. Para este tipo de ecuaciones elípticas es posible aplicar los métodos espectrales en los que tanta experiencia tiene el grupo de Meudon.

Una propiedad interesante de la FCF es que es una generalización natural de la aproximación relativista de las ecuaciones de Einstein conocida como CFC (de Conformally Flat Condition) [37, 38]. La aproximación CFC ha sido usada en muchas aplicaciones astrofísicas, tales como el colapso de los núcleos en rotación de estrellas masivas [39, 40, 41, 42] o supermasivas [43], el colapso inducido por una transición de fase de estrellas de neutrones en rotación [44], o modelos de equilibrio de estrellas de neutrones en rotación [45, 46], así como fusiones de binarias de estrellas de neutrones [47, 48, 49, 50]. CFC se puede recuperar como caso particular de la formulación FCF, simplemente imponiendo que la diferencia entre las métricas plana y conforme sea nula. CFC consta de un conjunto de ecuaciones elípticas para la función paso, el vector desplazamiento y el factor conforme. Es la formulación FCF, por tanto, una manera en la práctica sencilla de extender la aproximación CFC a una formulación completamente relativista, añadiendo nuevos términos en las fuentes de las ecuaciones elípticas e incluyendo el nuevo sistema de evolución.

1.4 Aspectos matemáticos

Tres puntos serán tratados en esta sección, que resume una importante parte del trabajo teórico presentado en la tesis: por un lado, la existencia local de foliaciones maximales en espacios-tiempo con simetría esférica [51] (más detalles en la Sección 5.1); por otro lado, propiedades de unicidad local de las ecuaciones elípticas en la formulación FCF [52] (más detalles en la Sección 5.2); y, finalmente, las propiedades de hiperbolicidad de las ecuaciones de evolución en la formulación FCF para la diferencia de las métricas plana y conforme [53] (más detalles en la Sección 5.3).

En 1944 Lichnerowicz [22] introdujo una foliación particular del espacio-tiempo, que se conoce con el nombre de maximal slicing (MS): la traza de la curvatura extrínseca es nula. Este tipo de foliaciones tiene propiedades interesantes como la conocida capacidad de evitar las singularidades, está bien adaptada a la propagación de ondas gravitatorias, y proporciona la natural aproximación Newtoniana cuando además se impone sobre cada hoja que la métrica espacial sea conformemente plana. Esta foliación ha sido recientemente uti-

lizada, como ya hemos mencionado anteriormente, en la FCF de las ecuaciones de Einstein. El estudio de este tipo de foliaciones ha estado motivado principalmente por la resolución de problemas de datos iniciales, y también por la correspondiente evolución de dichos datos iniciales. Esta idea fue popularizada por Smarr y York [25, 54]. Dada una clase de espacio-tiempo, la construcción de una foliación con una cierta propiedad podía ser acoplada dinámicamente en un esquema de evolución: suponiendo la existencia de una hipersuperficie inicial con esa propiedad, las ecuaciones de Einstein eran usadas para evolucionar localmente las correspondientes ligaduras adicionales. Esta estrategia puede ser aplicada tanto analítica como numéricamente, como así se ha hecho [55, 56] para construir MS en la geometría extendida de Schwarzschild, que fue obtenida también por Reinhart [57] de manera independiente con un método diferente esencialmente geométrico. Ejemplos parecidos de MS han sido estudiados en la geometría de Reissner-Nordström [58], y también en espacios-tiempo dinámicos en simetría esférica de colapso de polvo [59] usando coordenadas isotrópicas.

A pesar de su extendido uso, la existencia de MS en espacios-tiempo con simetría esférica ha sido probada solamente para vacío y para algunos casos particulares de contenido energético (véase [37, 55, 56, 57, 58, 59, 60]). No existe, al menos que sepamos, un teorema que afirme la existencia de MS en cualquier espacio-tiempo con simetría esférica. Para ello, seguiremos un procedimiento puramente geométrico, independiente de las ecuaciones de Einstein, complementario a la estrategia de evolución estándar.

El estudio de los espacio-tiempo con simetría esférica es de particular interés en diferentes campos de la Relatividad General: clasificación de soluciones exactas de las ecuaciones de Einstein, modelos simplificados de escenarios astrofísicos y cosmológicos (véase, por ejemplo, [61]), soluciones para testeo de códigos numéricos dinámicos completamente relativistas que evolucionan la materia en campos gravitatorios intensos (véanse, por ejemplo, [59, 62, 63, 64]), etc. Por todas estas razones, nuestro análisis comienza en simetría esférica, y deja abierta para futuros trabajos su extensión a espacios-tiempo con una simetría más débil.

Este procedimiento parte de la descomposición de los campos coordenados en el sistema de coordenadas final en función de los campos coordenados de la métrica en la forma de partida. Tras imponer las condiciones exigidas de MS, que la métrica espacial sea conformemente plana, y las condiciones de integrabilidad de los nuevos campos, se llega a un sistema desacoplado de

ecuaciones casi-lineales en derivadas parciales para las incógnitas planteadas (ver más detalles en la Sección 5.1). Suponiendo que las componentes de la métrica de partida son funciones continuamente diferenciables, el problema de valores iniciales con respecto al conjunto de ecuaciones obtenidas tiene siempre solución local. Por tanto, podemos concluir que todo espacio-tiempo con simetría esférica puede ser foliado localmente por una familia de hipersuperficies espaciales maximales. El ejemplo simple del espacio-tiempo de Minkowski, en coordenadas esféricas inerciales, puede estudiarse mediante este procedimiento, obteniendo incluso otra familia de hipersuperficies maximales distinta a la de partida. Este teorema de existencia viene a rellenar un pequeño vacío en la parte teórica de la literatura científica, y su carácter constructivo ofrece un procedimiento para obtener MS en los distintos casos particulares. Además, gracias a este trabajo, es posible proveer de una serie de ejemplos para la comprobación independiente de espacios-tiempo dinámicos, obtenidos numéricamente por la comunidad científica de relativistas numéricos y astrofísicos, a través de sofisticados códigos numéricos.

El segundo punto que vamos a tratar en esta Sección es la unicidad local de las ecuaciones elípticas en la formulación FCF. La no unicidad de soluciones proviene de la no linealidad de las ecuaciones de ligadura y ha sido estudiada en la formulación llamada XCTS (de eXtended Conformal Thin Sandwich) [65, 66, 67] para el problema de datos iniciales en Relatividad General. En [68], una rama parabólica fue numéricamente encontrada como solución de las ecuaciones en XCTS para un espacio-tiempo perturbado de Minkowski, suministrando la primera evidencia de la no unicidad en este sistema elíptico. El análisis teórico llevado a cabo en este sistema [69] sugiere la presencia de un signo en un cierto término de la ecuación elíptica para la función paso, responsable de la pérdida de unicidad, esencialmente porque impide la aplicación de un principio de máximo que la garantice. Algunos formalismos de evolución ligados que incorporan elecciones elípticas para los grados de libertad en sus esquemas, contienen sistemas elípticos que tienen puntos en común con el sistema mencionado anteriormente. La unicidad del subsistema elíptico es, por supuesto, un aspecto crucial para garantizar que el sistema elíptico-hiperbólico completo sea bien puesto. En implementaciones numéricas, este problema puede depender del esquema numérico empleado, en particular, o de la capacidad de éste de permanecer cerca de una de las soluciones, al menos siempre que estemos en la parte de la solución suficientemente lejos del punto

de ramificación de soluciones.

En este trabajo el interés se centra en la formulación FCF como objetivo final, aunque estudiaremos por el momento cuestiones de unicidad referentes a la aproximación CFC, sin imponer ningún tipo de simetría espacial. Esta elección está justificada ya que el esquema CFC ya contiene el sistema elíptico relevante de la formulación FCF, pero de tal modo que problemas adicionales relacionados con la parte hiperbólica no van a mezclarse con el problema específico de unicidad que queremos tratar. Una modificación del esquema CFC se va a proponer, en donde las líneas de razonamiento de un principio de máximo pueden usarse para deducir la unicidad local de las soluciones.

Aunque no vamos a dar más detalles de las ecuaciones de evolución de la parte hidrodinámica, necesitaremos trabajar con variables conservadas en vez de las variables usuales hidrodinámicas, que son en realidad las que se evolucionan, una vez las ecuaciones se escriben como un sistema de ecuaciones en derivadas parciales. Las ecuaciones elípticas en CFC pueden escribirse en función de estas variables conservadas. El uso de estas variables no sólo tiene importancia para el problema de unicidad. Algunos de los términos que aparecen en la fuente de una de las ecuaciones elípticas no puede calcularse sin conocer previamente el factor conforme, pero éste es una de las incógnitas del sistema elíptico que hay que resolver. Varias estrategias para resolver este problema pueden usarse, pero los problemas de unicidad local que subyacen a estas ecuaciones provocan que estas estrategias no sean válidas en simulaciones numéricas de configuraciones más compactas como el colapso del núcleo estelar o de una estrella de neutrones a agujero negro. Para estos escenarios con una intensa gravedad, se produce la convergencia de las ecuaciones a una métrica físicamente incorrecta o incluso la no convergencia de los algoritmos.

Para un tipo concreto de ecuaciones elípticas (ver más detalles en el Capítulo 5), es posible aplicar un principio de máximo [70, 25, 71, 72] que garantiza la unicidad local de soluciones, siempre y cuando se cumpla un cierto criterio de signos (ver Capítulo 5). En el caso de la aproximación CFC no tenemos una ecuación elíptica escalar, sino un sistema no lineal de ecuaciones elípticas acopladas. Para el caso de las ecuaciones elípticas para la función paso y el factor conforme es posible observar el signo problemático, una vez que el cuadrado de la curvatura extrínseca se escribe explícitamente en función de las incógnitas del sistema. Un reescalado apropiado de la función paso no puede solucionar el problema para la ecuación elíptica que satisface el factor

conforme, y no podemos usar el principio de máximo para inferir la unicidad local de las soluciones. En estas condiciones, la convergencia a una solución no deseada puede ocurrir. Esta patología ha sido ilustrada con ejemplos analíticos sencillos de ecuaciones escalares del tipo concreto que estamos estudiando [69], en implementaciones numéricas de las ecuaciones de Einstein en vacío [68], así como en simulaciones numéricas en la formulación FCF (véase el ejemplo numérico mostrado en la Sección 5.2).

A pesar de los problemas mencionados, Shapiro y Teukolsky [73] fueron capaces de estudiar numéricamente el problema físico del colapso a agujero negro en simetría esférica, usando coordenadas isotrópicas, sin encontrar problemas de no convergencia o inestabilidades numéricas. Este esquema puede extenderse al caso tridimensional en CFC, usando para ello dos reescalados conformes diferentes y dos descomposiciones de la parte sin traza en parte longitudinal y transversa (ver más detalles en la Sección 5.2). La ligadura de momento en CFC puede escribirse usando las cantidades hidrodinámicas reescaladas, suponiendo una aproximación que es totalmente compatible con la aproximación CFC. Dicha ecuación se reduce a una ecuación elíptica vectorial con un sólo vector como incógnita, y que puede ser resuelta. Una vez conocida esta incógnita, la ecuación elíptica para el factor conforme se escribe como una ecuación elíptica cuya única incógnita es el factor conforme, y en la que el principio de máximo puede aplicarse para deducir la unicidad local. Una vez calculado el factor conforme, la ecuación elíptica para la función paso tiene a esta variable como única incógnita, que puede calcularse, y de nuevo el principio de máximo puede aplicarse para deducir unicidad local de las soluciones. Una ecuación elíptica para el vector desplazamiento puede deducirse en donde las fuentes son conocidas. En resumen, una ecuación vectorial extra aparece en la resolución de las ecuaciones, pero el sistema se desacopla de una manera jerárquica, y las ecuaciones para la función paso y el factor conforme son compatibles con la aplicación del principio de máximo.

El buen comportamiento de estas ecuaciones ha sido mostrado en experimentos numéricos como el test de migración de una estrella de neutrones en rotación desde la rama inestable a la rama estable, y también en el caso del colapso de una estrella de neutrones esférica o en rotación a agujero negro [52], usando un código numérico llamado CoCoNuT [39, 40]. Estas simulaciones son consistentes con otros resultados previos. Para el caso del test de migración, el esquema original en CFC conducía a una solución incorrecta, con

una masa ADM sensiblemente diferente; este problema es resuelto satisfactoriamente con el nuevo esquema propuesto. Para el caso del colapso a agujero negro, el esquema permite llegar hasta la formación del agujero negro; debido a la condición MS impuesta, no se alcanza la singularidad, y la función paso en el centro se aproxima rápidamente a cero una vez que el horizonte aparente se ha formado. El horizonte aparente se forma en un radio finito y contiene en su interior, en ese momento, una fracción significativa de la masa total de la estrella.

Las ideas teóricas usadas en la aproximación CFC pueden ser generalizadas de una manera sencilla a la formulación FCF. La formulación FCF consta de un conjunto de ecuaciones elípticas para la función paso, el vector desplazamiento y el factor conforme, y, acoplado con este conjunto de ecuaciones elípticas, un sistema de segundo orden de ecuaciones en derivadas parciales para la evolución de la diferencia entre la métrica plana y la conforme, que denotamos por el tensor $\bar{h}^{ij}$. El sistema de segundo orden se escribe como un sistema de primer orden. Las variables de este sistema pueden descomponerse en parte longitudinal y transversal, y las partes transversales se evolucionan haciendo uso de unos potenciales que garantizan el cumplimiento de las condiciones transversal y sin traza que han de satisfacer. En las ecuaciones elípticas pueden seguirse las mismas líneas de razonamiento para resolver de manera jerárquica el resto de ecuaciones elípticas que se desacoplan: la ligadura de momento, escrita con las descomposiciones introducidas, resuelve la parte longitudinal de la curvatura extrínseca sin traza; a continuación se puede obtener el factor conforme a partir de su correspondiente ecuación elíptica. Una vez calculado el factor conforme, se puede obtener la función paso de su correspondiente ecuación y, finalmente, el vector desplazamiento resolviendo otra ecuación elíptica vectorial. En ambas ecuaciones escalares se puede aplicar el principio de máximo para deducir la unicidad local de las soluciones.

El tercer punto importante de esta Sección es el análisis de la hiperbolicidad de este sistema de primer orden. Para ello, vamos a considerar fijas las variables de las ecuaciones elípticas. Este será un primer paso para el estudio del sistema completo en un futuro. En este estudio no vamos a tener en cuenta los efectos de las fuentes no lineales del sistema, a efectos de las propiedades de hiperbolicidad del sistema. El siguiente paso es introducir variables auxiliares para escribir el sistema como un sistema de primer orden en forma conservativa (con flujos y fuentes), usando como variables las componentes del propio tensor $\bar{h}^{ij}$, de

su derivada temporal y de sus derivadas covariantes espaciales. Pretendemos obtener explícitamente las expresiones de las características en términos de las variables de las ecuaciones elípticas y de la métrica espacial, sin profundizar en otros aspectos como por ejemplo existencia, unicidad, o problema bien puesto.

Podemos plantearnos el correspondiente problema de autovalores y autovectores a partir de las matrices del sistema. La primera conclusión es que la elección del gauge de Dirac generalizado es una condición suficiente para garantizar la hiperbolicidad del sistema. Aunque es un paso importante para nuestro análisis, este hecho era de esperar desde la estructura general del sistema y de las propiedades de otros gauges similares como el de Coulomb en electromagnetismo. El objetivo principal es obtener las expresiones explícitas. Los correspondientes autovalores del sistema de dimensión 30 para un vector espacial arbitrario dado, ζ^i, son: cero, con multiplicidad 12, y otros dos autovalores más que denotaremos con signos positivo y negativo, de multiplicidad 6 cada uno. Todos son reales. Podemos obtener asimismo la matriz de autovectores asociada al conjunto de los anteriores autovalores. Esta matriz define un sistema completo si y sólo si: i) la función paso no se anula; ii) la proyección del vector de evolución sobre el plano formado por el vector normal a las hipersuperficies y el vector ζ^i es un vector no nulo. Tras un análisis de las posibles elecciones del vector espacial ζ^i, se puede concluir que el sistema es fuertemente hiperbólico si el vector de evolución tiene carácter temporal, es decir, la función paso no se anula y el cuadrado de la función lapso es mayor que el cuadrado del módulo del vector desplazamiento.

Una propiedad interesante del sistema que estamos estudiando es que los campos característicos son linealmente degenerados (ver más detalles en el Capítulo 5). Esta propiedad muestra la coherencia del gauge de Dirac con la estructura cuasilineal del sistema de evolución, ya que, hablando desde el lenguaje de la dinámica de fluidos, significa que no pueden aparecen choques que se propaguen a lo largo de estas curvas, y las discontinuidades tendrían que ser, en todo caso, discontinuidades de contacto. Al interpretar el significado de los autovalores que hemos obtenido en el estudio de hiperbolicidad del sistema, es clara la relación entre la velocidad de la luz y los autovalores, cuando consideramos las contribuciones únicamente en una dirección dada.

Gracias a la elección de gauge en la formulación FCF es posible encontrar un sistema equivalente escrito en forma conservativa. Esto permite trabajar con este sistema equivalente e introducir la noción de flujos, usada en la dinámica

clásica de fluidos, para hacer referencia a las funciones que hemos encontrado. Las nuevas matrices tienen el mismo conjunto de autovalores, aunque no el mismo sistema de autovectores, ligeramente diferente, que sin embargo es completo en los mismos casos en los que lo era antes.

Podemos plantearnos usar como variables del sistema, en vez de las componentes del tensor h^{ij}, las de su derivada temporal y las de sus derivadas covariantes espaciales, las componentes de la curvatura extrínseca sin traza en lugar de las componentes de la derivada temporal del tensor h^{ij}, por las propiedades de unicidad local deducidas del conjunto de las ecuaciones elípticas. Las matrices de este sistema son diferentes del sistema anterior, pero los campos característicos siguen siendo linealmente degenerados, se obtienen los mismos autovalores y el sistema de autovectores ligeramente diferente es completo en los mismos casos en los que lo era anteriormente.

1.5 Agujeros negros geométricos y numéricos

Las expresiones explícitas para las velocidades características o autovalores son especialmente útiles en el cálculo de las condiciones de contorno interiores en el contexto de espacios-tiempo de agujeros negros en donde la singularidad se evita eliminando del dominio numérico una parte que la contiene. Cabe resaltar que la formulación FCF puede ser usada en combinación con las técnicas convencionales para tratar numéricamente espacios-tiempo que contengan la singularidad de un agujero negro, como, por ejemplo, la excisión, la punción, la punción móvil, o el rellenar la singularidad (ver más detalles en el Capítulo 7). Sin embargo, el uso de métodos espectrales para resolver las ecuaciones elípticas favorece la técnica de excisión; los métodos espectrales son usados en las ecuaciones elípticas con singularidades analíticas, pero es difícil tratar numéricamente singularidades no analíticas (y también discontinuidades) en el método de punción (móvil) (ver más detalles en la Sección 7.1).

El análisis de la hiperbolicidad del sistema para h^{ij} puede usarse para sacar conclusiones sobre las condiciones de contorno interiores de un agujero negro tratado numéricamente con excisión, al evaluar las curvas características en la superficie que forma el contorno. Las características apuntan siempre hacia el agujero negro [74], algo esperable desde la intuición física, y por tanto no hay ninguna libertad en la prescripción de las condiciones de contorno interiores durante la evolución. El sistema está completamente determinado y debemos

únicamente garantizar que los valores de las variables que evolucionamos sean consistentes con el gauge de Dirac.

Numéricamente, existen diferentes técnicas para tratar la singularidad definida por un agujero negro. La técnica de excisión [75] es una de ellas, y requiere la imposición de condiciones de contorno interior para la resolución de las ecuaciones elípticas (diferentes propuestas son explicadas con más detalle en el Capítulo 7). Otra opción es el relleno de los agujeros negros; es un método simple basado en que ningún tipo de información física puede escapar del interior de un agujero negro. El relleno consiste es suavizar el interior de cada agujero negro, pero puede generar la violación de las ligaduras.

Otra herramienta para tratar numéricamente agujeros negros es la punción [76]; la hipersuperficie espacial consiste típicamente en dos o más copias de $\mathbb{R}^3$ con varias esferas eliminadas, identificados los contornos esféricos interiores. De esta manera, varias regiones asintóticamente planas se conectan por puentes o gargantas (ver detalles y figura en el Capítulo 7). La evolución de binarias de agujeros negros en Relatividad Numérica es un problema que ha sido resuelto en 2005 por varios grupos, usando el método más sencillo y actualmente más popular, la punción móvil [77]. Se parte de unos datos iniciales idénticos que en el caso de la punción, pero son cruciales las elecciones particulares de la formulación, el gauge, y, sobretodo, el tratamiento de la singularidad en cada punción. En el caso de la punción móvil, el factor conforme se evoluciona sin ningún tipo de hipótesis analítica y las punciones son capaces de moverse en la malla numérica.

Bruegmann y otros colaboradores [78] presentaron en 2004 simulaciones numéricas de binarias de agujeros negros capaces de girar entorno a un período orbital. Ocho grupos, Pretorius [79], el grupo en Texas [80], el grupo de la NASA [81], el grupo en Penn State [82], Sperhake [83], el grupo de CalTech/Cornell [84], el grupo de Jena [85] y el grupo del AEI [86] (ver más detalles técnicos de los elementos empleados por cada uno de ellos en el Capítulo 7), han conseguido llevar a cabo simulaciones numéricas de binarias de agujeros negros de larga duración cubriendo varias órbitas. Seis de ellos usan la técnica de punción móvil, lo que muestra la potencia de esta técnica.

1.6 Implementando un nuevo código

El trabajo numérico que se ha llevado a cabo durante esta tesis es parte de un programa a medio plazo que tiene el objetivo de extender el código CoCoNuT [87] para que sea capaz de evolucionar la materia en espacios-tiempo dinámicos, en la formulación FCF de las ecuaciones de Einstein, incluyendo campo magnético. Todas las simulaciones realizadas evolucionan el sistema para el tensor h^{ij}, escrito como un sistema de primer orden. La función paso, el vector desplazamiento, el factor conforme y el contenido energético van a ser considerados como parámetros procedentes de otras simulaciones numéricas o de expresiones analíticas. En el caso general, y en un futuro próximo, todas las variables se evolucionarán de manera conjunta.

De acuerdo con las propiedades mencionadas anteriormente en otras Secciones, sabemos que el sistema es linealmente degenerado y por lo tanto no pueden aparecer ondas de choque, como era de esperar desde la intuición física del comportamiento de las componentes de la métrica del espacio-tiempo. Éste es el motivo que nos lleva a no usar métodos de captura de choques en nuestro esquema numérico, como es habitual en las simulaciones hidrodinámicas. Las derivadas espaciales son tratadas con esquemas en diferencias finitas estándares de diferentes órdenes de precisión, y la evolución temporal con métodos de Runge-Kutta.

El código utiliza un sistema de coordenadas esféricas ortonormales. Es un código axisimétrico y simétrico con respecto al plano ecuatorial, que se traduce en el uso de únicamente dos componentes, una radial y otra angular. Las condiciones de contorno interiores han de ser impuestas en el centro, en el eje y en el plano ecuatorial, con la ayuda de puntos auxiliares en la malla numérica y de las simétrias de las componentes de la métrica conforme. Aunque en principio la coordenada radial se extiende hasta el infinito, el dominio numérico termina en un radio finito y hay que imponer condiciones de contorno exteriores, que vienen dadas por la condición de Sommerfeld. Esta es una condición que intenta dejar pasar la posible radiación que llega a la frontera exterior, suponiendo que esta radiación viaja sobre un fondo plano, sin curvatura. Los autovalores del sistema que queremos evolucionar pueden ser interpretados como las velocidades, que toman el valor asintótico de la velocidad de la luz, y que es el valor que suponemos dado que estamos suficientemente lejos del origen. Una malla equiespaciada es utilizada para las direcciones temporal y angular, y una malla

logarítmica para la dirección radial.

Los métodos de Runge-Kutta (RK) utilizados tienen la propiedad de disminuir la variación total (TVD) (más detalles en el Capítulo 8). Métodos RK-TVD de primer, segundo, tercer y cuarto orden han sido implementados en el código. Un filtro de ruido de alta frecuencia o alternativamente un término disipativo están implementados para eliminar el ruido numérico de alta frecuencia, que aparece en la evolución de las variables del sistema en simulaciones de larga duración. El añadir viscosidad no sería una buena solución porque, además de reducir la amplitud de este ruido de alta frecuencia, también reduciría la amplitud de las ondas gravitatorias que estamos interesados en estudiar. El filtro es sencillo de implementar y funciona muy bien, pero a priori el número de iteraciones entre aplicación y aplicación del filtro es diferente para diferentes simulaciones. El término disipativo tiene relación con incluir una derivada de orden par de alto orden, y es más conveniente que el filtro a la hora de llevar a cabo estudios de convergencia, ya que la adición de dicho término puede interpretarse como una modificación del algoritmo que mantiene el orden del error de truncamiento.

Algunos casos particulares pueden ser de gran utilidad a la hora de validar el código numérico y garantizar futuros resultados en escenarios más complejos. Consideremos en primer lugar el sistema de ecuaciones de Einstein linealizado en vacío, con función paso y factor conforme igual a uno, y vector de desplazamiento nulo. Los datos iniciales usados corresponden a una combinación de ondas de Teukolsky [88] regulares en el origen de amplitud 10^{-5}. Estas ondas son solución analítica de la ecuación linealizada en vacío, satisfacen el gauge de Dirac y tienen traza nula (que es la aproximación lineal de la condición sobre el valor del determinante de la métrica espacial). Esta solución analítica permite una comparación exacta con los resultados numéricos que se van obteniendo.

Usando diferentes valores del orden del RK, del orden de las derivadas espaciales y diferentes CFL (condición sobre el paso de tiempo), el código numérico siempre falla debido a la formación de una inestabilidad en el origen. Las inestabilidades en el origen son problemas comunes en problemas con simetría esférica, ya que el propio sistema de coordenadas no está bien definido en el origen. Esta singularidad coordenada no tiene relación ni con el formalismo ni con el algoritmo numérico utilizados. El tratamiento más común suele ser la redefinición de las variables dinámicas en base a sus desarrollos de Taylor cerca del origen (véase por ejemplo [89], o más recientemente [90]). En este

caso, el hecho de usar coordenadas ortonormales garantiza que los desarrollos de Taylor de las variables dinámicas son apropiados para la evolución numérica del sistema. Cabe distinguir, entre todas las variables del sistema que evolucionamos, dos grupos atendiendo a la manera en que se obtienen dichas variables y también a razones numéricas. El problema de la inestabilidad puede resolverse con una combinación de métodos explícitos e implícitos a la hora de evolucionar numéricamente las ecuaciones. La solución analítica en el régimen lineal se recupera, así como la velocidad y amplitud de la onda (ver más detalles y figuras que muestran la evolución de los datos en el Capítulo 8). La condición de contorno exterior funciona correctamente a nivel lineal.

En el segundo test vamos a considerar una estrella de neutrones en rotación en equilibrio, cuyos datos iniciales han sido obtenidos de una librería de métodos espectrales llamada LORENE [91]. La función paso, el factor conforme y el vector desplazamiento tienen valores generales, pero van a seguir siendo considerados como parámetros fijos durante la simulación. La malla en la dirección radial se divide en varios dominios. El primero se llamará dominio de la materia, y contiene a la estrella. El segundo es el dominio de propagación, en donde las ondas están bien resueltas. El tercer y último dominio es el de amortiguación, que tiene una resolución pobre y el objetivo es el de dejar a la onda viajar lo suficientemente lejos antes de llegar al radio exterior de la malla.

En los datos iniciales incluimos unas diferencias en las componentes de la curvatura extrínseca sin traza, que generan una perturbación que se propaga hacia el exterior. Una vez la onda ha pasado, se recupera la solución estacionaria. Este test puede permitir comprobar si realmente se recupera la estacionaridad en el sistema, y además permite validar la condición de contorno exterior implementada. Con estas simulaciones se comprueba que el radio exterior debe situarse al menos a unas 300 veces el radio de la estrella. Si inicialmente partimos de los datos estacionarios para todas las variables del sistema, no se genera ninguna onda artificial (ver más detalles en el Capítulo 8).

En el último test realizado se parte de una estrella de neutrones perturbada no esféricamente, por lo que cabe esperar la emisión de radiación gravitatoria del sistema. Las ecuaciones hidrodinámicas que evolucionan la materia también se resuelven, aunque la función paso, el factor conforme y el vector desplazamiento se siguen manteniendo fijos a lo largo de la evolución (suponemos que no van a variar significativamente). Con este test se pretende obtener infor-

mación del radio de extracción de las ondas gravitatorias, que serán calculadas con una aproximación del escalar de Weyl Ψ_4. Las ondas que se obtienen corresponden a las ondas gravitatorias físicas que produce la estrella perturbada al evolucionar las ecuaciones hidrodinámicas. Se observa que el radio de extracción debe estar situado lejos de la fuente, pero dentro del dominio de propagación. Es suficiente con cubrir la longitud de onda con cinco puntos al final del dominio de propagación.

La onda en principio debería oscilar sobre el valor 0. Puede observarse (ver figuras en el Capítulo 8) un off-set, o desplazamiento medio de las oscilaciones de las ondas gravitatorias, inicialmente, antes de que la onda alcance un determinado radio; puede solucionarse simplemente extendiendo el dominio de propagación hasta un radio más alejado de la fuente. El off-set en las propias ondas gravitatorias parece disminuir conforme el radio de extracción es mayor, pero es una cuestión aún pendiente de resolver. El origen de este problema puede ser debido a: i) la existencia de una pequeña inconsistencia entre los datos iniciales del tensor de energía momento de la estrella perturbada y los datos iniciales de la métrica del espacio-tiempo; ii) el procedimiento para estimar la aproximación del escalar de Weyl Ψ_4 no es el más preciso. Esperamos mejorar estos aspectos en la versión extendida del código CoCoNuT. Gracias a estas simulaciones, puede deducirse que es razonable situar el radio de extracción al menos a unas 30 veces el radio de la estrella.

El código CoCoNuT, al que nos hemos referido ya varias veces, es un código relativista magneto-hidrodinámico, que evoluciona también la métrica del espacio-tiempo. Este código numérico permitirá estudiar escenarios astrofísicos en donde la Relatividad General puede jugar un papel importante. El proyecto fue iniciado por H. Dimmelmeier en su tesis doctoral. Posteriormente, fue extendido a un código tridimensional haciendo uso de la librería LORENE para evolucionar las ecuaciones CFC, en colaboración con J. Novak, y de métodos de captura de choques para evolucionar las ecuaciones hidrodinámicas. Recientemente, P. Cerdá-Durán ha implementado una extensión magneto-hidrodinámica. Una vez que los principales aspectos para extender CFC a la formulación FCF han sido establecidos y los primeros tests llevados a cabo de manera satisfactoria, es el momento de incorporar el nuevo sistema hiperbólico al código. Este trabajo está en progreso, en colaboración con P. Cerdá-Durán, aunque algunos pasos importantes ya se han dado. Algunas de las herramientas implementadas en CoCoNuT serán de gran utilidad

para futuros desarrollos y aplicaciones; por ejemplo, los métodos espectrales serán muy útiles para el cálculo del escalar de Weyl, y el buscador de horizontes ya implementado será una herramienta importante en las simulaciones de colapso de una estrella de neutrones a agujero negro. Será igualmente interesante el estudio de la radiación gravitatoria procedente de estrellas de neutrones en rotación con diferentes ecuaciones de estado, y la comparación con otras aproximaciones (como la fórmula cuadrupolar).

1.7 Conclusiones

Durante el período de la tesis doctoral he dedicado tiempo tanto a investigaciones teóricas como numéricas, como dos ingredientes importantes y complementarios, poniendo énfasis en el campo de los formalismos de las ecuaciones de Einstein y en particular en la FCF. He completado, en gran parte, el análisis de las propiedades matemáticas del sistema elíptico-hiperbólico de las ecuaciones de Einstein en esta reciente formulación. Estos estudios tratan principalmente de las propiedades de unicidad local de las ecuaciones elípticas y de la estructura característica de las ecuaciones hiperbólicas. El análisis de las ecuaciones hiperbólicas ha sido aplicado al estudio de las condiciones de contorno sobre los horizontes atrapados de los espacio-tiempo dinámicos de los agujeros negros. También he llevado a cabo algunos estudios de existencia de foliaciones maximales en el caso de espacios-tiempo con simetría esférica.

Sobre la parte numérica de la tesis, he realizado progresos en la puesta a punto del código numérico responsable de evolucionar el sistema que contiene la radiación gravitatoria en la FCF, y también en su implementación numérica en la nueva versión del código CoCoNuT. Algunos aspectos clave para la evolución del sistema, como el radio de extracción de la señal gravitatoria o aspectos que tienen relación con la frontera exterior, han sido obtenidos. El código está preparado para simular numéricamente la evolución tanto del tensor de energía como del tensor métrico completo (teniendo en cuenta todas las ecuaciones elípticas e hiperbólicas del formalismo FCF).

Pueden plantearse un conjunto de posibles extensiones o aplicaciones de mi trabajo en distintos campos.

Desde un punto de vista puramente geométrico, el estudio de la existencia de foliaciones maximales en simetría esférica y la técnica empleada para dicho estudio, puede (y debería) ser extendida a casos más generales, como los

espacio-tiempo axisimétricos, por un lado, y a otras foliaciones, por otra parte. Como propuesta añadida de este análisis, sería interesante también generar numéricamente espacios-tiempo dinámicos, y compararlos con los resultados generados usando nuestro análisis geométrico.

Desde un punto de vista puramente matemático, considero muy relevante (y urgente) completar el estudio de si el sistema elíptico-hiperbólico de las ecuaciones de Einstein para la FCF es un problema matemáticamente bien puesto. Hasta el momento, únicamente se habían realizado estudios de los sistemas de ecuaciones que gobiernan la evolución de la radiación gravitatoria en la FCF y las ecuaciones que gobiernan la evolución de los campos de materia por separado, de manera independiente uno y otro sistema de ecuaciones. En particular, sería interesante profundizar en la comprensión de las propiedades hiperbólicas del sistema de ecuaciones acoplado.

Desde un punto de vista puramente matemático, considero muy relevante (y urgente) completar el estudio de si el conjunto de ecuaciones elíptico-hiperbólico del formalismo FCF es un problema bien puesto. Hasta el momento, únicamente se han realizado estudios independientes del sistema que gobierna la evolución de la radiación gravitatoria en FCF y de la parte (magneto-)hidrodinámica de la evolución de la materia. En particular, sería interesante profundizar en la comprensión de las propiedades de hiperbolicidad del sistema acoplado de ecuaciones.

Desde un punto de vista astrofísico, es el momento oportuno para usar un procedimiento exacto (sin aproximaciones) para extraer la señal gravitatoria procedente de escenarios astrofísicos como el colapso de los núcleos estelares. Es el siguiente paso natural a esta tesis, después de los tests llevados a cabo satisfactoriamente. Es necesario una comparación rigurosa con los estudios previos realizados con otras aproximaciones para extraer la señal gravitatoria, como es el caso de la fórmula cuadrupolar. El diseño del código CoCoNuT es tal que está preparado para aplicaciones en tres dimensiones espaciales, y es natural la extensión del código para incluir la FCF de las ecuaciones de Einstein. Un esfuerzo para la mejora en los aspectos de paralelización es necesario.

Como resumen de las simulaciones numéricas propuestas a llevar a término con la versión actualizada de código CoCoNuT, caben mencionar las siguientes: i) obtener y comparar las señales gravitatorias resultantes de diferentes simulaciones de estrellas de neutrones en rotación con varias ecuaciones de estado; ii) calcular de una manera más precisa la evolución de la métrica completa del

espacio-tiempo de una estrella de neutrones que gira y colapsa a agujero negro. Otras simulaciones, en las que las coordenadas esféricas están bien adaptadas al problema específico, son posibles en escenarios con un campo gravitatorio fuerte, una vez que la extensión a la formulación completamente relativistica ha sido implementada en CoCoNuT.

2. INTRODUCTION

The topic treated along this thesis is the theoretical and numerical study of formalisms of Einstein equations, with the final aim of applications to black holes and gravitational waves. Both mathematics and physics play a fundamental role, complementing one another, concerning the tools used and the results presented in this work. Comunication among different specific branches of knowledge can lead to important improvements, and sometimes provides additional original points of view in the strategy for solving a problem.

The black hole concept was introduced by John Michell in 1783 in an article sent to the Royal Society: *"If the semi-diameter of a sphere of the same density as the Sun were to exceed that of the Sun in the proportion of five hundred to one, a body falling from an infinite height towards it, would have acquired at its surface greater velocity than that of light, and consequently supposing light to be attracted by the same force in proportion to its mass, with other bodies, all light emitted from such a body would be made to return towards it by its own proper gravity"*. He introduced this concept in the sense of an object having a surface gravity such that even light could not scape from it. In 1796, the French mathematician Pierre-Simon Laplace explained the same idea in his book *Exposition du Système du Monde:"Un astre lumineux de même densité que la terre, et dont le diamètre seroit deux cent cinquante fois plus grand que celui du soleil, ne laisseroit en vertu de son attraction, parvenir aucun de ses rayons jusquà nous; il est donc possible que les plus grands corps lumineux de lunivers, soient par cela même, invisibles..."*. The General Relativity theory of Albert Einstein (1915) postulated that light and trajectories of all particles are curved by the geometry of spacetime. Just a few months later, Karl Schwarzschild found a solution of Einstein equations which describes a non-rotating black hole, but at that epoch it was interpreted as a mathematical solution. It was in 1967 when John Wheeler introduced the term *black hole* during a conference in New

York.

From a geometrical point of view, a black hole can be seen as a solution of Einstein equations which contains a singularity (infinite curvature) in the metric of spacetime. From an astrophysical point of view, a black hole can be seen as the final result of some kind of collapse of a particular stellar object. However, it is not clear if the outcome of the collapse is the formation of a singularity, firstly, because such regions of spacetime are not accesible and, secondly, because quantum effects need a careful analysis in the context of a consistent theory of quantum gravity.

One of the predicted consequences of General Relativity, not detected yet, is the existence of gravitational waves. Enormous experimental, theoretical and numerical efforts have been made in the last forty years, in order to detect, predict and study the gravitational waves released from different astrophysical and cosmological scenarios. It will be a completely new way of looking at the universe, it will even be a way to unveil some places of the universe, hidden up to now, as black holes.

In order to deep into the knowledge of all these scenarios and interesting objects a formalism of Einstein equations is required. The different formulations, and the mathematical properties of the resulting set of partial differential equations, like well-posedness or local uniqueness, can have a huge importance and they have not always deserved attention. A hard theoretical work has been made in this topic by important mathematicians and physicists. We have to recognize the capability of the most used formulations, as the so-called BSSN (see more details in Chapter 4), crucial for the success of recent simulations of binary black holes. But we do not have to forget the formalisms introduced in the last years, as the FCF, which will be the object of study in this thesis, because they can offer new ideas and more realistic comparisons between numerical results.

Finally, the numerical tools available nowadays have made possible important advances. For example, supercomputers are able to show us how the universe evolves to the macroscopic homogenous structure and to filaments in a small scale; without computers, it is almost imposible to imagine the simulations of the evolution of non-linear systems of equations governing complex processes such as the evolution of stars, the dynamics of binary compact objects, the jets associated to galaxies... and a long etcetera.

2.1 Organization of the manuscript

I start with a list of publications, and the Chapters based on them. The outline is briefly described.

Chapter 1 contains the introduction, an overview which summarizes the main ideas and the conclusions of the thesis in Spanish.

Chapter 2 contains the introduction and the organization of the thesis. In Chapter 3, a brief analysis of black holes from the astrophysical point of view is made. A classification of black holes depending on their origin and masses, and some detection methods are reviewed.

Chapter 4 is a review of the main formalisms of Einstein equations, namely 2+2 or null formalism, and 3+1 formalism. The Kojima-Oohara-Nakamura (KON) formulation which used the 3+1 formalism, was proposed in 1987. The most popular formulation of the 3+1 formalism, the so-called Baumgarte-Shapiro-Shibata-Nakamura (BSSN) formulation is described. This formulation represents the state-of-art in the field of Numerical Relativity involving the succesfully binary black hole simulations. A recent one, the fully constrained formulation (FCF), is analyzed paying particular attention to their mathematical properties. This thesis is basically devoted to theoretical and numerical studies based on FCF.

Chapters 5 and 6 contain the core of the theoretical work. In Chapter 5, the local existence of maximal slicings is discussed. It focuses on the properties concerning the elliptic and hyperbolic equations of the FCF formalism. In Chapter 6 the properties of the hyperbolic system studied in Chapter 5 are applied to geometric aspects of black holes as the inner boundary conditions on the horizon.

Chapters 7 and 8 contain the numerical work. In Chapter 7 the methods for the numerical evolution of black holes and the present status of this kind of simulations are summarized. In Chapter 8, a numerical code is presented. It evolves the non-conformal part of the metric of spacetime in the FCF formulation, described by the hyperbolic system of non-linear partial differential equations. Some basic tests are shown, confirming the goodness of the numerical implementation of the equations. This code has been developed during the thesis independently from other codes, but the intention is to incorporate it to an existing numerical code, CoCoNuT. Previous version of CoCoNuT was able to numerically evolve the magneto-hydrodynamic equations using the

CFC approximation of Einstein equations. The addition of the new FCF of Einstein equations will extend the approximation to a fully general relativistic formalism.

Chapter 9 is a summary of the thesis and some future plans.

3. ASTROPHYSICAL BLACK HOLES

From a classical point of view a black hole (BH) is a compact object whose surface gravitational potential approaches half the square of the speed of light. A BH is an object sufficiently compactified which does not let light escape from it. The theoretical tool to describe mathematically a BH is General Relativity (GR). The boundary of the BH is a surface generally called the horizon. There are some quantities scaling with mass, M, as the radius $R = GM/c^2 \approx 1.47\,(M/M_\odot)\,\mathrm{km}$, where G is the universal gravitational constant, c is the velocity of light and $M_\odot$ is the solar mass, or the average mass density $\rho \equiv 3M/4\pi R^3 \approx 1.5 \times 10^{17}\,(M_\odot/M)^2\,\mathrm{g\ cm^{-3}}$, which tells us that massive BHs have low density.

3.1 Schwarzschild and Kerr BHs

The non-rotating and rotating BHs are described, mathematically, by the Schwarzschild and the Kerr metric, respectively. In this Section we are going to use m instead of M for denoting the parameter which is interpreted as the mass of the BH.

3.1.1 Schwarzschild BH

The Schwarzschild metric describes a static BH [1, 2]. This metric can be formulated in terms of different set of coordinates:

(i) If we use Schwarzschild coordinates $(t_S, r, \theta, \varphi)$, with $r > 2m$, the line element is given by:

$$ds^2 = -\left(1 - \frac{2m}{r}\right) dt_S^2 + \left(1 - \frac{2m}{r}\right)^{-1} dr^2 + r^2 d\Omega^2, \qquad (3.1)$$

where $d\Omega^2 = d\theta^2 + \sin^2\theta d\varphi^2$ is the metric of a 2-sphere, and m is the gravitational mass.

(ii) If we use isotropic coordinates $(t_S, \tilde{r}, \theta, \varphi)$, the line element is given by:

$$ds^2 = -\left(\frac{1-\frac{m}{2\tilde{r}}}{1+\frac{m}{2\tilde{r}}}\right)^2 dt_S^2 + \left(1+\frac{m}{2\tilde{r}}\right)^4 \left(d\tilde{r}^2 + \tilde{r}^2 d\Omega^2\right), \tag{3.2}$$

where the relation between this set of coordinates and the first one is given by $r = \tilde{r}\left(1+\frac{m}{2\tilde{r}}\right)^2$.

(iii) If we use Painlevé-Gullstrand-Lemaître coordinates, (T, r, θ, φ), the line element is given by:

$$ds^2 = -\left(1-\frac{2m}{r}\right) dT^2 + 2\sqrt{\frac{2m}{r}} dT dr + dr^2 + r^2 d\Omega^2, \tag{3.3}$$

where the relation between this set of coordinates and the first one is given by $dT = dt_S + \frac{\sqrt{\frac{2m}{r}}}{1-\frac{2m}{r}} dr$.

(iv) If we use Eddington-Finkelstein coordinates (t, r, θ, φ), the line element is given by:

$$ds^2 = -\left(1-\frac{2m}{r}\right) dt^2 + \frac{4m}{r} dt dr + \left(1+\frac{2m}{r}\right) dr^2 + r^2 d\Omega^2, \tag{3.4}$$

where the relation between this set of coordinates and the first one is given by $t = t_S + 2m \ln\left|\frac{r}{2m} - 1\right|$.

The induced metric on the spatial hypersurfaces t_S = constant is conformally flat; it is easy to check it in the isotropic coordinates. As a general procedure, one can calculate the Cotton tensor in a set of coordinates. In three dimensions, the metric is conformally flat if and only if the Cotton tensor is zero (in more dimensions, the Cotton tensor must be replaced by the Weyl tensor). The induced metric on the spatial hypersurfaces $T = constant$ is flat.

The first and second set of coordinates are singular at the horizon $\mathcal{H}$, which corresponds to $r = 2m$, $\tilde{r} = m/2$ and $t_S \to +\infty$. The spatial hypersurfaces $t_S = constant$ are an example of maximal slicing (the trace of the extrinsic curvature is zero, see next Section); they do not intersect the horizon except at a 2-sphere that is common for all of them. The two last set of coordinates are regular at the horizon $\mathcal{H}$ which is located at $r = 2m$; in both of them we have always a timelike coordinate, T or t.

3.1.2 Kerr BH

A rotating BH is described by the Kerr metric [3]. There are several sets of coordinates we can use:

(i) If we use Boyer-Lindquist coordinates (t, r, θ, φ), the line element is given by:

$$ds^2 = -\left(\frac{\rho\sqrt{\Delta}}{\Sigma}\right)^2 dt^2 + \tilde{\omega}^2 \left(d\varphi - \omega dt\right)^2 + \rho^2/\Delta dr^2 + \rho^2 d\theta^2, \qquad (3.5)$$

where:

$$\begin{aligned} \Delta &= r^2 - 2mr + a^2, & (3.6)\\ \rho^2 &= r^2 + a^2\cos^2\theta, & (3.7)\\ \Sigma^2 &= \left(r^2 + a^2\right)^2 - a^2\Delta\sin^2\theta, & (3.8)\\ \omega &= 2amr/\Sigma^2, & (3.9)\\ \tilde{\omega} &= \Sigma\sin\theta/\rho, & (3.10) \end{aligned}$$

a being the specific angular momentum of the BH. Setting $a = 0$ in equation (3.5) we recover the Schwarzschild BH in Schwarzschild coordinates.

(ii) If we use Kerr-Schild coordinates $\left(\tilde{t}, r, \theta, \tilde{\varphi}\right)$, the line element is given by:

$$\begin{aligned} ds^2 \quad - \quad & -(1 - Z)\, d\tilde{t}^2 - 2a\sin^2\theta\, Z d\tilde{t} d\tilde{\varphi} - 2\epsilon Z^k d\tilde{t} dr + \frac{Z^{2k} - 1}{Z - 1} dr^2 \\ & + 2a\,\epsilon\sin^2\theta\,\frac{Z^{k+1} - 1}{Z - 1} dr d\tilde{\varphi} + \rho^2 d\theta^2 \\ & + \sin^2\theta\,\rho^2[1 + Y(1 + Z)] d\tilde{\varphi}^2, \qquad (3.11) \end{aligned}$$

where $Y = a^2 \sin^2\theta/\rho^2$, $Z = 2mr/\rho^2$, k is a non-negative integer that can be considered as a parameter, and $\epsilon = +1(-1)$ regularizes the future (past) horizon of a rotating BH. The relation between this set of coordinates and the Boyer-Lindquist one is given by

$$d\tilde{\varphi} = d\varphi - \epsilon \frac{a}{\Delta} dr, \tag{3.12}$$

$$d\tilde{t} = dt - \epsilon \left[\frac{1+Y}{1+Y-Z} - \frac{1-Z^k}{1-Z} \right] dr. \tag{3.13}$$

The function Δ is called the horizon function, which is zero at the horizon. This implies that the component g_{tt} of the metric, i.e, the coeficient of dt^2, vanishes.

For static Schwarzschild BHs, $a = 0$, there is only one horizon located at $r = 2m$; but for rotating Kerr BHs there are in fact two horizons located at:

$$r_\pm = m \pm \sqrt{m^2 - a^2}, \tag{3.14}$$

where r_+ is called the outer horizon and r_- the inner or Cauchy horizon. The outer horizon is the event horizon.

3.2 Classification

We can classify BHs in three types according to their origin: those that arise from stellar collapse (stellar BH), those that may come from merging and accretion processes and are named supermassive black holes (SMBH), and those which may be relics of the dense highly inhomogeneous medium in the early universe (primordial black holes –PBH).

According to their masses BHs can be classified: PBH, which have a very low mass, for which there are no observations; low mass BH, $3 - 10M_\odot$, as the stellar ones; intermediate mass BH (IMBH), $10 - 10^6 M_\odot$, for which the observational evidence is pretty weak [92]; and SMBH, up to $10^8 M_\odot$.

3.2.1 Stellar BHs

Stellar BHs, i.e., BHs as the outcome of the stellar evolution can be formed in the following cases:

(i) The final evolution of Population I massive stars with $M \geq M_c$, where M_c is typically much higher than $10M_\odot$ (see figure 3.1).

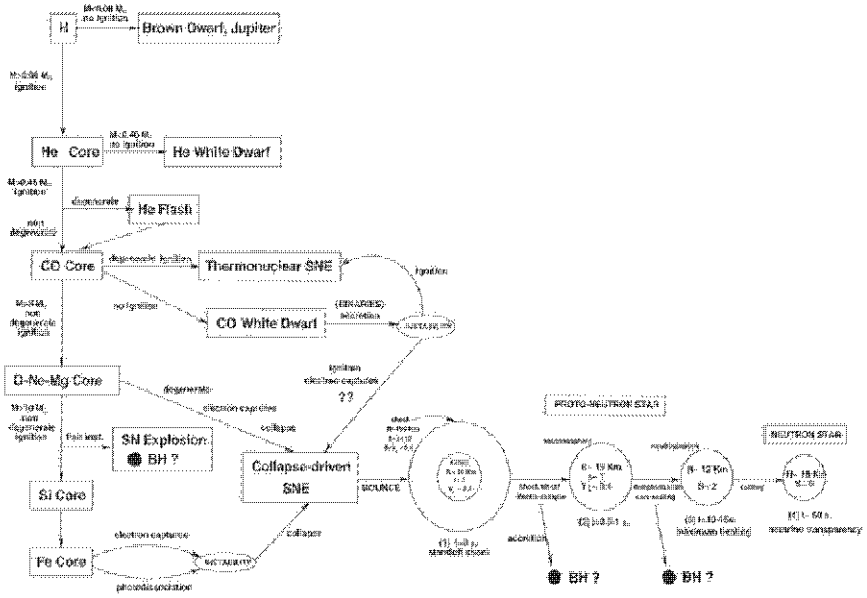

Fig. 3.1: Evolution of Pop I stars (J.A. Pons, private communication).

(ii) The final evolution of Population II massive stars as before. Roughly speaking, we can say that the evolution of Pop II follows the same track as do the stars of Pop I, generating the same mass spectrum of BHs as in the case (i).

(iii) The final evolution of Pop III massive stars ([93]). Notice that in this case the theory predicts the formation of IMBHs (see figure 3.2).

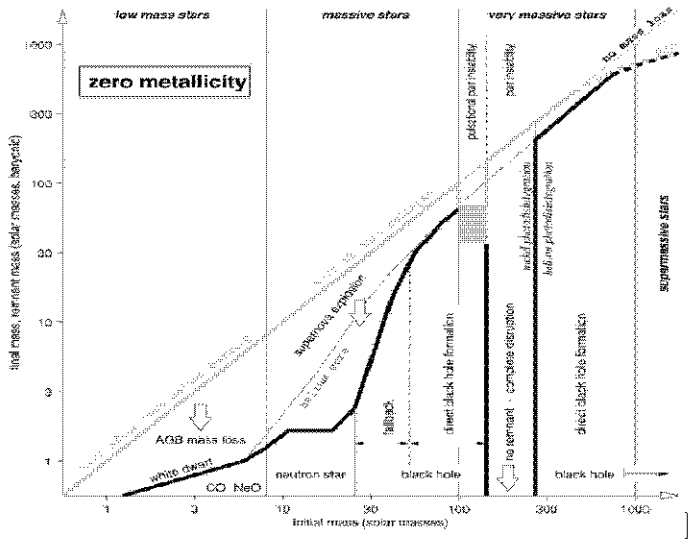

Fig. 3.2: The y-axis gives both the final mass of the collapsed remnant (thick black curve) and the mass of the star when the event that produces that remnant (e.g., mass loss in AGB stars, supernova explosion for those stars that make a neutron star, etc; thick gray curve) begins [93].

3.2.2 SMBH

In this case there can be some processes lumping together such as: accretion onto a stellar BH, merger of massive stars that collapse, gas cloud extremely dense that collapses, merger of IMBH, SMBH in the center of the galaxies as seed of the proper galaxy. The presence of them in late-type systems is reasonable if they form by accretion. There are relations between the mass and the velocity dispersion (see the detection methods) in early type disk galaxy bulges (Magorrian's law [5]) supporting the joint growth hypotesis. Other processes as mergers of BHs can be regarded.

The Milky Way has in its center a SMBH located at SgrA*. A cluster of stars is observed within 0.02 pc of it, and the orbital motion of some of them

with velocities up to 1350 km s^{-1} have been monitored during many years. Well determined acceleration vectors for several of the stars point at SgrA* and the data allow an estimate of the central mass about $(4.31 \pm 0.38) \times 10^6 M_\odot$ [94]. This massive object cannot itself be a cluster of smaller objects due to the following arguments: i) $10^6 M_\odot$ of ordinary stars would be visible; ii) if it were formed from brown dwarfs, then it would be so densely packed that they would collide, merge and become luminous beyond observable limits; iii) if they were formed from collapsed stars, then they would be rapidly expelled out by evaporation [95, 96].

Accretion onto SMBHs is the most efficient mechanism of energy generation. The physical picture to compute the maximum efficiency is an accretion disk in which matter slowly spirals inward. This spiralling motion stops at the innermost stable circular orbit (ISCO), which is the innermost radius an accretion disk can have. The efficiency of a BH is one minus the fraction of the original rest mass finally accreted by the BH. The upper limit efficiency for a Schwarzschild BH for point particles is 0.0572, while for an extreme Kerr BH it reaches 0.42; a BH accretion disk can convert mass into energy up to two orders of magnitude more efficiently than the one generated in the nuclear burning of hydrogen into helium (see more details in [97]).

There are reasons to expect that an accretion disk surrounding the BH can be formed. The angular momentum of gas around it can prevent the gas from immediately falling into the BH, and it will rather swirl around. Rotation of the galaxy hosting the BH will impose swirling of different gas streams; they will collide and the angular momentum vectors will align leading to the formation of a thin disk. A BH in an active galactic nucleus (AGN) spins rapidly because the disk feeds the hole with a high angular momentum to mass ratio. Let us start from a non-rotating BH with an initial mass, and let $l = g_{\varphi t} dt/d\tau + g_{\varphi\varphi} d\varphi/d\tau$ be the specific angular momentum, where $g_{\varphi t}$, $g_{\varphi\varphi}$ are the corresponding components of the metric, and τ and t are, respectively, the proper and coordinate time. When a unit mass in the disk reaches ISCO, it plummets into the BH without changing its energy E and angular momentum l, then $\delta M = E$, and $\delta(aM) = l$. We define $a_* = ca/GM$, that satisfies $a_* \leq 1$. Doing some calculations and evaluating at $r = r_{ISCO}$ (see [97]), one obtains

the differential equation:

$$da_* = \left[\frac{\rho(a_*)^2 - 2a_*\rho(a_*)^{1/2} + a_*^2}{\rho(a_*)^{1/2}[\rho(a_*) - 2] + a_*} - 2a_* \right] d\ln M, \tag{3.15}$$

where $\rho(a_*) \equiv c^2 (GM)^{-1} r_{ISCO}$ is a complicated function. Integrating numerically from $a_* = 0$ at the initial mass shows that the spin parameter reaches $a_* = 0.3058\,(a_* = 0.7689)$ when the mass grows by 10% (40%), and it can reach $a_* = 0.9875$ when the BH has doubled its initial mass. So if a SMBH has changed its mass substantially by accretion from its disk, it must be rotating rapidly.

3.2.3 PBH

There are no observational confirmation of their existence. They could be the seeds from which SMBHs grow. Only in the early universe we find densities which are orders of magnitude above nuclear density. The post-inflation radiation era is the first relevant one in connection with the formation of this kind of BHs. The time of formation of a PBH of mass M is $t \approx 4.9 \times 10^{-24} (M/M_\odot)\, s$. The less massive the PBH, the earlier it forms. The Hawking radiation, associated with the temperature of the BH, produces an energy loss, and PBH with less mass than a critical value have nowadays evaporated. The primordial density fluctuations spectrum are in the origin of the posible formation of PBHs. The search for PBH may provide important information about the conditions in the very early universe.

3.3 Detection methods

We can distinguish between direct and indirect methods to detect BHs. By direct methods we understand those aiming at showing the existence of the event horizon and the curvature singularity. Due to the cosmic censorship conjecture by R. Penrose [98], BH intrinsic singularities are hidden by an event horizon, so the only posibility is to prove the existence of an event horizon. It means to find strong evidence for a zero-emission region. This is almost imposible due to the innacuracies in the measurements and the fact that BH event horizons radiate

according to quantum gravity description. Only the detection of gravitational waves can be a strongly direct evidence of the existence of BHs.

Let us comment some of the observational strategies to detect event horizons [4]:

Kinematical methods

They are very popular and successful. Moving objects around the BH feel its deep gravitational potential. Hence, their dynamics can be used to derive properties as the mass and spin of the BH; the values obtained can be used to rule out other compact object alternatives such as white dwarfs or neutron stars. This is the case of the radio source SgrA* mentioned before. It is an indirect method which can be applied to luminous stars, gas or flaring objects. Typically the tracer of the objects close the BH surrounds it on Keplerian orbits, and the tracking time scale is determined by the Keplerian time scale at a given radius.

Stars that follow their orbits in groups can also be used, like in, e.g., galaxies. The study of galaxy samples shows evidence for a strong correlation between the mass of the central BH, M, and the stellar velocity dispersion, σ, called the $M-\sigma$ (Magorrian) relation [5]:

$$\log\left(M/M_{\odot}\right) = \alpha + \beta \log\left(\sigma/\sigma_0\right), \tag{3.16}$$

where $\sigma_0 = 200$km/s is a reference value, and β a fit value for the slope ($\beta \approx 4.0$). BH masses are measured from continuum luminosities and the width of Hβ lines. Narrow [OIII] line widths serve as tracers to determine the velocity dispersions. This relation is not valid at very high redshifts and recently a non-linear $M-\sigma$ relation has been suggested [99].

Other technique that involves the emission of gas is reverberation mapping. Broad line regions (BLRs) in AGNs are supposed to be luminous matter clouds consisting mainly of hydrogen that surrounds a galactic core; due to their fast motions, emission lines are significantly broadened by the Doppler effect and their width is a measure for the velocity of the BLRs, σ. We name r the distance of the BLRs to the center of the galaxy; we can determine it by comparing the emission from the galactic core with the one from the BLRs. From the Virial theorem, the central mass deduced is:

$$M \approx r\sigma^2/G. \tag{3.17}$$

This is very useful to detect SMBH in the center of a galaxy. NGC 5548 and other galaxies studied in [100] are some examples where this method has been applied.

Water masers can be found in the molecular torus placed at the pc scale of a galaxy. The microwave emission from Keplerian rotating gas orbiting the SMBH can be used to measure the central mass. In the nucleus of the spiral galaxy NGC 4258 the radial Doppler velocities can be fit by rotation of a circumnuclear disk of pc scale with a Keplerian rotation velocity profile reaching up to 1080 km s^{-1}. This implies a point mass at the center of around $4 \times 10^7 M_\odot$, that cannot be a cluster of brown dwarfs or collapsed objects inside because the disk's inner radius is at 0.13 pc [95, 96].

There are techniques to measure the spin of a BH, J, but, since $\omega \propto r^{-3}$, rotation of spacetime is extraordinarily strong only very close to the BH.

Finally, a comparison of the observations of quasi-periodic flare emission close to the galactic center BH with characteristic frequencies associated with accretion disks (i.e. Keplerian orbital, vertial, and radial epicyclic frequency) can also be used to detect BH and measure parameters as the rotation of the BH [101].

Spectro relativistic methods

Relativistic effects present in observed spectra are used to establish BH properties. The main method is the analysis of the Fe lines. There can be a line profile in the rest frame of the source, like a rotating disk around the BH that extends only a few gravitational radii away from the event horizon. A remote observer will see a line profile very different from the one observed at the rest frame due to some physical effects affecting the path of the photons on their way. We have to regard a Doppler redshift at the receding part and a Doppler blueshift at the approaching part. One expects a broadened line with two peaks when the disk is sufficiently inclined towards the observer. If the inclination is important the Keplerian velocities are comparable to the speed of light and the observer radiation intensity is amplified with respect to the rest frame; this intensifies the blue line wing. Moreover, the BH deviates the trajectory of photons by strong spacetime curvature; the observed photon energy is redshifted relative to the rest frame energy and the spectral line flux is lower in the observer's frame. See more details in [6].

Gathering together all the mentioned effects, an asymmetric and skewed relativistic emission line profile is produced. X-ray astronomers often observe such kind of profiles as iron K fluorescent lines, as part of the so-called 'reflection bump', as response of the ionized accretion disk. The most important iron fluorescent line is the neutral Fe Kα line. It has been observed in galaxies, quasars and stellar BHs. With sufficient spectral resolution, the gravitational redshift can be used as a new detection method for BHs to derive masses with multi-wavelength data. We can also get information about BH spin. The standard disk extends down to the ISCO which depends on the BH spin: the event horizon is placed at $r_{ISCO} = r_g = GM/c^2$ for rapidly spinning Kerr BHs, to be compared with the case of the Schwarzschild BHs for which $r_{ISCO} = 6r_g$. The line emission comes from regions that are deeper in the gravitational potential if the BH rotates. The line shape is broader and shows an extended broad red wing for Kerr BHs.

Thin accretion disks are known to have a temperature profile with a maximum close to the inner disk edge [102]. If we divide the disk into rings each one with a specific temperature, a disk blackbody spectrum (called multitemperature blackbody spectrum) is built up by the blackbody temperature of each ring. If the disk is close enough to the BH, GR influences the blackbody radiation. There is a proposed model [103] that is able to measure BH spins.

Accretive methods

Matter accreting onto a BH can cause luminous effects. In a simple scheme of an AGN, there is a torus around the BH. The matter of the torus flows due to instabilities into the center of the AGN. Depending mainly on the accretion rate a geometrically thick and optically thin advection-dominated accretion flow at several tens of gravitational radii away from the central SMBH can be formed. Magnetic effects close to the SMBH favor strong luminous outflows, the jets, that can be used as fingerprints of the activity of the SMBH. There are several groups working in simulations, and radio astronomers working in observations of these objects, trying to deepen the knowledge of this field. Eddington's relation links luminosity to accretion rate and BH mass. From the observed luminosity of SMBH or binaries that contain stellar BHs for example, it is possible to estimate the BH mass.

The Bondi-Hoyle astrophysical scenario around a Kerr BH (see [104]) traces the presence of the BH and could help observers to detect its presence.

Eruptive methods

The main example of an eruptive event is a gamma-ray burst (GRB). They are placed among the most luminous events known in the universe since the Big Bang, with energies $E_{GRB} \gtrsim 10^{51} erg$. They are flashes of γ-rays, coming from seemingly random places on the sky and at random times. Their duration spans from 10^{-3} seconds to 10^{3} seconds and they are often followed by an afterglow emission at longer wavelengths: X-ray, optical, and radio. According to the observed duration, they are classified in two classes: short GRBs (sGRBs), of less than 2 seconds of duration, and long GRBs (lGRBs), of more than 2 seconds of duration. The rate of the lGRBs is 1 per day and the rate of the sGRBs is 0.3 per day. They have a high variability. The spectrum is non-thermal, of 0.1–100 MeV. The cosmological redshifts are between $z = 0.085$ and 8.2, $< z >\sim 1.3$, for lGRBs, and between $z = 0.12$ and 4.6, $< z >\sim 0.3$, for sGRBs. The knowledge about their progenitors is only indirect; the progenitors are $10^{-6} - 10^{-7}$ times dimmer than GRBs themselves and we cannot observe them. Interested readers are addressed to references [7] for lGRBs and [8] for sGRBs.

There exists some evidence for an association between lGRBs and supernovae (SN); the two main indications are: i) photometry: like GRB980425 and SN1998bw in a nearby galaxy [105]; ii) spectroscopy: like GRB030329 and SN20003dh [106]. The hosts of lGRBs are star-forming, low metallicity galaxies, but bluer than typical starburst galaxies with little dust and masses lower than current ellipticals; so they are the typical environments of formation of massive stars. Concerning their distribution in the galaxy, lGRBs follow the light distribution that is approximately the density of star formation distribution. If we study the rates of SNIbc and the rate of the lGRBs, only a few percent of SNIbc can be associated with lGRBs; additional conditions must be imposed on the progenitors.

The knowledge of sGRBs is poor and can be improved, because there are only several dozen observations. However, we can say that the hosts of sGRBs are star-forming and elliptical (old) galaxies; this is consistent with the fact that sGRBs are associated with NS+NS/BH (NS≡neutron star) mergers, if one assumes that there are fast evolutionary tracks to form mergers. They are typically found in the outer parts of their hosts galaxies. Only a few percent of NS+NS mergers need to produce sGRBs; additional conditions must be

imposed on the progenitors.

Numerical modeling of progenitors systems involving a new-born BH has allowed to gain a refined understanding of the dynamics and global properties of relativistic outflows generated in these systems.

Another eruptive detection method for BHs concerns stellar tidal disruption events. A star with mass M_* and radius R_* approaches a BH of mass M. The star is strongly deformed by tidal forces of the BH. At the tidal radius, $R_T \approx R_* \left(\frac{M}{M_*}\right)^{1/3}$, BH's tidal forces overcome the selfgravity of the star and the star is disrupted. The stellar debris extends to a region close to the BH and can be partially accreted. If that happens (it is a rare event), a characteristic X-ray flare develops. This flare has typical signatures for a tidal disruption. It is thermal radiation with typical timescales of months and the integrated luminosity yields an energy output comparable to supernovae, that need simultaneous optical observations to exclude flares from AGN. The BH mass can be derived from blackbody spectral fits.

Finally, let us mentioned the Hawking evaporation. In the early Seventies it was shown that, even in a semi-classical approach with quantized scalar fields on the background of non-quantized 4D BH spacetimes, it is possible that BHs are not totally black [107]. The horizon is illuminated by Hawking radiation. Currently, the signal-to-noise ratio does not allow to detect dim Hawking emission and there are more intense radiation of other kind surrounding the BH. For typical cosmic BHs the decay due to energy loss by Hawking radiation can be neglected because the decay time scales with $\tau \propto M^{-3}$; this can be interesting for PBH, but there are not observations yet.

Obscurative methods

One can use the blackness of the BH to detect it. If there is something bright in the environment, like the accretion flow or the cosmic microwave background (CMB), the BH emerges in the foreground. Spectral flux is reduced by higher powers of a factor proportial to Δ, the horizon function. This function, and therefore also the spectral flux, vanishes at the horizons.

For Kerr BHs the intrinsic shape of the event horizon is spherically symmetric since there is no angle dependence. But the appearance of the event horizon by an observer placed at infinity depends strongly on the inclination angle of the observer and the rotation of the BH [9]. These deformations can

be used to determine BH properties by observations. It is introduced the notion of black spot (BS) to refer to this. We have to be careful because the BS shapes are model dependent. Constraining the inclination angle of the BH's rotation axis to the observer, then the BH spin, and BH mass can be deduced with detailed studies if its distance is known, that could be obtained by interferometric techniques. If we consider the CMB in which the BH emerges, the BH can be detected, independently of having something accreting into it.

Aberrative methods

The Astronomy of Gravitational Lenses is a very active field of Modern Astronomy. The search and detection of gravitational lenses can help observers to infer, among other issues, properties of the lens. In particular, BHs cause strong gravitational lensing effects that distort the appearance of close objects. Astronomers use photometric methods by measuring light amplification of background sources from lensing BHs in the foreground [10]. Several null geodesics coming from the source can arrive at the observer and multiple images and also rings can form. Galaxies, stars or planets can play the role of lenses. A BH distorts the orbits around it. BH masses and other properties can be deduced with these tecniques. For example, Meudon's group (J.A. Marck, [108]) have analyzed the null geodesics of photons emitted from the accretion disk around a Kerr BH. Other example about measurements of BH can be found in [109].

Gravitational wave–induced methods

This is the only direct method for detecting BHs. These waves can be viewed as ripples in the curvature of spacetime caused by accelerations of matter, provided that the motion is not perfectly spherically symmetric. Their propagation speed is the speed of light; the Gravitational Waves (GWs) do not travel through spacetime, it is the proper spacetime which oscillates. GW emission implies emission of energy. The first indirect detection of GWs was in 1974 by Hulse and Taylor from their observation of the binary pulsar system PSR B1913+16, consisting of two neutron stars orbiting each other closely and rapidly, a discovery for which they were awarded the Nobel Prize in Physics; its orbital period decreases just as it was predicted by GR if the system were losing energy by radiationg GWs.

Their strength weakens proportionally to its distance from the source. As these waves pass, distances between objects will increase and decrease rhythmically; the magnitude of this effect for very strong sources mesured at Earth is very small, changes in size at most 1 in 10^{20}, and so the difficulty to measuring them. GWs have not been detected directly yet. Huge experimental efforts are, currently, done in this field. The first attempt was due to Weber with a resonant bar; modern Weber bars are still operating, but they are not sensitive enough to detect anything but extremely powerful GWs [11]. More sensitive detectors are ground-based interferometers, as VIRGO [12], GEO600 [13], TAMA300 [14] or LIGO [15], and their advanced versions. Space-based interferometers, as LISA [16], are being developed. Scientific community expect that GW observatories will detect signals in a near future. A new window of information will be opened allowing us to see things that we cannot observe by means of other kind of messengers (photons, neutrinos...).

Binaries of NSs, NS+BH, or BHs, SN explosions, accretion onto BHs, non-spherical pulsating objects are sources of GWs (see Section 7 and talks in a recent workshop held in Valencia (Spain) [17]). Numerical simulations are providing useful templates for extracting GWs from data analysis in case of detection by the GW observatories. In the last few years this field has advanced enormously, and it is a nice example of synergy between observations and numerical simulations.

4. FORMALISMS OF EINSTEIN EQUATIONS

Two of the main formalisms of Einstein equations are the 2+2 or null formalism, and the 3+1 formalism. A review of them will be presented in this Section, as well as some formulations of 3+1.

4.1 2+2 formalism

The metric of Minkowski spacetime is:

$$\begin{aligned} ds^2 &= g_{\alpha\beta}dx^\alpha dx^\beta = \eta_{\alpha\beta}dx^\alpha dx^\beta \\ &= -dt^2 + dr^2 + r^2 d\Omega^2, \quad (4.1) \end{aligned}$$

where $d\Omega^2$ corresponds to the metric of the 2-sphere.

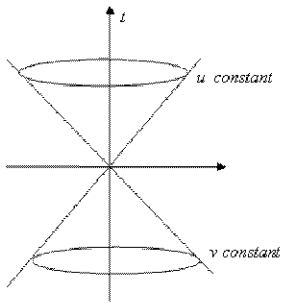

Fig. 4.1: Null cone.

The variable t is taken as a time variable and r as a radius. The velocity of light $c = 1$ splits the Minkowski spacetime into two regions which are called, because of causality reasons, future cone ($t > 0$) and past cone ($t < 0$). For a constant value of t, there is a 2-sphere of radius r, that can be seen as a 1-sphere in Fig. 4.1. The future and past cones of slope 1 are constituted by the null vectors k, which satisfy $\eta_{\alpha\beta}k^\alpha k^\beta = 0$. The timelike vectors are inside the cone, and the spacelike ones outside.

If one fixes the coordinates of the 2-sphere $d\Omega^2$ and imposes $ds^2 = 0$, there are two solutions: $dt = \pm dr$. We can define two new variables as

coordinate scalars: the advanced time, $v := t + r$, and the retarded time, $u := t - r$. The derivatives ∂_u and ∂_v along these coordinate directions define null vectors. The hypersurfaces defined by u = constant and v = constant are called characteristic hypersurfaces, because these coordinate scalars satisfy $\eta^{\alpha\beta}\partial_\alpha u \partial_\beta u = 0 = \eta^{\alpha\beta}\partial_\alpha v \partial_\beta v$. Using one of these variables instead of t, the metric can be rewritten as:

$$ds^2 = -du^2 - 2\,du\,dr + r^2 d\Omega^2 = -dv^2 + 2\,dv\,dr + r^2 d\Omega^2. \tag{4.2}$$

Now a general curved spacetime will be considered.

The characteristic surfaces for the gravitational field equations are null hypersurfaces in a curved space. Solutions of the equation

$$g^{\mu\nu}\partial_\mu u\,\partial_\nu u = 0 \tag{4.3}$$

define a family of $u = constant$ null hypersurfaces. The normal directions to the surface, $k^\mu = g^{\mu\nu}\partial_\nu u$, are also tangent to the surface since null vectors are self-orthogonal. A two-parameter system of null geodesics tangent to k^μ, called rays, generate a single null hypersurface.

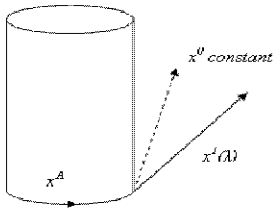

Fig. 4.2: Null coordinate system.

In null coordinate systems, $u = x^0$, the retarded time, is one of the coordinates; one wants to know the information coming from the system. Once a family of null hypersurfaces has been incorporated by the previous coordinate, two additional coordinates, x^A, $A = 2, 3$, are chosen as parameters constant along each ray:

$$k^\mu \partial_\mu x^A = 0. \tag{4.4}$$

These coordinates can be visualized as optical angles, and are named $\theta = x^2$, $\phi = x^3$. The choice of the coordinate scalars u, θ, ϕ, and the conditions (4.3) and (4.4), give the constraints $g^{uu} = g^{uA} = 0$ to the contravariant metric components. Since $g^{\alpha\beta}g_{\beta\mu} = \delta^\alpha_\mu$ one has furthermore $g_{11} = g_{1A} = 0$. The only coordinate varying along a given light ray is x^1. It is usually taken to be

the luminosity distance r from the source [18, 19]. This set of coordinates is illustrated in Fig. 4.2.

In the particular case of Minkowski spacetime, the retarded time labels a family of null cones which are generated by light rays emanating from the origin. This variable can be seen as the x^0 coordinate. Moreover, r can be seen as x^1 and the polar angles in the metric of the 2-sphere $d\Omega^2$ as x^A.

Bondi was the first in using null coordinates to describe radiation fields. His work was followed by a rapid development of other null formalisms. These were distinguished either as metric based approaches, as developed for axisymmetry by Bondi, Metzner and van den Burg [20] and generalized by Sachs [18], or as null tetrad approaches developed by Newman and Penrose [21] in which the Bianchi identities appear as part of the set of equations.

Let us consider an isolated worldtube [19]. The most general metric in this system of coordinates is [18]:

$$\begin{aligned} ds^2 &= -\left(\frac{V}{r}e^{2\beta} - r^2 h_{AB}U^A U^B\right) du^2 \\ &\quad -2e^{2\beta}drdu - 2r^2 h_{AB}U^B dx^A du + r^2 h_{AB}dx^A dx^B, \end{aligned} \tag{4.5}$$

where:

(i) $g_{ur} = -e^{2\beta}$,

(ii) $g_{AB} = r^2 h_{AB}$,

(iii) $g_{uA} = -r^2 h_{AB}U^B$,

(iv) $g_{uu} = -\left(\frac{V}{r}e^{2\beta} - r^2 h_{AB}U^A U^B\right)$.

The function V can be interpreted as a Newtonian potential. The functions U^A are the angular shift on the light cone. The function β is the redshift between the hypersurfaces u_0 and $u_0 + \Delta u$, or more physically, the expansion rate of light rays.

Notice that we have two degrees of freedom in the choices of the functions h_{AB}, that are going to be represented by the functions γ, δ. We can write them in terms of the new functions, if and only if we impose that the determinant of h_{AB} is equal to $\sin^2\theta$, as:

$$\begin{aligned} h_{AB}dx^A dx^B &= e^{2\gamma}\cosh(2\delta)\, d\theta^2 + 2\sinh(2\delta)\sin\theta d\theta d\phi \\ &\quad + e^{2\gamma}\cosh(2\delta)\sin^2\theta d\phi^2. \end{aligned} \tag{4.6}$$

In the linear approximation γ is connected with the plus polarization and δ with the cross polarization of the gravitational wave.

Given u one can make a change from any set of variables $\left(x^A, r\right)$ to any other allowed set by choosing two arbitrary functions of three variables $x'^A = G^A\left(u, x^B\right)$. This degree of freedom can be avoided by introducing a suitable tetrad system. Bars will be used to denote complex conjugation. For a given k^μ we have:

$$g^{\mu\nu} = k^\mu m^\nu + m^\mu k^\nu + \bar{t}^\mu t^\nu + t^\mu \bar{t}^\nu,\ m^\mu = \bar{m}^\mu$$
$$\Leftrightarrow k^\mu m_\mu = t^\mu \bar{t}_\mu = 1,\ m^\mu m_\mu = k^\mu k_\mu = t^\mu t_\mu = m^\mu t_\mu = k^\mu t_\mu = 0; \quad (4.7)$$
$$m^\mu \nabla_\mu k_\nu \propto k_\nu. \quad (4.8)$$

An algebraic consequence of (4.3) is that there is one and only one, necessarily null-like, real vector m^μ satisfying (4.7) and (4.8). Notice that m^μ is leading out of the hypersurface, and not laying in the hypersurface, because the x^A span a spacelike hypersurface. This vector is useful because it defines a unique direction leading out of the hypersurfaces $u = constant$. To interpret m^μ one can again imagine the rays realized by photons; then an observer sees the rays always coming from the same direction in his own rest frame if and only if his velocity lies in the plane spanned by k^μ and m^μ. The vector t^μ is determined up to the transformations $t'^\mu = e^{i\omega} t^\mu$, with ω any real spacetime function.

Next, let us consider what are the restrictions that Einstein field equations place on the metric functions. If we denote them by $E_{\mu\nu} \equiv G_{\mu\nu} - 8\pi T_{\mu\nu} = 0$, where $G_{\mu\nu} = R_{\mu\nu} - \frac{1}{2} g_{\mu\nu} R$, $R_{\mu\nu}$ is the Ricci tensor, R the scalar curvature and $T_{\mu\nu}$ the energy-momentum tensor (e.g., a perfect fluid), these equations automatically split into four groups:

(i) Four hypersurface equations: $E_{r\mu}$.

(ii) Two propagating equations: E_{AB}.

(iii) Four conservation equations: $E_{u\mu}$.

(iv) One trivial equation: $g^{AB} E_{AB}$.

The equation for E_{rr} gives a relation of the kind $\mathcal{A}_1\left(\beta, \gamma, \delta\right)$. Imposing initial conditions on $\gamma, \delta, \rho, h, u_r$, where ρ, h, u_r are the matter fields, i.e., the rest mass density, enthalpy and radial velocity respectively, we can obtain from

$\mathcal{A}_1(\beta,\gamma,\delta)$ the function β. The equations for E_{rA} give relations of the kind $\mathcal{A}_2\left(\beta,U^A,\gamma,\delta\right)$. With β,u_A and the previous initial conditions, one can integrate $\mathcal{A}_2\left(\beta,U^A,\gamma,\delta\right)$ to get the functions U^A. The equation for $g^{AB}E_{AB}$ gives a relation of the kind $\mathcal{A}_3\left(V,\beta,U^A,\gamma,\delta\right)$. With β,U^A,p, where p is the pressure of the fluid, and the initial conditions, from $\mathcal{A}_3\left(V,\beta,U^A,\gamma,\delta\right)$, one obtains the function V. Although E_{ur} is not in the proposed hierachy, it gives g_{uu} and so V as well [19].

Then, one has to solve the propagation equations for E_{AB} along u, which are two wave equations for γ,δ. The procedure starts again with E_{rr} on the next hypersurface. All the remaining Einstein equations are inmediately fulfilled when the integration hierachy is valid, because these remaining equations are connected to the others by the Bianchi identities. The evolution of the matter fields is responsible of generating the gravitational waves, that reach infinity.

The spacetime is assumed to have Euclidean topology at large distances from the source, is asymptotically flat, and the gravitational radiation obeys the outgoing Sommerfeld radiation condition:

$$\lim_{r\to\infty}\left.\frac{\partial r\gamma}{\partial r}\right|_{u=const}=0. \tag{4.9}$$

The following three conditions are sufficient for satisfying both the above topological condition and the Sommerfeld radiation condition:

(i) For some choice of u one can go to the limit $r\to\infty$ along each ray.

(ii) For some choice of θ and ϕ and the above choice of u:

$$\lim_{r\to\infty}(V/r) = -1, \tag{4.10}$$

$$\lim_{r\to\infty}\left(rU^A\right) = \lim_{r\to\infty}\beta=\lim_{r\to\infty}\gamma=\lim_{r\to\infty}\delta=0, \tag{4.11}$$

with u, θ and ϕ fixed.

(iii) Over the coordinate ranges $u_0\le u\le u_1$, $r_0\le r\le\infty$, $0\le\theta\le\pi$, and $0\le\phi\le 2\pi$ all the metric components and other quantities of interest can be expanded in powers of r^{-1} with at most a finite pole at $r=\infty$. Such power series can be added, multiplied, differentiated, etc.

It can be shown that condition (i) does not depend on the choice of θ and ϕ even though the definition of r does depend on this choice, because r has been prescribed to be a luminosity distance along the null rays. The topological restrictions are contained in the form of the metric and in the assumed coordinate ranges ($\phi = 0 \equiv \phi = 2\pi$). There is no assumption about the topology of the region $r < r_0$; one can see, from specific examples, that in any reasonably general coordinates u, r, θ, ϕ which have all the required properties will become singular for sufficiently small r, whether or not the space itself has physical singularities at small luminosity distances.

Whether boundary conditions (i), (ii) and (iii) are necessary is an unsolved question; probably (i) and (ii) cannot be weakened, but probably (iii) can and should be weakened. Coordinate systems in which these conditions hold can be introduced for static, axially symmetric fields with compact support sources and suitable topologies. In gravitational fields that have geodesic rays, and in all algebraically special vacuum fields in particular, the quantities of interest can be expanded in power series of the kind required for (iii) ([18]).

Winicour's article [110] is an updated view of the formalism and its numerical applications. With this formalism the Einstein equations have a nice form, which can be solved in a hierarchical way. Gravitational radiation at infinity can be extracted directly with this formalism, because future null infinity can be taken on the numerical grid with the compactification of the radial luminosity distance, e.g., $r \to 1/(1+x)$ with this formalism. A problem is the formation of caustics, points where two or more light rays intersects; they can be found, for example, in binary black hole (BBH) simulations, e.g., a light ray emmited next to BH1 travelling outwards to BH2, around BH2 going back to BH1 and crossing on the way its own path. On that crossing point causality breaks down.

4.2 3+1 formalism

This formalism was introduced in the works of Lichnerowicz (1944) [22], Choquet-Bruhat (1952) [23], Arnowitt, Deser and Misner (1962) [24]. York's seminal article [25], Baumgarte & Shapiro's article [26], Gourgoulhon's review [27] and Alcubierre's review [28], can be useful for an introduction and recent applications in numerical relativity.

Let t be a function with timelike gradient (similar comments can be said

about a function with spatial gradient that lead to a foliation by timelike hypersurfaces). The spatial hypersurfaces Σ_t, defined by $t = constant$, constitute a foliation of the spacetime. The normal vector of this foliation is:

$$\boldsymbol{n} = \frac{dt}{|dt|}. \tag{4.12}$$

It is an unitary timelike covector, $\boldsymbol{g}(\boldsymbol{n}, \boldsymbol{n}) = -1$, where $\boldsymbol{g}$ denotes the metric. The vector field $\xi \equiv \partial_t$ fulfills $\mathcal{L}_\xi t = 1$, where $\mathcal{L}_\xi$ denotes the Lie derivative along the vector ξ. The uniparametric group of diffeomorphisms, φ_t, generated by ξ transports the spatial hypersurface Σ_0 into the spatial hypersurface Σ_t.

We can decompose the field ξ into a part proportional to $\boldsymbol{n}$, seen as the dual vector of the defined covector, and a part tangent to Σ_t. To do it, the lapse function N, and the shift vector $\boldsymbol{\beta}$, tangent to Σ_t, are defined:

$$\xi = N\boldsymbol{n} + \boldsymbol{\beta}. \tag{4.13}$$

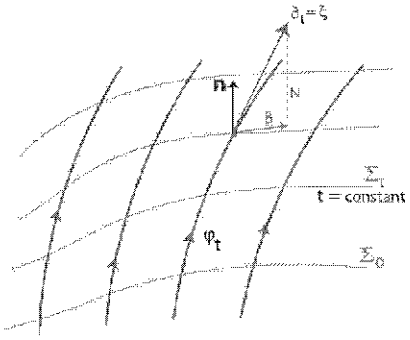

Fig. 4.3: Decomposition of the evolution vector in 3+1 formalism.

If (x^i) are the coordinates on the hypersurfaces Σ_t, we can write the shift vector as $\boldsymbol{\beta} = \beta^i \partial_i$. And from (4.13), $\boldsymbol{n}$ can be written as $\boldsymbol{n} = N^{-1}\left(\partial_t - \beta^i \partial_i\right)$.

From the fact that $\boldsymbol{n}$, as covector, is proportional to the 1-form dt, and taking into account that $\boldsymbol{n}$ is unitary, $\boldsymbol{n} = -Ndt$.

Let us make some comments about the meaning of the lapse function and the shift vector introduced above. From $\boldsymbol{n} = -Ndt$, the lapse function measures the proper time of the observer $\boldsymbol{n}$ between two slices of the foliation. This function depends on the slice and the point of the slice, $N = N\left(t, x^i\right)$, so different lapse functions give different foliations and viceversa. The shift vector belongs to the tangent plane of the slice. It is the difference between the vectors $N\boldsymbol{n}$ and ξ, i.e., the displacement between the integral curves of the vector field $\boldsymbol{n}$ and the difeomorphisms φ_t. This vector identifies univocally the points from a slice to the next one.

We define the metric of the spacetime restricted to the hypersurfaces Σ_t by $\boldsymbol{\gamma} = \gamma_{ij} dx^i dx^j = \gamma^{ij} \partial_i \partial_j$. So the spacetime metric in this system of coordinates is written as:

$$ds^2 = g_{\alpha\beta} dx^\alpha dx^\beta = -N^2 dt^2 + \gamma_{ij} \left(dx^i + \beta^i dt\right) \left(dx^j + \beta^j dt\right). \tag{4.14}$$

And the contravariant components are: $g^{00} = -N^{-2}$, $g^{0i} = N^{-2}\beta^i$ and $g^{ij} = \gamma^{ij} - N^{-2}\beta^i\beta^j$.

We denote by ∇ the covariant derivative associated to the spacetime metric $\boldsymbol{g}$. We define by $\boldsymbol{K} := -\frac{1}{2}\mathcal{L}_n \boldsymbol{\gamma}$ the symmetric tensor extrinsic curvature or second fundamental form of Σ. We denote by D the covariant derivative associated to the induced metric $\boldsymbol{\gamma}$, that it is the projection of the covariant derivative onto Σ_t, $D = (\perp\nabla)|_{\Sigma_t}$. The Gauss-Weingarten formula connects these three quantities: if X, Y are fields tangent to Σ_t, $\nabla_X Y = D_X Y - K(X,Y)\boldsymbol{n}$. We denote the trace of the extrinsic curvature by K. For an integral observer like $\boldsymbol{n}$, $-\boldsymbol{K}$ is the deformation of $\boldsymbol{n}$, $-K$ is the expansion of $\boldsymbol{n}$ and $-\boldsymbol{K} + \frac{1}{3}K\boldsymbol{\gamma}$ is the distorsion of $\boldsymbol{n}$.

The decomposition of the Ricci tensor with respect to $\boldsymbol{n}$ is:

$$Ric(\boldsymbol{g}) = i^2(\boldsymbol{n})\, Ric(\boldsymbol{g})\, \boldsymbol{n} \otimes \boldsymbol{n} - \boldsymbol{n} \tilde{\otimes} \perp i(\boldsymbol{n})\, Ric(\boldsymbol{g}) + \perp Ric(\boldsymbol{g}), \tag{4.15}$$

where

$$2i^2(\boldsymbol{n})\, Ric(\boldsymbol{g}) = -[R(\boldsymbol{g}) - R(\boldsymbol{\gamma})] + K^2 - \mathrm{tr}\boldsymbol{K}^2, \tag{4.16}$$

$$\perp i(\boldsymbol{n})\, Ric(\boldsymbol{g}) = DK - D \cdot K, \tag{4.17}$$

$$\perp Ric(\boldsymbol{g}) = Ric(\boldsymbol{\gamma}) - \left(2\boldsymbol{K}^2 - K\boldsymbol{K} + \mathcal{L}_{\boldsymbol{n}} \boldsymbol{K} + Da\right) - a \otimes a, \tag{4.18}$$

$a = \nabla_{\boldsymbol{n}}\boldsymbol{n}$, i represents the contraction, $\tilde{\otimes}$ represents the symmetrized tensor product, R the scalar curvature of the corresponding metric between parenthesis and $\perp$ the projection onto the spatial hypersurfaces orthogonal to $\boldsymbol{n}$.

Einstein equations are written as:

$$G(\boldsymbol{g}) :- Ric(\boldsymbol{g}) - \frac{R(\boldsymbol{g})}{2}\boldsymbol{g} - \kappa\boldsymbol{T}, \tag{4.19}$$

where $\kappa = 8\pi G/c^4$ and $\boldsymbol{T}$ is the energy-momentum tensor. The decomposition of $\boldsymbol{T}$ with respect to $\boldsymbol{n}$ is:

$$\boldsymbol{T} = \rho\boldsymbol{n}\otimes\boldsymbol{n} + \boldsymbol{n}\tilde{\otimes}\boldsymbol{q} + \boldsymbol{S}, \tag{4.20}$$

where $\rho = \boldsymbol{T}(\boldsymbol{n},\boldsymbol{n})$ is the energy density, $\boldsymbol{q} = -\perp i(\boldsymbol{n})\boldsymbol{T}$ is the momentum density, and $\boldsymbol{S} = \boldsymbol{T}_{\perp}$ the stress tensor. We are going to denote $S = tr\boldsymbol{S}$.

Replacing the decompositions of $Ric(\boldsymbol{g})$ and $\boldsymbol{T}$ with respect to $\boldsymbol{n}$, Einstein equations are expressed in terms of a set of constraint equations

$$R(\boldsymbol{\gamma}) + K^2 - tr\boldsymbol{K}^2 = 2\kappa\rho, \tag{4.21}$$

$$D\cdot(\boldsymbol{K} - K\boldsymbol{\gamma}) = \kappa\boldsymbol{q}, \tag{4.22}$$

and other set of evolution equations

$$\mathcal{L}_{\boldsymbol{n}}\boldsymbol{\gamma} = -2\boldsymbol{K}, \tag{4.23}$$

$$\mathcal{L}_{\boldsymbol{n}}\boldsymbol{K} = -\kappa\left(\boldsymbol{S} + \frac{1}{2}(\rho - S)\boldsymbol{\gamma}\right) + Ric(\boldsymbol{\gamma}) + K\boldsymbol{K} - 2\boldsymbol{K}^2 - Da - a\otimes a. \tag{4.24}$$

By virtue of the Bianchi identities, the conservation law of the energy-momentum tensor and the dynamical equations, if the constrained equations are fulfilled in a given hypersurface then they are fulfilled in the subsequent hypersurfaces.

Regarding the decomposition of the evolution vector, $\frac{\partial}{\partial t} = N\boldsymbol{n} + \boldsymbol{\beta}$, the constraint equations (4.21) and (4.22) have the same expressions and the dynamical equations can be rewritten in terms of ∂_t, the lapse function N and the shift vector $\boldsymbol{\beta}$:

$$\partial_t\boldsymbol{\gamma} = -2N\boldsymbol{K} + \mathcal{L}_{\boldsymbol{\beta}}\boldsymbol{\gamma}, \tag{4.25}$$

$$\partial_t\boldsymbol{K} = -DDN - \kappa N\left(\boldsymbol{S} + \frac{1}{2}(\rho - S)\boldsymbol{\gamma}\right) + N\left(Ric(\boldsymbol{\gamma}) + K\boldsymbol{K} - 2\boldsymbol{K}^2\right) + \mathcal{L}_{\boldsymbol{\beta}}\boldsymbol{K}. \tag{4.26}$$

The lapse function and the shift vector do not appear in the constraint equations. We have the freedom to choose the foliation and the evolution field along we evolve the equations, i.e., the lapse function and the shift vector. These quantities and their spatial derivatives appear in the dynamical equations, but not the derivates with respect to t. The dynamical variables are γ_{ij} and K_{ij}.

In the non-vacuum case, we have to take into account the conservation laws for the energy-momentum tensor. A simple way to write these equations in a covariant way, independently of the formalism used, is:

$$\nabla_\mu(\rho u^\mu) = 0, \tag{4.27}$$
$$\nabla_\mu T^\mu_{\ \nu} = 0, \tag{4.28}$$

where u^μ is the 4-velocity of the fluid.
In the 3+1 formalism, they are written as:

$$\partial_t \rho = N\left[K\rho + \mathrm{tr}\left(\boldsymbol{T}_\perp \times \boldsymbol{K}\right) - D\cdot\boldsymbol{q}\right] - 2i\left(\boldsymbol{q}\right)DN + \mathcal{L}_\beta\rho, \tag{4.29}$$
$$\partial_t \boldsymbol{q} = N\left[K\boldsymbol{q} + 2\boldsymbol{K}\left(\boldsymbol{q}\right) - D\cdot\boldsymbol{T}_\perp\right] - \rho DN - \boldsymbol{T}_\perp\left(DN\right) + \mathcal{L}_\beta\boldsymbol{q}. \tag{4.30}$$

It is posible to choose any set of dynamical variables as $\{\gamma_{ij}, \partial_t\gamma_{ij}\}$, $\left\{\gamma_{ij}, K^{ij}\right\}$ or $\left\{\gamma_{ij}, \Pi^{ij}\right\}$, where $\Pi^{ij} = \sqrt{\gamma}\left(K\gamma^{ij} - K^{ij}\right)$.

Taking the trace in the dynamical equations, the following equations can be derived:

$$\partial_t ln\left|\gamma\right| = -2NK + 2D\cdot\boldsymbol{\beta}, \tag{4.31}$$
$$\partial_t K = \mathcal{L}_\beta K + \frac{\kappa}{2}\left(\rho - S\right)N + N\mathrm{tr}\boldsymbol{K}^2 - \Delta N, \tag{4.32}$$

where $\Delta N = \gamma^{ij}D_iD_jN$ is the Laplacian operator. In the case of constant trace K in each hypersurface, the equations for the lapse function and the shift vector are decoupled.

There are indirect ways to impose the gauge freedom inherent to the kinematical variables, i.e. to choose the lapse function and the shift vector. For example, if we impose $K = 0$ (maximal slicing), we have a constraint equation for the lapse function:

$$\Delta N - N\left[\frac{\kappa}{2}\left(\rho + S\right) + \mathrm{tr}\boldsymbol{K}^2\right] - 0; \tag{4.33}$$

if, additionally, $D \cdot \beta = 0$, there will not appear coordinate singularities during the evolution (while $N \neq 0$).
The deformation and distorsion tensors are respectively:

$$\Theta :- N\boldsymbol{K} + \frac{1}{2}\mathcal{L}_{\beta}\boldsymbol{\gamma}, \tag{4.34}$$

$$\Sigma := \Theta - \frac{1}{3}tr\Theta\boldsymbol{\gamma}. \tag{4.35}$$

For example, if we impose $D \cdot \Theta = 0$ (minimal deformation), we have a constraint equation for the shift vector:

$$\Delta\boldsymbol{\beta} + DD \cdot \boldsymbol{\beta} + i\left(\boldsymbol{\beta}\right) Ric\left(\boldsymbol{\gamma}\right) = 2D \cdot \left(N\boldsymbol{K}\right). \tag{4.36}$$

Or we can impose $D \cdot \Sigma = 0$ (minimal distorsion), and we have the constraint equation:

$$\Delta\boldsymbol{\beta} + \frac{1}{3}DD \cdot \boldsymbol{\beta} + i\left(\boldsymbol{\beta}\right) Ric\left(\boldsymbol{\gamma}\right) = 2D \cdot \left(N\boldsymbol{K} - \frac{1}{3}NK\boldsymbol{\gamma}\right). \tag{4.37}$$

4.2.1 Baumgarte-Shapiro-Shibata-Nakamura (BSSN) formalism

The 3+1 system of Einstein equations is still not in the most convenient form for numerical implementation since it develops instabilities rapidly (see e.g. [29]). Kojima, Ooahara and Nakamura [30] presented in 1987 a conformal-traceless refomulation of the 3+1 system. In this formulation the trace of the extrinsic curvature is evolved separately and the mixed second derivatives in the Ricci tensor are eliminated with the introduction of auxiliary variables. Without these mixed derivatives, the 3+1 equations could be written as wave equations for the components of the spatial metric and they are manifestly hyperbolic. In addition, the conformal factor and the trace of the extrinsic curvature are evolved separately, which follows the strategy of separating transverse from longitudinal, or radiative from non-radiative degrees of freedom.

The most widespread version of this formalism is the one given by Shibata and Nakamura [32] and Baumgarte and Shapiro [31], known as the BSSN formulation. The robustness of this formalism has been compared with other ones (see 'Apples with Apples' project) and has some problems, although its robustness has been shown in numerical implementations based on particular

choices of gauges (see e.g. [33, 34]), as the so-called 1 + log slicing and the use of the so-called gamma driver shift. Long-term numerical simulations have been possible, even in spacetimes involving strong gravitational fields, such as black holes and neutron stars. Next, we explain this formulation (see [26] for details).

The spatial metric γ_{ij} is written as a product of a conformal factor ψ and an auxiliar metric, the conformally related or background metric $\tilde{\gamma}_{ij}$: $\gamma_{ij} = \psi^4 \tilde{\gamma}_{ij}$. The conformal factor is written as $\psi = e^{\phi}$, so that:

$$\tilde{\gamma}_{ij} = e^{-4\phi}\gamma_{ij}, \tag{4.38}$$

and by choosing it such that the determinant of the conformally related metric $\tilde{\gamma}_{ij}$ is unity, $\phi = (\ln \gamma)/12$, where γ is the determinant of the spatial metric γ_{ij}.

We conformally rescale the traceless part of the extrinsic curvature, $A_{ij} = K_{ij}^{\mathrm{TF}}$, where the superscript TF denotes the trace-free part of a tensor. Following [32] and [31], we choose the same conformal rescaling of A_{ij} chosen for the metric itsef:

$$\tilde{A}_{ij} = e^{-4\phi} A_{ij}. \tag{4.39}$$

Indices of $\tilde{A}_{ij}$ will be raised and lowered with the conformal metric $\tilde{\gamma}_{ij}$, so that $\tilde{A}^{ij} = e^{4\phi} A^{ij}$.

Evolution equations for ϕ and for the trace of the extrinsic curvature K are:

$$\partial_t \phi = -\frac{1}{6} NK + \beta^i \partial_i \phi + \frac{1}{6} \partial_i \beta^i \quad , \tag{4.40}$$

$$\partial_t K = -\gamma^{ij} D_j D_i N + N\left(\tilde{A}_{ij}\tilde{A}^{ij} + \frac{1}{3}K^2\right) + 4\pi N(\rho + S) + \beta^i \partial_i K. \tag{4.41}$$

Subtracting these from the evolution equations yields the traceless evolution equations for $\tilde{\gamma}_{ij}$ and $\tilde{A}_{ij}$:

$$\partial_t \tilde{\gamma}_{ij} = -2N\tilde{A}_{ij} + \beta^k \partial_k \tilde{\gamma}_{ij} + \tilde{\gamma}_{ik}\partial_j \beta^k + \tilde{\gamma}_{kj}\partial_i \beta^k - \frac{2}{3}\tilde{\gamma}_{ij}\partial_k \beta^k \quad , \tag{4.42}$$

$$\begin{aligned} \partial_t \tilde{A}_{ij} = {} & e^{-4\phi}\left(-(D_i D_j N)^{TF} + N\left(R_{ij}^{TF} - 8\pi S_{ij}^{TF}\right)\right) \\ & + N\left(K\tilde{A}_{ij} - 2\tilde{A}_{il}\tilde{A}^l{}_j\right) \\ & + \beta^k \partial_k \tilde{A}_{ij} + \tilde{A}_{ik}\partial_j \beta^k \tilde{A}_{kj}\partial_i \beta^k - \frac{2}{3}\tilde{A}_{ik}\partial_k \beta^k. \end{aligned} \tag{4.43}$$

In these equations the shift terms arise from Lie derivatives of the respective variable.

The Ricci tensor R_{ij} that appears in the source term of the previous evolution equation is split into two parts as follows:

$$R_{ij} = \tilde{R}_{ij} + R^{\phi}_{ij}, \tag{4.44}$$

where R^{ϕ}_{ij} is given by

$$R^{\phi}_{ij} = -2\tilde{D}_i\tilde{D}_j\phi - 2\gamma_{ij}\tilde{D}^k\tilde{D}_k\phi + 4\tilde{D}_i\phi\tilde{D}_j\phi - 4\gamma_{ij}\tilde{D}^k\phi\tilde{D}_k\phi \tag{4.45}$$

and $\tilde{D}_i$ is the covariant derivative with respect to the conformal metric $\tilde{\gamma}_{ij}$.

We can now define the "conformal connection functions"as:

$$\tilde{\Gamma}^i = \tilde{\gamma}^{jk}\tilde{\Gamma}^i_{jk} = -\tilde{\gamma}^{ij}{}_{,j} \quad , \tag{4.46}$$

where $\tilde{\Gamma}^{ij}_k$ are the connection coefficients associated with $\tilde{\gamma}_{ij}$, the subscript $(,j)$ stands for the partial derivative with respect to the corresponding variable and the last equality holds because $\tilde{\gamma} = 1$.

The conformal Ricci tensor, $\tilde{R}_{ij}$, can be written as:

$$\tilde{R}_{ij} - -\frac{1}{2}\tilde{\gamma}^{mn}\partial_{mn}\tilde{\gamma}_{ij} + \tilde{\gamma}_{k(i}\partial_{j)}\tilde{\Gamma}^k + \tilde{\Gamma}^k\tilde{\Gamma}_{(ij)k} + \tilde{\gamma}^{mn}\left(2\tilde{\Gamma}^k_{m(i}\tilde{\Gamma}_{j)kn} + \tilde{\Gamma}^k_{in}\tilde{\Gamma}_{kmj}\right), \tag{4.47}$$

where parenthesis denote symmetric indices (e.g., $2\tilde{\Gamma}^k_{m(i}\tilde{\Gamma}_{j)kn} = \tilde{\Gamma}^k_{mi}\tilde{\Gamma}_{jkn} + \tilde{\Gamma}^k_{mj}\tilde{\Gamma}_{ikn}$). All the second derivatives of $\tilde{\gamma}_{ij}$ have been absorbed into the first derivatives of $\tilde{\Gamma}^i$, except the ones in the Laplace operator $\tilde{\gamma}^{lm}\tilde{\gamma}_{ij,lm}$.

We consider the $\tilde{\Gamma}^i$ as independent functions, and hence it is necessary to derive their evolution equation. This can be done by permuting a time and space derivative in the definition of these functions:

$$\begin{aligned}
\partial_t\tilde{\Gamma}^i &= -\partial_j\left(2N\tilde{A}^{ij} - 2\tilde{\gamma}^{m(j}\beta^{i)}_{,m} + \frac{2}{3}\tilde{\gamma}^{ij}\beta^l{}_{,l} + \beta^l\tilde{\gamma}^{ij}{}_{,l}\right) \\
&= -2\tilde{A}^{ij}\partial_j N + 2N\left(\tilde{\Gamma}^i_{jk}\tilde{A}^{jk} - \frac{2}{3}\tilde{\gamma}^{ij}\partial_j K - 8\pi\tilde{\gamma}^{ij}S_j + 6\tilde{A}^{ij}\partial_j\phi\right) \\
&\quad +\beta^j\partial_j\tilde{\Gamma}^i - \tilde{\Gamma}^j\partial_j\beta^i + \frac{2}{3}\tilde{\Gamma}^i\partial_j\beta^j + \frac{1}{3}\tilde{\gamma}^{li}\beta^j{}_{,jl} + \tilde{\gamma}^{lj}\beta^i{}_{,lj},
\end{aligned} \tag{4.48}$$

where $S^i := q^i$ according to the notation used previously.

So the complete system of equations is formed by the set of constraint equations (4.23), (4.24) and (4.46), and the set of dynamical equations (4.40)-(4.43) and (4.48).

This conformal-traceless reformulation, with the appropiated choices of gauges, is widely used in Numerical Relativity. For instance, the robustness of this formulation has been shown in recent simulations of the merger of binary neutron stars [35], evolutions involving one black hole or two black holes (see Section 7.2, below), long-term evolution of neutron stars [34], and gravitational collapse of neutron stars to black holes [36].

4.2.2 Fully constrained formalism (FCF)

In the 3+1 formalism, the Meudon group has developed a fully constrained formalism (FCF) [111]. The extrinsic curvature, K^{ij}, can be written in terms of the lapse function, the shift vector and the 3-metric as:

$$K^{ij} := -\frac{1}{2N}\left(\partial_t \gamma^{ij} + D^i\beta^j + D^j\beta^i\right), \tag{4.49}$$

where D_i is the covariant derivative associated with the 3-metric γ^{ij}. This 3-metric on the spacelike slice is written in terms of a conformal metric. To do so, a metric f^{ij} is introduced, with the following properties:

(i) f^{ij} has a vanishing Riemann tensor (flat metric);

(ii) f^{ij} does not vary from one hypersuperface to the next along the spatial coordinates lines, i.e., $\dfrac{\partial}{\partial t} f^{ij} = 0$;

(iii) the asymptotic structure of the physical metric γ^{ij} is given by f^{ij}, $\gamma^{ij} \sim f^{ij}$ at spatial infinity.

Let us define the conformal factor:

$$\psi := \left(\frac{\gamma}{f}\right)^{1/12}, \tag{4.50}$$

where γ and f are the determinants of the metrics γ^{ij} and f^{ij}, respectively. The conformal factor is then a scalar field. Now, one can define the conformal metric, $\tilde{\gamma}^{ij}$, as

$$\tilde{\gamma}_{ij} := \psi^{-4}\gamma_{ij} \quad \text{or} \quad \tilde{\gamma}^{ij} := \psi^{4}\gamma^{ij}, \tag{4.51}$$

and a conformal extrinsic curvature

$$K^{ij} = \psi^{\zeta-8}\tilde{A}^{ij} + \frac{1}{3}K\gamma^{ij}, \tag{4.52}$$

where $K = \gamma^{ij}K_{ij}$ and $\zeta \in \mathbb{R}$. In [111], the choice $\zeta = 4$ is adopted, leading to the following expression for $\tilde{A}^{ij}$ in terms of the lapse N and the shift β^i:

$$\tilde{A}^{ij} := \psi^4\left(K^{ij} - \frac{1}{3}K\gamma^{ij}\right) = \frac{1}{2N}\left[(L\beta)^{ij} + \frac{\partial h^{ij}}{\partial t} - \mathcal{L}_\beta h^{ij} - \frac{2}{3}\mathcal{D}_k\beta^k h^{ij}\right], \tag{4.53}$$

where

$$(L\beta)^{ij} := \mathcal{D}^i\beta^j + \mathcal{D}^j\beta^i - \frac{2}{3}\mathcal{D}_k\beta^k f^{ij} \tag{4.54}$$

is the conformal Killing operator associated with the flat metric f^{ij} and applied to the vector field β^i.

There is a covariant derivative associated with this conformal metric, which is denoted by $\tilde{D}$. Notice that this definition of the conformal metric implies:

$$\det\tilde{\gamma}_{ij} = f. \tag{4.55}$$

A symmetric tensor field is introduced, h^{ij}, the difference between the conformal metric and the flat metric, defined by:

$$\tilde{\gamma}^{ij} =: f^{ij} + h^{ij}, \tag{4.56}$$

without introducing any bilinear form dual to it. The covariant derivative associated with f^{ij} is denoted by $\mathcal{D}$. If one defines the vector field H^{ij} as:

$$H^i := \mathcal{D}_j\tilde{\gamma}^{ij}, \tag{4.57}$$

by the previous decomposition of the conformal metric and the properties of the flat covariant derivative, it can be shown that H^{ij} is the divergence of h^{ij}:

$$H^i = \mathcal{D}_j h^{ij}. \tag{4.58}$$

Meudon's group choose maximal slicing which means that the trace of the extrinsic curvature is zero, $K = 0$. Following [111] (and references therein), this slicing leads to an elliptic equation for the lapse fuction, it has a singularity avoidance property, and it is well adapted to the propagation of gravitational waves. Moreover, they define the generalized Dirac gauge as:

$$\mathcal{D}_j \left[\left(\frac{\gamma}{f} \right)^{1/3} \gamma^{ij} \right] = 0, \tag{4.59}$$

that is nothing more than

$$H^i = 0. \tag{4.60}$$

These are the corresponding three degrees of freedom that one has to choose besides the constraint equation (4.55). These two relations define the gauge system in the FCF scheme. Since the gauge system has to be preserved in time, the following relations must also be satisfied

$$\partial_t K = 0, \quad \partial_t \left(\mathcal{D}_k \tilde{\gamma}^{ki} \right) = 0. \tag{4.61}$$

Gathering together all the above ingredients, Einstein equations lead to elliptic equations for the lapse function, for the shift vector and for the conformal factor. And there is an evolution system for the symmetric tensor h^{ij} (to be studied in the next Section). This system has, in principle, 6 degrees of freedom, but only two of them correspond to the propagation waves taking into account the constrained equations. There are 4 additional hyperbolic dynamical variables, similar to the harmonic generalized case (4 gauge sources) or to the Z4 one (an additional 4-vector). The FCF is fully constrained, because all the constraint equations are solved at each time step; this does not happen with free-evolution formalisms as BSSN, or partially constrained ones. The main motivation of this scheme is to get the maximum number of elliptic equations, that in principle are much more stable than the hyperbolic ones avoiding the violation of the constraints. For this kind of equations it is possible to apply spectral methods taking advantage of the Meudon's experience.

The difference between the Christoffel symbols of $\tilde{D}_i$ and those of $\mathcal{D}_i$ is the following tensor field:

$$\Delta^k_{ij} := -\frac{1}{2} \tilde{\gamma}^{kl} \left(\mathcal{D}_i \tilde{\gamma}_{lj} + \mathcal{D}_j \tilde{\gamma}_{il} - \mathcal{D}_l \tilde{\gamma}_{ij} \right). \tag{4.62}$$

Let us define the scalar $\tilde{R}_*$:

$$\tilde{R}_* := \frac{1}{4}\tilde{\gamma}^{kl}\mathcal{D}_k h^{mn}\mathcal{D}_l\tilde{\gamma}_{mn} - \frac{1}{2}\tilde{\gamma}^{kl}\mathcal{D}_k h^{mn}\mathcal{D}_n\tilde{\gamma}_{mn}. \tag{4.63}$$

The first of the gauge conditions (4.61), $\partial_t K = 0$, is enforced during the evolution by an elliptic equation for the lapse function. An elliptic equation can be used for the lapse function times conformal factor too, as a combination of the ellipic equation for the lapse and the elliptic equation for the conformal factor:

$$\begin{aligned}\Delta(N\psi) &= 2N\psi^5\pi(E+2S) + N\psi\frac{\tilde{R}_*}{8} - h^{kl}\mathcal{D}_k\mathcal{D}_l(N\psi) \\ &+\frac{7}{8}N\psi^5\frac{1}{(2N)^2}\tilde{\gamma}_{ik}\tilde{\gamma}_{jl}\left[(L\beta)^{ij} + \frac{\partial h^{ij}}{\partial t} - \mathcal{L}_\beta h^{ij} - \frac{2}{3}\mathcal{D}_k\beta^k h^{ij}\right] \\ &\left[(L\beta)^{kl} + \frac{\partial h^{kl}}{\partial t} - \mathcal{L}_\beta h^{kl} - \frac{2}{3}\mathcal{D}_k\beta^k h^{kl}\right],\end{aligned} \tag{4.64}$$

where S and the strain tensor S^{ij} have been defined previously, and $E = \rho$ is the energy density.

The Hamiltonian constraint can be written as an elliptic equation for the conformal factor:

$$\begin{aligned}\Delta\psi &= -2\pi E\psi^5 - h^{kl}\mathcal{D}_k\mathcal{D}_l\psi + \psi\frac{\tilde{R}_*}{8} \\ &-\frac{\psi^5}{8(2N)^2}\tilde{\gamma}_{ik}\tilde{\gamma}_{jl}\left[(L\beta)^{ij} + \frac{\partial h^{ij}}{\partial t} - \mathcal{L}_\beta h^{ij} - \frac{2}{3}\mathcal{D}_k\beta^k h^{ij}\right] \\ &\left[(L\beta)^{kl} + \frac{\partial h^{kl}}{\partial t} - \mathcal{L}_\beta h^{kl} - \frac{2}{3}\mathcal{D}_m\beta^m h^{kl}\right].\end{aligned} \tag{4.65}$$

An elliptic equation for the shift vector is derived using both the momentum constraint and the preservation in time of the Dirac gauge:

$$\begin{aligned}\Delta\beta^i + \frac{1}{3}\mathcal{D}^i\mathcal{D}_j\beta^j &= 16\pi N\psi^4 S^i - h^{kl}\mathcal{D}_k\mathcal{D}_l\beta^i - \frac{1}{3}h^{ik}\mathcal{D}_k\mathcal{D}_l\beta^l \\ &+\frac{\psi^6}{N}\mathcal{D}_j\left(\frac{N}{\psi^6}\right)\left[(L\beta)^{ij}\right] \\ &+\frac{\psi^6}{N}\mathcal{D}_j\left(\frac{N}{\psi^6}\right)\left[\frac{\partial h^{ij}}{\partial t} - \mathcal{L}_\beta h^{ij} - \frac{2}{3}\mathcal{D}_k\beta^k h^{ij}\right] \\ &-2N\Delta^i_{kl}A^{kl}, \end{aligned} \tag{4.66}$$

where the momentum density S^i has been defined previously.

An equation for the shift vector could be derived from the momentum constraint alone, but the coupling to the tensorial equation for h^{ij} would become more complicated due to the presence of a mixed time-space second order derivative of h^{ij}. This term is eliminated by the use of a Dirac, or a similar, gauge. Therefore, this elliptic equation for the shift vector enforces the momentum constraint, as long as the Dirac gauge is satisfied.

More details about the different systems and equations of this FCF can be seen in the next Chapter 5 and in Ref. [53].

4.2.3 Conformally flat condition (CFC)

One among many others interesting property of FCF is that it is a natural generalization of the conformally flat condition (CFC) [37, 38], that has been used in many astrophysical applications, as the collapse of rotating cores of massive stars [39, 40, 41, 42] or supermassive stars [43], the phase-transition-induced collapse of rotating neutron stars to hybrid quark stars [44], equilibrium models of rotating neutron stars [45, 46], as well as for binary neutron star merger [47, 48, 49, 50]. CFC is recovered just taking the symmetric tensor h^{ij} zero. FCF could be, in practice, an easy way to go from CFC to a complete general spacetime, just adding the new terms to the equations and the system for h^{ij}.

In CFC one has to consider the divergence of the energy-momentum tensor, and elliptic equations for the conformal factor, the lapse function and the shift

vector. In the previous elliptic equations we have written in black the corresponding part of CFC, and the new terms, coming from the non vanishing of h^{ij}, have been written in blue.

5. MATHEMATICAL ISSUES

This Section contains an important part of the theoretical work presented in this thesis. The local existence of maximal slicings, and properties concerning the elliptic and hyperbolic equations of the FCF formalism will be treated.

5.1 Local existence of maximal slicings in spherically symmetric spacetimes

This Subsection is based on [51]. In 1944 Lichnerowicz [22] introduced a particular foliation of spacetime, the so-called maximal slicing condition mentioned in Section 4.2, to solve Einstein constraint equations. This type of slicing has very nice properties as, for example: i) the well-known singularity avoidance capability [54], ii) it is well adapted to the propagation of gravitational waves [112, 32], and, iii) it gives the natural Newtonian analogous when, in addition, conformal flatness is imposed on each slice [37]. Maximal slicing condition has been recently used in the FCF of Einstein equations (see Section 4.2.2). In this Subsection, we will utilize the term maximal slicings (MS, in the next) when refering to those spacetimes sliced by maximal spacelike hypersurfaces.

The study of MS has been mainly motivated by the resolution of the initial value problem [22], and also by the associated time evolution. This idea was popularized by Smarr and York [25, 54]. Then, for a given class of spacetimes, the construction of a family of slices with a given property (e.g., maximal slicing and/or conformal flatness) may be dynamically accomplished in an evolution scheme: assuming the existence of an initial 3-surface with that property, Einstein equations are used to evolve locally the corresponding additional constraint.

This strategy can be applied both analytically and numerically, as it has been done in references [55, 56] to construct MS in the extended Schwarzschild

geometry. This maximal foliation of the Kruskal-Szekeres black hole was obtained independently by Reinhart [57] from a different approach. Reinhart procedure [57] does not make any use of Einstein equations, being essentially a geometrical (non dynamical) approach.

Similar examples of MS have been examined in the Reissner-Nordström geometry [58], and also in dynamical spherically symmetric spacetimes (SSSTs) of dust collapse scenarios [59], by using isotropic coordinates. Some general results and conjectures about the existence of Cauchy time functions whose level surfaces are maximal (or foliations with constant mean extrinsic curvature) have been given in [60] with applications to the Lemaître-Tolman-Bondi geometry. Of course, the study of the existence (and uniqueness) of other types of foliations deserves a lot of interest in SSST and more general spacetimes. That is the case of synchronizations by flat instants (Painlevé-Gullstrand slicings) and their generalizations (see, for example, [113, 114, 115, 116, 117, 118]).

In spite of their extended use, the existence of MS in SSSTs has been only established for vacuum and for some particular energy contents (see [37, 55, 56, 57, 58, 59, 60]). There is no, as far as we know, a theorem stating that always is possible to build a MS in a SSST.

In this Subsection, we aim to prove the local existence of MS in an arbitrary SSST. We will follow a purely geometrical approach, independent of Einstein equations, complementary to the standard time evolution strategy [37, 55, 56, 58, 59, 60]. Although our study is independent of the field equations, one by-product of our approach, which could be of interest in the field of Numerical Relativity, is the following: it will be possible to carry out a cross-checking of numerical solutions of Einstein equations.

Our analysis has focused on SSSTs. The study of SSSTs is of particular interest in different domains of general relativity: classification of exact solutions of Einstein equations, simplified models of astrophysical and cosmological scenarios (see, e.g. [61]), test-bed solutions for fully general-relativistic time-dependent numerical codes which evolve matter in strong gravitational fields (see, e.g., [59, 62, 63, 64]), etc. SSSTs provide the background for a perturbative theory. All these reasons advise us to start our analysis in such a simple symmetry and to defer for future works its extension to less strongly symmetric spacetimes.

5.1.1 Main equations

Without loss of generality, we start with the canonical form of the metric of a SSST (see [61]), that is

$$ds^2 = A\,dt^2 + 2C\,dt\,dr + B\,dr^2 + D\,d\Omega^2, \tag{5.1}$$

where $d\Omega^2 = d\theta^2 + \sin^2\theta d\varphi^2$ is the metric of the 2-sphere, A, B, C, D are smooth functions of t and r, and $AB - C^2 < 0$ to insure the Lorentzian character of the metric. In addition we choose the signature $(-,+,+,+)$, and accordingly $D > 0$. In this Section partial derivatives with respect to r will be denoted as $\frac{\partial f}{\partial r} = f'$, and with respect to t as $\frac{\partial f}{\partial t} = \dot{f}$. The spatial metric γ_{ij} induced on the hypersurfaces Σ_t, defined by $t = \text{const}$ is $\gamma_{ij} = \text{diag}(B, D, D\sin^2\theta)$, where $B > 0$ since we are considering spacelike hypersurfaces. Let $\boldsymbol{n}$ be the future pointing timelike unit normal to the hypersurfaces Σ_t,

$$\boldsymbol{n} = \frac{1}{\alpha}\left(\frac{\partial}{\partial t} - \frac{C}{B}\frac{\partial}{\partial r}\right), \quad \alpha = \sqrt{\frac{C^2}{B} - A}. \tag{5.2}$$

The mean extrinsic curvature K of Σ_t is minus the expansion of $\boldsymbol{n}$, $K = -\nabla\cdot\boldsymbol{n}$, that is

$$-K = \nabla_\mu n^\mu = \frac{1}{\sqrt{-g}}\partial_\mu(\sqrt{-g}n^\mu) = \frac{1}{H}\left[\left(\sqrt{B}D\right)^{\cdot} - \left(\frac{CD}{\sqrt{B}}\right)'\right] \tag{5.3}$$

where ∇ is the covariant derivative with respect to the spacetime metric $g_{\mu\nu}$ given by Eq. (5.1), $g = \det(g_{\mu\nu}) = -H^2\sin^2\theta$, $H = D\sqrt{C^2 - AB}$ and $\mu \in \{t, r, \theta, \phi\}$. Developing this relation, we obtain

$$K = \frac{1}{2\alpha B}\left(-\dot{B} - 2B\frac{\dot{D}}{D} + 2C' - C\frac{B'}{B} + 2C\frac{D'}{D}\right). \tag{5.4}$$

Therefore, the surfaces $t = \text{const}$ are maximal if, and only if, the maximal slicing condition $K = 0$ is fulfilled. In the following we assume that A, B, C and D are known functions. We aim to prove the local existence of a maximal slicing in spherical symmetry. From a kinematical point of view,

we look for the existence of a non-expanding observer $\boldsymbol{u}$ on the 2-surfaces defined by constant θ and φ, i.e., a unit and future directed radial timelike field $\boldsymbol{u} = u^\mu = (u^t(t,r), u^r(t,r), 0, 0)$ such that $\nabla \cdot \boldsymbol{u} = 0$, or equivalently

$$(u^t H)^{\cdot} + (u^r H)' = 0. \tag{5.5}$$

The condition $g(\boldsymbol{u}, \boldsymbol{u}) = -1$ suppose a relation between the components of $\boldsymbol{u}$,

$$A(u^t)^2 + B(u^r)^2 + 2Cu^t u^r = -1. \tag{5.6}$$

From Eq. (5.6), u^r may be written in terms of the u^t and the metric components. Replacing this expression of u^t in Eq. (5.5), one obtain a first order partial differential equations. The existence of solution of this equation is not sufficient to guarantee the existence of a maximal slicing. In fact, such a solution must be compatible with the algebraic constraint (5.6) and must be positive, $u^t > 0$, when the coordinate field ∂_t is future directed.

In order to bypass this difficulty, we consider a change of coordinates of the form $\left\{\tilde{t} = \tilde{t}(t,r), \tilde{r} = \tilde{r}(t,r), \theta, \varphi\right\}$, such that the coordinate hypersurfaces $\tilde{t} = \text{const}$ are maximal. Then, the above considered constraints will be satisfied as a consequence of the integrability conditions insuring the existence of the wanted coordinate system.

Let us introduce the following fields:

$$X \equiv \frac{\partial}{\partial \tilde{t}}, \; Y \equiv \frac{\partial}{\partial \tilde{r}}, \tag{5.7}$$

and decompose them as

$$Y = \lambda \bar{Y}, \quad \bar{Y}^2 = 1, \tag{5.8}$$

$$X = a\bar{Y} + b\bar{Y}^{\perp}, \quad \bar{Y} \cdot \bar{Y}^{\perp} = 0, \tag{5.9}$$

$b \neq 0$, $\lambda > 0$. The condition $\bar{Y}^2 = 1$ is equivalent to

$$\bar{Y} = f\frac{\partial}{\partial t} + P\frac{\partial}{\partial r}, \;\; P = B^{-1}\left(-fC + \epsilon\sqrt{f^2 l^2 + B}\right), \tag{5.10}$$

being $\epsilon = \pm 1$, $l^2 = -AB + C^2 > 0$. Moreover, $\bar{Y} \cdot \bar{Y}^{\perp} = 0$ leads to

$$\bar{Y}^{\perp} = \frac{\partial}{\partial t} + Q\frac{\partial}{\partial r}, \; Q = B^{-1}\left(-C + \frac{\epsilon f l^2}{\sqrt{f^2 l^2 + B}}\right). \tag{5.11}$$

Consequently, the resulting fields are

$$X = (af+b)\frac{\partial}{\partial t} + (aP+bQ)\frac{\partial}{\partial r}, \tag{5.12}$$

$$Y = \lambda\left(f\frac{\partial}{\partial t} + P\frac{\partial}{\partial r}\right) = \lambda\left(f\alpha\,\boldsymbol{n} + \frac{\epsilon}{B}\sqrt{f^2l^2+B}\frac{\partial}{\partial r}\right), \tag{5.13}$$

where we have taken into account Eqs. (5.2) and (5.10). This decomposition will reduce the maximal slicing condition $K=0$ to an equation involving only the unknown f. Notice that Eq. (5.13) makes clear the meaning of ϵ: relative to the Eulerian observer $\boldsymbol{n}$, the radial component of Y is outgoing or ingoing according to $\epsilon=1$ or $\epsilon=-1$.

The Jacobian matrix of the above change of coordinates can be written, in terms of the previous decompositions, as

$$\begin{pmatrix} \dot{\tilde{t}} & t' \\ \dot{\tilde{r}} & \tilde{r}' \end{pmatrix} = \begin{pmatrix} \frac{\partial t}{\partial \tilde{t}} & \frac{\partial t}{\partial \tilde{r}} \\ \frac{\partial r}{\partial \tilde{t}} & \frac{\partial r}{\partial \tilde{r}} \end{pmatrix}^{-1} = \begin{pmatrix} af+b & \lambda f \\ aP+bQ & \lambda P \end{pmatrix}^{-1}$$

$$= (b\,p\,\lambda)^{-1}\begin{pmatrix} \lambda P & -\lambda f \\ -(aP+bQ) & (af+b) \end{pmatrix}, \tag{5.14}$$

where $p = P - fQ = \dfrac{\epsilon}{\sqrt{f^2l^2+B}} \neq 0$. Then, in order to insure Eq. (5.7), the integrability conditions, $[X,Y]=0$, are:

$$\left[\frac{P}{bp}\right]' = \left[\frac{-f}{bp}\right]^{\cdot}, \tag{5.15}$$

$$\left[-\frac{aP+bQ}{bp\lambda}\right]' = \left[\frac{af+b}{bp\lambda}\right]^{\cdot}. \tag{5.16}$$

Taking into account the maximal slicing and the integrability conditions, we have 3 equations for 4 unknown functions, a, b, f, λ. But, due to D transforms as a scalar under the considered coordinate transformation, we can add without loss of generality, the coordinate condition

$$\tilde{r}^2\,Y^2 = D, \tag{5.17}$$

saying that the metric on the hypersurfaces $\tilde{t} = \text{const}$ is written in isotropic conformally flat form. Notice that Eq. (5.17) guarantees that the congruence of coordinate lines associated with the field $X = \dfrac{\partial}{\partial \tilde{t}}$ has minimal distorsion (see [27, 54]).

Now, from Eq. (5.4), the maximal slicing condition $\tilde{K} = 0$ for the new hypersurfaces $\tilde{t} = \text{const}$ is equivalent to

$$X(Y^2) + 2Y^2 \frac{X(D)}{D} - 2Y(X \cdot Y) + \left[\frac{Y(Y^2)}{Y^2} - 2\frac{Y(D)}{D} \right] X \cdot Y = 0, \quad (5.18)$$

and, taking into account the conformally flat coordinate condition (5.17), this expression is written as

$$2Y\,(X \cdot Y) - 3X\left(Y^2\right) + \left[\frac{4}{\tilde{r}} + \frac{Y\left(Y^2\right)}{Y^2} \right] X \cdot Y = 0. \quad (5.19)$$

In terms of the decompositions (5.12) and (5.13), Eqs. (5.17) and (5.19) are expressed as

$$\lambda = \sqrt{D}/\tilde{r} \quad (5.20)$$

$$f\dot{a} + Pa' - a\left(\frac{f\dot{\lambda} + P\lambda'}{\lambda} - \frac{2}{\sqrt{D}} \right) = 3b\,\frac{\dot{\lambda} + Q\lambda'}{\lambda}. \quad (5.21)$$

Eq. (5.20) can be viewed as a definition of $\tilde{r}$ in terms of λ, and from this equation we can derive

$$\frac{\lambda'}{\lambda} = \frac{D'}{2D} - \frac{af + b}{bp\sqrt{D}}, \quad \frac{\dot{\lambda}}{\lambda} = \frac{\dot{D}}{2D} + \frac{aP + bQ}{bp\sqrt{D}}. \quad (5.22)$$

At this point we have 5 equations, i.e., Eqs. (5.15), (5.16), (5.21) and (5.22), for 4 unknown functions, i.e., (a, b, f, λ). Eqs. (5.22) are equivalent to give quantity a in terms of the other unknowns,

$$a = b\sqrt{D}\left(\frac{\dot{\lambda} + Q\lambda'}{\lambda} - \frac{\dot{D} + QD'}{2D} \right), \quad (5.23)$$

and to the following equation

$$f\frac{\dot{\lambda}}{\lambda}+P\frac{\lambda'}{\lambda}=f\frac{\dot{D}}{2D}+P\frac{D'}{2D}-\frac{1}{\sqrt{D}}. \tag{5.24}$$

Once a has been eliminated, it can be seen that Eq. (5.16) can be obtained from Eq. (5.24). From Eq. (5.23), the field X is

$$X=b\,p\sqrt{D}\left(-\Lambda'\frac{\partial}{\partial t}+\dot{\Lambda}\frac{\partial}{\partial r}\right), \tag{5.25}$$

where $\Lambda=\log\lambda/\sqrt{D}$. So we have reduced the problem to solve 3 equations, i.e., Eqs. (5.15), (5.21) (replacing a), and (5.24), for 3 unknown functions, i.e., (b,f,λ). Eq. (5.15) can be rewritten as

$$f\frac{\dot{b}}{b}+P\frac{b'}{b}=P'-P\frac{p'}{p}+\dot{f}-f\frac{\dot{p}}{p}. \tag{5.26}$$

As it will be shown below in Eq. (5.27), f can be obtained from an equation which does not contain other variables. Then, Eq. (5.26) is a first order partial derivative equation (PDE) for b.

Eliminating a and its derivatives with Eq. (5.23), and using Eq. (5.26) to eliminate b, Eq. (5.21) is reduced to a second order PDE involving λ and f. Finally, making use of Eq. (5.24) for, firstly, reducing the order of the equation and, secondly, for eliminating λ, Eq. (5.21) is equivalent to the following one:

$$\frac{\dot{p}}{p}-\frac{\dot{D}}{D}-Q'+Q\left[\frac{p'}{p}-\frac{D'}{D}\right]=0. \tag{5.27}$$

Notice that previous equation involves only f when p and Q are written explicitely in terms of f from their definitions.

5.1.2 *Local existence of maximal slicings.*

We have found a decoupled system of quasi-linear PDEs (5.24), (5.26) and (5.27) according to the following steps: First, Eq. (5.27) can be solved for f. Second, Eq. (5.24) can be solved for λ. Third, Eq. (5.26) can be solved for b.

Finally, a can be obtained from Eq. (5.23). Assuming that all the metric components A, B, C, D are continuously differentiable functions, the initial value problem with respect to this set of equations has always local solution [119]. We have reached our main objective in this Section 5.1, that is to prove the following result:

Theorem: Any spherically symmetric spacetime can be locally sliced by a family of maximal spacelike hypersurfaces.

The proof of the theorem is, then, based on the explicit finding of the minimum set of equations to be solved in order to obtain MS in SSSTs. Let us analyze two different cases, $f = 0$ and $f \neq 0$, that will complement the theorem of existence of MS.

First case: If $f = 0$, Eq. (5.27) is reduced to $K = 0$, the maximal slicing condition provided by Eq. (5.4). In this case, from Eqs. (5.26), (5.24) and (5.23), it turns out that $b(t) \neq 0$ arbitrary, $\lambda = Z(t)\sqrt{D}\exp\left(-\epsilon\int_R^r \sqrt{B/D}dr\right)$, with $Z(t) > 0$, R constant, and $a = b\sqrt{D}\left[\dot{Z}/Z + \epsilon C/\sqrt{BD} - \epsilon\int_R^r \left(\sqrt{B/D}\right)^{\cdot} dr\right]$. The fields X and Y can be integrated according to the following result:

If the hypersurfaces $t = \text{const}$ in the metric expression (5.1) are maximal, the following change

$$\tilde{t} = \tilde{t}(t), \qquad \tilde{r} = Z^{-1}\exp\left(\epsilon\int_R^r \sqrt{B/D}dr\right), \tag{5.28}$$

with $\dot{\tilde{t}} = b^{-1}$, $Z(t) > 0$ and R constant, allows one to write the metric in isotropic form

$$\begin{aligned} ds^2 &= b^2\left[A + D\left(\frac{\dot{\tilde{r}}}{\tilde{r}}\right)^2 - 2\epsilon C\sqrt{\frac{D}{B}}\frac{\dot{\tilde{r}}}{\tilde{r}}\right]d\tilde{t}^2 + 2\frac{\epsilon b}{\tilde{r}}\sqrt{\frac{D}{B}}\left(C - \epsilon\sqrt{BD}\frac{\dot{\tilde{r}}}{\tilde{r}}\right)d\tilde{t}d\tilde{r} \\ &\quad + \frac{D}{\tilde{r}^2}\left(d\tilde{r}^2 + \tilde{r}^2 d\Omega^2\right). \end{aligned} \tag{5.29}$$

This metric form is adapted to the same initial maximal slices, that are now labeled as $\tilde{t} = \text{const}$. It remains invariant under the inversion $\tilde{r} \to T(\tilde{t})/\tilde{r}$ when,

in addition, the sign of the radial component of the field Y is reversed by the change $\epsilon \to -\epsilon$.

Second case: When $f \neq 0$, the explicit expressions of P/f and Q in terms of f, allow us to define the variable

$$F = \frac{\epsilon f}{\sqrt{f^2 l^2 + B}} \Leftrightarrow f = \epsilon F \sqrt{\frac{B}{1 - l^2 F^2}}, \tag{5.30}$$

so $\dfrac{P}{f} = \dfrac{1 - FC}{FB}$, $Q = \dfrac{-C + Fl^2}{B}$, and $p = \epsilon \sqrt{\dfrac{1 - l^2 F^2}{B}}$. Eqs. (5.26), (5.24) and (5.27) are rewritten, respectively, as

$$\dot{b} + \frac{1 - FC}{FB} b' = b \left\{ \frac{\dot{B} - C'}{B} + \frac{1}{1 - l^2 F^2} \right.$$
$$\left. \times \left[-(1 + l^2 F^2) \frac{\dot{F}}{F} + \frac{l^2 F(2 - FC) - C}{B} \frac{F'}{F} + F^2 (l^2)^{\cdot} + \frac{(1 - FC) F (l^2)'}{B} \right] \right\}, \tag{5.31}$$

$$\dot{\lambda} + \frac{1 - FC}{FB} \lambda' = \lambda \left[\frac{\dot{D}}{2D} + \frac{1 - FC}{FB} \frac{D'}{2D} - \frac{\epsilon \sqrt{1 - l^2 F^2}}{F \sqrt{BD}} \right], \tag{5.32}$$

$$\dot{F} + \frac{1 - FC}{FB} F' = -\frac{FB (l^2)^{\cdot} + (2 - l^2 F^2 - FC)(l^2)'}{2 l^2 B}$$
$$- L \left[\frac{\dot{B}}{2} + \frac{B \dot{D}}{D} + \frac{(C - Fl^2)(DB' - 2BD')}{2BD} - C' \right], \tag{5.33}$$

where $L = (1 - l^2 F^2)/(l^2 FB)$. The solution can be obtained numerically solving the quasilinear Eqs. (5.33), (5.32) and (5.31) for, respectively, F, λ and b, given initial data for $t = t_0$. These equations are of hyperbolic type, analogous to the well-known advective equation in classical fluid dynamics. The three equations have a common "advective velocity": $V = (1 - FC) F^{\ 1} B^{\ 1}$. This velocity can be interpreted as the radial component of the light velocity in the modified metric $d\tilde{s}^2 = ds^2 - \dfrac{1}{f^2} dt^2$.

Finally, from Eq. (5.14), we obtain the following result:

For any given SSST a maximal slicing can be built up according to the following steps:

i) To start with the metric form (5.1), with $l^2 \equiv C^2 - AB > 0$, $B > 0$ and $D > 0$, to solve Eq. (5.33) for F, and then, to solve Eq. (5.31) for b, and to define

$$\Gamma := b^{-1}(1 - l^2F^2)^{-1}\left[(1 - FC)dt - FBdr\right] \tag{5.34}$$

which is necessarily a closed 1-form.

ii) To find a potential $\tilde{t}(t, r)$ of Γ, $\Gamma = d\tilde{t}$. Then, the level surfaces of $\tilde{t}$ are spacelike and maximal.

Analogously, $\tilde{r}$ can be integrated once F and λ are solved. The change of coordinates is completely defined, the fields X, Y can be obtained and the metric derived in the new set of coordinates. The new slices are maximal and the first case, $f = 0$, can again be applied.

In order to see how the method may be applied in practice, let us consider the above procedure in the simple case of the Minkowski spacetime and inertial spherical coordinates, $ds^2 = -dt^2 + dr^2 + r^2 d\Omega^2$. According to the results in the first case, $f = 0$, the change of coordinates $\tilde{t} = \tilde{t}(t)$ can be derived, with $\dot{\tilde{t}} = b^{-1}$, $\tilde{r} = r^\epsilon\, Z^{-1}$, and the resulting metric is

$$\begin{aligned} ds^2 &= \left[-b^2 + \left(\tilde{r}^\epsilon\, Z^{\epsilon-1}\frac{dZ}{d\tilde{t}}\right)^2\right] d\tilde{t}^2 + 2\left(\tilde{r}\, Z\right)^{2\epsilon-1}\frac{dZ}{d\tilde{t}}d\tilde{t}\, d\tilde{r} \\ &\quad + \left(\tilde{r}^{\epsilon-1}\, Z^\epsilon\right)^2\left(d\tilde{r}^2 + \tilde{r}^2 d\Omega^2\right), \end{aligned} \tag{5.35}$$

$b = b(\tilde{t}) \neq 0, Z = Z(\tilde{t}) > 0$ being arbitrary functions. Hence, we have the same slicing that the initial inertial one (this foliation is totally geodesic, i.e., its extrinsic curvature tensor vanishes). However, other maximal slicings (non-inertial, en general) can be obtained as a consequence of the second case $f \neq 0$. According to it, Eq. (5.33) reads

$$\dot{F} + F^{-1}\, F' = -2r^{-1}(1 - F^2). \tag{5.36}$$

The general solution of this equation can be given in terms of an implicit function, $\Phi_1\left(m(F) + t\, r^{-1}\left(F^{-2} - 1\right)^{1/4}, r^{-1}\left(F^{-2} - 1\right)^{1/4}\right) = 0$, $0 < F^2 < 1$, Φ_1 being an arbitrary function, and $m(F) = \sqrt{|F|}\ {}_2\mathrm{F}_1\left(1/4,\ 3/4;\ 5/4;\ F^2\right)$, ${}_2\mathrm{F}_1$ being the classical standard hypergeometric series [120]. Once F is known,

the general solution of Eqs. (5.31) and (5.32) are, respectively, $\Phi_2(I_1, I_2)$ and $\Phi_3(I_1, I_3)$, where Φ_2 and Φ_3 are arbitrary functions, and

$$I_1 = r - \int_0^t F^{-1} dt, \tag{5.37}$$

$$I_2 = b^{-1} \exp\left[\int_0^t \left(-\frac{(1+F^2)\dot{F}}{F} + 2F'\right)\frac{dt}{1-F^2}\right], \tag{5.38}$$

$$I_3 = \lambda^{-1} \exp\left(r^{-1}\int_0^t F^{-1}(1-\epsilon\sqrt{1-F^2})dt\right). \tag{5.39}$$

This study can be extended to the Schwarzschild spacetime using different metric forms, specially those that are regular at the horizon, like the Painlevé-Gullstrand form and other similar ones [121]. MS can also be constructed in other spacetimes (Reissner-Nordtröm, Vaidya, Lemaître-Tolman-Bondi, etc.) and the results compared with previous works [55, 56, 57, 58, 59].

To end, let us summarize. Two basic results have been displayed: (i) A theorem insuring the existence of MS in any SSST. (ii) A geometrical method to build up such slices by solving three decoupled first order quasi-linear PDEs (5.24), (5.26) and (5.27). The first result aims to fill a theoretical gap in the scientific literature. The second one tries to achieve an algorithmic procedure to obtain MS. As an example, in a flat spacetime, the equations leading to obtain MS, which are not inertial in general, can be solved analytically. An interesting by-product for Numerical Relativity of the approach presented in this work has to do with the assessment of 3D codes written, as customary, in Cartesian coordinates. Let us consider two codes NC1 and NC2 such that only NC1 uses a gauge which is maximal. Hence, the evolution with code NC2 of any initial data admitting a spherically symmetric limit could be compared to the evolution produced by code NC1, by simply using our procedure to generate a SSST satisfying the maximal slicing condition.

We have outlined a method that should be extended to deal with the construction of a constant mean curvature slicings. The results on maximal slicings we have presented here can be considered as a step to gain some insights in this direction.

5.2 Mathematical properties of the elliptic equations in CFC and local uniqueness

This Subsection and Section 5.3.5 are based on [52]. The non-uniqueness of solutions stems from the non-linearity of the constraint equations and has been studied within the so-called extended conformal thin sandwich (XCTS) [65, 66, 67] approach to the initial data problem in general relativity. In Ref. [68] a parabolic branching was numerically found in the solutions to the XCTS equations for perturbations of Minkowski spacetime, providing the first evidence of non-uniqueness in this elliptic system. First analytical studies have been carried out in [69, 122], finding support for the genericity of this non-uniqueness behavior. More specifically, the XCTS elliptic system is formed by the Einstein constraint equations in a conformal thin sandwich (CTS) decomposition [65] supplemented with an additional elliptic equation for the lapse function, which follows from the maximal slicing condition. Although no general results on the existence and uniqueness for the XCTS system are available (in contrast to the CTS case and similar elliptic systems encompassing only the constraints; see, e.g., [123, 124, 25, 65, 66]), the analysis in [69] strongly suggests the presence of a wrong sign in a certain term of the lapse equation as the culprit for the loss of uniqueness, essentially because it spoils the application of a maximum principle to guarantee uniqueness. Moreover, under these circumstances (namely, the existence of a non-trivial kernel for the XCTS elliptic operator) it is shown in [122] that the parabolic behavior found in [68] is indeed generic.

Certain constrained evolution formalisms which incorporate elliptic gauges in their schemes contain elliptic subsystems which share essential points with the XCTS equations. Non-uniqueness in the elliptic subsystem is certainly an issue for the well-posedness of the whole elliptic-hyperbolic evolution system. In numerical implementations this can depend on the employed numerical scheme, in particular, on its capability to remain close to one of the solutions, at least as long as the solution stays sufficiently far from the branching point. In fact, constrained or partially constrained evolutions have shown to be robust in a variety of contexts (see, e.g., the references in [125] and Sec. 5.2.2 of [126]). However, the problems described above have also emerged, for instance, in the axisymmetric case in [127, 128] (see also [129]). The analysis in [125] concludes that the reason behind the failures in these axisymmetric formulations is in fact related to the presence of wrong signs or, more precisely, to the indefinite

character of certain non-linear Helmholtz-like equations present in the scheme (see [125] for details and also for a parallel numerical discussion in terms of a class of relaxation methods for the convergence of the elliptic solvers). Regarding the full three-dimensional case, fully constrained formalisms have been presented in [111, 130, 53]. While the work in [111, 53] includes an elliptic subsystem closely related to the XCTS equations and therefore suffers potentially from these non-uniqueness problems, the uniqueness properties of the scheme of [130] must yet be studied. In both cases, the full numerical performance still has to be assessed.

Having the analysis of the FCF of [111, 53] as final aim, a scheme addressing the non-uniqueness issues of CFC approximation in the full three-dimensional case is going to be discussed first. This methodological choice is justified since the CFC scheme already contains the relevant elliptic system of FCF, but in a setting in which potential additional problematic issues related to the FCF hyperbolic part do not mix up with the specific problem to be addressed here. Therefore, modification of the CFC scheme (in the presence of matter) is going to be discussed in detail where maximum-principle lines of reasoning can be used to infer the uniqueness of the solutions.

Although no details about the hydrodynamical equations, (4.27) and (4.28), are going to be given here, the following rescaled matter quantities are introduced, following York [25]:

$$E^* := \sqrt{\gamma/f}\, E = \psi^6 E, \tag{5.40}$$

$$S^* := \sqrt{\gamma/f}\, S = \psi^6 S, \tag{5.41}$$

$$(S^*)_i := \sqrt{\gamma/f}\, S_i = \psi^6 S_i, \tag{5.42}$$

and CFC equations are written in terms of these rescaled quantities as

$$\Delta\psi = -2\pi\psi^{-1}\left[E^* + \frac{\psi^6 K_{ij}K^{ij}}{16\pi}\right], \tag{5.43}$$

$$\Delta(N\psi) = 2\pi N\psi^{-1}\left[E^* + 2S^* + \frac{7\psi^6 K^{ij}K_{ij}}{16\pi}\right], \tag{5.44}$$

$$\Delta\beta^i + \frac{1}{3}\mathcal{D}^i\mathcal{D}_j\beta^j = 16\pi N\psi^{-2}(S^*)^i + 2\psi^{10}K^{ij}\mathcal{D}_j\frac{N}{\psi^6}. \tag{5.45}$$

Conformal rescaling of the hydrodynamical variables is not only relevant for local uniqueness issues. The hydrodynamic equations (4.27) and (4.28) can be

reformulated as a first order hyperbolic system of conservation equations for the quantities $(D^*, (S^*)_i, E^*)$ [131, 132], where, similarly to equations (5.40)–(5.42), $D^* := \psi^6 D$, $D := Nu^0\,\rho$ being the baryon mass density as measured by the Eulerian observer. We can thus consider E^* and $(S^*)_i$ as known variables in the computation of the CFC metric. Note that these quantities differ from E and S_i by a factor ψ^6, and hence it is not possible to compute the non-starred quantities before knowing the value of ψ. If the energy-momentum tensor represents a fluid (i.e. $P \neq 0$), then the source of equation (5.44) cannot be explicitly expressed in terms of $(D^*, (S^*)_i, E^*)$, the reason for that being the dependence of S^* on the pressure P. The pressure can only be computed in terms of the "primitive" quantities, e.g., as a function $P(\rho, \epsilon)$ of the rest-mass density and the specific internal energy ϵ. The primitive quantities are, in general, recovered from (D, S_i, E) implicitly by means of an iteration algorithm. So far, two solutions of the problem related to the fact that S^* directly contains P have been used in numerical simulations performed with the CFC approximation.

The first approach [48] is to consider P, and hence also S^*, as an implicit function of ψ. Then Eqs. (5.43)–(5.45) can be solved as a coupled set of non-linear equations using a fixed-point iteration algorithm. The convergence of the algorithm to the correct solution depends not only on the proximity of the initial seed metric to the solution, but also on the uniqueness of this solution. The latter point is extensively discussed in the next Section. Furthermore, one problem of this approach is the necessity of performing the recovery of the primitive variables (which is numerically a time consuming procedure) to compute the pressure during each fixed point iteration. Because of the uniqueness problem, this approach can be only successfully applied in numerical simulations for, at most, moderately strong gravity (like stellar core collapse to a neutron star or the inspiral and initial merger phase of binary neutron stars), but fails for more compact configurations like the collapse of a stellar core or a neutron star to a black hole. For such scenarios with very strong gravity, one finds convergence of the metric to a physically incorrect solution of the equations or even nonconvergence of the algorithm.

A second approach proposed here to the recovery algorithm problem is the attempt to calculate P independently of the CFC equations. This can be

achieved by computing the conformal factor by means of the evolution equation

$$\frac{\partial \psi'}{\partial t} = \frac{\psi'}{6} \mathcal{D}_k \beta^k. \tag{5.46}$$

The conformal factor ψ' obtained in this way is analytically identical to the ψ from Eqs. (5.43)–(5.45), but here we use a different notation to keep track of the way it is computed. The value of ψ' is solely used to evaluate P, and the coupled system of Eqs. (5.43)–(5.45) is solved for determining ψ, N, and β^i. Although this approach allows one to avoid the problem of recovering the primitive variables at each iteration, it also suffers from the convergence problem, and the simulation of configurations with very strong gravity is still not feasible. Furthermore, new complications are introduced by using two differently computed values, ψ and ψ', of the same quantity. For some scenarios like the formation of a black hole from stellar collapse, the numerical values of these two quantities during the evolution of the system start to diverge significantly at some point. We find that this inconsistency cannot be avoided, since any attempt to artificially synchronize both values leads to numerical instabilities.

5.2.1 *Uniqueness of the elliptic equations and convergence of elliptic solvers*

Well-posed elliptic partial differential systems admit non-unique solutions whenever the associated differential operator has a non-trivial kernel. When discussing sufficient conditions guaranteeing uniqueness, it is illustrative to first consider the case of a scalar elliptic equation. In particular, for the class of scalar elliptic equations for the function u of the form

$$\Delta u + h u^p = g, \tag{5.47}$$

where h and g are known functions independent of u, a maximum principle can be used to prove local uniqueness of the solutions as long as the sign of the exponent p is different from the sign of the proper function h [70, 25, 71, 72].

In the CFC case, we are not dealing with a single scalar elliptic equation, but rather with the coupled non-linear elliptic system (5.43)-(5.45). Therefore, assessing whether or not the scalar equations (5.43) and (5.44) present the appropiated signs for the application of a maximum principle is an important step for understanding the uniqueness properties of the whole system. However, as

pointed out previously, the CFC equations for the conformal factor and the lapse possess the wrong signs in the quadratic extrinsic curvature terms (once everything is expressed in terms of the lapse and the shift). This problem can be fixed in equation (5.43) by an appropriate rescaling of the lapse, $N = \tilde{N}\psi^6$, but this strategy does not solve the problem for the lapse equation. Therefore we cannot use the maximum principle to infer local uniqueness of the solutions to the CFC equations. In these conditions of potential non-unique solutions, convergence to a non-desirable solution may happen. This pathology has been illustrated using simple analytical examples of scalar equations of the type (5.47) in [69], as well as in numerical implementations of the vacuum Einstein constraints in the XCTS approach [68] and certain constrained evolution formalisms (see, e.g., [125]).

In the context of the CFC approximation this sign issue has also appeared, in particular associated with the "recovery algorithm" problem discussed since it involves the evaluation of the conformal factor. Non-unique solutions of ψ, either due to the use of the non-conformally rescaled E or the quadratic extrinsic curvature term, spoil the convergence of the algorithm when density, and thus compactness, increases. We again emphasize that a possible synchronization of ψ and ψ' does not solve the problem in general, since numerical instabilities eventually arise at sufficiently high compactness.

The non-uniqueness of solutions has also been observed in numerical simulations in FCF, as described in the following example. Let us consider a vacuum spacetime, with initial data formed by a Gaussian wave packet, as in [111], but with much higher amplitude $\chi_0 = 0.9$ instead of $\chi_0 = 10^{-3}$ in [111] (see the latter references for notations). The integration technique and numerical settings are the same as in [111], but contrary to the results for small amplitudes obtained in that reference, the wave packet does not disperse to infinity and instead starts to collapse. Fig. 5.1. displays the time evolution of the central lapse N_c at $r = 0$ and of the system's Arnowitt-Deser-Misner (ADM) mass M_{ADM}, which, in the present conformal decomposition, can be expressed as

$$\begin{aligned} M_{\rm ADM} &= -\frac{1}{2\pi}\oint_\infty \left(\mathcal{D}_i\psi - \frac{1}{8}\mathcal{D}^j\tilde{\gamma}_{ij}\right) d\mathcal{A}^i \\ &= -\frac{1}{2\pi}\oint_\infty \mathcal{D}_i\psi \, d\mathcal{A}^i, \end{aligned} \tag{5.48}$$

where the integral is taken over a sphere of radius $r = \infty$ and the second

equality follows from the use of Dirac gauge.

The very sudden change at $t \simeq 0.4$ in both the central lapse and the ADM mass, which is also present in, e.g., the central conformal factor ψ_c, originates from the convergence of the elliptic system (4.64)-(4.66) to another solution with a different (unphysical) value of the ADM mass, as it is shown in Fig. 5.1. The good conservation of $M_{\rm ADM}$ and the smooth evolution of N_c for $t \gtrsim 0.4$ indicate that this other solution remains stable until $t \simeq 2$, when high-frequency oscillations appear. These oscillations may be due to the overall inconsistency of the system, destabilizing the whole scheme. On the other hand, the time evolution of h^{ij} does not show any such type of behavior, and h^{ij} exhibits a continuous radial profile at all times. This is numerical evidence that, also for the full Einstein case (i.e. without approximation), the generalized elliptic equations suffer from a similar convergence problem as in the CFC case.

The same subject is also exemplified when one tries to calculate the space-time metric for an equilibrium neutron star model from the unstable branch using either Eqs. (4.64)–(4.66) in the FCF case or Eqs. (5.43)–(5.45) in the CFC approximation. Even for the simple setup of a polytrope with adiabatic index $\Gamma = 2$ in spherical symmetry, those metric equations yield – when converging at all – a grossly incorrect solution if the matter quantities (D, S_i, E) in the source terms are held fixed. Both the metric components as well as the ADM mass can deviate from the physical solution by a few tens of percent, even though that incorrect metric satisfies the asymptotic flatness condition. The reason why numerical codes for constructing rotating relativistic neutron star models, like the KEH code [133], the RNS code [134], or the BGSM code [135], are not obstructed by this non-uniqueness problem is apparently that they all utilize an iteration over both the metric and the hydrodynamic equations simultaneously, thereby allowing the matter quantities to change during the calculation of the metric.

We want to stress here that these non-convergence issues in the CFC case are not related to the approximation that is made. If one considers this system in the spherical (one-dimensional) case, CFC is no longer an approximation, but is the choice of the so-called isotropic gauge. Even then, the elliptic system (5.43)-(5.45) no longer converges to the proper (physical) solution.

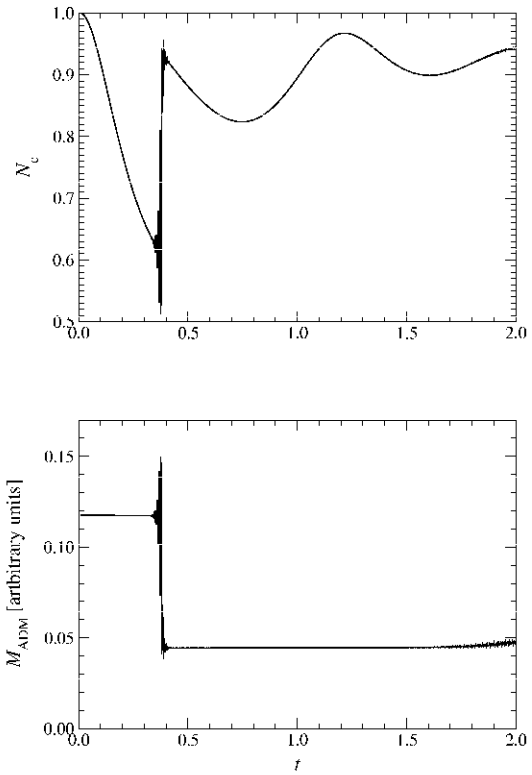

Fig. 5.1: Time evolution of the central lapse N_c (top panel) and the ADM mass M_{ADM} (bottom panel) for a collapsing packet of gravitational waves, using the integration scheme proposed in [111]. The unit of t is given by the initial width of the wave packet

5.2.2 The new scheme and its theoretical properties

Despite the above mentioned convergence problems, numerically simulating the physical problem of spherical collapse to a black hole in isotropic coordinates has been successfully studied by Shapiro and Teukolsky in [73]. Because of the spherical symmetry, there exists only one independent component of the extrinsic curvature. It is then possible to compute directly a conformal extrinsic curvature, $\psi^6 K^r_r$, from the conserved hydrodynamical variables. The elliptic equation for ψ then decouples from the other elliptic equations by introducing this conformal extrinsic curvature and using the conserved hydrodynamical variables in the source. This source term presents no problem for proving local uniqueness, and the equation for ψ always converges to the physically correct solution. Once the conformal factor, the extrinsic curvature (from the conformal factor and the conformal extrinsic curvature), and the conserved hydrodynamical variables are known, the elliptic equation for $N\psi$ can be solved and, again, the source exhibits no local uniqueness problem. This follows from the fact that the extrinsic curvature is not expressed in terms of the lapse and the shift. This contrasts with the CFC equation (5.44) where a division by N^2 occurs in the last term when the extrinsic curvature is expressed in terms of its constituents N, ψ, and β^i. In adition, there is no need to use ψ'. Finally, the elliptic equation for the shift vector can be solved. In summary, no problems of instabilities or non-uniqueness are encountered.

We now generalize this scheme to the CFC case in three dimensions. This involves the use of two different conformal decompositions of the extrinsic curvature: first, two different conformal rescaling and, second, two different decompositions of the traceless part into longitudinal and transverse parts. Adopting maximal slicing, $K = 0$, a generic conformal decomposition can be written as

$$K^{ij} = \psi^{\zeta-8}(A^{(\zeta)})^{ij} := \psi^{\zeta-8}\left(\frac{1}{\sigma}(LX)^{ij} + A^{ij}_{\rm TT}\right), \tag{5.49}$$

where ζ is a free parameter and σ a free function, $A^{ij}_{\rm TT}$ is transverse traceless and L is the conformal Killing operator defined by equation (4.54). We implicitly make use of a flat conformal metric, with respect to which $A^{ij}_{\rm TT}$ is transverse although, in principle, it would be more general to use the metric $\tilde{\gamma}^{ij}$ and the conformal Killing operator associated with it, $\tilde{L}$. But such a decomposition would introduce many technical difficulties in our treatment. In

particular, it is numerically easier to handle tensors which are divergence-free with respect to the flat metric in the generalization to FCF. The vector X^i, on which L is acting, is therefore called the longitudinal part of $(A^{(\zeta)})^{ij}$. The first decomposition we use is the one introduced in equations (4.52) (4.53) with the choice $\zeta = 4$ and $\sigma = 2N$. This corresponds to a CTS-like decomposition of the traceless part, so that X^i is given by the shift vector β^i and $A^{ij}_{\rm TT}$ can be expressed in terms of the time derivative of the conformal metric. We denote this traceless part as $\tilde{A}^{ij} := (A^{(4)})^{ij}$. In the CFC approximation this becomes

$$K^{ij} = \psi^{-4}\tilde{A}^{ij}, \qquad \tilde{A}^{ij} = \frac{1}{2N}(L\beta)^{ij}. \tag{5.50}$$

The second conformal decomposition,

$$K^{ij} = \psi^{-10}\hat{A}^{ij}, \qquad \hat{A}^{ij} = (LX)^{ij} + \hat{A}^{ij}_{\rm TT}, \tag{5.51}$$

refers to $\zeta = -2$ and $\sigma = 1$. It instead corresponds to a conformal tranverse traceless (CTT) decomposition of the traceless part of extrinsic curvature introduced by Lichnerowicz [22]. Notice that we have defined $\hat{A}^{ij} := (A^{(-2)})^{ij}$, not to be confused with $\tilde{A}^{ij} := (A^{(4)})^{ij}$. The relation between $\hat{A}^{ij}$ and $\tilde{A}^{ij}$ is given by

$$\hat{A}^{ij} = \psi^{10}K^{ij} = \psi^6\tilde{A}^{ij}. \tag{5.52}$$

In terms of $\hat{A}^{ij}$, the CFC momentum constraint can be written as

$$\mathcal{D}_j\hat{A}^{ij} = 8\pi\psi^{10}S^i = 8\pi\psi^6 f^{ij}S_j = 8\pi f^{ij}S^*_j. \tag{5.53}$$

Consistency between the CTT-like decomposition (5.51) and the CTS-like (5.50) generically requires a non-vanishing tranverse part $\hat{A}^{ij}_{\rm TT}$ in equation (5.51). However, as it is shown in Appendix A, this $\hat{A}^{ij}_{\rm TT}$ is smaller in amplitude than the non-conformal part h^{ij} of the spatial metric and $\hat{A}^{ij}$ can be approximated on the CFC approximation level as

$$\hat{A}^{ij} \approx (LX)^{ij} = \mathcal{D}^iX^j + \mathcal{D}^jX^i - \frac{2}{3}\mathcal{D}_kX^kf^{ij}. \tag{5.54}$$

From equations (5.51) and (5.53), an elliptic equation for the vector X^i can be derived,

$$\Delta X^i + \frac{1}{3}\mathcal{D}^i\mathcal{D}_jX^j = 8\pi f^{ij}S^*_j, \tag{5.55}$$

from which X^i can be obtained. With this vector field, one can calculate the tensor $\hat{A}^{ij}$ via (5.54). Notice that in the case of spherical symmetry, $\hat{A}^{rr} = \psi^{10}K^{rr} = \psi^6 K^r{}_r$ is the quantity used by Shapiro and Teukolsky [73].

The elliptic equation for the conformal factor can be rewritten in terms of the conserved hydrodynamical variables and $\hat{A}^{ij}$:

$$\Delta\psi = -2\pi\psi^{-1}E^* - \psi^{-7}\frac{f_{il}f_{jm}\hat{A}^{lm}\hat{A}^{ij}}{8}. \tag{5.56}$$

This equation can be solved in order to obtain the conformal factor. Once the conformal factor is known, the procedure to implicitly recover the primitive variables from the conserved ones is possible, the pressure P can be computed using the equation of state, and therefore S^* is at hand. The elliptic equation for $N\psi$ can be reformulated by means of the conserved hydrodynamical variables, $\hat{A}^{ij}$, and the conformal factor:

$$\Delta(\psi N) = 2\pi N\psi^{-1}\left(E^* + 2S^*\right) + N\psi^{-7}\frac{7f_{il}f_{jm}\hat{A}^{lm}\hat{A}^{ij}}{8}. \tag{5.57}$$

From this equation $N\psi$ can then be obtained, and, consequently, the lapse function N. Note that, since $\hat{A}^{ij}$ is already known at this step, no division by N^2 spoils the good sign compatible with the maximum principle.

Using the relation between the two conformal decompositions of the extrinsic curvature, $\hat{A}^{ij} = \psi^6\tilde{A}^{ij}$, equation (5.50) can be expressed as $(L\beta)^{ij} = 2N\psi^{-6}\hat{A}^{ij}$. Taking the divergence, we arrive at an elliptic equation for the shift vector,

$$\Delta\beta^i + \frac{1}{3}\mathcal{D}^i\left(\mathcal{D}_j\beta^j\right) = \mathcal{D}_j\left(2N\psi^{-6}\hat{A}^{ij}\right), \tag{5.58}$$

where the source is completely known. This elliptic equation can be solved in order to obtain the shift vector β^i consistent with $\partial_t\tilde{\gamma}_{ij} = 0$, as required by the CFC approximation.

In this recast of the CFC equations, an extra elliptic vectorial equation for the vector field X^i is introduced. However, now the signs of the exponents of ψ and N are compatible with the maximum principle for scalar elliptic equations, and the problem is linearization stable. While this does not guarantee global uniqueness of the solutions, it provides a sufficient result for local uniqueness. This strongly relies on the fact that the system decouples in a hierarchical way, which we summarize here once more:

1. With the hydrodynamical conserved quantities at hand, solve equation (5.55) for X^i, and thus for $\hat{A}^{ij}$.

2. Solve equation (5.56) for ψ, where local uniqueness is now guaranteed. Then S^* can be calculated consistently.

3. Solve equation (5.57) for $N\psi$, a linear equation where the maximum principle can be applied and uniqueness and existence follow with appropriate boundary conditions.

4. As the source of equation (5.58) is then fully known, solve it for β^i.

The same augmented CFC scheme as that discussed here has been introduced already by Saijo [43] to compute gravitational collapse of differentially rotating supermassive stars. However, in this work the inconsistency between equation (5.50) and equation (5.54), i.e., setting to zero the transverse traceless part of $\hat{A}^{ij}$, has not been pointed out. On the contrary, we have analyzed this inconsistency in detail (cf. Appendix A) and have shown that it leads to an error of the same order as that of the CFC approximation. In addition, we have shown here that the introduction of the vector potential X^i is the key ingredient for solving the non-uniqueness issue. The same scheme, but without the conformal rescaling of the matter quantities, has also been used recently by Shibata and Uryu [136, 137] in the context of computing initial data. As in [43], the inconsistency resulting from setting to zero the transverse traceless part $\hat{A}^{ij}$ and the uniqueness issue are not discussed in their work. These studies [43, 136, 137] do not discuss the extension of the new scheme to the non-conformally flat case, as it is done in 5.3.5.

We finally comment on the recent work by Rinne [125], where uniqueness issues related to the Hamiltonian constraint equation are solved by adopting an appropriate rescaling of the extrinsic curvature. On the other hand, problems associated with the slicing condition are tracked to the substitution in that equation of the extrinsic curvature by its kinematical expression in terms of the (shift and the) lapse. The latter spoils the uniqueness properties by reversing the sign of the relevant term in the slicing equation. This problem is solved by enlarging the elliptic system with an additional vector so as to re-express the relevant components of the extrinsic curvature without resorting to the lapse. The resulting elliptic system presents also a hierarchical structure. Although

the spirit of such approach is close to the one presented here, the specific manner of introducing the additional vector variable in [125] critically relies on the two dimensionality of the axisymmetric problem; specifically, on a choice of a particular gauge and on the fact that vectors and rank-two traceless symmetric tensors have the same number components in two dimensions, a property lost in three dimensions. On the contrary, the introduction of the vector X^i through the decomposition (5.54) is properly devised to work in three dimensions.

The new CFC metric equations presented here not only allow us to evolve the hydrodynamical equations and recover the metric variables from the elliptic equations in a consistent way (no auxiliary quantity ψ' is needed), but they also permit to introduce initial perturbations in the hydrodynamical variables (strictly speaking, in the conserved quantities) in a set of previously calculated initial data and directly delivers the correct values for the metric. It is even possible to perturb only the primitive quantities, and consistently resolve for the metric by iterating until the conformal factor ψ, which links the primitive to the conserved quantities, converges. We have found that such an iteration method fails for sufficiently strong gravity if the original CFC formulation is used.

5.2.3 Numerical simulations with the new scheme

The good behaviour of these equations have been shown in numerical simulations as the migration test, and the spherical and rotational collapse to a black hole [52]. The numerical simulations presented in [52] were performed using the numerical code CoCoNuT [39, 40] and the initial models were general relativistic $\Gamma = 2$ polytropes in equilibrium with a polytropic constant $K = 100$ (see more details of different models and grid setup in [52]). Figure 5.2 shows the time evolution of the central values of the rest-mass density and the lapse in the migration test. As the star expands, ρ_c decreases while N_c grows until the new stable equilibrium configuration is reached. In the polytropic case, there are no physical mechanisms to damp the strong pulsations, and the final state resembles a star oscillating around the equilibrium configuration until numerical dissipation finally damps the oscillations.

In the ideal gas case, shock waves are formed at every pulsation, and they dissipate kinetic energy into thermal energy, thereby damping the oscillations. As these shocks reach the surface of the star, a small amount of mass is expelled

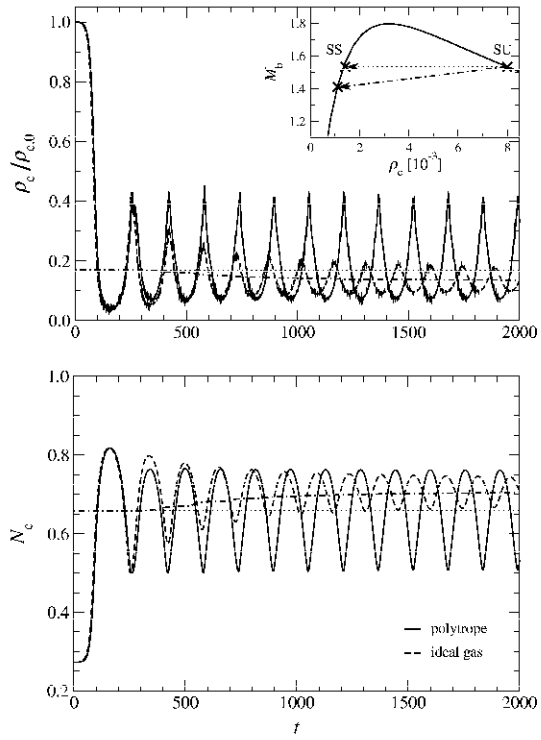

Fig. 5.2: Time evolution of the central rest-mass density ρ_c (top panel) and the central lapse N_c (bottom panel) for the migration of the unstable neutron star model to the stable branch, with either a polytropic (solid lines) or an ideal gas (dashed lines) equation of state. The dotted horizontal lines mark the value of ρ_c and N_c for the equilibrium configuration from the stable branch with the same gravitational mass $M_{\rm ADM}$, while the dash-dotted lines are obtained from a series of equilibrium models where mass shedding as in the migration model with an ideal gas equation of state is taken into account. In the inset the $M_{\rm ADM}$–ρ_c relation for this model setup is displayed. The unstable models (initial models) and the equilibrium configuration (final state for a polytropic equation of state) as well as the final state for an ideal gas equation of state are marked. The arrows symbolize the respective migration paths.

from the star and matter is ejected outwards into the surrounding artificial low-density atmosphere until it leaves the grid across the outer numerical boundary. The shock waves leaving the computational domain exceed the escape velocity and therefore the lost mass is gravitationallly unbounded. As the oscillations are damped, the shocks become weaker and the mass expelled at each oscillation is smaller. At the end of the simulation the star has lost about 10% of its initial baryon mass, approaching a state of constant baryon mass. As a consequence, the final equilibrium configuration on the stable branch is not the inital model anymore but, rather, the corresponding model from the stable branch with lower baryon mass and central density.

These simulations are consistent with the results from a fully relativistic three-dimensional code in [138]. Similar simulations of this test, with the original, unmodified CFC scheme, lead to a completely incorrect solution with a grossly incorrect ADM mass. When running with the new improved CFC scheme, it is obtained $M_{\rm ADM} = 1.451 M_\odot$ and initial values for the conformal factor and lapse of $\psi_{\rm c} = 1.561$ and $N_{\rm c} = 0.273$, respectively. On the other hand, with the unmodified conventional CFC scheme, the metric solver already initially converges to a solution with $M_{ADM} = 0.647 M_\odot$ (55%), $\psi_{\rm c} = 1.221$ (61%) and $N_{\rm c} = 0.532$ (63%), where the relative differences to the physically correct solution are given in parentheses.

The second test is the collapse to a black hole, which is triggered by reducing the polytropic constant (and, hence, the pressure) by 2% in the initial models. The top panel of figure 5.3 shows the evolution of the rest-mass density and lapse at the center. Due to the maximal slicing condition the singularity cannot be reached in a finite time, and, consequently, N_c rapidly approaches zero once the apparent horizon has formed. In parallel, ρ_c grows, which results in a decrease of the numerical time step due to the Courant condition. The evolution is terminated as the central region of the collapsing star inside the apparent horizon becomes increasingly badly resolved numerically. By refining the radial grid, the evolution is able to follow the collapse to even higher densities. Therefore, the only limitation to perform a stable evolution after the apparent horizon formation is the numerical resolution used. Note, however, that the spatial gauge condition is fixed in CFC, and thus the usual method of exploiting the gauge freedom for the radial component of the shift vector in order to effectively increase the central resolution cannot be used.

In the bottom panel of figure 5.3 the time evolution of the apparent horizon

radius is displayed. As expected, the apparent horizon appears at a finite radius and already encompasses a significant fraction of the total mass of the star (~70-80%) at that time. Later on, its radius grows as the surrounding matter falls inside beyond the horizon. The fraction of the rest mass remaining outside the horizon is also plotted in the figure.

These ideas can be generalized easily to the FCF formalism of the full Einstein equations (see Section 5.3.5).

5.3 Mathematical properties of FCF

This Section focuses on some properties of the hyperbolic equations in FCF. Some comments about the coupled elliptic-hyperbolic system will be discussed.

5.3.1 The evolution system and its hyperbolicity

Using FCF, a set of elliptic equations for the lapse function, the shift vector and the conformal factor is derived. Moreover, coupled with the set of the elliptic equations, there is a second order system of partial differential equations for the evolution of the difference between the flat metric and the conformal metric, h^{ij}. The work here focuses on this last set of equations. More specifically, this is a preliminary analysis of the hyperbolic part of the fully constrained evolution system. Rather than studying the whole coupled elliptic-evolution system, following a systematic line like the one developed in [139], we consider the fields in the elliptic part, that is ψ, N and β^i, as given fixed functions acting as parameters for the evolution system. This is therefore a first approach to the study of the whole coupled system.

In addition of considering ψ, N and β^i as fixed functions, we construct the differential operator governing the evolution in terms of the connection associated with the flat metric $\mathcal{D}_i$, instead of the one corresponding to the conformal metric $\tilde{D}_i$. The main motivation for this simplification is the numerical scheme proposed in [111] for the resolution of the evolution problem, which heavily relies on the use of spherical coordinates. The correction terms linking the flat connection with the conformal one are moved to the sources. In this work we do not consider the effects of the non-linear sources on the features of the hyperbolic system. In particular, an analysis of these sources will be carried out elsewhere.

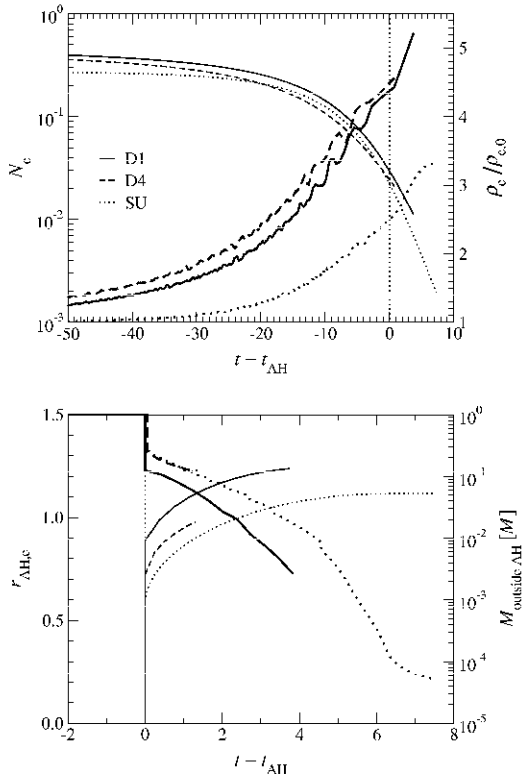

Fig. 5.3: Collapse to a black hole for the spherical model (SU), and the rotating models (D1 and D4). The top panel shows the time evolution of the central lapse N_c (thin lines) and the central rest-mass density ρ_c relative to the initial value $\rho_{c,0}$ (thick lines). The bottom panel shows the time evolution of the apparent horizon radius $r_{AH,e}$ in the equatorial plane (thin lines) and the rest mass $M_{outside\,AH}$ remaining outside the apparent horizon relative to the total rest mass M (thick lines). The dashed vertical lines mark the time when the apparent horizon first appears.

The system for the difference between the conformal metric and the flat metric, h^{ij}, is:

$$\begin{aligned}
&\frac{\partial^2 h^{ij}}{\partial t^2} - \frac{N^2}{\psi^4}\tilde{\gamma}^{kl}\mathcal{D}_k\mathcal{D}_l h^{ij} - 2\mathcal{L}_\beta\frac{\partial h^{ij}}{\partial t} + \mathcal{L}_\beta\mathcal{L}_\beta h^{ij} = \\
&\quad \mathcal{L}_{\hat{\beta}} h^{ij} + \frac{4}{3}\mathcal{D}_k\beta^k\left(\frac{\partial}{\partial t} - \mathcal{L}_\beta\right)h^{ij} - \frac{N}{\psi^6}\mathcal{D}_k Q\left(\mathcal{D}^i h^{jk} + \mathcal{D}^j h^{ik} - \mathcal{D}^k h^{ij}\right) \\
&\quad + \left[\left(\frac{\partial}{\partial t} - \mathcal{L}_\beta\right)lnN\right]\left[\left(\frac{\partial}{\partial t} - \mathcal{L}_\beta\right)h^{ij} - \frac{2}{3}\mathcal{D}_k\beta^k h^{ij} + (L\beta)^{ij}\right] \\
&\quad + \frac{2}{3}\left[\left(\frac{\partial}{\partial t} - \mathcal{L}_\beta\right)\mathcal{D}_k\beta^k - \frac{2}{3}\left(\mathcal{D}_k\beta^k\right)^2\right]h^{ij} - \left(\frac{\partial}{\partial t} - \mathcal{L}_\beta\right)(L\beta)^{ij} \\
&\quad + \frac{2}{3}\mathcal{D}_k\beta^k(L\beta)^{ij} + \frac{2N}{\psi^4}Z^{ij} + (2N)^2\left[\tilde{\gamma}_{kl}\tilde{A}^{ik}\tilde{A}^{jl} - 4\pi\left(\psi^4 S^{ij} - \frac{1}{3}S\tilde{\gamma}^{ij}\right)\right] \\
&\quad - 2N\psi^{-6}\left[\tilde{\gamma}^{ik}\tilde{\gamma}^{jl}\mathcal{D}_k\mathcal{D}_l Q + \frac{1}{2}\left(h^{ik}\mathcal{D}_l h^{lj} + h^{jk}\mathcal{D}_k h^{il} - h^{kl}\mathcal{D}_k h^{ij}\right)\mathcal{D}_l Q\right. \\
&\qquad \left. - \frac{1}{3}\tilde{\gamma}^{ij}\tilde{\gamma}^{kl}\mathcal{D}_k\mathcal{D}_l Q\right],
\end{aligned} \tag{5.59}$$

where $Q := N\psi^2$ and

$$\begin{aligned}
Z^{ij} \;=\; & N\left[\tilde{R}_*^{ij} + 8\psi^{-2}\left(\tilde{\gamma}^{ik}\mathcal{D}_k\psi\right)\left(\tilde{\gamma}^{jl}\mathcal{D}_l\psi\right)\right] + 4\psi^{-1}\left(\tilde{\gamma}^{ik}\mathcal{D}_k\psi\right)\left(\tilde{\gamma}^{jl}\mathcal{D}_l N\right) \\
& + 4\psi^{-1}\left(\tilde{\gamma}^{jk}\mathcal{D}_k\psi\right)\left(\tilde{\gamma}^{il}\mathcal{D}_l N\right) - \frac{1}{3}N\left[\tilde{R}_* + 8\psi^{-2}\mathcal{D}_k\psi\left(\tilde{\gamma}^{kl}\mathcal{D}_l\psi\right)\right]\tilde{\gamma}^{ij} \\
& - \frac{8}{3}\psi^{-1}\mathcal{D}_k\psi\left(\tilde{\gamma}^{kl}\mathcal{D}_k N\right)\tilde{\gamma}^{ij}.
\end{aligned} \tag{5.60}$$

The symmetric tensor $\tilde{R}_*^{ij}$ is defined by

$$\begin{aligned}
\tilde{R}_*^{ij} \;:=\; & \frac{1}{2}\left[-\mathcal{D}_l h^{ik}\mathcal{D}_k h^{jl} - \tilde{\gamma}_{kl}\tilde{\gamma}^{mn}\mathcal{D}_m h^{ik}\mathcal{D}_n h^{jl}\right. \\
& \left. + \tilde{\gamma}^{nl}\mathcal{D}_k h^{mn}\left(\tilde{\gamma}^{ik}\mathcal{D}_m h^{jl} + \tilde{\gamma}^{jk}\mathcal{D}_m h^{il}\right)\right] \\
& + \frac{1}{4}\tilde{\gamma}^{ik}\tilde{\gamma}^{jl}\mathcal{D}_k h^{mn}\mathcal{D}_l\tilde{\gamma}_{mn}
\end{aligned} \tag{5.61}$$

The scalar $\tilde{R}_*$ has been introduced previosly in equation (4.63).

Let us write the equations for h^{ij} as a first-order system. We define the following auxiliary variables:

$$u^{ij} := \frac{\partial h^{ij}}{\partial t}, \tag{5.62}$$

$$w_k^{ij} := \mathcal{D}_k h^{ij}. \tag{5.63}$$

With these new variables the system for h^{ij} can be cast into:

$$\begin{aligned} &\frac{\partial u^{ij}}{\partial t} - \frac{N^2}{\psi^4}\tilde{\gamma}^{kl}\mathcal{D}_k w_l^{ij} - 2\beta^k \mathcal{D}_k u^{ij} + \beta^k\beta^l \mathcal{D}_k w_l^{ij} \\ &\qquad = \phi^{ij}\left(\beta^k, N, \psi, \partial_\mu\beta^k, \partial_\mu N, \partial_\mu\psi, h^{ij}, u^{ij}, w_k^{ij}\right), \end{aligned} \tag{5.64}$$

where ϕ^{ij} is a source term which does not contain partial derivatives of u^{ij} or w_k^{ij}. From definition (5.63) and taking into account that $\partial_t f^{ij} = 0$, we obtain:

$$\frac{\partial w_k^{ij}}{\partial t} = \mathcal{D}_k u^{ij}. \tag{5.65}$$

Then the system of equations (5.62), (5.64) and (5.65), can be written as:

$$\frac{\partial \bar{\mathbf{v}}}{\partial t} + \mathbf{A}^l \mathcal{D}_l \bar{\mathbf{v}} = \mathbf{g}\left(\beta^k, N, \psi, \partial_\mu\beta^k, \partial_\mu N, \partial_\mu\psi, h^{ij}, u^{ij}, w_k^{ij}\right), \tag{5.66}$$

where the vectors $\bar{\mathbf{v}}$ and $\mathbf{g}$, corresponding respectively to the variables of the first-order system and the sources, are defined as:

$$\bar{\mathbf{v}} = \begin{pmatrix} (h^{ij}) \\ (u^{ij}) \\ (w_k^{ij}) \end{pmatrix}, \quad \mathbf{g}\left(\beta^k, N, \psi, \partial_\mu\beta^k, \partial_\mu N, \partial_\mu\psi, h^{ij}, u^{ij}, w_k^{ij}\right) = \begin{pmatrix} (u^{ij}) \\ (\phi^{ij}) \\ (0) \end{pmatrix}. \tag{5.67}$$

In these equations, $\bar{\mathbf{v}}$ and $\mathbf{g}$ are vectors of dimension 30, as it results from the symmetry properties of h^{ij}, u^{ij}, and w_k^{ij}. Let us remind that, besides the above symmetry properties, the following algebraic constraints have to be satisfied: i) $\det \tilde{\gamma}_{ij} = \det f_{ij}$; and $w_i^{ij} = 0$, which is equivalent to Dirac's gauge. Indices run as $1 \le i \le 3$, $i \le j \le 3$, $1 \le k \le 3$. In order to write the

matrices of the system in a simple way, the following auxiliary quantities are defined:

$$q^{ij} := \beta^i\beta^j - N^2\psi^{\ 4}\tilde{\gamma}^{ij}, \tag{5.68}$$

$$Q^i := \begin{pmatrix} q^{1i} & q^{2i} & q^{3i} \end{pmatrix}, \tag{5.69}$$

$$-\delta^i := \begin{pmatrix} -\delta^i_1 \\ -\delta^i_2 \\ -\delta^i_3 \end{pmatrix}. \tag{5.70}$$

Then, the explicit form of the matrices $\mathbf{A}^l$, for each value of $l = 1, 2, 3$, are:

$$\left(\begin{array}{c|ccc} 0_{6\times6} & \multicolumn{3}{c}{0_{6\times24}} \\ \hline 0_{24\times6} & \multicolumn{2}{c}{-2\beta^l I_6} & \begin{array}{cc} Q^l & 0 \\ & \ddots \\ 0 & Q^l \end{array} \\ \hline & \begin{array}{c|c} -\delta^l & 0_{3\times5} \\ \hline 0_{15} & \begin{array}{c|c} -\delta^l & 0_{3\times4} \\ \hline 0_{12} & \begin{array}{c|c} -\delta^l & 0_{3\times3} \\ \hline 0_9 & \begin{array}{c|c} -\delta^l & 0_{3\times2} \\ \hline 0_6 & \begin{array}{c|c} -\delta^l & 0_3 \\ \hline 0_3 & -\delta^l \end{array} \end{array} \end{array} \end{array} \end{array} & 0_{18\times18} \end{array}\right)$$

Once we dispose of the first-order evolution scheme (5.66), we study some basic hyperbolicity issues, mainly attempting to obtain explicit expressions of the characteristics in terms of the functions ψ, N, β^i and $\tilde{\gamma}^{ij}$, with the practical goal of determining the freedom to impose boundary conditions for h^{ij} on the inner excised boundary. This will be done in the next Section. In particular, our analysis is far from being exhaustive and we do not investigate issues like existence, uniqueness or well-posedness (see for instance [140]). The excision method is one of the most common methods for simulating numerically the evolution of black holes, among other ones (see more details in Section 7.1). It is very used when elliptic equations are solved with spectral methods, as it will be our case.

The next step is therefore the study of the hyperbolicity of the system (5.66) of first order with respect to the evolution vector ∂_t, whose components are $\xi^\alpha = (1, 0, 0, 0)$. As a notation we define $\mathbf{A}^0 = I$. The following relation is

satisfied: $\det(\mathbf{A}^{\alpha}\xi_{\alpha}) = \det(I) = 1 \neq 0$. Let $\zeta_{\alpha} = (0, \zeta_i)$ be a generic spacelike covector; we can choose it orthogonal to the evolution vector and we suppress the part proportional to it. The associated eigenvalue problem we have to solve is (see, e.g., Ref. [141]):

$$\left[\mathbf{A}^{l}\zeta_{l} - \lambda\mathbf{I}\right]\mathbf{X}_{\lambda} = 0, \tag{5.71}$$

where λ denotes the eigenvalue and $\mathbf{X}_{\lambda}$ the corresponding eigenvector.

Apparently, the system (5.66) looks like a hyperbolic system with sources. But that conclusion is far to be obvious. Imposing Dirac's gauge in (4.59) indeed guarantees the real character of the eigenvalues corresponding to matrices $\mathbf{A}^{l}$, and therefore the hyperbolicity of the evolution system. Even though this is not a prerogative of the Dirac gauge, other prescriptions for H^i in condition (4.59) lead to a more complicated structure of the resulting sources. As mentioned after equation (4.66), a more important point is the fact that other choices of H^i will generally introduce time derivatives of h^{ij} in the elliptic equations, complicating further the complete PDE system. Of course, if any gauge is not imposed at all, one can check that the $\mathbf{A}^{l}$ matrices admit complex eigenvalues. This reflects the property that Einstein equations by themselves do not have a definite type, without the specification of a gauge. When imposing $H^i = 0$, the eigenvalues of the linear combination $\mathbf{A}^{l}\zeta_{l}$ are real. So the first conclusion is that Dirac's gauge is a sufficient condition for the hyperbolicity of the system (5.66). Even though this is a crucial result for our analysis, this was also expected from the general structure of equation (5.64) and the properties of gauges analogous to the Dirac one, like the Coulomb gauge in electromagnetism.

The main goal of the work here is to obtain explicit expressions for the characteristics of the hyperbolic system. It is easy to see that there are six eigenvectors associated to the eigenvalue 0, and the rest eigenvectors have to be linearly independent with respect to these six vectors. Therefore, the rest eigenvectors can be studied independently. The eigenvalues associated with the chosen spatial vector are:

$$\lambda_0 = 0, \tag{5.72}$$

$$\lambda_{\pm}^{(\zeta)} = -\beta^{\mu}\zeta_{\mu} \pm \frac{N}{\psi^2}\left(\tilde{\gamma}^{\mu\nu}\zeta_{\mu}\zeta_{\nu}\right)^{1/2} = -\beta^{\mu}\zeta_{\mu} \pm N\left(\zeta^{\mu}\zeta_{\mu}\right)^{1/2}, \tag{5.73}$$

where λ_0 has multiplicity 12, and $\lambda_{\pm}^{(\zeta)}$ has each one multiplicity 6.

We define some quantities in order to write the set of eigenvectors in a simple matrix:

$$\mathbf{C}_1 := \begin{pmatrix} -\zeta_i q^{i2} & -\zeta_i q^{i3} \\ \zeta_i q^{i1} & 0 \\ 0 & \zeta_i q^{i1} \end{pmatrix} \tag{5.74}$$

$$\mathbf{C}_2 := \begin{pmatrix} \zeta_1 \\ \zeta_2 \\ \zeta_3 \end{pmatrix} \tag{5.75}$$

If we consider the (right) eigenvectors of the eigenvalue λ_0, the ones of the eigenvalue $\lambda_+^{(\zeta)}$ and the ones of the eigenvalue $\lambda_-^{(\zeta)}$, the corresponding matrix, $\mathbf{R}$, having the (right) eigenvectors as columns, is:

$$\left(\begin{array}{c|c} I_6 & 0_{6\times 24} \\ \hline 0_{24\times 6} & \begin{array}{c|c|c} 0_{6\times 12} & -\lambda_+^{(\zeta)} I_6 & -\lambda_-^{(\zeta)} I_6 \\ \hline \begin{array}{cc} \mathbf{C}_1 & 0 \\ & \ddots \\ 0 & \mathbf{C}_1 \end{array} & \begin{array}{cc} \mathbf{C}_2 & 0 \\ & \ddots \\ 0 & \mathbf{C}_2 \end{array} & \begin{array}{cc} \mathbf{C}_2 & 0 \\ & \ddots \\ 0 & \mathbf{C}_2 \end{array} \end{array} \end{array}\right)$$

It is easy to see that one can do linear combinations to change the roles of $\zeta_i q^{ij}$ in $\mathbf{C}_1$. The determinant of this matrix is $\left(\zeta_i q^{i1}\right)^6 \left(\lambda_+^{(\zeta)} - \lambda_-^{(\zeta)}\right)^6 \left(\zeta_i \zeta_j q^{ij}\right)^6$. Taking into account the above comment, about the change of the roles of the quantities in $\mathbf{C}_1$, the determinant of the (right) eigenvectors matrix change as $\left(\zeta_i q^{ij}\right)^6 \left(\lambda_+^{(\zeta)} - \lambda_-^{(\zeta)}\right)^6 \left(\zeta_i \zeta_j q^{ij}\right)^6$. The conditions to be satisfied for an incomplete basis of eigenvectors are:

(i) $\lambda_+^{(\zeta)} = \lambda_-^{(\zeta)}$: Since

$$\lambda_+^{(\zeta)} = \lambda_-^{(\zeta)} \Leftrightarrow N^2 \psi^{-4} \zeta_i \zeta_j \tilde{\gamma}^{ij} = N^2 \zeta_i \zeta^i = 0 \ , \tag{5.76}$$

and $\zeta_i \zeta^i$ does not vanish (ζ^i is a spatial vector different from zero) non-completeness only occurs if the lapse N vanishes.

(ii) $\zeta_i\zeta_j q^{ij} = 0$: From the definition of q^{ij}, it follows

$$\zeta_i\zeta_j\left(\beta^i\beta^j - N^2\psi^{-4}\tilde{\gamma}^{ij}\right) = 0 \Leftrightarrow \left(\zeta_i\beta^i\right)^2 = N^2\left(\zeta_i\zeta^i\right)^2. \tag{5.77}$$

One can see that the previous equality depends only on the direction of the vector ζ^i (i.e. $\zeta^i\zeta_i = 1$). From now up to the end of the study of the different cases, the vector ζ^i will be considered to be unitary. So (5.77) leads to:

$$\zeta_i\zeta_j\left(\beta^i\beta^j - N^2\psi^{-4}\tilde{\gamma}^{ij}\right) = 0 \Leftrightarrow \left(\zeta_i\beta^i\right)^2 = N^2. \tag{5.78}$$

Decomposing β^i into parallel and normal components to ζ^i, we write $\beta^i = \left(\beta^{\parallel}\right)\zeta^i + \left(\beta^{\perp}\right)^i$, where $\left(\beta^{\parallel}\right) = \zeta_i\beta^i$ and $\zeta_i\left(\beta^{\perp}\right)^i = 0$. From (5.78), we conclude:

$$\zeta_i\zeta_j q^{ij} = 0 \Leftrightarrow \left(\beta^{\parallel}\right)^2 = N^2 \quad . \tag{5.79}$$

Note that this case is independent of the choice of ζ^i, since it corresponds to $\left(\beta^{\parallel}\right)^i\left(\beta^{\parallel}\right)_i$, i.e. $|\zeta^i\beta_i|^2$. Therefore, non-completeness occurs if

$$|\beta^{\parallel}| = N. \tag{5.80}$$

(iii) $\zeta_i q^{ij} = 0$, $\forall j = 1,2,3$: This is a stronger case than the previous one. Again from the definition for q^{ij}, we have:

$$\zeta_i\left(\beta^i\beta^j - N^2\psi^{-4}\tilde{\gamma}^{ij}\right) = 0 \Leftrightarrow \left(\zeta_i\beta^i\right)\beta^j = N^2\zeta^j. \tag{5.81}$$

From this, and the decomposition $\beta^i = \left(\beta^{\parallel}\right)\zeta^i + \left(\beta^{\perp}\right)^i$, it follows:

$$\zeta_i q^{ij} = 0 \Leftrightarrow \left(\beta^{\perp}\right)^i = 0 \quad \text{and} \quad \left(\beta^{\parallel}\right)^2 = N^2 \tag{5.82}$$

This is just a stronger version of the previous second case.

As a consequence of the above analysis, the (right-)eigenvectors associated with the matrix $\mathbf{A}^l\zeta_l$ define a complete system iff i) the lapse N does not vanish, and ii) the projection of the evolution vector onto the plane spanned by n^μ and ζ^μ, i.e. $\left(t^{\parallel}\right)^\mu = Nn^\mu + b_\beta\zeta^\mu$, is non-null, i.e. $\left(\beta^{\parallel}\right)^2 \neq N^2$.

In the eigenvalue problem (5.71), ζ^i stands for an arbitrary spatial vector. In particular, we can always choose $\zeta^i = \beta^i$. In that case, the degeneracy

condition in cases 2 and 3 above reduces to $\beta^i\beta_i = N^2$. This happens if the vector t^μ becomes null. Moreover, if the vector t^μ is spacelike then we fall in case 2, since then there exists a vector ζ^i (in fact, a cone obtained by the rotation of the non-vanishing β^i by an appropriate angle) such that the projection of β^i onto that ζ^i, refered to as $\left(\beta^\parallel\right)^i$, satisfies $\left(\beta^\parallel\right)^i\left(\beta^\parallel\right)_i = \left(\zeta_i\beta^i\right)^2 = N^2$. We conclude that the system (5.66) is strongly hyperbolic if t^μ is timelike, i.e. if

$$N \neq 0 \quad \text{and} \quad N^2 - \beta^i\beta_i > 0. \tag{5.83}$$

In some particular cases, degeneracy in the eigenvalues can occur. In particular, it could happen that one of the eigenvalues λ_+ or λ_- coincides with λ_0. These degeneracies can appear if:

$$\lambda_+^{(\zeta)}\lambda_-^{(\zeta)} = 0 \Leftrightarrow \left(\beta^\mu\zeta_\mu\right)^2 = N^2\left(\zeta^\mu\zeta_\mu\right). \tag{5.84}$$

Again, one can consider ζ^i to be unitary. Hence, either λ_+ or λ_- vanishes when $\left(\beta^\parallel\right)^2 = N^2$. As seen in (5.78), in this case the system of eigenvectors is incomplete.

Let us introduce new auxiliary quantities in order to write in a simple way the inverse of the matrix of eigenvectors:

$$\Delta_1 := \frac{1}{\zeta_i\zeta_j q^{ij}}, \tag{5.85}$$

$$\Delta_2 := \frac{1}{\lambda_+^{(\zeta)} - \lambda_-^{(\zeta)}}, \tag{5.86}$$

$$\Delta_3 := \frac{1}{\zeta_j q^{1j}}, \tag{5.87}$$

$$\mathbf{D_1} := \begin{pmatrix} -\zeta_2\zeta_j q^{1j} & \zeta_1\zeta_j q^{1j} + \zeta_3\zeta_j q^{3j} & -\zeta_2\zeta_j q^{3j} \\ -\zeta_3\zeta_j q^{1j} & -\zeta_3\zeta_j q^{2j} & \zeta_1\zeta_j q^{1j} + \zeta_2\zeta_j q^{2j} \end{pmatrix} \tag{5.88}$$

$$\mathbf{D_2} := -\lambda_-^{(\zeta)} \begin{pmatrix} \zeta_j q^{1j} & \zeta_j q^{2j} & \zeta_j q^{3j} \end{pmatrix} \tag{5.89}$$

$$\mathbf{D_3} := -\lambda_+^{(\zeta)} \begin{pmatrix} \zeta_j q^{1j} & \zeta_j q^{2j} & \zeta_j q^{3j} \end{pmatrix} \tag{5.90}$$

The inverse of the eigenvectors matrix, $\mathbf{R}^{-1}$, is:

$$\left(\begin{array}{c|c|cc} I_6 & \multicolumn{3}{c}{0_{6\times 24}} \\ \hline & & \Delta_1\Delta_3\mathbf{D}_1 & 0 \\ & 0_{12\times 6} & & \ddots \\ & & 0 & \Delta_1\Delta_3\mathbf{D}_1 \\ \hline & & \Delta_1\Delta_2\mathbf{D}_2 & 0 \\ 0_{24\times 6} & -\Delta_2 I_6 & & \ddots \\ & & 0 & \Delta_1\Delta_2\mathbf{D}_2 \\ \hline & & \Delta_1\Delta_2\mathbf{D}_3 & 0 \\ & \Delta_2 I_6 & & \ddots \\ & & 0 & \Delta_1\Delta_2\mathbf{D}_3 \end{array}\right)$$

This form of the inverse matrix can be problematic from the numerical point of view, due to possible zero values in the denominators of the above expressions (e.g., in case of using the eigenvalues and eigenvectors of the system with a conservative scheme of fluxes; see more details in [142]). Taking advantage of the fact that the eigenvectors are indefined up to a normalization factor, we choose the following inverse matrix, which we name again $\mathbf{R}^{-1}$:

$$\left(\begin{array}{c|c|cc} I_6 & \multicolumn{3}{c}{0_{6\times 24}} \\ \hline & & \mathbf{D}_1 & 0 \\ & 0_{12\times 6} & & \ddots \\ & & 0 & \mathbf{D}_1 \\ \hline & & \Delta_1\mathbf{D}_2 & 0 \\ 0_{24\times 6} & -I_6 & & \ddots \\ & & 0 & \Delta_1\mathbf{D}_2 \\ \hline & & \Delta_1\mathbf{D}_3 & 0 \\ & I_6 & & \ddots \\ & & 0 & \Delta_1\mathbf{D}_3 \end{array}\right)$$

5.3.2 Some properties

One interesting property of this system is that all the characteristic fields are linearly degenerate, i.e.,

$$\mathbf{D}\lambda_p(\bar{v}) \cdot r_p(\bar{v}) \equiv 0, \tag{5.91}$$

where r_p is the eigenvector associated with the eigenvalue λ_p, and the operator $\mathbf{D}$ is defined in the space of the variables of the system. The reasons are:

(i) The first six eigenvectors has the eigenvalue $\lambda_0 = 0$, so the derivative of the eigenvalue is zero too, and the expression is identical to zero for $p = 1, ..., 6$.

(ii) In the expressions of the eigenvalues associated with the rest of the eigenvectors, $\lambda_{\pm}^{(\zeta)} = -\beta^{\mu}\zeta_{\mu} \pm N\psi^{-2}\left(\tilde{\gamma}^{\mu\nu}\zeta_{\mu}\zeta_{\nu}\right)^{1/2} = -\beta^{\mu}\zeta_{\mu} \pm N\left(\zeta^{\mu}\zeta_{\mu}\right)^{1/2}$, only the first six variables of the system can appear, so the partial derivatives with respect to the last 24 ones are zero. Moreover, the eigenvectors have zero in their first six components. Hence the expression is identical to zero for $p = 7, ..., 30$.

This property shows the coherence of the Dirac gauge with the quasilinear structure of the evolution system, since, in the language from fluid dynamics, it means that no shocks can be propagated along these curves, in particular gauge shocks. Hence, if there were discontinuities, they have to be contact discontinuities.

Now we are going to interpret the meaning of the eigenvalues we have obtained. If we impose in the metric $ds^2 = 0$, we get:

$$\left(\frac{dx}{dt} + \beta\right)^{\mu}\left(\frac{dx}{dt} + \beta\right)_{\mu} = N^2. \tag{5.92}$$

The solutions for λ in the equation

$$\left(\lambda + \beta^{\mu}\zeta_{\mu}\right)^2 = N^2\left(\zeta^{\mu}\zeta_{\mu}\right) \tag{5.93}$$

are the eigenvalues. If we take an unitary vector $\boldsymbol{\zeta}$, (5.93) leads to:

$$\left(\lambda + \beta^{\mu}\zeta_{\mu}\right)^2 = N^2. \tag{5.94}$$

Taking into account only the contributions of β^i and $\left(\frac{dx}{dt}\right)^i$ in the direction of ζ^i, i.e., $\beta^\mu = \beta\zeta^\mu$ and $\left(\frac{dx}{dt}\right)^\mu = \frac{dx}{dt}\zeta^\mu$, we can write (5.92) and (5.94) respectively as:

$$\left(\frac{dx}{dt} + \beta\right)^2 = N^2, \tag{5.95}$$

$$(\lambda + \beta)^2 = N^2. \tag{5.96}$$

From them we can see clearly that $\lambda = \frac{dx}{dt}$. We can conclude that there is a relation between the speed of light and the eigenvalues when we consider the contributions in a fixed direction.

5.3.3 Fluxes

In the last years, the high-resolution shock-capturing (HRSC) schemes to solve the equations of classical fluid dynamics have been succesfully extended to the relativistic case [143, 144]. They have been specifically designed to solve hyperbolic systems of conservation laws (HSCL). These numerical techniques exploit the hyperbolic and conservative character of the system of equations. Let

$$\partial_t u + \mathrm{D}_i f^i(u) = 0 \tag{5.97}$$

be a system where we can identify the set of unknowns, i.e., the vector of conserved quantities u, and their corresponding fluxes $f^i(u)$. If the Jacobian matrix associated to $f^i(u)$, $\frac{\partial f^i(u)}{\partial u}$, has real eigenvalues and a complete set of eigenvectors then Eq. (5.97) is said to be a HSCL.

In our case, once the equations have been written in conservation form, almost every high resolution method devised to solve hyperbolic systems of conservation laws can be applied. To this aim, we easily notice that the matrices A^l in Eq. (5.66) cannot be the Jacobian ones associated with any possible flux (i.e., any possible function of 30 components). On one hand, the first six columns of the matrices are zero, so all the components of the functions can

not depend on the first variables, that represent the components h^{ij}; on the other hand, in the last 24 columns appear the first variables and this means that the derivative of the components of the functions depends on them, and in particular the components of the functions depend on the first six variables too.

But we have not taken into account the gauge we are using. Let us take the following functions, where $k, l = 1, 2, 3$, and $i, j = 1, 2, 3$, with $j > i$:

$$\mathbf{f}^l := \begin{pmatrix} (0_6) \\ \left(-2u^{ij}\beta^l + w_k^{ij}\left[\beta^k\beta^l - N^2\psi^{-4}\tilde{\gamma}^{kl}\right]\right) \\ \left(-u^{ij}\delta_k^l\right) \end{pmatrix}. \tag{5.98}$$

By calculating the corresponding Jacobian matrices, we get the matrices $\mathbf{A}^l$ of Eq. (5.66) with an extra term, corresponding to the partial of the components 7 to 12 of $\mathbf{f}^l$ with respect to the variables h^{lk}, that is:

$$-N^2\psi^{-4}w_k^{ij}. \tag{5.99}$$

In general, this term is not zero, but in the equations it does not appear alone. Hence, we have:

$$\frac{\partial \mathbf{f}^{7-12,l}}{\partial h^{lk}}\mathcal{D}_l h^{lk} = -N^2\psi^{-4}w_k^{ij}\mathcal{D}_l h^{lk} = -N^2\psi^{-4}w_k^{ij}H^k. \tag{5.100}$$

Let us remind the expression of the gauge, $H^i = 0$, then the right-hand side of Eq. (5.98) is zero.

We define the new matrices $\left(\mathbf{A}^*\right)^l$ as:

$$\left(\begin{array}{c|c|c}
\multicolumn{3}{c}{0_{6\times30}} \\
\frac{-N^2}{\psi^4}\mathbf{E}^l & -2\beta^l I_6 & \begin{matrix} Q^l & & 0\\ & \ddots & \\ 0 & & Q^l\end{matrix} \\ \hline
0_{18\times6} & \begin{array}{c|c|c|c|c|c}
-\delta & \multicolumn{5}{c}{0_{3\times5}} \\ \cline{1-6}
0_{15} & -\delta^l & \multicolumn{4}{c}{0_{3\times4}} \\ \cline{2-6}
 & 0_{12} & -\delta^l & \multicolumn{3}{c}{0_{3\times3}} \\ \cline{3-6}
 & & 0_9 & -\delta^l & \multicolumn{2}{c}{0_{3\times2}} \\ \cline{4-6}
 & & & 0_6 & -\delta^l & 0_3 \\ \cline{5-6}
 & & & & 0_3 & -\delta^l
\end{array} & 0_{18\times18}
\end{array}\right),$$

where

$$\begin{aligned}
\mathbf{E}^{ij,l} &:= \left(\begin{array}{cccccc} w_1^{ij}\delta_1^l & w_{(1}^{ij}\delta_{2)}^l & w_{(1}^{ij}\delta_{3)}^l & w_2^{ij}\delta_2^l & w_{(2}^{ij}\delta_{3)}^l & w_3^{ij}\delta_3^l \end{array} \right), \\
\mathbf{E}^l &:= \left(\begin{array}{c} \mathbf{E}^{11,l} \\ \mathbf{E}^{12,l} \\ \mathbf{E}^{13,l} \\ \mathbf{E}^{22,l} \\ \mathbf{E}^{23,l} \\ \mathbf{E}^{33,l} \end{array} \right),
\end{aligned} \tag{5.101}$$

and the parentheses in the subindices represent a symmetric sum, e.g., $w_{(1}^{ij}\delta_{2)}^l = w_1^{ij}\delta_2^l + w_2^{ij}\delta_1^l$.

Thanks to the choice of the gauge, we have found the functions having the matrices $\left(\mathbf{A}^*\right)^l$ as the Jacobians. It is clear that $\left(\mathbf{A}^*\right)^l \neq \mathbf{A}^l$, but we have at the end the following equivalent system:

$$\begin{aligned}
\frac{\partial \bar{\mathbf{v}}}{\partial t} + \mathbf{A}^l \mathcal{D}_l \bar{\mathbf{v}} &= \frac{\partial \bar{\mathbf{v}}}{\partial t} + \left(\mathbf{A}^*\right)^l \mathcal{D}_l \bar{\mathbf{v}} \\
&= \mathbf{g}\left(\beta^k, N, \psi, \partial_\mu \beta^k, \partial_\mu N, \partial_\mu \psi, h^{ij}, u^{ij}, w_k^{ij}\right).
\end{aligned} \tag{5.102}$$

It is easy to check that the eigenvalues of the matrices $\left(\mathbf{A}^*\right)^l$ and $\mathbf{A}^l$ are the same and the set of eigenvectors is the same except for the first six ones. The system is linearly degenerate as before (see Section 5.3.2). If we order the eigenvectors for $\left(\mathbf{A}^*\right)^l$ as we did above for $\mathbf{A}^l$, the corresponding matrix, $\mathbf{R}^*$, is:

$$\left(\begin{array}{c|ccc|ccc|ccc} I_6 & \multicolumn{3}{c|}{0_{6\times 12}} & \multicolumn{3}{c|}{0_{6\times 6}} & \multicolumn{3}{c}{0_{6\times 6}} \\ \hline 0_{6\times 6} & \multicolumn{3}{c|}{0_{6\times 12}} & \multicolumn{3}{c|}{-\lambda_+^{(\zeta)} I_6} & \multicolumn{3}{c}{-\lambda_-^{(\zeta)} I_6} \\ \hline & \mathbf{C}_1 & & 0 & \mathbf{C}_2 & & 0 & \mathbf{C}_2 & & 0 \\ \mathbf{C}_3 & & \ddots & & & \ddots & & & \ddots & \\ & 0 & & \mathbf{C}_1 & 0 & & \mathbf{C}_2 & 0 & & \mathbf{C}_2 \end{array}\right),$$

where

$$\mathbf{C}_3 := \frac{N^2\psi^{-1}}{\zeta_j q^{1j}} \begin{pmatrix} \zeta_l \mathbf{E}^{11,l} \\ 0_{2\times 6} \\ \zeta_l \mathbf{E}^{12,l} \\ 0_{2\times 6} \\ \zeta_l \mathbf{E}^{13,l} \\ 0_{2\times 6} \\ \zeta_l \mathbf{E}^{22,l} \\ 0_{2\times 6} \\ \zeta_l \mathbf{E}^{23,l} \\ 0_{2\times 6} \\ \zeta_l \mathbf{E}^{33,l} \\ 0_{2\times 6} \end{pmatrix}. \tag{5.103}$$

Again, one can construct linear combinations to change the roles of $\zeta_i q^{ij}$ in $\mathbf{C}_1$; moreover, one can change the roles of the same quantities and the positions of the zeros in $\mathbf{C}_3$. The determinant is $\left(\zeta_i q^{i1}\right)^6 \left(\lambda_+^{(\zeta)} - \lambda_-^{(\zeta)}\right)^6 \left(\zeta_i \zeta_j q^{ij}\right)^6$. It is the same value that we got for the matrices $\mathbf{A}^l$. All the comments mentioned above can be repeated here.

The inverse of the eigenvectors matrix, $\left(\mathbf{R}^*\right)^{-1}$, is:

$$\left(\begin{array}{c|c|ccc} I_6 & 0_{6\times 6} & \multicolumn{3}{c}{0_{6\times 18}} \\ \hline & & \Delta_1\Delta_3\mathbf{D}_1 & & 0 \\ N^2\psi^{-4}\Delta_1\Delta_3\mathbf{D}_4 & 0_{12\times 6} & & \ddots & \\ & & 0 & & \Delta_1\Delta_3\mathbf{D}_1 \\ \hline & & \Delta_1\Delta_2\mathbf{D}_2 & & 0 \\ -N^2\psi^{-4}\lambda_-^{(\zeta)}\Delta_1\Delta_2\zeta_l\mathbf{E}^l & -\Delta_2 I_6 & & \ddots & \\ & & 0 & & \Delta_1\Delta_2\mathbf{D}_2 \\ \hline & & \Delta_1\Delta_2\mathbf{D}_3 & & 0 \\ N^2\psi^{-4}\lambda_+^{(\zeta)}\Delta_1\Delta_2\zeta_l\mathbf{E}^l & \Delta_2 I_6 & & \ddots & \\ & & 0 & & \Delta_1\Delta_2\mathbf{D}_3 \end{array}\right),$$

where

$$\mathbf{D}_4 := \left(\begin{array}{c} \mathbf{D}_5\zeta_l\mathbf{E}^{11,l} \\ \mathbf{D}_5\zeta_l\mathbf{E}^{12,l} \\ \mathbf{D}_5\zeta_l\mathbf{E}^{13,l} \\ \mathbf{D}_5\zeta_l\mathbf{E}^{22,l} \\ \mathbf{D}_5\zeta_l\mathbf{E}^{23,l} \\ \mathbf{D}_5\zeta_l\mathbf{E}^{33,l} \end{array}\right), \tag{5.104}$$

(5.105)

$$\mathbf{D}_5 := \left(\begin{array}{c} \zeta_2 \\ \zeta_3 \end{array}\right). \tag{5.106}$$

This form of the inverse matrix can be problematic from the numerical point of view because of the same reasons as before, due to possible zero values in the denominators of the expressions involved in the matrix. We choose the following renormalized inverse matrix, and we name it again $(\mathbf{R}^*)^{-1}$:

$$\left(\begin{array}{c|c|ccc} I_6 & 0_{6\times 6} & \multicolumn{3}{c}{0_{6\times 18}} \\ \hline & & \mathbf{D}_1 & & 0 \\ N^2\psi^{-4}\mathbf{D}_4 & 0_{12\times 6} & & \ddots & \\ & & 0 & & \mathbf{D}_1 \\ \hline & & \Delta_1\mathbf{D}_2 & & 0 \\ -N^2\psi^{-4}\lambda_-^{(\zeta)}\Delta_1\zeta_l\mathbf{E}^l & -I_6 & & \ddots & \\ & & 0 & & \Delta_1\mathbf{D}_2 \\ \hline & & \Delta_1\mathbf{D}_3 & & 0 \\ N^2\psi^{-4}\lambda_+^{(\zeta)}\Delta_1\zeta_l\mathbf{E}^l & I_6 & & \ddots & \\ & & 0 & & \Delta_1\mathbf{D}_3 \end{array}\right).$$

5.3.4 *Modified system.*

Motivated by Section 5.2, it is reasonable to split the second order evolution system for the symmetric tensor h^{ij} into a first order system, equivalent to the systems (5.66) and (5.102), but using the tensor $\hat{A}^{ij}$ instead of the tensor $u^{ij} = \partial_t h^{ij}$. The tensor $\hat{A}^{ij}$ introduced in Section 5.2, is defined, taking into account the condition of maximal slicing, as $\hat{A}^{ij} := \psi^{10}K^{ij}$, as in the CFC

case. The system can be written then as:

$$\frac{\partial h^{ij}}{\partial t} = 2N\psi^{-6}\hat{A}^{ij} + \beta^k w_k^{ij} - \tilde{\gamma}^{ik}\mathcal{D}_k\beta^j - \tilde{\gamma}^{kj}\mathcal{D}_k\beta^i + \frac{2}{3}\tilde{\gamma}^{ij}\mathcal{D}_k\beta^k \ , \tag{5.107}$$

$$\begin{aligned}\frac{\partial \hat{A}^{ij}}{\partial t} + \mathcal{D}_k\left(-\frac{N\psi^2}{2}\tilde{\gamma}^{kl}w_l^{ij} - \beta^k\hat{A}^{ij}\right) &= -\hat{A}^{kj}\mathcal{D}_k\beta^i - \hat{A}^{ik}\mathcal{D}_k\beta^j + \frac{2}{3}\hat{A}^{ij}\mathcal{D}_k\beta^k \\ &+2N\psi^{-6}\tilde{\gamma}_{kl}\hat{A}^{ik}\hat{A}^{jl} - 8\pi N\psi^6\left(\psi^4 S^{ij} - \frac{S\tilde{\gamma}^{ij}}{3}\right) \\ &+N\left(\psi^2\tilde{R}_*^{ij} + 8\tilde{\gamma}^{ik}\tilde{\gamma}^{jl}\mathcal{D}_k\psi\mathcal{D}_l\psi\right) + 4\psi\left(\tilde{\gamma}^{ik}\tilde{\gamma}^{jl}\mathcal{D}_k\psi\mathcal{D}_l N + \tilde{\gamma}^{ik}\tilde{\gamma}^{jl}\mathcal{D}_k N\mathcal{D}_l\psi\right) \\ &-\frac{1}{3}\left[N\left(\psi^2\tilde{R}_* + 8\tilde{\gamma}^{kl}\mathcal{D}_k\psi\mathcal{D}_l\psi\right) + 8\psi\tilde{\gamma}^{kl}\mathcal{D}_k\psi\mathcal{D}_l N\right]\tilde{\gamma}^{ij} \\ &-\frac{1}{2}\left(\tilde{\gamma}^{ik}w_k^{lj} + \tilde{\gamma}^{kl}w_k^{il}\right)\mathcal{D}_l Q - \tilde{\gamma}^{ik}\tilde{\gamma}^{jl}\mathcal{D}_k\mathcal{D}_l Q + \frac{1}{3}\tilde{\gamma}^{ij}\tilde{\gamma}^{kl}\mathcal{D}_k\mathcal{D}_l Q, \end{aligned} \tag{5.108}$$

$$\begin{aligned}\frac{\partial w_k^{ij}}{\partial t} + \mathcal{D}_k\left(-\beta^l w_l^{ij} - 2N\psi^{-6}\hat{A}^{ij}\right) &= -w_k^{il}\mathcal{D}_l\beta^j \\ &-\tilde{\gamma}^{il}\mathcal{D}_k\mathcal{D}_l\beta^j - w_k^{lj}\mathcal{D}_l\beta^i - \tilde{\gamma}^{lj}\mathcal{D}_k\mathcal{D}_l\beta^i + \frac{2}{3}\tilde{\gamma}^{ij}\mathcal{D}_k\mathcal{D}_l\beta^l + \frac{2}{3}w_k^{ij}\mathcal{D}_l\beta^l. \end{aligned} \tag{5.109}$$

Moreover, we have to add the constraints of the Dirac gauge to the above system, $w_i^{ij} = 0$, and the determinant of the conformal metric, $\tilde{\gamma} = f$. This way to write the second order system for h^{ij} has the advantage of getting rid of partial derivatives with respect to t of the lapse N, the shift β^i, or the conformal factor ψ in the sources. In the CFC case, there is only the equation for the evolution for the tensor $\hat{A}^{ij}$, but it has been shown that this tensor can be neglected in a consistent way with the CFC approximation.

The system of equations (5.107)-(5.109) can be written as

$$\frac{\partial \bar{\mathbf{v}}'}{\partial t} + \mathbf{A}'^l\mathcal{D}_l\bar{\mathbf{v}}' = \mathbf{g}'\left(\beta^k, N, \psi, \partial_\mu\beta^k, \partial_\mu N, \partial_\mu\psi, h^{ij}, \hat{A}^{ij}, w_k^{ij}\right), \tag{5.110}$$

where the vectors $\bar{\mathbf{v}}' = \begin{pmatrix} (h^{ij}) \\ (\hat{A}^{ij}) \\ (w_k^{ij}) \end{pmatrix}$ and $\mathbf{g}'$, are, respectively, the conserved variables and the sources. Matrices $\mathbf{A}'^l$ are the corresponding Jacobian ones

associated to the following fluxes

$$\mathbf{f}'^{l} := \begin{pmatrix} (0_6) \\ \left(-2\hat{A}^{ij}\beta^l - \frac{N\psi^2}{2}\tilde{\gamma}^{ml}w_m^{ij}\right) \\ \left(-\delta_k^l\left[\beta^m w_m^{ij} + 2N\psi^{-6}\hat{A}^{ij}\right]\right) \end{pmatrix}. \tag{5.111}$$

The explicit form of $\mathbf{A}'^{l}$ is:

$$\left(\begin{array}{cc|c} & & 0_{6\times 30} \\ \hline -\mathbf{E}'^{l} & -2\beta^l I_6 & \begin{array}{ccc} Q'^{l} & & 0 \\ & \ddots & \\ 0 & & Q'^{l} \end{array} \\ \hline 0_{18\times 6} & \sigma^l & \begin{array}{c|c} -\beta\delta^l & 0_{3\times 5} \\ \hline 0_{15} & \begin{array}{c|c} -\beta\delta^l & 0_{3\times 4} \\ \hline 0_{12} & \begin{array}{c|c} -\beta\delta^l & 0_{3\times 3} \\ \hline 0_9 & \begin{array}{c|c} -\beta\delta^l & 0_{3\times 2} \\ \hline 0_6 & \begin{array}{c|c} -\beta\delta^l & 0_3 \\ \hline 0_3 & -\beta\delta^l \end{array} \end{array} \end{array} \end{array} \end{array} \end{array}\right),$$

where

$$\begin{aligned} -\mathbf{E}'^{l} &:= -\frac{N\psi^2}{2}\mathbf{E}^l, \\ Q'^{l} &:= -\frac{N\psi^2}{2}\begin{pmatrix} \tilde{\gamma}^{1l} & \tilde{\gamma}^{2l} & \tilde{\gamma}^{3l} \end{pmatrix}, \\ \sigma^l &:= -\frac{2N}{\psi^6}\left(\begin{array}{c|c} \delta^l & 0_{3\times 5} \\ \hline 0_{15} & \begin{array}{c|c} \delta^l & 0_{3\times 4} \\ \hline 0_{12} & \begin{array}{c|c} \delta^l & 0_{3\times 3} \\ \hline 0_9 & \begin{array}{c|c} \delta^l & 0_{3\times 2} \\ \hline 0_6 & \begin{array}{c|c} \delta^l & 0_3 \\ \hline 0_3 & \delta^l \end{array} \end{array} \end{array} \end{array} \end{array}\right), \\ -\beta\delta^l &:= \begin{pmatrix} -\beta^1\delta_1^l & -\beta^2\delta_1^l & -\beta^3\delta_1^l \\ -\beta^1\delta_2^l & -\beta^2\delta_2^l & -\beta^3\delta_2^l \\ -\beta^1\delta_3^l & -\beta^2\delta_3^l & -\beta^3\delta_3^l \end{pmatrix}. \end{aligned}$$

The eigenvalues of the matrices $\mathbf{A}^l$ and $\mathbf{A}'^{l}$ are the same. The system is linearly degenerate as before (see Section 5.3.2). The corresponding matrix of

eigenvectors for $\mathbf{A}'^{l}$ (with the usual ordenation), $\mathbf{R}'$, is:

$$\left(\begin{array}{c|ccc|c|cc|cc} I_6 & \multicolumn{3}{c|}{0_{6\times 12}} & \multicolumn{2}{c|}{0_{6\times 6}} & \multicolumn{2}{c}{0_{6\times 6}} \\ \hline & \mathbf{C}_5 & & 0 & & & & \\ \mathbf{C}_4 & & \ddots & & -\frac{\psi^6(\zeta_i\zeta^l)^{1/2}}{2} I_6 & & \frac{\psi^6(\zeta_i\zeta^l)^{1/2}}{2} I_6 & \\ & 0 & & \mathbf{C}_5 & & & & \\ \hline & \mathbf{C}_1 & & 0 & \mathbf{C}_2 & 0 & \mathbf{C}_2 & 0 \\ \mathbf{C}_3 & & \ddots & & & \ddots & & \ddots \\ & 0 & & \mathbf{C}_1 & 0 & \mathbf{C}_2 & 0 & \mathbf{C}_2 \end{array}\right),$$

where

$$\mathbf{C}_4 := -\frac{N\psi^2\beta^1}{2\zeta_j q^{1j}} \begin{pmatrix} \zeta_l \mathbf{E}^{11,l} \\ \zeta_l \mathbf{E}^{12,l} \\ \zeta_l \mathbf{E}^{13,l} \\ \zeta_l \mathbf{E}^{22,l} \\ \zeta_l \mathbf{E}^{23,l} \\ \zeta_l \mathbf{E}^{33,l} \end{pmatrix}, \tag{5.112}$$

$$\mathbf{C}_5 := \frac{\psi^6}{2N} \begin{pmatrix} \beta^1\zeta_j q^{2j} - \beta^2\zeta_j q^{1j} & \beta^1\zeta_j q^{3j} - \beta^3\zeta_j q^{1j} \end{pmatrix}. \tag{5.113}$$

As before, one can construct linear combinations to change the roles of $\zeta_j q^{ij}$ in $\mathbf{C}_1$, $\mathbf{C}_4$ and $\mathbf{C}_5$, as well as the same quantities and the positions of the zeros in $\mathbf{C}_3$. The determinant is $\psi^{36}\left(\zeta_l\zeta^l\right)^3\left(\zeta_j q^{1j}\right)^6\left(\zeta_i\zeta_j q^{ij}\right)^6$. It is not exactly the same value that we got for the matrices $\mathbf{A}^l$, but all the comments mentioned there, about the different cases in which the determinant is zero, can be repeated here again (notice than the lapse N has to be different from zero because the definition of $\mathbf{C}_5$).

The inverse of the eigenvectors matrix, $(\mathbf{R}')^{-1}$, is:

$$\left(\begin{array}{c|c|ccc} I_6 & 0_{6\times 6} & \multicolumn{3}{c}{0_{6\times 18}} \\ \hline & & \Delta_1\Delta_3\mathbf{D}_1 & & 0 \\ N^2\psi^{-4}\Delta_1\Delta_3\mathbf{D}_4 & 0_{12\times 6} & & \ddots & \\ & & 0 & & \Delta_1\Delta_3\mathbf{D}_1 \\ \hline & & \Delta_1\mathbf{D}_6 & & 0 \\ \frac{-N\psi^{-4}\Delta_1}{2}\left(\frac{\beta^1}{(\zeta_l\zeta^l)^{1/2}}+N\right)\zeta_l\mathbf{E}^l & \frac{-1}{\psi^6(\zeta_l\zeta^l)^{1/2}}I_6 & & \ddots & \\ & & 0 & & \Delta_1\mathbf{D}_6 \\ \hline & & \Delta_1\mathbf{D}_6 & & 0 \\ \frac{N\psi^{-4}\Delta_1}{2}\left(\frac{\beta^1}{(\zeta_l\zeta^l)^{1/2}}-N\right)\zeta_l\mathbf{E}^l & \frac{1}{\psi^6(\zeta_l\zeta^l)^{1/2}}I_6 & & \ddots & \\ & & 0 & & \Delta_1\mathbf{D}_6 \end{array}\right),$$

where

$$\mathbf{D}_6 \;:=\; \frac{1}{2}\begin{pmatrix} \zeta_l q^{l1} & \zeta_l q^{l2} & \zeta_l q^{l3} \end{pmatrix}. \tag{5.114}$$

This form of the inverse matrix can be problematic from the numerical point of view because of the same reasons as before, due to possible zero values in the denominators of the expressions involved in the matrix. We choose the following renormalized inverse matrix, and we name it again $(\mathbf{R}')^{-1}$:

$$\left(\begin{array}{c|c|ccc} I_6 & 0_{6\times 6} & \multicolumn{3}{c}{0_{6\times 18}} \\ \hline & & \mathbf{D}_1 & & 0 \\ N^2\psi^{-4}\mathbf{D}_4 & 0_{12\times 6} & & \ddots & \\ & & 0 & & \mathbf{D}_1 \\ \hline & & \mathbf{D}_6 & & 0 \\ \frac{-N\psi^{-4}}{2}\left(\frac{\beta^1}{(\zeta_l\zeta^l)^{1/2}}+N\right)\zeta_l\mathbf{E}^l & \frac{-\zeta_l q^{l1}}{\psi^6(\zeta_l\zeta^l)^{1/2}}I_6 & & \ddots & \\ & & 0 & & \mathbf{D}_6 \\ \hline & & \mathbf{D}_6 & & 0 \\ \frac{N\psi^{-4}}{2}\left(\frac{\beta^1}{(\zeta_l\zeta^l)^{1/2}}-N\right)\zeta_l\mathbf{E}^l & \frac{\zeta_l q^{l1}}{\psi^6(\zeta_l\zeta^l)^{1/2}}I_6 & & \ddots & \\ & & 0 & & \mathbf{D}_6 \end{array}\right)$$

5.3.5 The coupled elliptic-hyperbolic system

We are going to finish this Section with some comments regarding the elliptic part and its coupling with the hyperbolic one. The elliptic part in FCF can be rewritten, using the tensor $\hat{A}^{ij}$, as:

$$\begin{aligned}\tilde{\gamma}^{kl}\mathcal{D}_k\mathcal{D}_l\psi &= -2\pi\psi^{-1}E^* - \psi^{-7}\frac{\tilde{\gamma}_{il}\tilde{\gamma}_{jm}\hat{A}^{lm}\hat{A}^{ij}}{8} \\ &\quad +\psi\frac{\tilde{R}_*}{8}, \qquad (5.115)\\ \tilde{\gamma}^{kl}\mathcal{D}_k\mathcal{D}_l\left(\psi N\right) &= (N\psi)\left[\frac{2\pi}{\psi^2}\left(E^*+2S^*\right)+\frac{7\tilde{\gamma}_{il}\tilde{\gamma}_{jm}\hat{A}^{lm}\hat{A}^{ij}}{8\psi^8}\right] \\ &\quad +(N\psi)\frac{\tilde{R}_*}{8}, \qquad (5.116)\\ \tilde{\gamma}^{kl}\mathcal{D}_k\mathcal{D}_l\beta^i+\frac{1}{3}\tilde{\gamma}^{ik}\mathcal{D}_k\mathcal{D}_l\beta^l &= 16\pi N\psi^{-6}\tilde{\gamma}^{ij}(S^*)_j+\hat{A}^{ij}\mathcal{D}_j\left(2N\psi^{-6}\right) \\ &\quad -2N\psi^{-6}\Delta^i_{kl}\hat{A}^{kl}. \qquad (5.117)\end{aligned}$$

The blue terms are the extra ones which do not appear in the CFC case.

We are going to show a procedure to solve all the elliptic and hyperbolic equations in the FCF general case. On the one hand, the variables of the evolution of the hyperbolic system are going to be directly used in the elliptic equations. On the other hand, the elliptic equations will keep the nice properties of local uniqueness as in the CFC case.

The strategy to evolve the two symmetric tensors h^{ij} and $\hat{A}^{ij}$ relies on a decomposition of these tensors in longitudinal and transverse traceless parts. The longitudinal parts (divergences with respect to the flat metric) are either known a priori, or are determined by the elliptic equations. More specifically, the divergence of h^{ij} vanishes according to the Dirac gauge. The tensor $\hat{A}^{ij}$ can be decomposed, as in the CFC case, as

$$\hat{A}^{ij} = (LX)^{ij} + \hat{A}^{ij}_{TT}, \qquad (5.118)$$

where $\mathcal{D}_i\hat{A}^{ij}_{TT} = 0$ and the vector X^i will be determined by the momentum constraint (see below). Consequently, we focus on the transverse traceless parts of these tensors. From h^{ij} and $\hat{A}^{ij}_{TT}$, it is possible to define two scalar

potentials, described in [53], for each tensor, that contain all the information of these tensors. These potentials are evolved according to the evolution equation (5.107) for h^{ij}, and the transverse traceless part of the evolution equation (5.108) for $\hat{A}^{ij}$ by applying consistently the previous decomposition (5.118). Once the scalar potentials on the next time slice are determined, the tensors h^{ij} and $\hat{A}^{ij}_{TT}$ can be reconstructed completely, satisfying the divergence-free conditions. The tensor w^{ij}_k can be computed too.

From (5.118), the momentum constraint can be written as

$$\mathcal{D}_j \hat{A}^{ij} = 8\pi\tilde{\gamma}^{ij}(S^*)_j - \Delta^i_{kl}\hat{A}^{kl}, \tag{5.119}$$

which is equivalent to the following elliptic equation for the vector X^i

$$\begin{aligned}
&\mathcal{D}_j\mathcal{D}^j X^i - \frac{1}{3}\mathcal{D}^i\mathcal{D}_k X^k \\
&+\tilde{\gamma}^{im}\left(\mathcal{D}_k\tilde{\gamma}_{ml} - \frac{\mathcal{D}_m\tilde{\gamma}_{kl}}{2}\right)\left(\mathcal{D}^k X^l + \mathcal{D}^l X^k - \frac{2}{3}f^{kl}\mathcal{D}_p X^p\right) = \\
&\qquad 8\pi\tilde{\gamma}^{ij}(S^*)_j - \tilde{\gamma}^{im}\left(\mathcal{D}_k\tilde{\gamma}_{ml} - \frac{\mathcal{D}_m\tilde{\gamma}_{kl}}{2}\right)\hat{A}^{kl}_{TT},
\end{aligned} \tag{5.120}$$

where $\mathcal{D}^i = f^{ij}\mathcal{D}_j$. This elliptical equation for the vector X^i is linear. Since h^{ij} and $\hat{A}^{ij}_{TT}$ have been calculated previously, the elliptic equation can be solved to obtain the vector X^i. With this method, the Dirac gauge and the momentum constraint are satisfied (by construction). Then, $\hat{A}^{ij}$ is reconstructed from $\hat{A}^{ij}_{TT}$ and X^i.

At this point, since the tensors h^{ij} and $\hat{A}^{ij}$ are known, we can follow exactly the same scheme as in the CFC case to solve, in a hierarchical way, the elliptic equations. First, the conformal factor is obtained from equation (5.115), then the lapse function from equation (5.116), and finally the shift vector from equation (5.117). These equations are decoupled in the order mentioned. No non-uniqueness problems are exhibited in the scalar elliptic equation and therefore the maximum principle can be applied.

The scheme presented here is augmented by an additional vector elliptic equation for X^i, while the elliptic character of the system of metric equations is preserved. The new scheme reformulates the elliptic equations in a CTT shape (one scalar and one vector elliptic equation), and then solves, for the

lapse and the shift one additional scalar and one vector elliptic equation. The new formulation not only corrects the problem of local uniqueness in the scalar elliptic equations, but also introduces a hierarchical structure that decouples the system. It has not been tested numerically yet.

6. GEOMETRICAL BLACK HOLES

In this Section we are going to introduce some definitions related with horizons of BHs, and we are going to discuss an application of the characteristic analysis to the inner boundary conditions of trapping horizons.

6.1 Definitions of horizons

The definitions and calculations of this part have been taken from [145], in which all the details can be found.

Let a hypersurface $\mathcal{H}$ of $\mathcal{M}$ be the image of a 3-dimensional manifold $\mathcal{H}_0$ by an embedding $\Phi : \mathcal{H}_0 \to \mathcal{M}$, $\mathcal{H} = \Phi(\mathcal{H}_0)$. The pull-back of the bilinear form $\boldsymbol{g}$, i.e. the spacetime metric, defines the induced metric on $\mathcal{H}$, also called the first fundamental form of $\mathcal{H}$: $\boldsymbol{q} := \Phi^* \boldsymbol{g}$. The hypersurface $\mathcal{H}$ is said to be null if, and only if, the induced metric $\boldsymbol{q}$ is degenerate; this means if, and only if, there exists a vector field $\boldsymbol{l}$ in $\mathcal{T}(\mathcal{H})$, the space of smooth vector fields on $\mathcal{M}$, that satisfies $\forall \boldsymbol{v} \in \mathcal{T}(\mathcal{H})$, $\boldsymbol{q}(\boldsymbol{l},\boldsymbol{v}) = 0$. In null hypersurfaces their normal vectors are both orthogonal and tangent to them.

For any hypersurface, the "bending" of $\mathcal{H}$ in $\mathcal{M}$ or extrinsic curvature of $\mathcal{H}$ is described by the Weingarten map or shape operator, which is the endomorphism of $\mathcal{T}_p(\mathcal{H})$, the tangent space of vectors at p, which associates to each vector tangent to $\mathcal{H}$ the variation of the normal $\boldsymbol{l}$ along that vector, with respect to the space-time connection $\overline{\boldsymbol{\nabla}}$:

$$\begin{aligned} \boldsymbol{\chi} : \mathcal{T}_p(\mathcal{H}) &\longrightarrow \mathcal{T}_p(\mathcal{H}) \\ v &\longmapsto \boldsymbol{\nabla}_v \boldsymbol{l} \end{aligned} \tag{6.1}$$

This application is well defined since $\boldsymbol{l} \cdot \boldsymbol{\chi}(v) = \boldsymbol{l} \cdot \boldsymbol{\nabla}_v \boldsymbol{l} = 1/2\, \boldsymbol{\nabla}_v (\boldsymbol{l} \cdot \boldsymbol{l}) = 0$. The Weingarten map depends on the specific choice of the normal $\boldsymbol{l}$; a rescaling of $\boldsymbol{l}$

acts as follows on $\boldsymbol{\chi}$: $\boldsymbol{l} \to \boldsymbol{l}' = \alpha \boldsymbol{l} \Rightarrow \boldsymbol{\chi} \to \boldsymbol{\chi}' = \alpha \boldsymbol{\chi} + \langle \boldsymbol{d}\alpha, \cdot \rangle \, \boldsymbol{l}$. The fundamental property of this application is to be self-adjoint with respect to the metric $\boldsymbol{q}$.

This property implies the symmetry of the bilinear form defined on $\mathcal{H}$'s tangent space by:

$$\begin{aligned} \boldsymbol{\Theta} : \mathcal{T}_p(\mathcal{H}) \times \mathcal{T}_p(\mathcal{H}) &\longrightarrow \mathbb{R} \\ (u, v) &\longmapsto u \cdot \boldsymbol{\chi}(v) \end{aligned} \tag{6.2}$$

It is called the second fundamental form of $\mathcal{H}$ with respect to $\boldsymbol{l}$. It is symmetric only because $\boldsymbol{l}$ is normal to some hypersurface. Actually, it is nothing but the pull-back of the bilinear form $\boldsymbol{\nabla}\underline{\boldsymbol{l}}$ onto $\mathcal{T}_p(\mathcal{H})$ induced by the embedding Φ of $\mathcal{H}$ in $\mathcal{M}$: $\boldsymbol{\Theta} = \boldsymbol{\Phi}^* \boldsymbol{\nabla} \underline{\boldsymbol{l}}$. As for $\boldsymbol{\chi}$, $\boldsymbol{\Theta}$ depends on the choice of the normal $\boldsymbol{l}$; its transformation under a rescaling of $\boldsymbol{l}$ is: $\boldsymbol{l} \to \boldsymbol{l}' = \alpha \boldsymbol{l} \Rightarrow \boldsymbol{\Theta} \to \boldsymbol{\Theta}' = \alpha \boldsymbol{\Theta}$.

If we take into account the foliation provided by the family of spacelike hypersurfaces that foliates the space-time in the 3+1 formalism, we have some extra-structure on $\mathcal{M}$. From now on, $\mathcal{H}$ is assumed to be a null hypersurface. We will define unambiguously a transverse direction to $\mathcal{H}$ and an associated projector $\boldsymbol{\Pi}$.

Each spacelike hypersurface Σ_t of the 3+1 slicing intersects the null hypersurface $\mathcal{H}$ on some 2-dimensional surface: $\mathcal{S}_t := \mathcal{H} \cap \Sigma_t$. As a submanifold of Σ_t, each $\mathcal{S}_t$ is necessarily a spacelike surface. The $\mathcal{S}_t$'s constitute a foliation on $\mathcal{H}$. The coordinate t can then be used as a parameter. We can normalize the null normal $\boldsymbol{l}$ of $\mathcal{H}$ by demanding that $\boldsymbol{l}$ is the tangent vector associated with this parametrization, or equivalently demanding that $\boldsymbol{l}$ is a vector field dual to the 1-form $\boldsymbol{dt}$: $\boldsymbol{\nabla}_{\boldsymbol{l}} t = 1$.

Let $\boldsymbol{s}$ be the unit vector of Σ_t, normal to $\mathcal{S}_t$ and directed towards the exterior of $\mathcal{S}_t$. Let $\boldsymbol{b} \in \mathcal{T}_p(\mathcal{S}_t)$, $\boldsymbol{b} := \vec{\boldsymbol{\gamma}}(\boldsymbol{l})$. Due to the normalization on the null normal $\boldsymbol{l}$, it can be expressed as $\boldsymbol{l} = N\boldsymbol{n} + \boldsymbol{b}$. It can be deduced that $\boldsymbol{b}$ is a vector of Σ_t which is normal to $\mathcal{S}_t$; then it is necessarily colinear to $\boldsymbol{s}$. Because $\boldsymbol{l}$ is null, $\boldsymbol{l} = N(\boldsymbol{n} + \boldsymbol{s})$. Since $\vec{\boldsymbol{\gamma}}(\boldsymbol{l}) = N\boldsymbol{s}$ with $N > 0$, we say that $\boldsymbol{l}$ is an outgoing null vector with respect to $\mathcal{S}_t$.

We need some direction transverse to $\mathcal{H}$ to define a projector. The slicing has already provided the timelike direction $\boldsymbol{n}$ and the spacelike direction $\boldsymbol{s}$, both normal to the 2-surfaces $\mathcal{S}_t$. We may also think about the null directions normal to $\mathcal{S}_t$. The ingoing direction is defined by the null vector $\boldsymbol{k} = 1/2N \ (\boldsymbol{n} - \boldsymbol{s})$. This null vector satisfies $\boldsymbol{l} \cdot \boldsymbol{k} = -1$. Each pair $(\boldsymbol{n}, \boldsymbol{s})$ or $(\boldsymbol{l}, \boldsymbol{k})$ forms a basis of the vectorial plane orthogonal to $\mathcal{S}_t$.

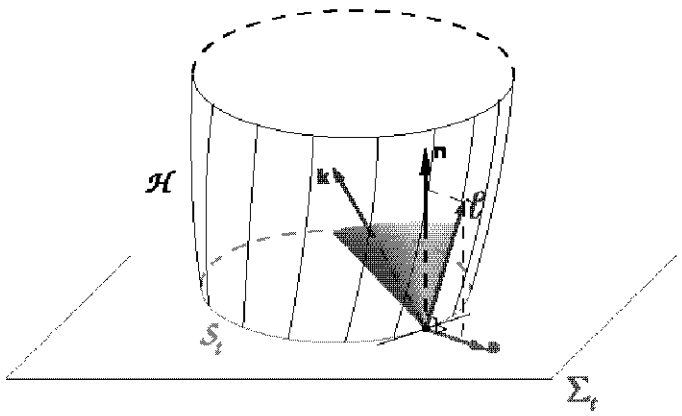

Fig. 6.1: Null vector $\boldsymbol{l}$ normal to $\mathcal{H}$, unit timelike vector $\boldsymbol{n}$ normal to Σ_t, unit spacelike vector $\boldsymbol{s}$ normal to $\mathcal{S}_t$ and ingoing null vector $\boldsymbol{k}$ normal to $\mathcal{S}_t$, from [145].

We can now define the projector onto $\mathcal{H}$ along $\boldsymbol{k}$ by:

$$\begin{aligned} \boldsymbol{\Pi} : \mathcal{T}_p(\mathcal{M}) &\longrightarrow \mathcal{T}_p(\mathcal{H}) \\ v &\longmapsto v + (\boldsymbol{l}\cdot v)\,\boldsymbol{k} \end{aligned} \tag{6.3}$$

It is well defined. It leaves invariant any vector in $\mathcal{T}_p(\mathcal{H})$. It satisfies $\boldsymbol{\Pi}(\boldsymbol{k}) = 0$ and $\boldsymbol{\Pi}(\boldsymbol{l}) = \boldsymbol{l}$. Its definition does not depend on the normalization of $\boldsymbol{l}$ and $\boldsymbol{k}$ as long as they satisfy the relation $\boldsymbol{l}\cdot\boldsymbol{k} = -1$; the application is determined only by the foliation $\mathcal{S}_t$ of $\mathcal{H}$ and not by the scale of $\mathcal{H}$'s null normal.

Once introduced the projector $\boldsymbol{\Pi}$ onto $\mathcal{H}$, we can extend the definition of the Weingarten map of $\mathcal{H}$ to all vectors of $\mathcal{T}_p(\mathcal{M})$ by:

$$\begin{aligned} \boldsymbol{\chi} : \mathcal{T}_p(\mathcal{M}) &\longrightarrow \mathcal{T}_p(\mathcal{H}) \\ v &\longmapsto \boldsymbol{\chi}_{\mathcal{H}}(\boldsymbol{\Pi}(v)), \end{aligned} \tag{6.4}$$

where $\boldsymbol{\chi}_{\mathcal{H}}$ denotes de Weingarten map introduced on $\mathcal{T}_p(\mathcal{H})$. Similary, we make use of the projector to extend the definition of the second fundamental form of

$\mathcal{H}$ with respect to the normal $\boldsymbol{l}$ by $\boldsymbol{\Theta} := \boldsymbol{\Pi}^* \boldsymbol{\Theta}_{\mathcal{H}}$, where $\boldsymbol{\Theta}_{\mathcal{H}}$ denotes the second fundamental form of $\mathcal{H}$ with respect to $\boldsymbol{l}$ introduced before; explicitly:

$$\begin{aligned} \boldsymbol{\Theta} : \mathcal{T}_p(\mathcal{M}) \times \mathcal{T}_p(\mathcal{M}) &\longrightarrow \mathbb{R} \\ (u, v) &\longmapsto \boldsymbol{\Theta}_{\mathcal{H}}(\boldsymbol{\Pi}(u), \boldsymbol{\Pi}(v)). \end{aligned} \tag{6.5}$$

Actually, it is nothing but the pull-back of the bilinear form $\nabla \underline{l}$ onto $\mathcal{T}_p(\mathcal{M})$ induced by the projector $\vec{q}$: $\Theta = \vec{q}^* \nabla \underline{l}$. The bilinear form $\boldsymbol{\Theta}$ has at least two degeneracy directions, $\boldsymbol{l}$ and $\boldsymbol{k}$; then, we can conclude that any vector in the plane orthogonal to $\mathcal{S}_t$ is also a degeneracy direction for $\boldsymbol{\Theta}$.

We define the tensor of deformation rate with respect to $\boldsymbol{l}$ of the 2-surface $\mathcal{S}_t$ as half the Lie derivative of $\mathcal{S}_t$'s metric $\boldsymbol{q}$ along the vector field $\boldsymbol{l}$: $\boldsymbol{Q} := 1/2\ {}^{\mathcal{S}}\mathcal{L}_{\boldsymbol{l}}\, \boldsymbol{q}$, where $\boldsymbol{q}$ is considered as a bilinear form field on $\mathcal{S}_t$ and ${}^{\mathcal{S}}\mathcal{L}_{\boldsymbol{l}}$ is the Lie derivative intrinsic to $\mathcal{S}_t$ which arises from the Lie-dragging of $\mathcal{S}_t$ by $\boldsymbol{l}$. It can be deduced that:

$$\boldsymbol{\Theta} - \vec{q}^* \boldsymbol{Q} - \frac{1}{2} \vec{q}^*\, {}^{\mathcal{S}}\mathcal{L}_{\boldsymbol{l}} \boldsymbol{q} - \frac{1}{2} \vec{q}^* \mathcal{L}_{\boldsymbol{l}}\, \boldsymbol{q}. \tag{6.6}$$

Let us split the second fundamental form, now considered as the deformation rate of the 2-surfaces $\mathcal{S}_t$, into a trace part and a traceless part with respect to $\mathcal{S}_t$'s metric $\boldsymbol{q}$:

$$\boldsymbol{\Theta} = \frac{1}{2} \theta \boldsymbol{q} + \boldsymbol{\sigma}, \tag{6.7}$$

where

$$\theta := tr\vec{\boldsymbol{\Theta}}, \tag{6.8}$$

$$\boldsymbol{\sigma} := \boldsymbol{\Theta} - \frac{1}{2} \theta \boldsymbol{q}, \tag{6.9}$$

are the trace of the endomorphism $\vec{\boldsymbol{\Theta}}$ canonically associated with $\boldsymbol{\Theta}$ by the metric $\boldsymbol{g}$ and $\boldsymbol{\sigma}$ is the traceless part of $\boldsymbol{\Theta}$ respectively. The trace θ is called the expansion scalar of $\mathcal{S}_t$ and $\boldsymbol{\sigma}$ the shear tensor of $\mathcal{S}_t$. If we denote by q the determinant of the components of the metric $\boldsymbol{q}$ with respect to the coordinates in $\mathcal{S}_t$, the expansion scalar satisfies $\theta = {}^{\mathcal{S}}\mathcal{L}_{\boldsymbol{l}} \ln \sqrt{q}$, that justifies its name, for $\sqrt{q}$ is related to the surface element ${}^2\epsilon$ of $\mathcal{S}_t$. θ depends only upon the null normal $\boldsymbol{l}$ to $\mathcal{H}$, so the dependence of θ with respect to the foliation $\mathcal{S}_t$ is only

through the normalization of $\boldsymbol{l}$ induced by the $\mathcal{S}_t$ slicing and not on the precise shape of this slicing.

By analogy with the expression (6.6) of $\boldsymbol{\Theta}$, we define the transversal deformation rate of the 2-surface $\mathcal{S}_t$ as the projection onto $\mathcal{T}(\mathcal{S}_t)$ of the Lie derivative of $\mathcal{S}_t$'s metric $\boldsymbol{q}$ along the null transverse vector $\boldsymbol{k}$:

$$\boldsymbol{\Xi} := \frac{1}{2}\vec{\boldsymbol{q}}^{*}\mathcal{L}_{\boldsymbol{k}}\,\boldsymbol{q}, \tag{6.10}$$

where $\boldsymbol{q}$ is considered as 4-dimensional bilinear form, and $\mathcal{L}_{\boldsymbol{k}}\,\boldsymbol{q}$ is its Lie derivative within the 4-manifold $\mathcal{M}$. Since the vector field $\boldsymbol{k}$ does not Lie drag the surfaces $\mathcal{S}_t$, we do not have an object such as the 2-dimensional Lie derivative analog of ${}^{\mathcal{S}}\mathcal{L}_{\boldsymbol{l}}$. It can be deduced that $\boldsymbol{\Xi} = \vec{\boldsymbol{q}}^{*}\boldsymbol{\nabla}\underline{\boldsymbol{k}}$. A rescaling of $\boldsymbol{l}$ acts as follows: $\boldsymbol{l} \to \boldsymbol{l}' = \alpha\boldsymbol{l} \Rightarrow \boldsymbol{\Xi} \to \boldsymbol{\Xi}' = \alpha^{-1}\boldsymbol{\Xi}$.

Similary to the definition of the expansion scalar θ as the trace of the deformation rate $\boldsymbol{\Theta}$, we define the transversal expansion scalar $\theta_{(k)}$ as the trace of $\boldsymbol{\Xi}$

We say that the null hypersurface $\mathcal{H}$ is a non-expanding horizon (NEH) if, and only if, the following properties hold:

(i) $\mathcal{H}$ has the topology of $\mathbb{R}\times\mathbb{S}^2$;

(ii) the expansion scalar θ vanishes on $\mathcal{H}$: $\theta \overset{\mathcal{H}}{=} 0$;

(iii) the matter stress-energy tensor $\boldsymbol{T}$ obeys the null dominant energy condition on $\mathcal{H}$, namely the "energy-momentum current density" vector $\boldsymbol{W} := -\vec{\boldsymbol{T}}\cdot\boldsymbol{l}$ is future directed timelike or null on $\mathcal{H}$.

Properties (ii) and (iii) do not depend upon the choice of a specific null normal $\boldsymbol{l}$; the property of being a NEH is an intrinsic property of the null hypersurface $\mathcal{H}$, and in particular it does not depend upon the space-time foliation by the hypersurfaces Σ_t.

A trapped surface has been defined by Penrose (1965) as a closed (i.e. compact without boundary) spacelike 2-surface $\mathcal{S}$ such that the two systems of null geodesics emerging orthogonally from $\mathcal{S}$ converge locally at $\mathcal{S}$, i.e. they have non-positive scalar expansions. In the present context, demanding that the spacelike 2-surface $\mathcal{S}_t = \mathcal{H}\cap\Sigma_t$ be a trapped surface is equivalent to $\theta \le 0$ and $\theta_{(k)} \le 0$. The subcase $\theta = 0$ or $\theta_{(k)} = 0$ is referred to as a marginally

trapped surface (or simply marginal surface). Penrose's definition is purely local since it involves only quantities defined on the surface $\mathcal{S}$.

According to Hawking [146], an outer trapped surface is an orientable compact spacelike 2-surface $\mathcal{S}$ contained in the future development of a partial Cauchy hypersurface Σ_0 and which is such that the outgoing null geodesics emerging orthogonally from $\mathcal{S}$ converge locally at $\mathcal{S}$. The definition of outgoing null geodesics is based on the asumption of asymptotic flatness. In the present context, demanding that the spacelike 2-surface $\mathcal{S}_t = \mathcal{H} \cap \Sigma_t$ is an outer trapped surface is equivalent to:

(i) the spacelike hypersurface Σ_t is asymptotically flat and the scalar field u defining $\mathcal{H}$ has been chosen so that the exterior or $\mathcal{S}_t$ contains the asymptotically flat region, so that $\boldsymbol{l}$ is an outgoing null normal in the sense of Hawking;

(ii) the expansion scalar of $\boldsymbol{l}$ is negative or null: $\theta \leq 0$.

The subcase $\theta = 0$ is referred to as a marginally trapped surface. This definition does not assume anything on $\theta_{(k)}$.

An apparent horizon was introduced by Hawking [146] and it is defined as a 2-surface $\mathcal{A}$ inside a Cauchy spacelike hypersurface Σ such that $\mathcal{A}$ is a connected component of the outer boundary of the trapped region of Σ. By a trapped region, it is meant the set of points of Σ through which there is an outer trapped surface lying in Σ. It can be deduced that an apparent horizon is a marginally outer trapped surface.

We can connect the above definitions with a NEH: if $\mathcal{H}$ is an NEH in an asymptotically flat spacetime, then each slice $\mathcal{S}_t$ is a marginally outer trapped surface. If, in addition, $\theta_{(k)} \leq 0$, then $\mathcal{S}_t$ is a marginally trapped surface. In general, $\boldsymbol{k}$ being the inward null normal to $\mathcal{S}_t$, $\theta_{(k)}$ is always negative; however, there exist some pathological situations for which $\theta_{(k)} > 0$ at some points of $\mathcal{S}_t$.

6.2 *Trapping horizons in dynamical spacetimes of BHs: inner boundary conditions*

This Section is based on the Refs. [53, 147, 148, 74]. The explicit expressions for the characteristic speeds obtained in Section 5.3 are specially useful in the as-

sessment of the boundary conditions to be imposed on a given boundary. This is illustrated by considering inner boundaries in the context of excised black hole spacetimes. Let us point out that FCF can be employed in combination with any of the standard techniques dealing with the black hole singularity in numerical evolutions of black hole spacetimes, namely excision, punctures, moving punctures or stuffed black holes (see next Section). However, the excision technique is favoured if the elliptic subsystem of the FCF is implemented by means of spectral methods; spectral methods are used in elliptic equations with analytical singularities, but it is difficut to treat numerically non-analytical singularities (and also discontinuities) in the (moving) puncture method (see Section 7.1 for more details).

We are going to consider the problem of inner boundary conditions of trapping horizons of black holes, following Ref. [147]. We are going to identify a quasi-local horizon as a world tube $\mathcal{H}$ of apparent horizons, i.e.:

(i) $\mathcal{H} \approx \mathbb{S}^2 \times \mathbb{R}$ is foliated by marginally trapped 2-surfaces ($\theta = 0$ and $\theta_{(k)} < 0$);

(ii) the condition of future outer trapping horizon, $\mathcal{L}_{\boldsymbol{k}}\,\theta_{(l)} < 0$, has to be verified;

(iii) the condition of dynamical horizon (DH), $\mathcal{H}$ is spacelike, has to be verified.

Given a DH $\mathcal{H}$, the foliation by marginally trapped surfaces is unique, and it defines a unique vector $\boldsymbol{h}$, which can be written as $\boldsymbol{h} = N\boldsymbol{n} + b\boldsymbol{s}$ (see [147]). $\mathcal{H}$ is spacelike as long as $\boldsymbol{h}$ be spacelike, i.e., $b - N > 0$.

A coordinate system adapted to the horizon is one such that $\boldsymbol{t}$ is tangent to $\mathcal{H}$. In a coordinate system all the spheres $\mathcal{S}_t$ stay at the same coordinate position, say $r = \text{const} = r_0$. If we write the decomposition of the shift vector with respect to $\boldsymbol{s}$ as $\boldsymbol{\beta} = \beta^{\perp}\boldsymbol{s} - \boldsymbol{V}$, the condition of $\boldsymbol{t}$ tangent to $\mathcal{H}$ means $\beta^{\perp} = b$; in this case, $\boldsymbol{h}$ spacelike means $\beta^{\perp} - N > 0$.

The previous analysis of the evolution system for h^{ij} can be applied to the inner boundary conditions problem in an excised approach to black hole evolutions. A crucial point in such an approach to black hole evolution is to assess the freedom to impose boundary conditions on the excised surface. To this aim we must determine the characteristics on the excised surface.

We now specify the generic vector ζ^i as the unitary outgoing radial vector on the horizon, s_i. By definition $\beta^{\perp} = \beta^{\mu}s_{\mu}$, so the expressions of the eigenvalues

associated to (5.66) which are not identical to zero are just $\lambda_{\pm}^{(\zeta)} = -\beta^{\perp} \pm N$. Because of the conditions mentioned before, that are linked with the boundary conditions of the elliptic equations, we have $-\beta^{\perp} + N < 0$ on the excised surface (which coincides with the black hole horizon). Since the lapse function is positive, then $-\beta^{\perp} - N < 0$. This shows that the characteristics on the excised surface associated with the vector s^i points outwards with respect to the integration domain. There is a key interplay between the elliptic boundary conditions and the properties of the hyperbolic degrees of freedom. All the equations, elliptic and hyperbolic ones, must be considered as a whole strongly coupled system.

The fact that all the characteristic curves are ingoing into the black hole (or outgoing with respect to the integration domain) is something we could expect from the physical intuition. In consequence, there is no residual freedom in the prescription of the inner boundary conditions of h^{ij} during the evolution. The system is fully determined and we must only guarantee that the values of h^{ij} are consistent with the choice of the Dirac gauge (something that can actually be tricky in the numerical implementation).

Of course, it is not obvious how to choose dynamically an inner boundary $\mathcal{H}$ that is guaranteed to be spacelike during the evolution. One can adopt a coordinate system in order to guarantee $\mathcal{H}$ to be spacelike and the characteristics are still outgoing from the integration domain (see [53] for more details).

7. NUMERICAL BLACK HOLES

7.1 Numerical treatments for BHs

In this section we are going to analyze the different techniques to treat, numerically, the singularity defined by a BH.

7.1.1 Excision method

A tool to treat numerically the black holes has been the excision method [75]. In the 3+1 formalism in which a conformal spatial metric and a conformal factor are introduced,

$$\begin{aligned} \gamma_{ij} &= \psi^4 \tilde{\gamma}_{ij}, \\ K_{ij} &= \psi^{-2} \tilde{K}_{ij}, \end{aligned} \tag{7.1}$$

one question arises, that is what boundary conditions should be imposed to the conformal factor to specify a unique and physically meaningful solution in the elliptic equation for it. We first consider the outer boundary. Asymptotic flatness of the physical space gives $lim_{r\to\infty}\psi = 1$, which suggests taking $\psi = 1$ on the outer boundary. However, there are other alternatives like the one proposed by York and Piran (1982), $\dfrac{\partial\psi}{\partial r} + \dfrac{\psi - 1}{r} = O\left(\dfrac{1}{r^3}\right) \approx 0$, as a more accurate boundary condition, which cancels out the leading $O(M/r)$ term in ψ, where (r, θ, ϕ) stands for the spherical coordinates in the conformal flat metric f_{ij}.

Let us consider the problem of choosing an inner boundary condition for the black hole "surfaces". We first review the approach suggested by Bowen and York (1980) which starts by considering the case of a single black hole only.

The equations for $\tilde{K}_{ij}$ and ψ, are,

$$\tilde{\nabla}^j \tilde{K}_{ij} = 0, \tag{7.2}$$

$$\nabla^2 \psi + \frac{1}{8} \tilde{K}_{ij} \tilde{K}^{ij} \psi^{-7} = 0, \tag{7.3}$$

where $\tilde{\nabla}$ is the connection associated to $\tilde{\gamma}_{ij}$. Bowen (1979) has shown that the previous equation for $\tilde{K}_{ij}$ can be solved analytically through the use of a vector potential. For a single black hole at the origin with momentum P^i and no spin, he gives the solution:

$$\begin{aligned} \tilde{K}_{ij} = & \frac{3}{2r^2} \left[P_i n_j + P_j n_i - (f_{ij} - n_i n_j) P^k n_k \right] \\ & -\kappa \frac{3a^2}{2r^2} \left[P_i n_j + P_j n_i - (f_{ij} - 5 n_i n_j) P^k n_k \right], \end{aligned} \tag{7.4}$$

where n^i is the unit normal vector pointing outwards the 2-sphere of radius r centred at the origin, a is an arbitrary parameter and $\kappa = \pm 1$. For a single black hole at the origin with spin J^i and no linear momentum, Bowen gives the solution:

$$\tilde{K}_{ij} = \frac{3}{r^3} J^l n^k \left(\epsilon_{kil} n_j + \epsilon_{kjl} n_i \right), \tag{7.5}$$

where ϵ_{ijk} is the usual Levi-Civita symbol.

Bowen and York (1980) impose that the space be 3-conformally isometric under the "reflection mapping":

$$r/a \to a/r, \tag{7.6}$$

with a and r defined as in their solutions (7.4) and (7.5), both of which do indeed satisfy this requirement. They then interpret the resulting space as the union of two distinct asymptotically flat spaces, joined at $r = a$ by an Einstein-Rosen bridge which they take as a model for the black hole, as it is shown in Fig. 7.1.

They observe that it suffices to solve (7.3) on only one of these spaces, the "outside"one defined by $r \geq a$, provided that an inner boundary condition enforcing the conformal isometry of the two spaces under the mapping (7.6) is chosen. They propose:

$$\frac{\partial \psi}{\partial r} + \frac{\psi}{2r} = 0, \tag{7.7}$$

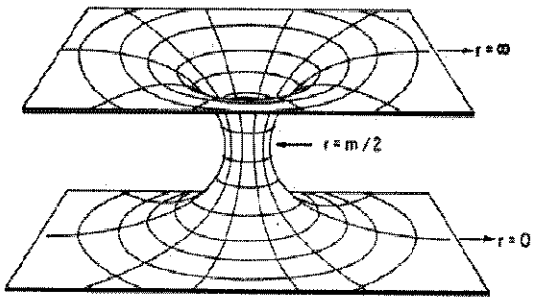

Fig. 7.1: A two-dimensional diagram, similar to the Schwarzschild-Kruskal manifold, is shown isometrically imbedded in flat three-space. The sheets at the top and bottom of the funnel continue to infinity and represent the asymptotically flat regions of the manifold.

at $r = a$ as the desired "reflection symmetric" boundary condition for enforcing this.

York and Piran (1982) [149], Choptuik (1982) [150] and Rauber (1986) [151] have found that the choice of Eq. (7.7) as an inner boundary condition leads to interesting results. However, it has the following drawbacks: first, its generalisation to a space containing multiple black holes is complicated, due to the need of ensuring conformal isometry of the space under a reflection mapping through any of the black hole positions; second, this boundary condition results in the interior of each black hole being in some sense a "mirror image" (common method used also in electrostatics) of the rest of the space, which we consider somewhat unnatural (in the sense that physically it does not have to be symmetric, although numerically is an option): why should the interior of a black hole depend at all on the contents of the "outside world"?

As an alternative boundary condition, Unruh (1984) [152] has suggested requiring that the inner boundary be a marginally trapped surface. This allows the exclusion of black hole interiors from the computational domain. This exclusion of black hole interiors is the key motivation behind this boundary condition, since these interiors cannot causally affect the rest of the space, there is no need to waste grid points by modelling them. This boundary condition

can be extended to spaces containing multiple black holes in a simple way.

Another advantage of excluding black hole interiors from the computational domain is that this also excludes all "censored" singularities. In a time evolution calculation, this relaxes the lapse function N from having to freeze the evolution before hitting a singularity. This should allow the grid stretching near black hole horizons and avoid the problems of stability near the origin. And there is an important practical advantage as well: no computer time has to be wasted evolving black hole interiors.

One difficulty with this boundary condition is that the marginally trapped surface in question may not be an outer trapped surface (apparent horizon). In particular, if we have two black holes close enough together then Čadež (1974) [153] has found that a third (outer) marginally trapped surface forms, enclosing both the inner ones. This outer one is the desired inner grid boundary. One solution to this difficulty is to search the space for any additional marginally trapped surfaces and use the outermost found, if any. According to Thornburg (1987), this search could be quite expensive if it is performed at each time step. However, there is no numerical necessity to search for the outermost marginally trapped surface as inner boundary (Eric Gourgoulhon, private communication). Since black hole interiors cannnot causally influence the rest of spacetime, their exclusion from the computational domain does not affect the well-posedness of the 3+1 equations.

How to choose a suitable set of spatial coordinates for spaces containing multiple (say, two) black holes? The numerical treatment of boundary conditions is much more simple if they occur only at constant coordinate surfaces, so we want that the surface of each black hole be a constant coordinate surface of the coordinate system. We would like our coordinates to approach polar spherical (centred on the black hole's centre) in order to reflect its approximate spherical symmetry. Because of our space is asymptotically flat, we want that our coordinates display the asymptotic spherical symmetry that this implies by approaching polar spherical coordinates at large distances from the strong field region containing the black holes. Our outer boundary grid should be a constant coordinate surface, for the same reasons as the black hole surfaces, and its outward directed normal should be fairly close to a radial one. It is a reasonable requirement too that our coordinate system be free of singularities at least exterior to the black holes.

All the conditions cannot be satisfied by any single coordinate system, that

cannot make a continuous transition form having two spheres as constant coordinate surfaces to only one. One option is to relax the requirement of being free of singularities. For example, using bispherical coordinates place a coordinate singularity at spatial infinity, but these coordinates fail badly to approach polar spherical at large distances from the black holes. One alternative solution is the use of stereographic coordinates. Other alternative solution to the coordinate choice problem could be the use of multiple coordinate patches: spherical ones centred on each black hole, a polar spherical one centred on some convenient origin for the outer region of the numerical grid, and the volume between them can be filled with, for example, a rectangular coordinate one. One has to be cautious with the way to comunicate the patches, i.e., the values of all the variables from one patch to its neighbour ones.

7.1.2 Punctures

Other tool to treat numerically the black holes is the puncture method [76]. The Einstein-Maxwell equations of gravitation and electromagnetism admit many nontrivial solutions of physical interest if the underlying manifold is permitted to have a sufficiently general topology. In particular, these equations have been discussed in multiply connected manifolds, like the maximum analytic continuation of the solution of Schwarzschild for a spherically symmetric geometry endowed with mass and charge. The spatial slice typically consists of two or more copies of $\mathbb{R}^3$ with several spheres removed and identifications of the various spherical inner boundaries, such as it has been explained before. In this way several asymptotically flat regions are obtained that are connected by bridges or throats.

We are going to take into account the conformal metric and the equations (7.1), (7.2) and (7.3). The simplest example comes from the Schwarzschild spacetime in quasi-isotropic coordinates. Considered as a problem on $\mathbb{R}^3$ minus the point $r = 0$, the constraint equations (7.2) and (7.3) are solved:

$$\begin{aligned} \psi &= 1 + \frac{m}{2r}, \\ K_{ij} &= 0, \end{aligned} \tag{7.8}$$

where m is the mass and r the isotropic radius. Conecting with the above throat picture, it exists an isometry given by $r \to m^2/4r$ which leaves the coordinate

sphere $r = m/2$ invariant and which maps the entire exterior asymptotically flat space into that sphere. Consequently, there exists a second asymptotically flat region near $r = 0$. Equivalently, one can display this solution to the constraints on a space consisting of two copies of $\mathbb{R}^3$ with a sphere excised and appropriate identification at the spheres.

For several black holes and nonvanishing extrinsic curvature, York et al. (J. York, in *Frontiers in Numerical Relativity*, 1989) have developed a sophisticated method to solve the constraints for two asymptotically flat spaces that are connected by as many throats as black holes, and that are isometric copies of each other. Note that there are explicit solutions to the momentum constraint (7.2) that characterize a single black hole with a given momentum $\boldsymbol{P}^i$, and spin $\boldsymbol{S}^i$, as the ones mentioned before, or, for example, the Bowen-York solution:

$$\begin{aligned} K^{ij}_{PS} &= \frac{3}{2r^2}\left[P^i n^j + P^j n^i - \left(\gamma^{ij} - n^i n^j\right) P^k n_k\right] \\ &\quad + \frac{3}{r^3}\left(\epsilon^{ikl} S_k n_l n^j + \epsilon^{jkl} S_k n_l n^i\right). \end{aligned} \tag{7.9}$$

By the method of images it is possible to obtain an infinite series based on the previous equation for K^{ij} which solves the momentum constraint and satisfies an isometry condition at any number of spheres. Given such a solution, one has to solve the equation (7.3), which is an elliptic equation on $\mathbb{R}^3 - S^n$ ($\mathbb{R}^3$ minus several spheres), with the inner boundary given by the isometry and the outer boundary determined by asymptotic flatness. The approach is very complicated for numerical implementations.

Let us return to the Schwarzschild solution of the constraints on a "punctured" $\mathbb{R}^3$. As noted by Misner and Wheeler [154] and studied in detail by Brill and Lindquist [155] (MWBL), the Schwarzschild solution to the constraints generalizes trivially to N black holes for time symmetry:

$$\begin{aligned} \psi &= 1 + \sum_{i=1}^{N} \frac{m_{(i)}}{2\left|\vec{r} - \vec{r}_{(i)}\right|}, \\ K_{ij} &= 0, \end{aligned} \tag{7.10}$$

where $m_{(i)}$ characterizes the mass and $\vec{r}_{(i)}$ is the location of the ith black hole. For regularity of the conformal factor, the MWBL solution is considered on a

single $\mathbb{R}^3$ with the points $\vec{r} = \vec{r}_{(i)}$ removed. We refer to the $\vec{r}_{(i)}$ as punctures. The isometry present in the Schwarzschild solution is lost, although there still exist minimal surfaces characterizing the throats [155].

An idea to find data for multiple black holes with arbitrary boosts and spins is to compactify the internal asymptotically flat regions in order to obtain a simple domain of integration. We solve the momentum constraint by setting:

$$K^{ij} = \sum_{i=1}^{N} K^{ij}_{PS(i)}, \tag{7.11}$$

where each term is defined by (7.9) with its own origin $\vec{r}_{(i)}$, momentum $\vec{\boldsymbol{P}}_{(i)}$, and spin $\vec{\boldsymbol{S}}_{(i)}$. These parameters correspond to the 3+1 quantities in the limit that the separation of the holes is very large. The equation (7.2) defines the solution to the momentum constraint, and it is not just the starting point for the method of images that is usually used to obtain an isometric solution.

Given K^{ij}, we solve the Hamiltonian constraint (7.3). We rewrite the conformal factor in terms of functions α and u given by:

$$\begin{aligned} \psi &= \frac{1}{\alpha} + u, \\ \frac{1}{\alpha} &= \sum_{i=1}^{N} \frac{m_{(i)}}{2\left|\vec{r} - \vec{r}_{(i)}\right|}. \end{aligned} \tag{7.12}$$

On the punctured $\mathbb{R}^3$, the Laplacian of $1/\alpha$ is zero. The Hamiltonian constraint equation becomes:

$$\Delta u + \beta \left(1 + \alpha u\right)^{-7} = 0, \tag{7.13}$$

$$\beta = \frac{1}{8}\, \alpha^7 K^{ij} K_{ij}. \tag{7.14}$$

And we have to specify boundary conditions for u. For asymptotic flatness at infinity we require $u - 1 = O\left(r^{-1}\right)$ for large distances to the punctures. And the key question is what condition we want to impose on u close to the punctures. To build in asymptotically flat regions, as are present in the MWBL data near the punctures, it suffices to solve (7.13) everywhere on $\mathbb{R}^3$ without any points excised.

It can be shown that there exists a unique solution for the conformal factor $\psi = u + 1/\alpha$ on the puncture $\mathbb{R}^3$. Given a solution u, each puncture represents the "point at infinity" for another asymptotically flat spacetime; solving (7.13) on $\mathbb{R}^3$ involves a particular compactification of N out of $N+1$ asymptotically flat regions, one of which is distinguished by our choice of K^{ij}.

By comparision with the isometric wormhole approach, the MWBL one has two numerical advantages. The solution K^{ij} to the momentum constraint is all the information that we need, i.e., since we do not impose the isometry condition there is no need for the method of images. And second, in the solution of the Hamiltonian constraint we avoid the numerical complications due to an inner boundary. The punctures can be part of the numerical grid since there are no physical singularities on the initial slice. For a long term evolution of black holes, one may start with data obtained by either the throat or puncture construction, and then cut out the interior regions at the apparent horizon to avoid the physical singularities on future slices.

7.1.3 Moving punctures

The black hole binary evolutions in numerical relativity have been solved in 2005 by several groups. The easiest method to implement, and currently the most popular, is the "moving puncture" approach; details of this method can be found in [77]. One starts with initial data that possess a Brill-Lindquist wormhole topology [155] and each asymptotic end is compactified to a single point on $\mathbb{R}^3$ called puncture, such as it has been explained previously. They represent black holes on $\mathbb{R}^3$ without excision. The initial data slices avoid the curvature singularity of each black hole. It is well understood how to construct puncture initial data for any number of boosted, spinning black holes. It can be crucial in successful numerical techniques the choice of the particular formulation of the evolution equations, gauge conditions and, most important, the treatment of the coordinate singularity at each puncture.

Before the "moving punctures", "fixed puncture" evolutions factored the singularity into a fixed analytically prescribed conformal factor and a regular function f that is evolved numerically. The apparent problem with the conformal factor is that it diverges at the puncture, and will presumably behave in a pathological way if it would be evolved directly. In "fixed puncture" evolutions one avoids this problem by writing the initial isotropic Schwarzschild conformal

factor as we have mentioned in the last Section:

$$\psi = \left(1 + \frac{M}{2r}\right) f, \tag{7.15}$$

where $f = 1$ only at the beginning of the evolution. The evolution of f keeps the divergent part fixed. The method is tailored so that the wormhole topology remains throughout the evolution. This means that even in black hole binary simulations, where the black holes have physical motion, the punctures are kept fixed on the grid.

These methods met with some success, but long-term stable evolutions of general configurations of black hole binaries, specially orbiting, were not achieved. The only detailed analytical study of the properties of fixed puncture evolutions, applied to the Schwarzschild spacetime, showed that such evolutions would never reach a stationary state: nontrivial evolution of the slices of Schwarzschild would continue indefinitely. One way of seeing this is that if they did, the lapse would have to pass through zero at the throat, but the slicing choices used in puncture evolutions preclude this.

Recently two groups [80, 81] independently introduced similar methods to deal with the puncture singularities. The singular conformal factor ψ is evolved without any analytical assumptions, by introducing a new auxiliary variable, either $\chi = \psi^{-4}$ in [80] or $\phi = ln\psi$ in [81], and the punctures are able to move on the numerical grid. Both variables behave sufficiently well at the puncture to allow stable evolutions. These methods have met with spectacular success, and the "moving puncture" method is now the most popular one for evolving black hole binaries.

When the first results obtained using moving punctures were published, some questions were raised. What happens to the punctures during the evolution? Does the evolution reach a final, stationary state, or do gauge dynamics persist, as in the fixed puncture case? Is the method accurate or it may fail at higher resolutions or for longer evolutions? Hannam et al. (gr-qc/0606099) studied moving puncture evolutions of the Schwarzschild spacetime, and they showed that the evolution quickly reaches a stationary state.

7.1.4 Stuffed BHs

This is a simple method based on the fact that no physical information can escape from the interior of a BH. The method consists on smoothing the interior of each BH with arbitrary data. This change in the interior of the BH can generate constraint violations, and the form of the equations must not allow constraint violations to propagate outside. The method has to guarantee that the evolutions will proceed to a smooth, regular end-states. Different versions of this method have been used by Bona and collaborators [156, 157, 158], Misner [159], or Brown et al. [160] more recently, for example.

7.2 BBHs evolutions

In 2004, Bruegmann et al. [78] presented numerical simulations of BBH system for about one orbital period. Since then, there are eight groups that have successfully performed long-term evolutions of BBHs covering several orbits, [80, 81, 79, 82, 83, 84, 85, 86]. Six of them use moving punctures; this shows the power of this technique. We are going to comment briefly the main ingredients of their codes.

Pretorius, [79]

He has obtained stable binary black hole merger evolutions. The main features of his code are:

(i) A generalized harmonic formulation of the field equations.

(ii) A discretization scheme where the only evolved quantities are the covariant metric elements and harmonic source. This procedure minimizes the number of constraint equations that need to be solved.

(iii) The use of a compactified coordinate system where the outer boundaries of the grid are at spatial infinity, hence the physically correct boundary conditions can be placed there.

(iv) The use of adaptive mesh refinement to adequately resolve the relevant length scales in the problem.

(v) Dynamical excision that tracks the motion of the black holes through the grid.

(vi) Addition of numerical dissipation to control high-frequency instabilities.

(vii) A time slicing that slows down the "collapse"of the lapse function that would otherwise occur in a pure harmonic time slicing.

(viii) The addition of "constraint-damping"terms to the field equations. These terms have a significant effect on how long a simulation with black holes can run with reasonable accuracy at a given resolution.

Pretorius discretizes the Einstein field equations written in the following form:

$$g^{\delta\gamma}g_{\alpha\beta,\gamma\delta} + g^{\gamma\delta}_{,\beta}g_{\alpha\delta,\gamma} + g^{\gamma\delta}_{,\alpha}g_{\beta\delta,\gamma} + 2H_{(\alpha,\beta)} - 2H_\delta\Gamma^\delta_{\alpha\beta} + 2\Gamma^\gamma_{\delta\beta}\Gamma^\delta_{\gamma\alpha} = -8\pi\left(2T_{\alpha\beta} - g_{\alpha\beta}T\right) - \kappa\left(n_\alpha C_\beta + n_\beta C_\alpha - g_{\alpha\beta}n^\gamma C_\gamma\right). \quad (7.16)$$

H_μ are source functions encoding the gauge freedom of the solution, $\Gamma^\delta_{\alpha\beta}$ are the Christoffel symbols, $T_{\alpha\beta}$ is the energy-momentum tensor with trace T, κ is a positive constant multiplying the new constraint-damping terms, $n^\mu = N^{-1}\left(\partial_t - \beta^i\partial_i\right)^\mu$ is the unit hypersurface normal vector with lapse function N and shift vector β^i, and C_μ are the constraints, $C_\mu \equiv H_\mu - g_{\mu\nu}\Box\, x^\nu$. In order to evolve the source functions, Pretorius uses the following equation:

$$\Box\, H_t - -\xi_1\frac{N-1}{N^\eta} + \xi_2 H_{t,\nu}n^\nu,\ H_i - 0, \quad (7.17)$$

where ξ_1 and η are positive constants, and ξ_2 an arbitrary one. Let us draw reader's attention to the fact that (7.17) is not the usual definition of spatial harmonic gauge. He uses black hole excision, whereby portions of the computational domain inside apparent horizons are excised to remove the singularities, and aparent horizon finder. The initial spatial metric and its first time derivative is conformally flat, and he specifies a slice that is maximal and harmonic. The Hamiltonian constraint is used to solve the conformal factor, the maximal conditions give the initial time derivative of the conformal factor and an elliptic equation for the lapse, the momentum constraints are used to solve the initial values of the shift vectors. The harmonic conditions are used to specify the initial first time derivatives for the lapse and shift.

Texas' group, [80]

They use the BSSN formulation. The metric on the initial slice is given by a conformal flat metric, $\gamma_{ij} = (\psi_{BL} + u)^4 \delta_{ij}$, with a Brill-Lindquist conformal factor ψ_{BL} as in (7.12). They use a unigrid high-order finite-difference code along with a nonuniform coordinate system that concentrates grid points in the central region containing the black holes in order to get highly accurate evolutions. They evolve a conformal metric, the conformal trace-free extrinsic curvature, the conformal exponent and the variables $\tilde{\Gamma}^i$ of the BSSN formulation. In order to regularize the system near the puncture, they replace the conformal exponent by the variable $\chi = \psi^{-4}$. They choose an initial lapse function equal to ψ_{BL}^{-2} which is $O\left(r^2\right)$, and the following gauge conditions:

$$\partial_t N = -2NK, \tag{7.18}$$

$$\partial_t \beta^i = B^i,\ \partial_t B^i = 3/4 \partial_t \tilde{\Gamma}^i - \eta B^i, \tag{7.19}$$

where η is an arbitrary parameter. At the pucnture χ vanishes, and the equation of its evolution implies that the puncture position obeys $\partial_t \vec{x}_{punct} = -\vec{\beta}\left(\vec{x}_{punct}\right)$. Texas' group track the puncture positions throughout the evolution by integrating this equation. Since the centers of the black holes remain in the $z = 0$ plane, they do not pass through grid points placed in the cell-centers.

NASA's group, [81]

They use the conformal flat metric with the same conformal factor as Texas' group, ψ_{BL}. They allow the punctures to move freely through the grid with initial data puncture technique. The centers of the black holes remain in the $z = 0$ plane and do not pass through grid points. They use a modified version of a common coordinate condition known as the Gamma-freezing shift vector. Specifically, they use:

$$\partial_t \beta^i = \frac{3}{4} B^i,\ \partial_t B^i = \partial_t \tilde{\Gamma}^i - \beta^j \partial_j \tilde{\Gamma}^i - \eta B^i, \tag{7.20}$$

where η is an arbitrary parameter (no related in principle with the η parameter of Texa's group); along with this shift condition, they use the standard singularity-avoiding 1+log slicing condition on the lapse N.

Penn State's group, [82]

The initial data are construted via the puncture method. The initial spatial metric is conformally flat, maximally sliced, and the extrinsic curvature is given by the Bowen-York solution to the momentum constraint; the conformal factor ψ is used to set the initial lapse as $N = \psi^{-2}$, while the initial shift is $\beta^i = 0$. The evolutions were carried out with a code based on the BSSN 3+1 formulation. The gauge conditions used were modified versions of the 1+log lapse and Γ-driver shifts, (7.18) and (7.20). These gauge choices were found to be important for long-term stable and accurate evolutions on head-on collisions without excision. They use mesh refinement.

U. Sperhake, [83]

He uses a BSSN formulation. He starts with a time-symmetric initial configuration of multiple black holes Brill-Lindquist data, or a superposed Kerr-Schild data. The gauge variables are evolved according to:

$$\partial_t N = \beta^i \partial_i N - 2NK; \tag{7.21}$$

$$\partial_t \beta^i = B^i,\ \partial_t B^i = \partial_t \tilde{\Gamma}^i - \eta B^i. \tag{7.22}$$

Initially, he has experimented with $\eta = 2$ but the choice $\eta = 1$ cures an instability in the outermost boundary. These gauge conditions make more easy a method to track the black hole position; the coordinate velocity of the puncture is given by $\dfrac{dx^i}{dt} - -\beta^i$. He prescribes analytic trajectories for the two black holes and calculates the resulting gauge functions by superposing the analytic gauge of the individual holes. He uses excision method in order to evolve the initial data and a horizon finder to track the black hole motion and to move accordingly the excision region.

CalTech/Cornell group, [84]

They use two distinct coordinate systems; tensors like the metric are represented by their components in the coordinate basis of the first one, and Einstein equations are used to determine these tensor components as functions of the second coordinate system. The method applies to the generalized harmonic form of the Einstein equations. The gauge freedom is represented by four

freely specifiable gauge source functions H_μ, which determine the evolution of the lapse and shift. The harmonic constraint equation $0 = \mathcal{C}_\mu := \Gamma_\mu + H_\mu$ must be satisfied. They use spectral methods. In their approach the black holes move across the coordinate grid. They evolve Schwarzschild initial data with uniformly rotating coordinates. For this test, the inertial coordinates are the standard asymptotically Cartesian ones associated with the Kerr-Schild representation of the Schwarzschild geometry, and the other coordinates rotate uniformly with respect to these inertial coordinates. The second one allows them to track the motion of the individual black holes in a binary through a feedback control system. The coordinate maps could be constructed in such a way that keep the shape of the apparent horizons spherical and their locations close to the excision boundary.

Jena's group, [85]

They use the moving puncture method of simulating black hole spacetimes without excision and use moving boxes mesh refinement. They model N-black hole initial data by adopting the Brill-Lindquist wormhole topology with $N+1$ asymptotically flat ends for our initial geometry, thus enforcing the presence of N throats. The asymptotically flat ends are compactified and identified with points. They use a conformal flat metric and maximal slicing. As initial values for the lapse and shift they regard $N = 1$ or $N = \psi^{-2}$, and $\beta^i = 0$. They evolve the initial data with the BSSN system. The entire conformal factor is evolved in the moving puncture approach like in [80], where the singularity is not cut out of the numerical grid, it is avoided by the choice of gauge. The choices of the gauge are:

$$\partial_t N = -2NK, \tag{7.23}$$

$$\partial_t \beta^i = \frac{3}{4} B^i,\ \partial_t B^i = \partial_t \tilde{\Gamma}^i - \eta B^i, \tag{7.24}$$

where η is an arbitrary parameter (no related in principle with η parameter of previous groups).The hierarchy of boxes in the mesh refinement evolves as the punctures move. They use the shift to track the position of a puncture by integrating the expression $\partial_t x^i_{punct} = -\beta^i \left(x^i_{punc}\right)$.

AEI's group, [86]

They use BSSN formulation of Einstein equations where the constraints are not actively enforced during the evolution. They use as dynamic gauge conditions the Bona-Massó slicing, Γ-driver shift and co-rotating frame:

$$\partial_t N - \beta^j \partial_j N = -N^2 f(N) K, \tag{7.25}$$

$$\partial_t \beta^i - \beta^j \partial_j \beta^i = \frac{3}{4} B^i,\ \partial_t B^i - \beta^j \partial_j B^i = \partial_t \tilde{\Gamma}^i - \beta^j \partial_j \tilde{\Gamma}^i - \eta \beta^i, \tag{7.26}$$

where η is an arbitrary parameter (no related in principle with η parameter of previous groups). AEI's group uses the moving puncture method, and apply a smoothing to the initial data in order to avoid singularities in the case that the punctures are positioned on a grid point. They use mesh refinement, and determine the horizon location during an evolution.

8. IMPLEMENTING A NEW CODE

The numerical work we are going to explain in this chapter is part of a middle term program aiming at extending CoCoNuT's code [87] to evolve numerically dynamical spacetimes, in the FCF of Einstein equations, and matter fields, including not only perfect fluids but magnetic fields too. According to FCF of Einstein equations (see Chapter 5), we are going to evolve the second order system for the deviations with respect to the flat metric, h^{ij}, viewed as a quasi-linear first order system for these quantities and their first derivatives (5.66), (5.102) and (5.110). Main assumption is: the lapse function, the shift vector, the conformal factor and the components of the energy-momentum tensor will be regarded as given parameters, i.e., all these quantities are frozen during the evolution and they will not be influenced by the conformal spatial metric (equivalently by h^{ij}) but will influence it (no back reaction of h^{ij} on the rest of equations). In this assumption, the values of these fields could be given from numerical simulations in which we do not take into account the conformal metric or simply they could come from analytical expressions. In the general case, all the set of variables will be evolved numerically, the conformal metric, the rest of components of the metric, and the components of the energy-momentum tensor containing the matter fields. In Section 8.1 we describe theenical details of the code. Section 8.2 is devoted to discuss the code testing. Geometrical units ($G = c = 1$) will be used in the simulations.

8.1 Structure of the code

According to the previous mathematical properties of the system studied in Section 5.3, we know that it is linearly degenerate (5.91) and therefore there can not appear shock waves, as one expect from the physical intuition about the variables representing the metric of the spacetime. That is the reason why

in the numerical scheme we are going to build up we are not going to use HRSC schemes unlike in the case of numerical hydrodynamics. The spatial derivatives are treated with standard finite differences of different orders of accuracy, and the time evolution with Runge-Kutta (RK) methods having the property of preserving TVD conditions (see below).

Coordinate system

A coordinate system of spherical type is introduced, (r, θ, φ), where $r \in [0, +\infty)$, $\theta \in [0, \pi]$ and $\varphi \in [0, 2\pi)$. The components of the flat metric f_{ij} with respect to these coordinates are:

$$f_{ij} = \mathrm{diag}\left(1, r^2, r^2 \sin^2\theta\right). \tag{8.1}$$

Its determinant is $f = r^4 \sin^2\theta$. From the natural vector basis associated with the previous system of coordinates, $\left(\partial/\partial x^i\right) = (\partial/\partial r, \partial/\partial\theta, \partial/\partial\varphi)$, the following vector fields are constructed:

$$\left(\boldsymbol{e}_r := \frac{\partial}{\partial r}, \boldsymbol{e}_\theta := \frac{1}{r}\frac{\partial}{\partial\theta}, \boldsymbol{e}_\varphi := \frac{1}{r\,\sin\theta}\frac{\partial}{\partial\varphi}\right). \tag{8.2}$$

This basis is orthonormal with respect to the flat metric $\boldsymbol{f}$: $f_{\hat{i}\hat{j}} = \mathrm{diag}\,(1,1,1)$.

Given a tensor field $\boldsymbol{T}$ of type $\binom{p}{q}$, the components of the covariant derivative $\mathcal{D}\boldsymbol{T}$ in the orthonormal basis $e_{\hat{i}_1} \otimes \ldots \otimes e_{\hat{i}_p} \otimes \ldots \otimes e^{\hat{j}_1} \otimes \ldots \otimes e^{\hat{j}_q} \otimes e^{\hat{k}}$ are given by (see [111]):

$$\begin{aligned}\mathcal{D}_{\hat{k}} T^{\hat{i}_1\ldots\hat{i}_p}{}_{\hat{j}_1\ldots\hat{j}_q} &= e_{\hat{k}}^{\ l}\frac{\partial}{\partial x^l} T^{\hat{i}_1\ldots\hat{i}_p}{}_{\hat{j}_1\ldots\hat{j}_q} \\ &\quad + \sum_{r=1}^{p} \hat{\Gamma}^{\hat{i}_r}{}_{\hat{l}\hat{k}} T^{\hat{i}_1\ldots\hat{l}\ldots\hat{i}_p}{}_{\hat{j}_1\ldots\hat{j}_q} - \sum_{r=1}^{q} \hat{\Gamma}^{\hat{l}}{}_{\hat{j}_r\hat{k}} T^{\hat{i}_1\ldots\hat{i}_p}{}_{\hat{j}_1\ldots\hat{l}\ldots\hat{j}_q}\end{aligned} \tag{8.3}$$

where $e_{\hat{k}}^{\ l} := \mathrm{diag}\,(1, 1/r, 1/(r\sin\theta))$ is the change-of-basis matrix defined by (8.2), and the $\hat{\Gamma}^{\hat{k}}{}_{\hat{i}\hat{j}}$ are the connection coefficients of $\mathcal{D}$ associated with the orthonormal frame (8.2); these coefficients all vanish, except for

$$\hat{\Gamma}^{r}{}_{\theta\theta} = -\hat{\Gamma}^{\theta}{}_{r\theta} = -r^{-1},\ \hat{\Gamma}^{r}{}_{\varphi\varphi} = -\hat{\Gamma}^{\varphi}{}_{r\varphi} = -r^{-1},\ \hat{\Gamma}^{\theta}{}_{\varphi\varphi} = -\hat{\Gamma}^{\varphi}{}_{\theta\varphi} = -\left(r\tan\theta\right)^{-1}. \tag{8.4}$$

Notice that this choice has the consequence of the non-symmetry of the connection symbols in the development of the covariant derivatives with respect to the flat metric that appear in the equations (5.66), (5.102) and (5.110). Expressions of covariant derivatives for tensors of several types are developed in Appendix B.

Symmetries and inner boundaries

The code has axisymmetry with respect to an axis that defines an equatorial plane; the code has equatorial symmetry with respect to the equatorial plane too. This is translated into the independence of the components of the conformal metric with respect to the coordinate φ and the use of only two coordinates (r, θ), with $0 \leq r$ and $0 \leq \theta \leq \pi/2$. Moreover, inner boundary conditions have to be imposed across the center, defined by $r = 0$, the polar axis, defined by $\theta = 0$, and the equatorial plane, defined by $\theta = \pi/2$. These inner boundary conditions are imposed with the help of auxiliary grid points and the knowledge of the symmetries of the components of the conformal spatial metric in those boundaries. The extra grid points included as auxiliary ones are placed at $-\epsilon \leq r < 0$ and $\pi/2 < \theta \leq \pi/2+\epsilon$, with ϵ a small quantity depending on the order of the finite differences scheme used for the spatial partial derivatives.

In these extra grid points, each component of the conformal spatial metric is mirrored either symmetrically or antisymmetrically across a symmetry boundary, depending on whether it should be continuous across the boundary or zero at the boundary. For a generic quantity q representing one of the components, and the subindices denoting the numbered grid points for (r, θ) from 1 to n_r or n_θ, the following notation is used:

$$q_{1-l,j} = \pm q_{l,j}, \tag{8.5}$$

$$q_{i,1-l} = \pm q_{i,l}, \tag{8.6}$$

$$q_{i,n_\theta+l} = \pm q_{i,n_\theta-l+1}, \tag{8.7}$$

for $l \in \{1, 2 \ldots\}$ and

$$\pm = \begin{cases} + & \text{symmetric,} \\ - & \text{antisymmetric.} \end{cases} \tag{8.8}$$

(8.5) corresponds to the inner boundary at the center, (8.6) to the polar axis and (8.7) to the equatorial plane.

The symmetry conditions for the tensor quantities are nontrivial. The components of the "physical" velocities in a spherical type coordinate system, that are going to be denoted by stars and subindices r, θ, φ, are related with the covariant components of the velocities for the orthonormal basis [161], denoted by the superindices r, θ, φ, through the conformal factor and the scalars that define the coordinate system:

$$v_r^* = \psi^2 v^r, \tag{8.9}$$
$$v_\theta^* = \psi^2 v^\theta, \tag{8.10}$$
$$v_\varphi^* = \psi^2 v^\varphi. \tag{8.11}$$

We know the symmetries for the physical velocities at all the inner boundaries, and we can deduce the symmetries for the components of the velocities for the orthonomal basis:

	v_r^*	v_θ^*	v_φ^*	v^r	v^θ	v^φ
center	$-$	$-$	$-$	$-$	$-$	$-$
axis	$+$	$-$	$-$	$+$	$-$	$-$
equator	$+$	$-$	$+$	$+$	$-$	$+$

Following [111], it is shown that the behaviour of the time derivatives of components for the deviations of the conformal metric with respect to the flat metric is the same as for the traceless part of the extrinsic curvature, $\partial_t h^{ij} \sim A^{ij}$. The behaviour for the time derivative of the traceless part of the extrinsic curvature is the same as for the strain tensor, that is the same as the product of the velocities, $\partial_t A^{ij} \sim S^{ij} \sim v^i v^j$. Due to the fact that the spatial symmetries we need do not depend on the partial derivatives with respect to t, we conclude that the components of the following quantities have the same behaviour: $h^{ij} \sim v^i v^j$. With the known symmetries for v^i, the ones for h^{ij} are:

	center	axis	equator
h^{rr}	$+$	$+$	$+$
$h^{r\theta}$	$+$	$-$	$-$
$h^{r\varphi}$	$+$	$-$	$+$
$h^{\theta\theta}$	$+$	$+$	$+$
$h^{\theta\varphi}$	$+$	$+$	$-$
$h^{\varphi\varphi}$	$+$	$+$	$+$

Partial derivatives with respect to r (to θ), or powers of r (of θ), change the symmetries at the center (at the axis and the equator). Partial derivatives with respect to φ change the symmetries at the equator. From the expressions of the covariant derivatives the behaviour of the quantities are summarized in the following tables:

	center	axis	equator
u^{rr}	+	+	+
$u^{r\theta}$	+	−	−
$u^{r\varphi}$	+	−	+
$u^{\theta\theta}$	+	+	+
$u^{\theta\varphi}$	+	+	−
$u^{\varphi\varphi}$	+	+	+

	center	axis	equator
$\hat{A}^{rr}$	+	+	+
$\hat{A}^{r\theta}$	+	−	−
$\hat{A}^{r\varphi}$	+	−	+
$\hat{A}^{\theta\theta}$	+	+	+
$\hat{A}^{\theta\varphi}$	+	+	−
$\hat{A}^{\varphi\varphi}$	+	+	+

	center	axis	equator
w_r^{rr}	−	+	+
w_θ^{rr}	−	−	−
w_φ^{rr}	−	−	+
$w_r^{r\theta}$	−	−	−
$w_\theta^{r\theta}$	−	+	+
$w_\varphi^{r\theta}$	−	+	−
$w_r^{r\varphi}$	−	−	+
$w_\theta^{r\varphi}$	−	+	−
$w_\varphi^{r\varphi}$	−	+	+
$w_r^{\theta\theta}$	−	+	+
$w_\theta^{\theta\theta}$	−	−	−
$w_\varphi^{\theta\theta}$	−	−	+
$w_r^{\theta\varphi}$	−	+	−
$w_\theta^{\theta\varphi}$	−	−	+
$w_\varphi^{\theta\varphi}$	−	−	−
$w_r^{\varphi\varphi}$	−	+	+
$w_\theta^{\varphi\varphi}$	−	−	−
$w_\varphi^{\varphi\varphi}$	−	−	+

Although r extends to infinity, the numerical domain ends at a finite radius where one has to impose outer boundary conditions. A Sommerfeld-like outer boundary condition has been implemented, but one has to be careful with the problems that can appear (see below in this chapter).

Grid

A regular grid in θ is used, being $\Delta\theta$ the spacing of grid points or cell size in the θ-direction. If $[0, \pi/2]$ is discretized by n_θ equally spaced grid points, then $\Delta\theta = \dfrac{\pi/2}{n_\theta - 1}$. A logarithmic grid is used in the radial direction; the spacing of grid points or cell size in this direction increases according to an amplification factor, f. If $[r_{\rm inner}, r_{\rm outer}]$ is discretized by n_r grid points, then Δr takes the values $\Delta r_{\rm innner}\, f^p$, with $\Delta r_{\rm inner}$ being the inner radial spacing, f satisfying $\dfrac{f^{n_r} - f}{f - 1} = \dfrac{r_{\rm outer}}{\Delta r_{\rm inner}}$, and $p = 1, \ldots n_r - 1$. The outer radial spacing is then $\Delta r_{\rm outer} = \Delta r_{\rm inner} f^{n_r - 1}$. The value $f = 1$ corresponds to a regular radial grid. A regular grid in t is used, being Δt the spacing of grid points in the t-direction.

A logarithmic grid is used with the corresponding amplification factor in each possible domain (depending on the requirements of number of domains of the simulation). The amplification factor, f, and the number of radial points, n_r, in a given subinterval can be calculated from the inner and outer radii of the region, $r_{\rm inner}$ and $r_{\rm outer}$ respectively, and the corresponding cell size chosen, $\Delta r_{\rm inner}$ and $\Delta r_{\rm outer}$ respectively, as

$$f = \frac{r_{\rm outer} - r_{\rm inner} - \Delta r_{\rm inner}}{r_{\rm outer} - r_{\rm inner} - \Delta r_{\rm outer}}, \quad n = \frac{\log\left(\frac{\Delta r_{\rm outer}}{\Delta r_{\rm inner}}\right)}{\log f} + 1. \tag{8.12}$$

The points of the mesh are positioned on the $r - \theta$ plane at $\left(r_{\rm inner} + \Delta r_{\rm inner}\dfrac{f^{i-1} - 1}{f - 1}, j\,\Delta\theta\right)$, with $i = 1, \ldots n_r$, $j = 1, \ldots n_\theta$. The discrete values of a function $u(r, \theta, t)$ at $\left(r_{\rm inner} + \Delta r_{\rm inner}\dfrac{f^{i-1} - 1}{f - 1}, j\,\Delta\theta, t^n \equiv n\Delta t\right)$ will be denoted by $u^n_{i,j}$.

The m^{th}-order spatial partial derivative uses a central difference scheme which couples $m + 1$ adjacent points. The values for m used are $m = 1, \ldots, 4$.

The necessity of extra grid points comes from calculating spatial partial derivatives close to the boundaries.

RK methods for the evolution

Numerical methods based on a nonlinear stability requirement are very desirable. Such methods were originally named total variation diminishing (TVD) and are also referred to as strong stability preserving (SSP) methods. If $U = U(t)$ is a vector of discretized variables, i.e., $[U(t)]_j = U_j(t) = u(x_j, t)$, and u_j^n is the numerical approximation to $u(x_j, t_n)$, then TVD discretizations have the property that the total variation

$$TV(U^n) = \sum_j \left| u_j^n - u_{j-1}^n \right| \tag{8.13}$$

of the numerical solution does not increase with time, i.e.,

$$TV\left(U^{n+1}\right) \leq TV(U^n). \tag{8.14}$$

A sequence $\{U^n\}$ is said to be strongly stable in a given norm $\|\cdot\|$ provided that $\left\|U^{n+1}\right\| \leq \|U^n\|$ for all $n \geq 0$. The choice of the norm is arbitrary, being the TV-norm, and the infinity norm, two natural possibilities.

A s-stage, explicit RK method for the equation $\partial_t U = L(U)$ is written in the form:

$$\begin{aligned} U^{(0)} &= U^n, \\ U^{(i)} &= \sum_{k=0}^{i-1} \left(\alpha_{ik} U^{(k)} + \Delta t \beta_{ik} L\left(U^{(k)}\right) \right), \ i = 1, 2, \ldots, s, \\ U^{n+1} &= U^{(s)}, \end{aligned} \tag{8.15}$$

where all the $\alpha_{ik} \geq 0$ and $\alpha_{ik} = 0$, only if $\beta_{ik} = 0$.

RK-TVD methods of first, second, third and fourth order have been derived. The second one

$$\begin{aligned} U^{(0)} &= U^n, \\ U^{(1)} &= U^n + \Delta t L(U^n), \\ U^{n+1} &- \frac{1}{2} U^n + \frac{1}{2} U^{(1)} + \frac{1}{2} \Delta t L\left(U^{(1)}\right), \end{aligned} \tag{8.16}$$

and the third one

$$\begin{aligned} U^{(0)} &= U^n, \\ U^{(1)} &= U^n + \Delta t L\left(U^n\right), \\ U^{(2)} &= \frac{3}{4}U^n + \frac{1}{4}U^{(1)} + \frac{1}{4}\Delta t L\left(U^{(1)}\right), \\ U^{n+1} &= \frac{1}{3}U^n + \frac{2}{3}U^{(2)} + \frac{2}{3}\Delta t L\left(U^{(2)}\right), \end{aligned} \tag{8.17}$$

are due to Shu and Osher [162]. Gottlieb and Shu [163] proved that these second and third order RK schemes are the optimal two-stage order-two SSPRK and three-stage order-three SSPRK ones. To achieve fourth order, a five-stage order-four SSPRK method has been proposed by Spiteri and Ruuth [164] (we are grateful to Prof. Marquina for providing us this reference), that follows the form of a RK method (8.15) with the coefficients:

	1		
	0.44437049406734	0.55562950593266	
α_{ik}	0.62010185138540	0	0.37989814861460
	0.17807995410773	0	0
	0.00683325884039	0	0.51723167208978
	0.82192004589227		
	0.12759831133288	0.34833675773694	

	0.39175222700392		
	0	0.36841059262959	
β_{ik}	0	0	0.25189177424738
	0	0	0
	0	0	0
	0.54497475021237		
	0.08460416338212	0.22600748319395	

Outer boundary

An important ingredient in our code is the treatment of the outer boundary. As it is said before, a Sommerfeld-like boundary condition is implemented in the code. This is an outgoing radiation condition, in an attempt to approximate the proper data for the exterior, assuming a flat background (this can be problematic in some simulations). This condition partially reflects an outgoing wave; however, nonlinear waves reflect back into the numerical domain. This error has an analytical origin, independent of the computational discretization. A reduction of this error can only be achieved by moving the computational boundary further away. In a general simulation this is very expensive, but in our case we can use the fact that our radial grid has not to be uniformly spaced, and, for example, we can use a logarithmic radial grid.

The Sommerfeld condition for a function f assumes that this function is of the form $f = f_0 + u(r - vt)/r$ close to the outer boundary, where r is the radial coordinate, v is the velocity of the outgoing wave, t stands for the coordinate time, f_0 is the asymptotic value of f when $r \to \infty$, and u is an arbitrary function with the only requirement that it depends on $r - vt$. With this hypothesis, the function satisfies the following PDE:

$$\partial_t f + \partial_r f + v\,(f - f_0)\,/\,r = 0. \tag{8.18}$$

The eigenvalues of the system we want to evolve, that can be interpreted as the velocities of the waves, have the asymptotical values of the speed of light, as it has been shown in Section 5.3. If the outer boundary is far enough from the origin we can take $v = 1$, and the previous PDE is reduced to:

$$\partial_t f + \partial_r f + (f - f_0)\,/\,r = 0. \tag{8.19}$$

We would like to apply this condition to the components h^{ij} of the tensor of the deviation with respect to the flat metric. The asymptotical values of all the components are zero. Taking into account that we are using an orthonormal basis, we assume that these components have the following behaviour:

$$\begin{aligned} h^{rr} &\approx \frac{g_1(r-t)}{r}, \qquad h^{\theta\theta} \approx \frac{g_4(r-t)}{r^3}, \qquad h^{\varphi\varphi} \approx \frac{g_6(r-t)}{r^3 \sin^2\theta} \\ h^{r\theta} &\approx \frac{g_2(r-t)}{r^2}, \qquad h^{r\varphi} \approx \frac{g_3(r-t)}{r^2 \sin\theta}, \qquad h^{\theta\varphi} \approx \frac{g_5(r-t)}{r^3 \sin\theta}. \end{aligned} \tag{8.20}$$

The functions g_i, $i = 1, ..., 6$, stand for arbitrary functions with the same role as u. From (8.20), one can derive the corresponding PDE for all the 30 variables of the system, i.e. the set (h^{ij}, u^{ij}, w^{ij}_k) or the set (h^{ij}, $\hat{A}^{ij}$, w^{ij}_k). Actually, this condition works there where the outer boundary is placed, far enough from the origin, where the background metric can be considered flat; there, the behaviour of u^{ij} and $\hat{A}^{ij}$ are the same. These PDEs will be applied to evolve quantities at the points near the outer boundary (see Appendix C).

Filter and dissipative term

Numerical noise, point to point, appears in all the variables during long term simulations. This noise can be viewed as a very high frecuency wave in each coordinate direction. Adding viscosity not only smoothes the high frecuencies out, but also the low ones. In the context of extracting gravitational waves this behaviour has to be avoided, for which there are two options. A filter of very high frecuency, proposed by Savitzky and Golay [165], can be applied after running a given number of (e.g. one hundred) iterations (in the radial and angular directions). This filter does not affect the amplitude of the physical waves. It works quite well and it is very easy to implement, but the number of iterations has to be known a priori and in general it is different for different simulations.

On the other hand, a dissipative term can be included, e.g. the Kreiss-Oliger one [166], in each direction. This dissipative term is an even derivative of high order, fourth order in our case, in the corresponding direction, that we are going to name generically as ∂_i^4, multiplied by a power, fourth power in our case, of the spacing of grid points in the corresponding r or θ-direction, Δr or $\Delta\theta$, that we are going to represent generically as Δ_i, and a constant:

$$-\frac{\epsilon}{16}\Delta_i^4\partial_i^4. \tag{8.21}$$

The constant ϵ can be regarded as the dissipative factor and it does not depend on the different simulations. The minus sign corresponds to $(-1)^n$ for $n = 1$, where $2(n + 1)$ is the order of the derivative. The fourth order derivative is calculated with a truncation error which goes as Δ_i. The addition of a dissipative term can be viewed as a modification of an algorithm, which is not exact. Hence, the inclusion of this dissipative term leads to a truncation error higher than the approximation of the spatial derivatives through the FD

method used, and it does not affect to the convergence order of the algorithm. The Kreiss-Oliger dissipative term is applied to the whole set of variables of the evolution system, acting this derivative of high order into the corresponding variable which is evolved in time in each equation of the system.

An alternative dissipative term [167] has been used with no remarkable differences. The idea is very similar to the Kreiss-Oliger method; in this case the derivative appearing in the dissipative term is applied to the variables of the system times the maximum characteristic speed at the specific grid point.

8.2 Testing the code

8.2.1 Teukolsky waves

Let us consider the linearized system of Einstein equations in vacuum,

$$\begin{cases} \partial_t h^{ij} = u^{ij} \\ \partial_t u^{ij} = f^{kl}\mathcal{D}_k w_l^{ij} \\ \partial_t w_k^{ij} = \mathcal{D}_k u^{ij} \end{cases} , \tag{8.22}$$

where we have fixed the values for the lapse function and the conformal factor equal to one, $N = \psi = 1$, and zero shift vector, $\beta^i = 0$. With our choice of coordinates, $f^{kl} = \delta^{kl}$. Notice that in this simple case $u^{ij} = 2\hat{A}^{ij}$; hence, there is no difference between both tensors. In general, it will be more convenient to use $\hat{A}^{ij}$ due to the reasons explained in Chapter 5. The condition for the determinant of the conformal metric, $det\left(\tilde{\gamma}^{ij}\right) = 1$, in the linear approximation is translated into the vanishing of the trace for h^{ij}.

The initial data used for h^{ij} and their derivatives correspond to a combination of ingoing and outgoing even-parity $m = 0$ (axisymmetric) Teukolsky waves [88], in order to construct regular initial data at the center $r = 0$. The amplitude chosen is 10^{-5}. These data are solution of the linearized wave equation in vacuum, satisfies the Dirac gauge and it is traceless (which is the linear approximation of $\tilde{\gamma} = 1$). Since the analytical expressions for all the components at each time are avalaible, the numerical solution is comparable with the analytical one. Time step preserves the Courant-Friedrichs-Lewy (CFL) condition.

In the following, we will say that a method is of order (p, q) if the RK method is of order p and the spatial partial derivatives of order q. Using

several orders of accuracy for the spatial derivatives and the RK method, and analyzing several CFL values, we have found that the code crashes due to the formation of an instability at the center $r = 0$. The time at which the code crashes depends on the values of p, q and CFL. We have plotted in Figs. 8.1 8.5 the variable $u^{\theta\theta}$, where the red lines correspond to the numerical values and the green lines to the analytical values. This variable has been chosen in order to display the behaviour of these instabilities. Computational domain is defined by $[0, 6] \times [0, \pi/2]$ on the $r - \theta$ plane, plus several extra grid points. We have used $n_r = 100$, and $n_\theta = 20$.

Fig. 8.1 shows the instability at the center $r = 0$. For a $(2, 2)$ method, decreasing CFL delays its formation. Tab. 8.1 displays the numerical values of $u^{\theta\theta}$ at its peak, for different CFL, compared with the analytical correct ones.

CFL	Coordinate time	Approximated numerical value at the peak	Approximated analytical
0.8	3.9×10^{-2}	-27.3	1.3×10^{-4}
0.4	3.9×10^{-2}	6.8×10^{-4}	1.3×10^{-4}
0.2	1.4×10^{-1}	7.9×10^{-4}	4.4×10^{-4}

Tab. 8.1: Numerical values of $u^{\theta\theta}$ at the peak, for a $(2, 2)$ method.

Fig. 8.2 corresponds to a $(2, 4)$ method. We can see again the same instability at the center. Tab. 8.2 displays the numerical values of $u^{\theta\theta}$ at the peak, for differents CFL, compared with the analytical correct ones. The main difference between Figs. 8.1 and 8.2 is that the appearence of the instability at the center is delayed when a high order method is used, but the problem is still unsolved.

CFL	Coordinate time	Approximated numerical value at the peak	Approximated analytical
0.8	3.9×10^{-2}	2×10^{-1}	1.3×10^{-4}
0.4	9×10^{-2}	8×10^{5}	2.9×10^{-4}
0.2	1.9×10^{-1}	1.2×10^{-4}	5.7×10^{-4}

Tab. 8.2: Numerical values of $u^{\theta\theta}$ at the peak, for a $(2, 4)$ method.

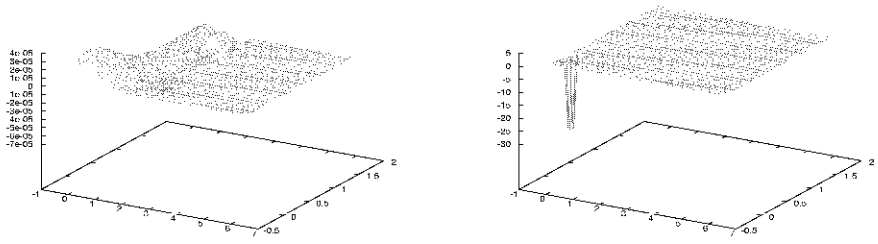

(a) CFL 0.8, $t = 9.9 \times 10^{-3}$ and $t = 3.9 \times 10^{-2}$.

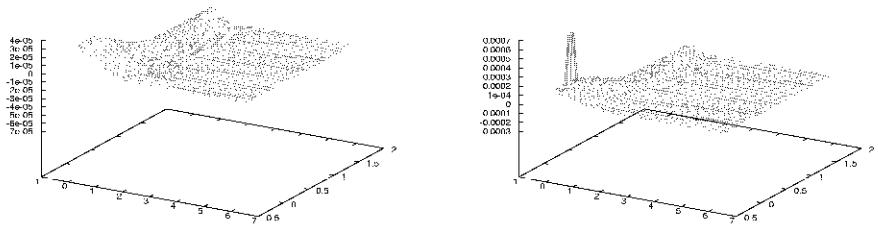

(b) CFL 0.4, $t = 9.9 \times 10^{-3}$ and $t = 3.9 \times 10^{-2}$.

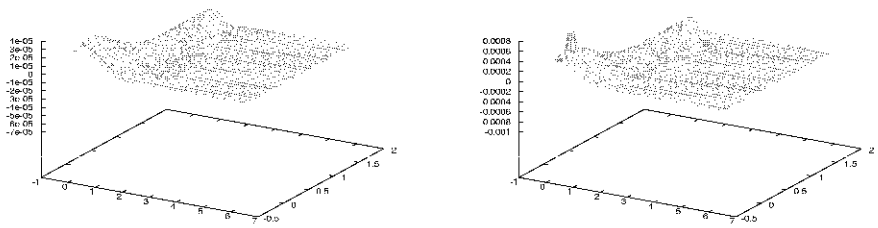

(c) CFL 0.2, $t = 9.9 \times 10^{-3}$ and $t = 1.4 \times 10^{-1}$.

Fig. 8.1: $u^{\theta\theta}.(2,2)$ method.

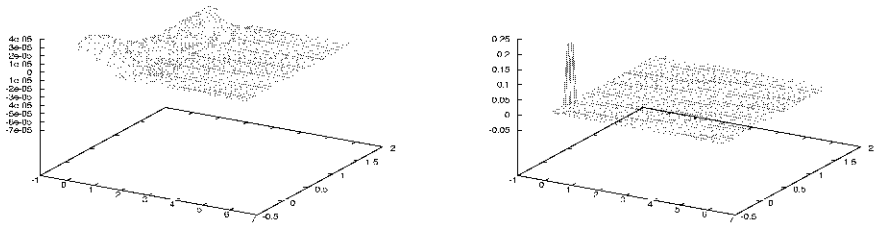

(a) CFL 0.8, $t = 9.9 \times 10^{-3}$ and $t = 3.9 \times 10^{-2}$.

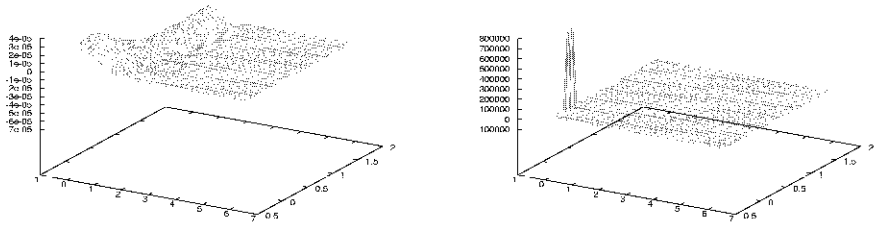

(b) CFL 0.4, $t = 9.9 \times 10^{-3}$ and $t = 9.0 \times 10^{-2}$.

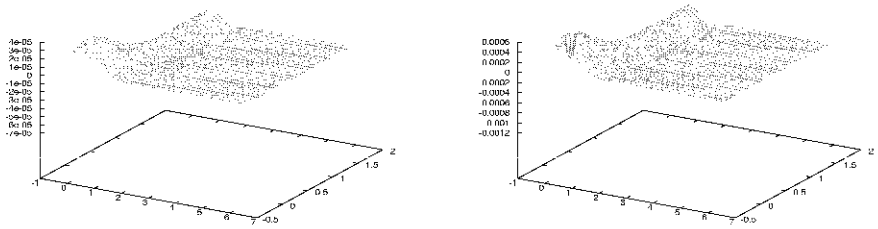

(c) CFL 0.2, $t = 9.9 \times 10^{-3}$ and $t = 1.9 \times 10^{-1}$.

Fig. 8.2: $u^{\theta\theta}.(2,4)$ method.

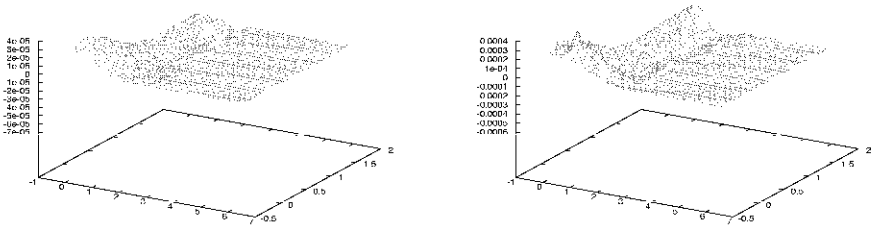

(a) CFL 0.8, $t = 9.9 \times 10^{-3}$ and $t = 7.0 \times 10^{-1}$.

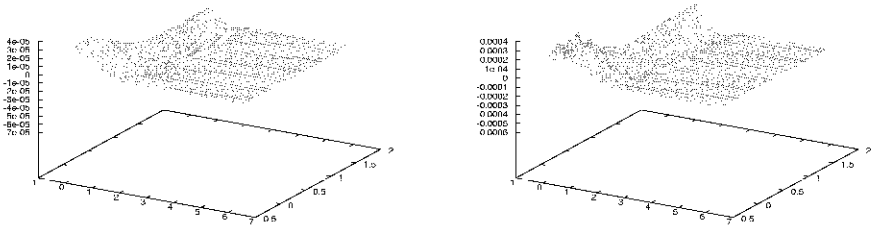

(b) CFL 0.4, $t = 9.9 \times 10^{-3}$ and $t = 7.0 \times 10^{-1}$.

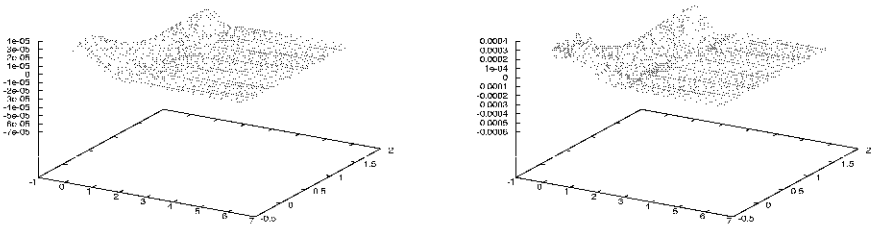

(c) CFL 0.2, $t = 9.9 \times 10^{-3}$ and $t = 7.0 \times 10^{-1}$.

Fig. 8.3: $u^{\theta\theta}.(4,4)$ method.

Results for a $(4,4)$ method are shown in Fig. 8.3. There is again an instability at the center, but not only at $r = 0 = \theta$; the instability appears for several values of θ around $\theta = 0$. The numerical values at $r = 0 = \theta$ and $t = 7 \times 10^{-1}$, for different CFL, are similar, around 2.8×10^{-4} compared with the analytical value 1.8×10^{-4}. Again, the difference between these results and the ones in Figs. 8.1 and 8.2 is that the development of the instability is delayed.

The formation of the instability at $r = 0$ is independent on the accuracy of the RK method used. The development of this instability is very fast. The instabilities at the origin are common problems in spherical symmetry, since the coordinate system is not well defined at the origin. This coordinate singularity is not related with the formalism used and neither with the numerical algorithm used. The usual treatment is the redefinition of the dynamical variables based on the Taylor development close to the origin (see e.g. [89], or more recently [90]). In this case, the fact of using orthonormal coordinates guarantee that the Taylor developments of the dynamical variables are appropiated for the numerical evolution of the system. What can be done in order to solve this problem?

We can notice that, according to the way they have been obtained, two groups in the 30 variables of the system can be considered: the first twelve variables, h^{ij} and u^{ij} (or h^{ij} and $\hat{A}^{ij}$ in a general simulation), that we will name G_1 in the next, and the last eighteen ones, w_k^{ij}, that we will name G_2 in the next. The variables G_1 have been obtained directly; however, the G_2 shows a time derivative acting on them. According to their numerical features, if we evolve the system with analytical values for the set G_1, the variables of G_2 are obtained numerically free of instabilities. And the same happens if we interchange G_1 and G_2.

As a consequence, we have used different ways to treat G_1 and G_2. G_1 is going to be evolved with an explicit scheme, while G_2 is going to be evolved with an implicit one. Moreover, it is crucial the use of fourth order methods for the spatial partial derivatives. When we take into account all these facts, the numerical instability at the center disappears.

We display in Fig. 8.4 the evolution of $u^{\theta\theta}$, with a $(2,4)$ method and a CFL value of 0.5. It can be seen that, for a $(2,4)$ method, there is a value of CFL, about 0.535, below which the instability dissapears.

We show in Fig. 8.5 the evolution of $u^{\theta\theta}$, with a $(4,4)$ method and a CFL of 0.8. It the case of a $(4,4)$ method, the maximum CFL for avoiding the

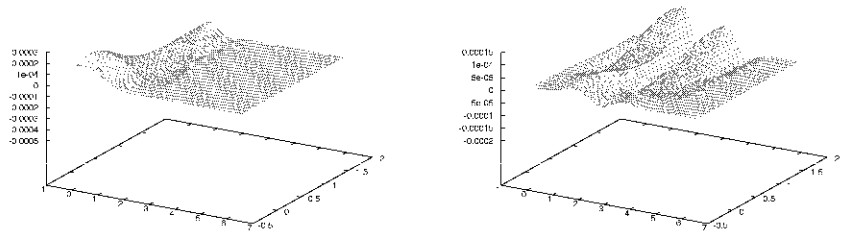

Fig. 8.4: $u^{\theta\theta}.(2,4)$ method, CFL 0.5. $t = 6.4 \times 10^{-2}$ and $t = 2.61$.

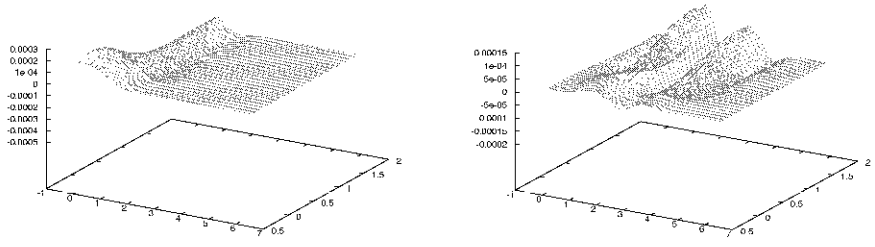

Fig. 8.5: $u^{\theta\theta}.(4,4)$ method, CFL 0.8. $t = 6.4 \times 10^{-2}$ and $t = 2.61$.

instability at the center is 1.

We have carried out convergence studies of these simulations. We display in Fig. 8.6 the numerical evolution of the component h^{rr} in terms of the radius r at $t = 6$, at the equator and at the pole, with different values of the number of radial and angular points, n_r and n_θ respectively. The analytical solution in linear regime is recovered, as well as the velocity and the amplitude of the wave, and the decay with the radius. The Sommerfeld condition at the outer boundary works well at the linear level. We obtain second order of convergence for all the non zero components of the tensor h^{ij} (Fig. 8.7). This second order is obtained even when 4th order R-K and FD methods are used. The reason of this low order of convergence is the influence of the inner boundary conditions, that can lead even to a first order of convergence. This fact can be checked with a short duration simulation and calculating the order of convergence in a region of the numerical domain far from the inner boundaries.

8.2.2 Equilibrium configuration of rotating neutron stars

In this numerical experiment the tensor $\hat{A}^{ij}$ is going to be used, instead of the time derivative of h^{ij}, due to all the properties analyzed in Chapter 5. We are going to consider an axisymmetric model: an uniformly rotating neutron star in equilibrium. The initial data has been obtained from LORENE [91], which is a library of spectral methods. These models, of different rotation parameters, have non-vanishing shift vector, lapse function, conformal factor and matter fields. All these variables will be kept fixed during the evolution of the tensor h^{ij}. In the figures we show the results corresponding to neutron stars with a rotation frequency of 550 Hz, a baryon mass of 1.6 $M_\odot$ and a coordinate equatorial radius of 12.86 km.

Fig. 8.8 shows a sketch of the grid, where the following domains have been defined: The first domain (matter domain, MD) is common to the hydrodinamic equations and contains the star. The second domain (propagation domain, PD) is the one where the waves are well-resolved. The region for extracting the gravitational radiation is placed at the outer boundary of the PD. The third and last domain (damping domain, DD) has a lower resolution in the radial direction. The wave travels far enough before reaching the outer boundary. Let $r_{\mathrm{MD-PD}}$ the radius which separates the MD and the PD, and $r_{\mathrm{PD-DD}}$ the radius which separates the PD and the DD. The star radius r_* is

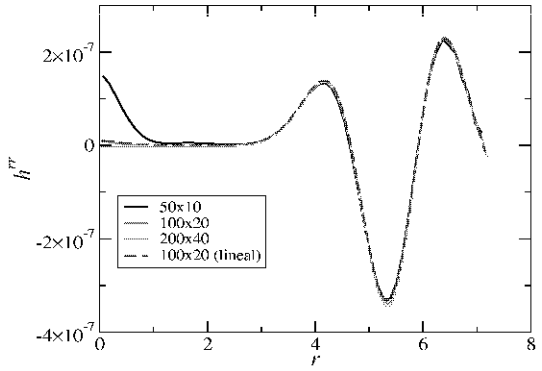

(a) Pole ($\theta = 0$).

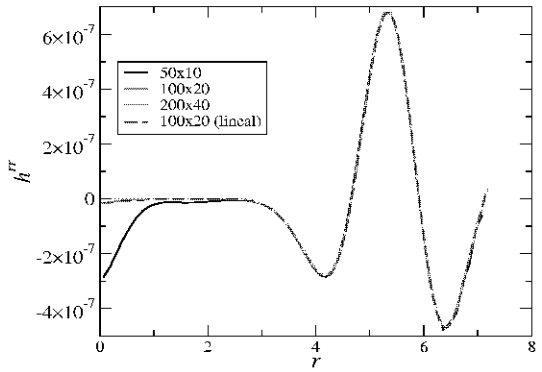

(b) Equator ($\theta = \pi/2$).

Fig. 8.6: h^{rr} at $t = 6$. Black line corresponds to $n_r = 50$ and $n_\theta = 100$ (radial and angular number of grid points), red line to $n_r = 100$ and $n_\theta = 20$, green line to $n_r = 200$ and $n_\theta = 40$, in non-linear evolutions. Dashed blue line corresponds to $n_r = 100$ and $n_\theta = 20$, in a linear evolution.

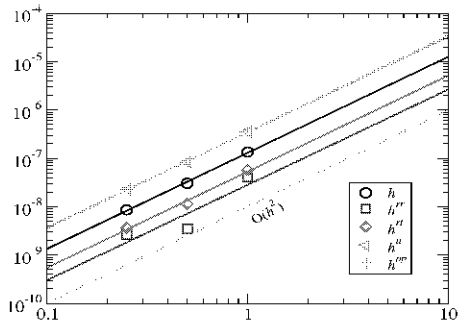

Fig. 8.7: Absolute errors (L2-norm) in terms of (scaled) grid size. Black line fits the errors for $\sum_{i,j} h^{ij}$, blue one for h^{rr}, red one for $h^{r\theta}$, orange one for $h^{\theta\theta}$ and green one for $h^{\varphi\varphi}$. Dash cyan line is the reference of second order of convergence.

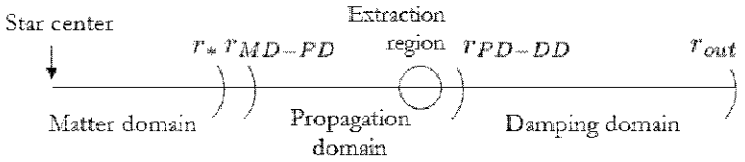

Fig. 8.8: Scheme of the radial grid used in the code for rotating neutron star simulations.

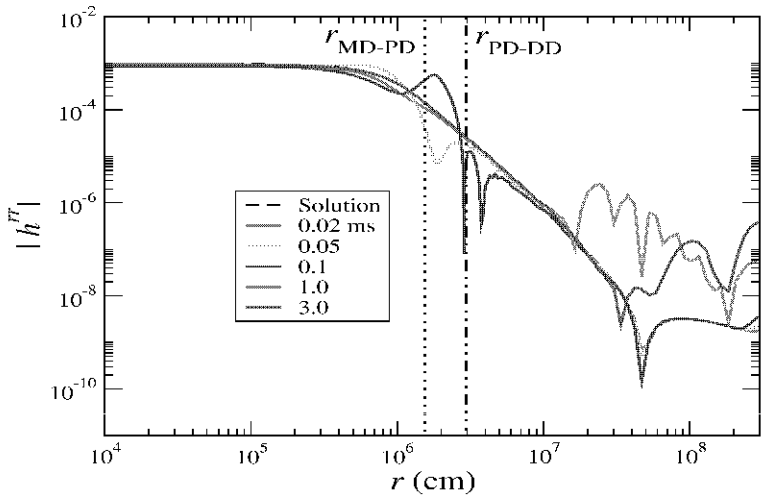

Fig. 8.9: $|h^{rr}|$ in terms of the radius. Black dash line corresponds to the stationary solution (as reference). Red, green, blue, grey and violet lines correspond to the evolution of the initial data at 0.02, 0.05, 0.1, 1.0 and 3.0 ms respectively. Vertical lines denote radius between domains.

close (but smaller) to $r_{\mathrm{MD-PD}}$. The logarithmic grid (in the radial direction) is a very useful tool for constructing this kind of grids with a reasonable number of points. We get the necessary accuracy in the MD and the PD, but we need a computational time for running the simulations smaller than the one required in an equally spaced radial grid.

We have used the following initial data: The stationary values for the tensor h^{ij}, on the one hand, and some differences from stationarity for $\hat{A}^{ij}$, on the other hand. In this general background, these differences from stationarity introduced in the initial data, generate a perturbation that propagates to the outer boundary, leaving behind the stationary solution. In Fig. 8.9, we have

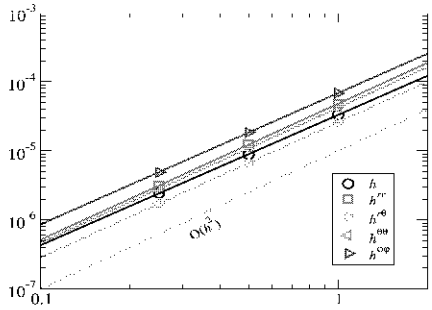

Fig. 8.10: Absolute errors (L2-norm) in terms of (scaled) grid size. Black, red, green, orange and blue lines fit the errors for $\sum_{i,j} h^{ij}$, h^{rr}, h^{r0}, h^{00} and $h^{\varphi\varphi}$. Dash cyan line represents second order of convergence (as reference).

plotted the absolute value of the component h^{rr} in terms of the radius for different times. We can see a first perturbation travelling towards the outer boundary, where the wave leaves the numerical domain. This error of the initial data is interpreted as a perturbation. Second order of convergence is obtained for all the non zero components of the tensor h^{ij} (Fig. 8.10), as previously.

The aim at introducing these initial differences from stationarity is two-fold: on the one hand, the recovering of stationarity from a perturbed initial data, and, on the other hand, testing the outer boundary condition imposed by the generation of the artificial wave.

This test is very useful in order to understand how the Sommerfeld condition at the outer boundary works. If the background, where the wave is travelling, is not flat enough, the slopes of the components of the tensor at the outer boundary can be interpreted as outgoing waves by the Sommerfeld condition. The outer boundary condition enforces the interpreted wave to leave the numerical domain in such a way that the values of the components increase or decrease arbitrary, and making the code crash. This behaviour can be seen in Fig. 8.11 for the simulation whose outer boundary is placed closer, at 3×10^7. We have found that Sommerfeld condition works properly for $r_{out} \gtrsim 3 \times 10^8$cm

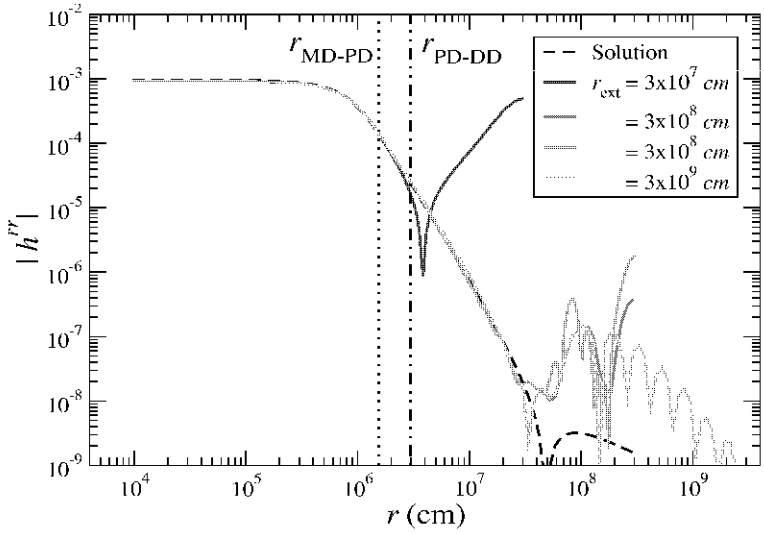

Fig. 8.11: $|h^{rr}|$ in terms of the radius at time $t = 3$ ms. Black dash line corresponds to the stationary solution (as reference). Blue, red and green lines correspond to the numerical evolution whose outer boundary are placed at 3×10^7, 3×10^8 and 3×10^9 cm respectively. Orange line correspond to the numerical evolution whose outer boundary is placed at 3×10^7 cm with more resolution than the simulation corresponding to the red line. Vertical lines denote radius between domains.

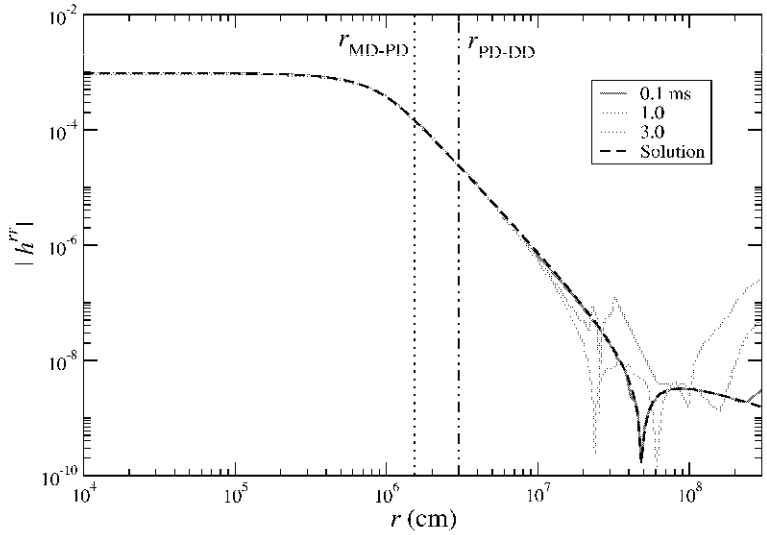

Fig. 8.12: $|h^{rr}|$ in terms of the radius. Black dash line corresponds to the stationary solution (as reference). Red, green and cyan lines correspond to the evolution of the initial data at 0.1, 1.0 and 3.0 ms respectively. Vertical lines denote radius between domains.

(around 300 stellar radius). In our calculations we have used 80 radial grid points in the MD, 80 points in the PD and around 50 in the DD.

Once the outer boundary radius has been fixed, we can use the stationary initial data for both h^{ij} and $\hat{A}^{ij}$ tensors. In Fig. 8.12 we show the absolute value of the component h^{rr}, in terms of the radius, for different times. No initial artificial wave is introduced. The noise comes from the outer boundary condition. The errors for the non zero components of the tensor h^{ij} grows up linearly, but again a second order of convergence is obtained.

8.2.3 A perturbed equilibrium configuration: extraction of gravitational radiation.

We consider a radially perturbed neutron star. The radial perturbation is proportional to $\sin(\pi\, r/r_*)$; since the star is rotating, the star radius depends on θ, and the perturbation is not spherically symmetric; hence, gravitational radiation is expected to be generated. The hydrodynamic equations governing the matter evolution will be solved. We keep fixed the CFC background, i.e., we fix the lapse function, the shift vector and the conformal factor during the evolution, assuming that they are not going to change very much during the evolution. This approximation will provide interesting information about where to place $r_{\rm PD-DD}$, and, consequently, where to extract the gravitational radiation.

In Fig. 8.13, an approximation of the real part of the Weyl scalar Ψ_4, h_+, (scaled with the radial coordinate) is plotted in terms of the retarded time, and for different radius at the equator. This approximation is accurate enough for the objectives of this test. The boundary of PD-DD domains, $r_{\rm PD-DD}$, is placed at 3×10^7cm (around 30 stellar radius). The waves correspond to the physical gravitational waves coming from the evolution of the perturbed star through the evolution of the hydrodynamic equations. The different curves in Fig. 8.13 refer to different radii where the gravitational radiation has been extracted. From the superposition of the waves extracted in the PD (the two first ones), we can deduce that the speed of the waves is the light velocity and they decay as $1/r$. We also see that the wave must be extracted far from the source but inside the PD, since the last wave does not reproduce the previous ones. Regarding with the resolution of the logarithmic grid, it is enough to cover a wavelength with five points at the end of the PD. As a consistency check, the frequencies extracted from the wave plotted in Fig. 8.13 coincide with the ones extracted by using the quadrupole formula.

The small initial off-set, before the waves reach the corresponding radius, can be cured just placing r_{PD-DD} far enough from the source. The off-set in the waves themselves seems to decrease with distance. This is an open question for now. The origin of the problem could be due to:

i) The existence of a mild inconsistency between the initial data of the energy-momentum tensor of the perturbed star and the initial data of the metric.

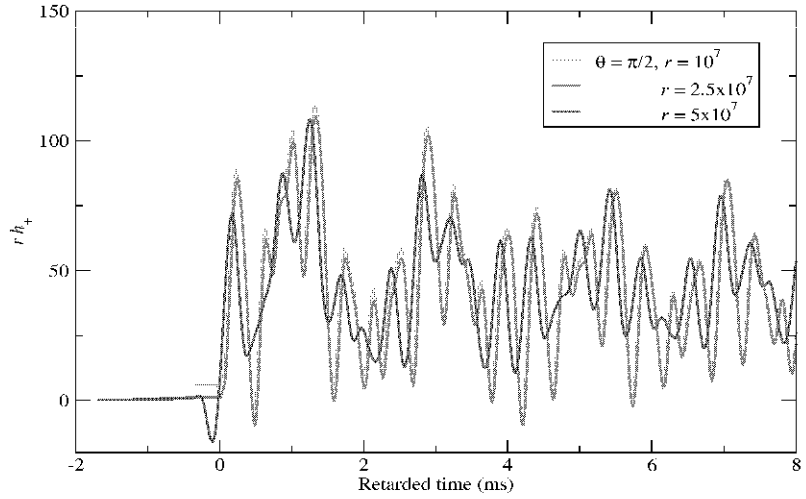

Fig. 8.13: rh_+ versus the retarded time. Green, magenta and violet lines are the corresponding wave extracted at $r = 10^7$, $r = 2.5 \times 10^7$ and $r = 5 \times 10^7$cm respectively, at the equator. $r_{\rm PD-DD}$ is placed at 3×10^7cm.

ii) Our procedure to estimate an approximation to the scalar Ψ_4. This procedure calculates Ψ_4 at the spatial infinity, assuming an asymptotically flat spacetime, but it is valid far enough from the source for getting a good approximation. It does not take into account the non-diagonal terms of the metric.

We hope to improve these points in the extended version of CoCoNuT (see next Section).

Furthermore, it will be important to know where to place $r_{\mathrm{PD-DD}}$. In Fig. 8.14, rh_+ is plotted in terms of the retarded time in simulations with different $r_{\mathrm{PD-DD}}$. The wave is extracted close to $r_{\mathrm{PD-DD}}$ in all the cases. From the figure, it is reasonable to place $r_{\mathrm{PD-DD}}$ at 3×10^7cm (around 30 stellar radius) or further.

The CoCoNuT code [87] is a general relativistic magneto-hydrodynamical code able to evolve matter in the CFC and FCF (current version, in progress) dynamical spacetime. This numerical code will allow us to study several astrophysical scenarios in which general relativity can play an important role, namely the collapse of rapidly rotating stellar cores and the evolution of isolated neutron stars. The project was started by H. Dimmelmeier at the Max-Planck Institute for Astrophysics (Garching, Germany) during his PhD thesis. It was extended to a three-dimensional code using Lorene's library for the CFC Einstein equations, and HRSC methods for the hydrodynamic equations [40], in collaboration with J. Novak from the LUTH at the Observatoire de Paris (Meudon, France). Recently, P. Cerdá-Durán has implemented a magneto-hydrodynamic extension of the code.

Regarding the metric evolution, the CFC approximation was originally used. Once the main elements of the extension from CFC to FCF are established and the first tests made, it is the moment for incorporating the new system of hyperbolic equations to the CoCoNuT code. This is a work in progress in collaboration with P. Cerdá-Durán at the Max-Planck Institute for Astrophysics (Garching, Germany). Important steps have already been done. Some of the tools included in CoCoNuT will be very useful for future developments; for example, the spectral methods (used for solving the elliptic equations of the metric) can be very useful for calculating the scalar Ψ_4, and the horizon finder implemented can be very useful for simulations of collapse of a neutron star to a black hole. It will also be very interesting the study of the gravitational

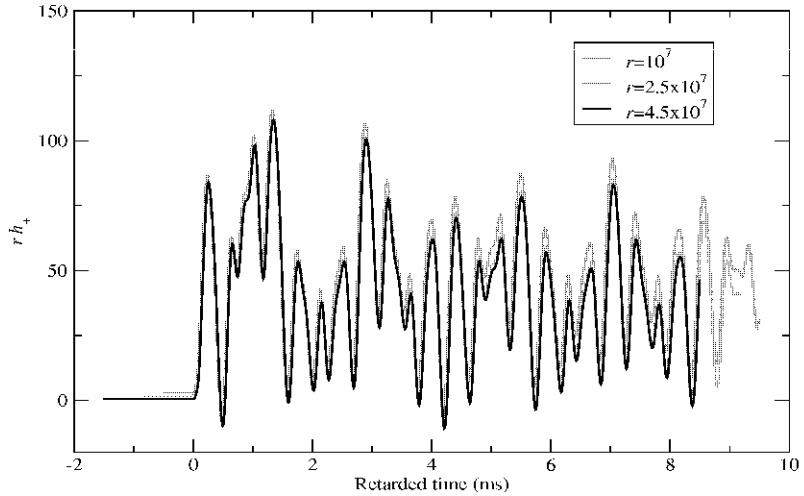

Fig. 8.14: rh_+ versus the retarded time, at the equator. Radii are expressed in cm. Orange line is the corresponding wave extracted at $r = 10^7$, where $r_{\mathrm{PD-DD}} = 1.5 \times 10^7$; turquoise line corresponds to $r = 2.5 \times 10^7$, where $r_{\mathrm{PD-DD}} = 3 \times 10^7$; black line corresponds to $r = 4.5 \times 10^7$, where $r_{\mathrm{PD-DD}} = 5 \times 10^7$.

radiation coming from neutron stars with different equations of state, comparision of the gravitational waves obtained with other approximations (quadrupole formula), etc.

9. SUMMARY AND OUTLOOK

During the period of time spent in my thesis I have been involved in both theoretical and numerical research, as two important and complementing ingredients, focusing on formulations of Einstein equations and mainly in the FCF. I have nearly completed the analysis of the mathematical properties of the elliptic-hyperbolic system of Einstein equations in this recent formulation. These studies have faced on the uniqueness properties of the elliptic equations and the characteristic structure of the hyperbolic equations. The analysis of the hyperbolic equations has been applied to the study of the boundary conditions at trapping horizons in dynamical spacetimes of BHs. I have also carried out some studies about the existence of maximal slicings in the spherically symmetric case.

Regarding the numerical part of the thesis, I have made progress in testing a numerical code responsible of evolving the system which contain the gravitational radiation in FCF, and in implementing this formulation in the new version of CoCoNuT's code. Some key pieces for the evolution of the system, such as the information about extracting the gravitational waves or outer boundaries, are known. The code is ready to carry out simulations evolving both the energy-momentum tensor and the whole metric tensor (all the elliptic and hyperbolic equations in FCF).

Hence, I foresee a set of possible extensions or applications of my work in different subfields.

From a purely geometrical point of view, the study about the existence of maximal slicings in spherical symmetry and procedure we have used can (and should) be extended to more general cases, as axisymmetric spacetimes, on one hand, and to other foliations (and gauges) on the other hand. As a by-product of this analysis, it should be interesting to generate numerically dynamical spacetimes, and to compare them with the one generated by our geometric

analysis.

From a purely mathematical (analysis) point of view, I consider very relevant (and urgent) to complete the study on the well-posed problem issue for the FCF elliptic-hyperbolic system of Einstein equations. Up to now, only independent studies of the system of equations governing the evolution of h^{ij} (gravitational radiation in FCF) and the (magneto-)hydrodynamic equations governing the evolution of matter fields have been done. In particular, it would be interesting to deepen the understanding of the hyperbolic properties of the coupled system of equations.

From the astrophysical point of view, it is time for an accurate procedure to extract information about the gravitational wave signal from astrophysical scenarios such as the stellar core collapse. It is the natural follow-up of this thesis, once all the succesful tests have been made. It is necessary to make a rigorous comparison with previous studies carried out with other approximations for extracting the gravitational radiation, as the quadrupole formula. CoCoNuT's code is already written in such a way that it is ready for 3D applications, and it is natural to complete the extension of the code to include the FCF of Einstein equations. An effort in its parallelization is necessary.

As a summary of the numerical simulations to be made with the upgraded CoCoNuT's code, I suggest the following ones: i) to obtain and compare the gravitational wave signals resulting from different simulations of rotating neutron stars with several equations of state; ii) to compute more exactly the evolution of the full metric for the spacetime of a collapsing and rotating neutron star to a black hole. Other simulations, in which spherical coordinates are well-adapted to the specific problem, can be done in scenarios with strong gravitational fields, once the extension to a fully relativistic formulation is implemented in CoCoNuT.

APPENDIX

A. APPROXIMATION OF THE CONFORMAL EXTRINSIC CURVATURE IN CFC CASE.

In the derivation of the new version of FCF/CFC we make use of the fact that $(LX)^{ij} \approx \hat{A}^{ij}$ in CFC. Here we are going to show next that this assumption is completely consistent at the accuracy level of the CFC approximation. First, we need to estimate the error of the CFC approximation itself. By definition, the CFC 3-metric deviates linearly with h^{ij} from the (exact) FCF case. It can be easily shown from the FCF equations (5.115)-(5.117) that the metric quantities behave as

$$\psi = \psi_{\rm CFC} + \mathcal{O}(h), \tag{A.1}$$
$$N = N_{\rm CFC} + \mathcal{O}(h), \tag{A.2}$$
$$\beta^i = \beta^i_{\rm CFC} + \mathcal{O}(h). \tag{A.3}$$

Therefore h^{ij} can be used as an estimator for the error of the CFC approximation.

Two limits in which CFC is exact will be considered. The first limit is spherical symmetry. In spherical symmetry the CFC metric system is an exact reformulation of Einstein equations since $h^{ij} = 0$ in the FCF metric. If the system is close to spherical symmetry (i.e. spheroidal), and if we were able to define a quasi-spherical surface of the system (e.g., the surface of a star or the apparent horizon of a BH) then the equatorial and polar circumferential proper radius, $R_{\rm e}$ and $R_{\rm p}$, can be computed, and we can define the ellipticity of the system as

$$e^2 := 1 - R^2_{\rm p}/R^2_{\rm e}. \tag{A.4}$$

Close to sphericity e^2 scales linearly with h^{ij}, and we can ensure that the error of CFC is $h^{ij} \sim \mathcal{O}(e^2)$. The second limit to consider is a post-Newtonian

expansion of the gravitational sources, i.e. the case where the post-Newtonian parameter $\max(v^2/c^2, GM/Lc^2)$ is much less than 1, where v, M, and L are the typical velocity, mass, and length of the system, respectively. In this case the CFC metric behaves like the first post-Newtonian approximation [168, 169], i.e.

$$\psi = \psi_{\rm CFC} + \mathcal{O}\left(1/c^4\right), \tag{A.5}$$

$$N = N_{\rm CFC} + \mathcal{O}\left(1/c^4\right), \tag{A.6}$$

$$c\,\beta^i = c\,\beta^i_{\rm CFC} + \mathcal{O}\left(1/c^4\right). \tag{A.7}$$

Note that, for clarity, we explicitly retain powers of the speed of light c as factors in the equations throughout this appendix. In the case that both limits are valid, i.e. close to sphericity and in the post-Newtonian expansion, the non-conformally-flat part of the 3-metric behaves like $h^{ij} \sim \mathcal{O}(e^2/c^4)$.

The next step is to compute the behavior of the CFC metric if we assume $(LX)^{ij} \approx \hat{A}^{ij}$, considering the two limiting cases introduced above.

In the spherically symmetric case the relation $(LX)^{ij} = \hat{A}^{ij}$ is trivially fulfilled. Therefore the behavior for a quasi-spherical configuration is also $h^{ij} \sim \mathcal{O}(e^2)$ even if $\hat{A}^{ij}_{\rm TT} = 0$ is assumed. This limit in the approximation is very important, since it is independent of the strength of the gravitational field. For example it allows us to evolve black holes, with the only condition that h^{ij} should be small, i.e. close to the sphericity.

To check the approximation in the post-Newtonian limit we need to compare $\beta^i_{\rm CFC}$ and X^i. This can be done by means of the post-Newtonian expansion of the sources of equations (5.45) and (5.55), respectively,

$$\Delta\beta^i_{\rm CFC} + \frac{1}{3}\mathcal{D}^i\mathcal{D}_j\beta^j_{\rm CFC} = 16\pi S^{*i} + \mathcal{O}\left(1/c^7\right), \tag{A.8}$$

$$\Delta X^i + \frac{1}{3}\mathcal{D}^i\mathcal{D}_j X^j = 8\pi S^{*i} + \mathcal{O}\left(1/c^7\right). \tag{A.9}$$

From the comparison of equations (A.8) and (A.9) we obtain that

$$c^3\,\frac{\beta^i_{\rm CFC}}{2} = c^3\,X^i + \mathcal{O}\left(1/c^2\right). \tag{A.10}$$

Thus $\hat{A}^{ij}$ can be computed in terms of X^i as

$$c^4\hat{A}^{ij} = \frac{\psi^6_{\rm CFC}}{2N_{\rm CFC}}c^4(L\beta_{\rm CFC})^{ij} = c^4(LX)^{ij} + \mathcal{O}\left(1/c^2\right), \tag{A.11}$$

where we make use of $\psi^6_{\rm CFC}/N_{\rm CFC} = 1 + \mathcal{O}(1/c^2)$. The effect of using $(LX)^{ij}$ instead of $\hat{A}^{ij}$ in the calculation of the CFC metric can be seen in the expressions

$$\begin{aligned} \psi_{\rm CFC} &= \Delta_{\rm s}^{-1}\mathcal{S}_{(\psi)}(N_{\rm CFC}, \psi_{\rm CFC}, \hat{A}^{ij}) \\ &= \Delta_{\rm s}^{-1}\mathcal{S}_{(\psi)}(N_{\rm CFC}, \psi_{\rm CFC}, (LX)^{ij}) \\ &\quad +\mathcal{O}\left(1/c^8\right), \end{aligned} \tag{A.12}$$

$$\begin{aligned} N_{\rm CFC} &= \psi_{\rm CFC}^{-1}\Delta_{\rm s}^{-1}\mathcal{S}_{(N\psi)}(N_{\rm CFC}, \psi_{\rm CFC}, \hat{A}^{ij}) \\ &= \psi_{\rm CFC}^{-1}\Delta_{\rm s}^{-1}\mathcal{S}_{(N\psi)}(N_{\rm CFC}, \psi_{\rm CFC}, (LX)^{ij}) \\ &\quad +\mathcal{O}\left(1/c^8\right), \end{aligned} \tag{A.13}$$

$$\begin{aligned} c\,\beta^i_{\rm CFC} &= c\,\Delta_{\rm v}^{-1}\mathcal{S}_{(\beta)}(N_{\rm CFC}, \psi_{\rm CFC}, \hat{A}^{ij}) \\ &= c\,\Delta_{\rm v}^{-1}\mathcal{S}_{(\beta)}(N_{\rm CFC}, \psi_{\rm CFC}, (LX)^{ij}) \\ &\quad +\mathcal{O}\left(1/c^6\right). \end{aligned} \tag{A.14}$$

where $\mathcal{S}_{(\psi)}$, $\mathcal{S}_{(N\psi)}$ and $\mathcal{S}_{(\beta)}$ are the sources of equations (5.56) (5.58), and $\Delta_{\rm s}^{-1}$ and $\Delta_{\rm v}^{-1}$ are just the inverse operators appearing in the right-hand-side of these equations (for the scalars ψ and $N\psi$, and for the vector β^i, respectively). When comparing equations (A.12)–(A.14) with equations (A.5)–(A.7) it becomes obvious that in all cases the error introduced by making the approximation $(LX)^{ij} \approx \hat{A}^{ij}$ is smaller than the error of the CFC approximation itself.

As an illustration of the above properties, we study the influence of the $\hat{A}^{ij}_{\rm TT}$ term in equation (5.54) when computing rotating neutron star models with a polytropic $\Gamma = 2$ equation of state. This setup contains the initial models used in section 5.2.3. They assume axial symmetry and stationarity, in combination with rigid rotation. We build a sequence of rotating polytropes with increasing rotation frequencies, while keeping the central enthalpy fixed, which produces models of increasing masses from $M = 1.33\,M_\odot$ (no rotation), to $M = 1.57 M_\odot$ (the Kepler limit; see below). For all these models, we use three gravitational field schemes: the exact Einstein equations using the stationary ansatz in FCF, and the two approximate ones, regular CFC and CFC neglecting the term $\hat{A}^{ij}_{\rm TT}$ in equation (5.54). The results are displayed on a logarithmic scale in Fig. A.1.

The top panel shows the maximal amplitudes of $\hat{A}^{ij}_{\rm TT}$ (relatively to $\hat{A}^{ij}$) in both FCF and regular CFC, as functions of the ellipticity e defined in equation (A.4). This quantity is physically and numerically limited by the minimal rotational period at the so-called mass-shedding limit (or Kepler limit), when centrifugal forces exactly balance gravitational and pressure forces at the star's equator. In the FCF case we plot the maximal amplitude of h^{ij}. This quantity is dimensionless and represents the deviation of the 3-metric from conformal flatness, which can be interpreted as the relative error one makes in the metric when using CFC instead of FCF. Note that this error on computing $\hat{A}^{ij}$ by discarding the $\hat{A}^{ij}_{\rm TT}$ term in the CFC approximation is roughly of the same order as the error on the metric in the CFC case. All these quantities decrease like $\mathcal{O}(e^2)$ as expected, except for stars rotating close to the Kepler limit. Indeed, the development in powers of e is equivalent to a slow-rotation approximation (see, e.g., [170]) by perturbing spherically symmetric configurations and, when comparing these slow-rotation results with the numerical "exact" ones for rigidly rotating stars (see, e.g., [171] in the two-fluids case), one sees that they usually agree extremely well, with the exception of those very close to the Kepler limit, where this "perturbed spherical symmetry" approach is no longer valid. Finally, because $\hat{A}^{ij}$ appears as a quadratic source term in the Poisson-like equations (5.43, 5.44), the overall errors on the lapse N or the conformal factor ψ are even smaller, as shown in the bottom panel of Fig. A.1. In the case of the central value $N_{\rm c}$ of the lapse, the error due to the CFC approximation is maximal at the Kepler limit and $\lesssim 10^{-4}$ for the studied sequence. The error due to neglecting $\hat{A}^{ij}_{\rm TT}$ within the CFC scheme amounts to $\lesssim 10^{-6}$ and decreases faster than the error due to the CFC approximation, namely as $\mathcal{O}(e^4)$, again except near the Kepler limit. Our tests show that for stationary rotating neutron star models this additional approximation induces an error which falls within the overall CFC approximation.

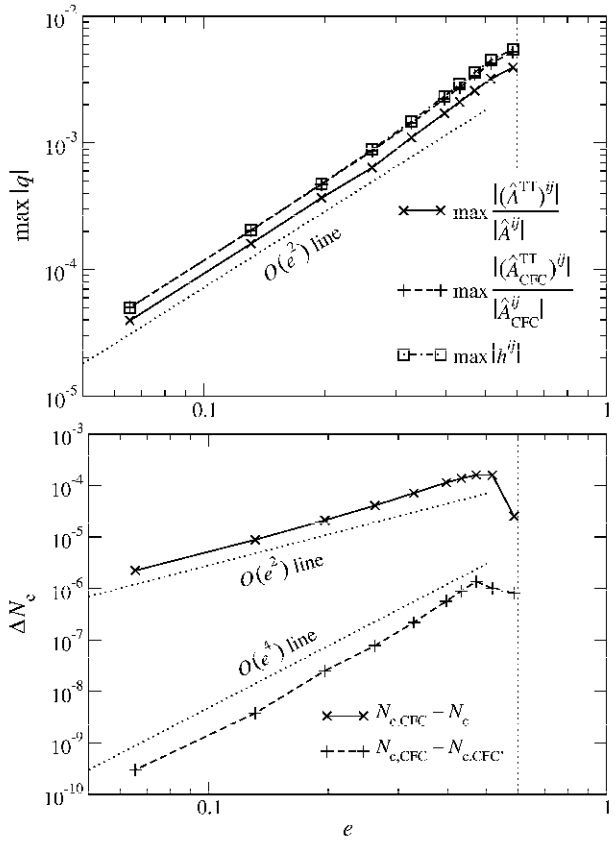

Fig. A.1: Consistency of the approximation for rotating neutron star models. In the top panel $\max |\hat{A}^{ij}_{\rm TT}/\hat{A}^{ij}|$ for FCF (solid line) and CFC (dashed line) as well as the maximum deviation from conformal flatness $\max |h^{ij}|$ for FCF (dash-dotted line) are plotted against the ellipticity e. The bottom panel shows the absolute difference $|N_{\rm c,CFC} - N_{\rm c}|$ in the central value of the lapse between CFC and FCF (solid line) and the absolute difference $|N_{\rm c,CFC} - N_{\rm c,CFC'}|$ between regular CFC and CFC neglecting $\hat{A}^{ij}_{\rm TT}$ in equations (5.54) (dashed line). The Kepler limit is marked by vertical dotted lines, while the slanted dotted lines represent the order of accuracy with respect to powers of e.

B. COVARIANT DERIVATIVES

As it is mentioned in chapter 8, given a tensor field $\boldsymbol{T}$ of type $\begin{pmatrix} p \\ q \end{pmatrix}$, the components of the covariant derivative $\mathcal{D}\boldsymbol{T}$ in the orthonormal basis $e_{\hat{i}_1} \otimes \ldots \otimes e_{\hat{i}_p} \otimes \ldots \otimes e^{\hat{j}_1} \otimes \ldots \otimes e^{\hat{j}_q} \otimes e^{\hat{k}}$ are given by:

$$\begin{aligned} \mathcal{D}_{\hat{k}} T^{\hat{i}_1 \ldots \hat{i}_p}{}_{\hat{j}_1 \ldots \hat{j}_q} &= e_{\hat{k}}^{\ l} \frac{\partial}{\partial x^l} T^{\hat{i}_1 \ldots \hat{i}_p}{}_{\hat{j}_1 \ldots \hat{j}_q} \\ &\quad + \sum_{r=1}^{p} \hat{\Gamma}^{\hat{i}_r}{}_{\hat{l}\hat{k}} T^{\hat{i}_1 \ldots \hat{l} \ldots \hat{i}_p}{}_{\hat{j}_1 \ldots \hat{j}_q} - \sum_{r=1}^{q} \hat{\Gamma}^{\hat{l}}{}_{\hat{j}_r \hat{k}} T^{\hat{i}_1 \ldots \hat{i}_p}{}_{\hat{j}_1 \ldots \hat{l} \ldots \hat{j}_q} \end{aligned} \tag{B.1}$$

where $e_{\hat{k}}^{\ l} := \operatorname{diag}\left(1, \frac{1}{r}, \frac{1}{r \sin\theta}\right)$ is the change-of-basis matrix defined by (8.2), and the $\hat{\Gamma}^{\hat{k}}{}_{\hat{i}\hat{j}}$ are the connection coefficients of $\mathcal{D}$ associated with the orthonormal frame (8.2); these cofficients all vanish, except for

$$\hat{\Gamma}^{r}{}_{\theta\theta} = -\hat{\Gamma}^{\theta}{}_{r\theta} = -r^{-1},\ \hat{\Gamma}^{r}{}_{\varphi\varphi} = -\hat{\Gamma}^{\varphi}{}_{r\varphi} = -r^{-1},\ \hat{\Gamma}^{\theta}{}_{\varphi\varphi} = -\hat{\Gamma}^{\varphi}{}_{\theta\varphi} = -\left(r \tan\theta\right)^{-1}. \tag{B.2}$$

As it is mentioned too, the basis is orthonormal with respect to the flat metric $\boldsymbol{f}$: $f_{\hat{i}\hat{j}} = \operatorname{diag}(1,1,1)$. This implics $f^{\hat{i}\hat{j}} = \operatorname{diag}(1,1,1)$, and

$$\mathcal{D}^{\hat{k}} T^{\hat{i}_1 \ldots \hat{i}_p}{}_{\hat{j}_1 \ldots \hat{j}_q} - f^{\hat{k}\hat{l}} \mathcal{D}_{\hat{l}} T^{\hat{i}_1 \ldots \hat{i}_p}{}_{\hat{j}_1 \ldots \hat{j}_q} - \delta^{\hat{k}\hat{l}} \mathcal{D}_{\hat{l}} T^{\hat{i}_1 \ldots \hat{i}_p}{}_{\hat{j}_1 \ldots \hat{j}_q} - \mathcal{D}_{\hat{k}} T^{\hat{i}_1 \ldots \hat{i}_p}{}_{\hat{j}_1 \ldots \hat{j}_q}. \tag{B.3}$$

In particular, we can develop the covariant derivatives of some types of tensors:

$\mathcal{D}_{\hat{k}}F$:

$$\begin{aligned}\mathcal{D}_r F &= \partial_r F;\\ \mathcal{D}_\theta F &= \tfrac{1}{r}\partial_\theta F;\\ \mathcal{D}_\varphi F &= \tfrac{1}{r\sin\theta}\partial_\varphi F.\end{aligned}$$

$\mathcal{D}_{\hat{k}}T^{\hat{i}}$:

$$\begin{aligned}&\mathcal{D}_r T^r = \partial_r T^r, \quad \mathcal{D}_\theta T^r = \tfrac{1}{r}\left(\partial_\theta T^r - T^\theta\right), \quad \mathcal{D}_\varphi T^r = \tfrac{1}{r}\left(\tfrac{1}{\sin\theta}\partial_\varphi T^r - T^\varphi\right);\\ &\mathcal{D}_r T^\theta = \partial_r T^\theta, \quad \mathcal{D}_\theta T^\theta = \tfrac{1}{r}\left(\partial_\theta T^\theta + T^r\right), \quad \mathcal{D}_\varphi T^\theta = \tfrac{1}{r\sin\theta}\left(\partial_\varphi T^\theta - \cos\theta\ T^\varphi\right);\\ &\mathcal{D}_r T^\varphi = \partial_r T^\varphi, \quad \mathcal{D}_\theta T^\varphi = \tfrac{1}{r}\partial_\theta T^\varphi, \qquad\quad \mathcal{D}_\varphi T^\varphi = \tfrac{1}{r}\left(\tfrac{1}{\sin\theta}\partial_\varphi T^\varphi + T^r + \tfrac{1}{\tan\theta}T^\theta\right).\end{aligned}$$

$\mathcal{D}_{\hat{k}}T^{\hat{i}\hat{j}}$, where the tensor is symmetric with respect to the superindices i, j:

$$\begin{aligned}&\mathcal{D}_r T^{rr} = \partial_r T^{rr}, \quad \mathcal{D}_\theta T^{rr} = \tfrac{1}{r}\left(\partial_\theta T^{rr} - 2T^{r\theta}\right),\\ &\qquad\qquad\quad \mathcal{D}_\varphi T^{rr} = \tfrac{1}{r}\left(\tfrac{1}{\sin\theta}\partial_\varphi T^{rr} - 2T^{r\varphi}\right);\\ &\mathcal{D}_r T^{r\theta} = \partial_r T^{r\theta}, \quad \mathcal{D}_\theta T^{r\theta} = \tfrac{1}{r}\left(\partial_\theta T^{r\theta} - T^{\theta\theta} + T^{rr}\right),\\ &\qquad\qquad\quad \mathcal{D}_\varphi T^{r\theta} = -\tfrac{1}{r}\left(\tfrac{1}{\sin\theta}\partial_\varphi T^{r\theta} + T^{\theta\varphi} + \tfrac{1}{\tan\theta}T^{r\varphi}\right);\\ &\mathcal{D}_r T^{r\varphi} = \partial_r T^{r\varphi}, \quad \mathcal{D}_\theta T^{r\varphi} = \tfrac{1}{r}\left(\partial_\theta T^{r\varphi} - T^{\theta\varphi}\right),\\ &\qquad\qquad\quad \mathcal{D}_\varphi T^{r\varphi} = \tfrac{1}{r}\left(\tfrac{1}{\sin\theta}\partial_\varphi T^{r\varphi} - T^{\varphi\varphi} + T^{rr} + \tfrac{1}{\tan\theta}T^{r\theta}\right);\\ &\mathcal{D}_r T^{\theta\theta} = \partial_r T^{\theta\theta}, \quad \mathcal{D}_\theta T^{\theta\theta} = \tfrac{1}{r}\left(\partial_\theta T^{\theta\theta} + 2T^{r\theta}\right),\\ &\qquad\qquad\quad \mathcal{D}_\varphi T^{\theta\theta} = \tfrac{1}{r\sin\theta}\left(\partial_\varphi T^{\theta\theta} - 2\cos\theta\ T^{\theta\varphi}\right);\\ &\mathcal{D}_r T^{\theta\varphi} = \partial_r T^{\theta\varphi}, \quad \mathcal{D}_\theta T^{\theta\varphi} = \tfrac{1}{r}\left(\partial_\theta T^{\theta\varphi} + T^{r\varphi}\right),\\ &\qquad\qquad\quad \mathcal{D}_\varphi T^{\theta\varphi} = \tfrac{1}{r}\left(\tfrac{1}{\sin\theta}\partial_\varphi T^{\theta\varphi} + \tfrac{1}{\tan\theta}\left(T^{\theta\theta} - T^{\varphi\varphi}\right)\right);\\ &\mathcal{D}_r T^{\varphi\varphi} = \partial_r T^{\varphi\varphi}, \quad \mathcal{D}_\theta T^{\varphi\varphi} = \tfrac{1}{r}\partial_\theta T^{\varphi\varphi},\\ &\qquad\qquad\quad \mathcal{D}_\varphi T^{\varphi\varphi} = \tfrac{1}{r}\left(\tfrac{1}{\sin\theta}\partial_\varphi T^{\varphi\varphi} + 2T^{r\varphi} + \tfrac{2}{\tan\theta}T^{\theta\varphi}\right).\end{aligned}$$

$\mathcal{D}_{\hat{k}} T^{\hat{i}}{}_{\hat{j}}$:

$$
\begin{aligned}
&\mathcal{D}_r T^r{}_r = \partial_r T^r{}_r, && \mathcal{D}_\theta T^r{}_r = \tfrac{1}{r}\left(\partial_\theta T^r{}_r - T^\theta{}_r - T^r{}_\theta\right),\\
&&& \mathcal{D}_\varphi T^r{}_r = \tfrac{1}{r}\left(\tfrac{1}{\sin\theta}\partial_\varphi T^r{}_r - T^r{}_\varphi - T^\varphi{}_r\right);\\
&\mathcal{D}_r T^r{}_\theta = \partial_r T^r{}_\theta, && \mathcal{D}_\theta T^r{}_\theta = \tfrac{1}{r}\left(\partial_\theta T^r{}_\theta - T^\theta{}_\theta + T^r{}_r\right),\\
&&& \mathcal{D}_\varphi T^r{}_\theta = \tfrac{1}{r}\left(\tfrac{1}{\sin\theta}\partial_\varphi T^r{}_\theta - T^\varphi{}_\theta - \tfrac{1}{\tan\theta}T^r{}_\varphi\right);\\
&\mathcal{D}_r T^r{}_\varphi = \partial_r T^r{}_\varphi, && \mathcal{D}_\theta T^r{}_\varphi = \tfrac{1}{r}\left(\partial_\theta T^r{}_\varphi - T^\theta{}_\varphi\right),\\
&&& \mathcal{D}_\varphi T^r{}_\varphi = \tfrac{1}{r}\left(\tfrac{1}{\sin\theta}\partial_\varphi T^r{}_\varphi - T^\varphi{}_\varphi + T^r{}_r + \tfrac{1}{\tan\theta}T^r{}_\theta\right);\\
&\mathcal{D}_r T^\theta{}_r = \partial_r T^\theta{}_r, && \mathcal{D}_\theta T^\theta{}_r = \tfrac{1}{r}\left(\partial_\theta T^\theta{}_r - T^r{}_r - T^\theta{}_\theta\right),\\
&&& \mathcal{D}_\varphi T^\theta{}_r = \tfrac{1}{r}\left(\tfrac{1}{\sin\theta}\partial_\varphi T^\theta{}_r - T^\theta{}_\varphi - \tfrac{1}{\tan\theta}T^\varphi{}_r\right);\\
&\mathcal{D}_r T^\theta{}_\theta = \partial_r T^\theta{}_\theta, && \mathcal{D}_\theta T^\theta{}_\theta = \tfrac{1}{r}\left(\partial_\theta T^\theta{}_\theta + T^r{}_\theta + T^\theta{}_r\right),\\
&&& \mathcal{D}_\varphi T^\theta{}_\theta = \tfrac{1}{r\sin\theta}\left(\partial_\varphi T^\theta{}_\theta - \cos\theta\left(T^\theta{}_\varphi + T^\varphi{}_\theta\right)\right);\\
&\mathcal{D}_r T^\theta{}_\varphi = \partial_r T^\theta{}_\varphi, && \mathcal{D}_\theta T^\theta{}_\varphi = \tfrac{1}{r}\left(\partial_\theta T^\theta{}_\varphi + T^r{}_\varphi\right),\\
&&& \mathcal{D}_\varphi T^\theta{}_\varphi = \tfrac{1}{r}\left(\tfrac{1}{\sin\theta}\partial_\varphi T^\theta{}_\varphi + \tfrac{1}{\tan\theta}\left(T^\theta{}_\theta - T^\varphi{}_\varphi\right)\right);\\
&\mathcal{D}_r T^\varphi{}_r = \partial_r T^\varphi{}_r, && \mathcal{D}_\theta T^\varphi{}_r = \tfrac{1}{r}\left(\partial_\theta T^\varphi{}_r - T^\varphi{}_\theta\right),\\
&&& \mathcal{D}_\varphi T^\varphi{}_r = \tfrac{1}{r}\left(\tfrac{1}{\sin\theta}\partial_\varphi T^\varphi{}_r - T^\varphi{}_\varphi + T^r{}_r + \tfrac{1}{\tan\theta}T^\theta{}_r\right);\\
&\mathcal{D}_r T^\varphi{}_\theta = \partial_r T^\varphi{}_\theta, && \mathcal{D}_\theta T^\varphi{}_\theta = \tfrac{1}{r}\left(\partial_\theta T^\varphi{}_\theta + T\varphi{}_r\right),\\
&&& \mathcal{D}_\varphi T^\varphi{}_\theta = \tfrac{1}{r}\left(\tfrac{1}{\sin\theta}\partial_\varphi T^\varphi{}_\theta + T^r{}_\theta + \tfrac{1}{\tan\theta}\left(T^\theta{}_\theta - T^\varphi{}_\varphi\right)\right);\\
&\mathcal{D}_r T^\varphi{}_\varphi = \partial_r T^\varphi{}_\varphi, && \mathcal{D}_\theta T^\varphi{}_\varphi = \tfrac{1}{r}\partial_\theta T^\varphi{}_\varphi,\\
&&& \mathcal{D}_\varphi T^\varphi{}_\varphi = \tfrac{1}{r}\left(\tfrac{1}{\sin\theta}\partial_\varphi T^\varphi{}_\varphi + T^r{}_\varphi + T^\varphi{}_r + \tfrac{1}{\tan\theta}\left(T^\theta{}_\varphi + T^\varphi{}_\theta\right)\right).
\end{aligned}
$$

Notice that in the code, due to the fact that the variables do not depend on the coordinate φ, in the hypothesis of axisymmetry, all the partial derivatives with respect to it are zero.

C. OUTER BOUNDARY

In section 8.1, we have assumed that the components h^{ij} have the following behaviour:

$$h^{rr} \approx \frac{g_1(r-t)}{r}, \quad h^{\theta\theta} \approx \frac{g_4(r-t)}{r^3}, \quad h^{\varphi\varphi} \approx \frac{g_6(r-t)}{r^3 \sin^2\theta}$$
$$h^{r\theta} \approx \frac{g_2(r-t)}{r^2}, \quad h^{r\varphi} \approx \frac{g_3(r-t)}{r^2 \sin\theta}, \quad h^{\theta\varphi} \approx \frac{g_5(r-t)}{r^3 \sin\theta}.$$

From the previous equations, it is easy to deduce the following PDEs for the components h^{ij}:

$$\begin{aligned}
\partial_t h^{rr} &= -\partial_r h^{rr} - \frac{h^{rr}}{r} \\
\partial_t h^{r\theta} &= -\partial_r h^{r\theta} - \frac{2h^{r\theta}}{r} \\
\partial_t h^{r\varphi} &= -\partial_r h^{r\varphi} - \frac{2h^{r\varphi}}{r} \\
\partial_t h^{\theta\theta} &= -\partial_r h^{\theta\theta} - \frac{3h^{\theta\theta}}{r} \\
\partial_t h^{\theta\varphi} &= -\partial_r h^{\theta\varphi} - \frac{3h^{\theta\varphi}}{r} \\
\partial_t h^{\varphi\varphi} &= -\partial_r h^{\varphi\varphi} - \frac{3h^{\varphi\varphi}}{r}
\end{aligned}$$

For the components u^{ij} and $\hat{A}^{ij}$ one can deduce similar PDEs. For the components w_k^{ij} one can deduce the following ones:

$$
\begin{aligned}
\partial_t w_r^{rr} &= -\partial_r w_r^{rr} - \frac{w_r^{rr}}{r} + \frac{h^{rr}}{r^2} \\
\partial_t w_0^{rr} &= -\partial_r w_0^{rr} - \frac{3w_\theta^{rr}}{r} \\
\partial_t w_\varphi^{rr} &= -\partial_r w_\varphi^{rr} - \frac{3w_\varphi^{rr}}{r} \\
\partial_t w_r^{r\theta} &= -\partial_r w_r^{r\theta} - \frac{2w_r^{r\theta}}{r} + \frac{2h^{r\theta}}{r^2} \\
\partial_t w_\theta^{r0} &- -\partial_r w_\theta^{r0} - \frac{2w_\theta^{r\theta}}{r} + \frac{2h^{\theta\theta}}{r^2} \\
\partial_t w_\varphi^{r0} &= -\partial_r w_\varphi^{r0} - \frac{3w_\varphi^{r0}}{r} + \frac{h^{\theta\varphi}}{r^2} \\
\partial_t w_r^{r\varphi} &= -\partial_r w_r^{r\varphi} - \frac{2w_r^{r\varphi}}{r} + \frac{2h^{r\varphi}}{r^2} \\
\partial_t w_0^{r\varphi} &- -\partial_r w_0^{r\varphi} - \frac{3w_0^{r\varphi}}{r} + \frac{h^{0\varphi}}{r^2} \\
\partial_t w_\varphi^{r\varphi} &= -\partial_r w_\varphi^{r\varphi} - \frac{2w_\varphi^{r\varphi}}{r} - \frac{h^{r\theta}\cos\theta}{r^2} + \frac{2h^{\varphi\varphi}}{r^2} \\
\partial_t w_r^{00} &= -\partial_r w_r^{00} - \frac{3w_r^{\theta\theta}}{r} + \frac{3h^{\theta\theta}}{r^2} \\
\partial_t w_\theta^{00} &- -\partial_r w_\theta^{00} - \frac{3w_\theta^{\theta\theta}}{r} \\
\partial_t w_\varphi^{00} &= -\partial_r w_\varphi^{00} - \frac{4w_\varphi^{00}}{r} \\
\partial_t w_r^{\theta\varphi} &- -\partial_r w_r^{\theta\varphi} - \frac{3w_r^{0\varphi}}{r} + \frac{3h^{0\varphi}}{r^2} \\
\partial_t w_0^{\theta\varphi} &- -\partial_r w_0^{\theta\varphi} - \frac{3w_0^{\theta\varphi}}{r} + \frac{h^{0\varphi}\cot\theta}{r^2} \\
\partial_t w_\varphi^{\theta\varphi} &- -\partial_r w_\varphi^{\theta\varphi} - \frac{4w_\varphi^{\theta\varphi}}{r} \\
\partial_t w_r^{\varphi\varphi} &- -\partial_r w_r^{\varphi\varphi} - \frac{3w_r^{\varphi\varphi}}{r} + \frac{3h^{\varphi\varphi}}{r^2} \\
\partial_t w_\theta^{\varphi\varphi} &= -\partial_r w_\theta^{\varphi\varphi} - \frac{4w_\theta^{\varphi\varphi}}{r} \\
\partial_t w_\varphi^{\varphi\varphi} &- -\partial_r w_\varphi^{\varphi\varphi} - \frac{3w_\varphi^{\varphi\varphi}}{r} - \frac{2h^{0\varphi}\cot\theta}{r^2}
\end{aligned}
$$

Actually, the terms in r^{-p} with $p > 1$ are not considered in the implemention of the code.

BIBLIOGRAPHY

[1] Letter from K. Schwarzschild to A. Einstein dated 22 December 1915, in "The Collected Papers of Albert Einstein", vol. **8**a, doc. #169.

[2] Berlineer Sitzungsberichte (*Phys. Math. Klasse*) 189-196, 3. Febr. (Mitt. 13. Jan. 1916).

[3] R. P. Kerr, *Phys. Rev. Lett.* **11**, 237 (1963).

[4] A. Mueller, astro-ph/0701228, 2007.

[5] K. G. et al., *Astrophys. J.* **539**, L13 (2000).

[6] A. Mueller and M. Wold, *Astron. Astrophys.* **457**, 485 (2006).

[7] M. A. Aloy, E. Mueller, J. M. Ibáñez, J. M. Martí, and A. MacFadyen, *Astrophys. J.* **531**, L119 (2000).

[8] M. A. Aloy, H.-T. Janka, and E. Mueller, *Astron. Astrophys.* **436**, 273 (2005).

[9] C. T. Cunningham and J. M. Bardeen, *Astrophys. J.* **183**, 237 (1973).

[10] P. Schneider, C. S. Kochanek, and J. Wambsganss, *Gravitational Lensing: Strong, Weak and Micro*, volume 33, Saas-Fee Advanced Courses, Springer-Verlag, Berlin Heidelberg, 2006.

[11] J. L. Levine, *Physics in Perspective* **6**, 42 (2004).

[12] http://www.virgo.infn.it/.

[13] http://www.geo600.de/.

[14] http://tamago.mtk.nao.ac.jp/.

[15] http://www.ligo.caltech.edu/.

[16] http://lisa.jpl.nasa.gov/.

[17] http://celeste.uv.es/ gw2008/.

[18] R. K. Sachs, *Proc. R. Soc. London, Ser. A* **270**, 103 (1962).

[19] L. A. Tamburino and J. H. Winicour, *Phys. Rev. A* **150**, 1039 (1966).

[20] H. Bondi, M. J. G. van der Burg, and A. W. K. Metzner, *Proc. R. Soc. London, Ser. A* **269**, 21 (1962).

[21] E. T. Newman and R. Penrose, *J. Math. Phys.* **3**, 566 (1962).

[22] A. Lichnerowicz, *J. Math. Pures Appl.* **23**, 37 (1944).

[23] Y. F.-B. (Y.Choquet-Bruhat), *Acta Mathematica* **88**, 141 (1952).

[24] R. Arnowitt, S. Deser, and C. W. Misner, The Dynamics of General Relativity, in *Gravitation: an introduction to current research*, edited by L. Witten, chapter 7, pp. 227 265, New York: Wiley, 1962, gr-qc/0405109.

[25] J. M. York, Kinematics and dynamics of general relativity, in *Sources of Gravitational Radiation*, edited by L. L. Smarr, p. 83, Cambridge: Cambridge University Press, 1979.

[26] T. W. Baumgarte and S. L. Shapiro, *Phys. Rep.* **376**, 41 (2003), gr-qc/0211028.

[27] E. Gourgoulhon, 3+1 Formalism and Bases of Numerical Relativity, gr-qc/0703035, 2007.

[28] M. Alcubierre, *Introduction to 3+1 numerical relativity*, Oxford: Oxford University Press, 2008.

[29] M. Alcubierre, G. Allen, B. Bruegmann, E. Seidel, and W.-M. Suen, *Phys. Rev. D* **62**, 124011 (2000).

[30] Y. Kojima, D. Oohara, and T. Nakamura, *Progress of Theoretical Physics Supplement* **90**, 1 (1987).

[31] T. W. Baumgarte and S. L. Shapiro, *Phys. Rev. D* **59**, 024007 (1999).

[32] M. Shibata and T. Nakamura, *Phys. Rev. D* **52**, 5428 (1995).

[33] M. Shibata, T. W. Baumgarte, and S. L. Shapiro, *Astrophys. J.* **542**, 453 (2000).

[34] J. A. Font and F. Daigne, *Mon. Not. R. Astron. Soc.* **334**, 383 (2002).

[35] M. Shibata and K. Uryu, Binary Neutron Star Mergers in Fully General Relativistic Simulations (Plenary Talk), in *20th Texas Symposium on relativistic astrophysics*, edited by J. Wheeler and H. Martel, volume 586 of *American Institute of Physics Conference Series*, 2001.

[36] L. Baiotti, I. Hawke, P. J. Montero, F. Loeffler, L. Rezzolla, N. Stergioulas, J. A. Font, and E. Seidel, *Phys. Rev. D* **71**, 024035 (2005).

[37] J. Isenberg, *Int. J. Mod. Phys. D* **17**, 265 (2008).

[38] J. Isenberg and J. Nester, *General Relativity and Gravitation*, volume 1, New York: Plenum, 1980.

[39] H. Dimmelmeier, J. A. Font, and E. Mueller, *Astron. Astrophys.* **393**, 523 (2002).

[40] H. Dimmelmeier, J. Novak, J. A. Font, J. M. Ibáñez, and E. Mueller, *Phys. Rev. D* **71**, 064023 (2005).

[41] C. D. Ott, H. Dimmelmeier, A. Marek, H.-T. Janka, I. Hawke, B. Zink, and E. Schnetter, *Phys. Rev. Lett.* **98**, 261101 (2007).

[42] P. Cerdá-Durán, J. A. Font, and H. Dimmelmeier, *Astron. Astrophys.* **474**, 169 (2007).

[43] M. Saijo, *Astrophys. J.* **615**, 866 (2004).

[44] E. B. Abdikamalov, H. Dimmelmeier, L. Rezzolla, and J. C. Miller, *Mon. Not. R. Astron. Soc.* **392**, 52 (2009).

[45] G. B. Cook, S. L. Shapiro, and S. A. Teukolsky, *Phys. Rev. D* **53**, 5533 (1996).

[46] H. Dimelmeier, N. Stergioulas, and J. A. Font, *Mon. Not. R. Astron. Soc.* **368**, 1609 (2006).

[47] R. Oechslin, S. Rosswog, and F.-K. Thielemann, *Phys. Rev. D* **65**, 103005 (2002).

[48] J. R. Wilson, G. J. Mathews, and P. Marronetti, *Phys. Rev. D* **54**, 1317 (1996).

[49] R. Oechslin, H.-T. Janka, and A. Marek, *Astron. Astrophys.* **467**, 395 (2007).

[50] J. A. Faber, P. Grandclément, and F. A. Rasio, *Phys. Rev. D* **69**, 124036 (2004).

[51] I. Cordero-Carrión, J. M. Ibáñez, and J. A. Morales-LLadosa, *in preparation*, 2009.

[52] I. Cordero-Carrión, P. Cerdá-Durán, H. Dimmermeier, J. L. Jaramillo, J. Novak, and E. Gourgoulhon, *Phys. Rev. D* **79**, 024017 (2009).

[53] I. Cordero-Carrión, J. M. Ibáñez, E. Gourgoulhon, J. L. Jaramillo, and J. Novak, *Phys. Rev. D* **77**, 084007 (2008).

[54] L. Smarr and J. W. York, *Phys. Rev. D* **17**, 2529 (1978).

[55] F. Estabrook, H. Wahlquist, S. Christensen, B. DeWitt, L. Smarr, and E. Tsiang, *Phys. Rev. D* **7**, 2814 (1973).

[56] R. Beig and N. O'Murchadha, *Phys. Rev. D* **57**, 4728 (1998).

[57] B. L. Reinhart, *J. Math. Phys.* **14**, 719 (1973).

[58] E. Malec, *Phys. Rev. D* **49**, 6475 (1994).

[59] L. I. Petrich, S. L. Shapiro, and S. A. Teukolsky, *Phys. Rev. D* **31**, 2459 (1985).

[60] D. M. Eardley and L. Smarr, *Phys. Rev. D* **19**, 2239 (1979).

[61] J. Plebański and A. Krasiński, *An Introduction to General Relativity and Cosmology*, Cambridge University Press: Cambridge, 2006.

[62] L. I. Petrich, S. L. Shapiro, and S. A. Teukolsky, *Phys. Rev. D* **33**, 2100 (1986).

[63] E. Gourgoulhon, Ph.D. Thesis, *Université de Paris VII*, 1992.

[64] J. V. Romero, J. M. Ibáñez, J. M. Martí, and J. A. Miralles, *Astrophys. J.* , 839 (1996).

[65] J. M. York, *Phys. Rev. Lett.* **82**, 1350 (1999).

[66] H. P. Pfeiffer and J. W. Y. Jr., *Phys. Rev. D* **67**, 044022 (2003).

[67] H. P. Pfeiffer, *J. Hyperbol. Diff. Equat.* **2**, 497 (2005).

[68] H. P. Pfeiffer and J. W. Y. Jr., *Phys. Rev. Lett.* **95**, 091101 (2005).

[69] T. W. Baumgarte, N. O'Murchadha, and H. P. Pfeiffer, *Phys. Rev. D* **75**, 044009 (2007).

[70] M. Protter and H. Weinberger, *Maximum principles in differential equations*, Prentice-Hall, Englewood Cliffs, 1967.

[71] M. Taylor, *Partial differential equations III. Nonlinear equations*, Applied Mathematical Sciences, Springer-Verlag, New York, 1996.

[72] L. C. Evans, *Partial differential equations*, American Mathematical Society, Providence, 1998.

[73] S. L. Shapiro and S. A. Teukolsky, *Astrophys. J.* **235**, 199 (1980).

[74] J. L. Jaramillo, E. Gourgoulhon, I. Cordero-Carrión, and J. M. Ibáñez, *Phys. Rev. D* **77**, 047501 (2008).

[75] J. Thornburg, *Class. Quantum Grav.* **4**, 1119 (1987).

[76] S. Brandt and B. Bruegmann, *Phys. Rev. Lett.* **78**, 3606 (1997).

[77] M. Hannam, S. Husa, B. Bruegmann, J. A. González, U. Sperhake, and N. O'Murchadha, *J. Phys. Conf. Ser.* **66**, 012047 (2007), gr-qc/0612097.

[78] B. Bruegmann, W. Tichy, and N. Jansen, *Phys. Rev. Lett.* **92**, 211101 (2004).

[79] F. Pretorius, *Phys. Rev. Lett.* **95**, 121101 (2005).

[80] M. Campanelli, C. O. Lousto, P. Marronetti, and Y. Zlochower, *Phys. Rev. Lett.* **96**, 111101 (2006).

[81] J. G. Baker, J. Centrella, D.-I. Choi, M. Koppitz, and J. van Meter, *Phys. Rev. Lett.* **96**, 111102 (2006).

[82] F. Herrmann, D. Shoemaker, and P. Laguna, gr-qc/0601026, 2006.

[83] U. Sperhake, gr-qc/0606079, 2006.

[84] M. A. Scheel, H. P. Pfeiffer, L. Lindblom, L. E. Kidder, O. Rinne, and S. A. Teukolsky, *Phys. Rev. D* **74**, 104006 (2006).

[85] B. B. et al., gr-qc/0610128, 2006.

[86] D. P. et al., Binary Black Hole evolutions using BSSN, Presented at the *New Frontiers in Numerical Relativity* meeting, Golm, 2006.

[87] http://www.mpa-garching.mpg.de/hydro/COCONUT.

[88] S. A. Teukolsky, *Phys. Rev. D* **26**, 745 (1982).

[89] A. Arbona and C. Bona, *Comp. Phys. Comm.* **118**, 229 (1999).

[90] D. Alic, C. Bona, C. Bona-Casas, and J. Massó, *Phys. Rev. D* **76**, 104007 (2007).

[91] http://www.lorene.obspm.fr/.

[92] T. J. Maccarone, A. Kundu, S. E. Zepf, and K. L. Rhode, *Nature* **445**, 05434 (2007).

[93] A. Heger and S. E. Woosley, *Astrophys. J.* **567**, 532 (2002).

[94] S. Gillessen, F. Eisenhauer, S. Trippe, T. Alexander, R. Genzel, F. Martins, and T. Ott, *ApJ* **692**, 1075 (2009).

[95] E. Maoz, *Astrophys. J.* **447**, L91 (1995).

[96] E. Maoz, *Astrophys. J.* **494**, L181 (1998).

[97] J. D. Bekenstein, astro-ph/0407560, 2004.

[98] R. Penrose, *Riv. Nuovo Cim.* **I**, 252 (1969).

[99] J. S. B. Wyithe, *MNRAS* **365**, 1082 (2006).

[100] B. M. Peterson and A. Wandel, *ApJ* **540**, L13 (2000).

[101] B. Aschenbach, N. Grosso, D. Porquet, and P. Predehl, *Astron. Astrophys.* **417**, 71 (2004).

[102] N. L. Shakura and R. A. Sunyaev, *Astron. Astrophys.* **24**, 337 (1973).

[103] L.-X. Li, E. R. Zimmerman, R. Narayan, and J. E. McClintock, *ApJS* **157**, 335 (2005).

[104] J. A. Font, J. M. Ibáñez, and P. Papadopoulos, *Astrophys. J.* **507**, L67 (1998).

[105] T. J. G. et al., *Astron. Astrophys. Suppl. Ser.* **138**, 465 (1999).

[106] K. Z. S. et al., *ApJ* **591**, L17 (2003).

[107] S. W. Hawking, *Commun. Math. Phys.* **43**, 199 (1975).

[108] J. A. Marck, *Class. Quantum Grav.* **13**, 393 (1996).

[109] D. Rusin, C. R. Keeton, and J. N. Winn, *Astrophys. J.* **627**, L93 (2005).

[110] J. H. Winicour, *Living Rev. Relativity* **8**, 72 (2005), http://www.livingreviews.org/lrr-2005-10.

[111] S. Bonazzola, E. Gourgoulhon, P. Grandclément, and J. Novak, *Phys. Rev. D* **70**, 104007 (2004).

[112] L. Smarr and J. W. York, *Phys. Rev. D* **17**, 1945 (1978).

[113] J. Guven and N. O'Murchadha, *Phys. Rev. D* **61**, 067503 (2000).

[114] V. Husain, A. Quadir, and A. A. Siddiqui, *Phys. Rev. D* **65**, 027501 (2001).

[115] R. Beig and A. A. Siddiqui, *Class. Quantum Grav.* **24**, 5435 (2007).

[116] C. Doran, *Phys. Rev. D* **61**, 067503 (2000).

[117] J. Natário, *Painlevé-Gullstrand Coordinates for the Kerr Solution*, Gen. Relativ. Gravit., 2009.

[118] C.-Y. Lin and C. Soo, *Phys. Lett. B* **671**, 493 (2009).

[119] E. Zauderer, *Partial differential equations of applied mathematics*, Second edition, John Wiley and Sons, New York, 1989.

[120] *Handbook of mathematical functions*, edited by M. Abramowitz and I.A. Stegun, Dover Publications, Inc., New York, p.556.

[121] P. Papadopoulos and J. A. Font, *Phys. Rev. D* **58**, 024005 (1998).

[122] D. Walsh, *Class. Quantum Grav.* **24**, 1911 (2007).

[123] N. O'Murchadha and J. W. Y. Jr., *J. Math. Phys.* **14**, 1551 (1973).

[124] N. O'Murchadha and J. W. Y. Jr., *Phys. Rev. D* **10**, 428 (1974).

[125] O. Rinne, *Class. Quantum Grav.* **25**, 135009 (2008).

[126] J. L. Jaramillo, J. A. V. Kroon, and E. Gourgoulhon, *Class. Quantum Grav.* **25**, 093001 (2008).

[127] M. W. Choptuik, E. W. Hirschmann, S. L. Liebling, and F. Pretorius, *Class. Quantum Grav.* **20**, 1857 (2003).

[128] O. Rinne, *PhD Thesis* University of Cambridge UK, 2006, gr-qc/0601064.

[129] O. Rinne and J. M. Stewart, *Comm. Math. Phys.* **22**, 1143 (2005).

[130] V. Moncrief, L. Buchman, H. P. Pfeiffer, O. Rinne, and O. Sarbach, Presented at *From geometry to numerics* workshop, Institut Henri Poincaré, Paris (2006), and private communication.

[131] F. Banyuls, J. A. Font, J. M. Ibáñez, J. M. Martí, and J. A. Miralles, *Astrophys. J.* **476**, 221 (1997).

[132] J. A. Font, *J. Phys. Conf. Ser.* **91**, 012002 (2007).

[133] H. Komatsu, Y. Eriguchi, and I. Hachisu, *Mon. Not. R. Astron. Soc.* **237**, 335 (1989).

[134] N. Stergioulas and J. L. Friedman, *Astrophys. J.* **444**, 306 (1995).

[135] S. Bonazzola, E. Gourgoulhon, M. Salgado, and J. A. Marck, *Astron. Astrophys.* **278**, 421 (1993).

[136] M. Shibata and K. Uryu, *Phys. Rev. D* **74**, 121503 (2006).

[137] M. Shibata and K. Uryu, *Class. Quantum Grav.* **24**, S125 (2007).

[138] J. A. Font, T. Goodale, S. Iyer, M. Miller, L. Rezzolla, E. Seidel, N. Stergioulas, W.-M. Suen, and M. Tobias, *Phys. Rev. D* **65**, 084024 (2002).

[139] L. Andersson and V. Moncrief, *Ann. H. Poincaré* **4**, 1 (2003), gr-qc/0110111.

[140] O. Reula, *J. Hyperbolic Differ. Equ.* , 251 (2004), gr-qc/0403007.

[141] A. Anile, *Relativistic fluids and magneto-fluids*, Cambridge: Cambridge University Press, 1989.

[142] L. Antón, *PhD Thesis* University of Valencia, Spain, 2008.

[143] J. M. Martí and E. Mueller, *Living Rev. Relativity* **2**, 3 (1999), http://www.livingreviews.org/lrr-1999-3.

[144] J. A. Font, *Living Rev. Relativity* **3**, 2 (2000), http://www.livingreviews.org/lrr-2000-2.

[145] E. Gourgoulhon and J. L. Jaramillo, *Phys. Rep.* **423**, 159 (2006), gr-qc/0503113.

[146] S. W. Hawking, The event horizon, in *Black holes, les astres occlus*, edited by C. DeWitt and B. S. DeWitt, Gordon and Breach, New York, 1973.

[147] J. L. Jaramillo, Presented in the *Spanish Relativity Meetings*, (EREs), 2006.

[148] I. Cordero-Carrión, J. M. Ibáñez, J. L. Jaramillo, and E. Gourgoulhon, Presented in the *Spanish Relativity Meetings*, (EREs), 2006.

[149] J. W. York and T. Piran, Spacetime and Geometry, in *The Alfred Schild Lectures*, edited by R. A. Matzner and L. C. Shepley, pp. 147–176, Austin: University of Texas Press, 1982.

[150] M. W. Choptuik, *MSc Thesis* University of British Columbia, 1982.

[151] J. D. Rauber, in *Dynamical Spacetimes and Numerical Relativity*, edited by J. M. Centrella, pp. 304 327, Cambridge: Cambridge University Press, 1986.

[152] W. G. Unruh, 1984.

[153] A. Čadež, *Ann. Phys. N.Y.* **83**, 449 (1974).

[154] C. Misner and J. Wheeler, *Ann. Phys.* **2**, 525 (1957).

[155] D. S. Brill and R. W. Lindquist, *Phys. Rev.* **131**, 471 (1963).

[156] A. Arbona, C. Bona, J. Carot, L. Mas, J. Massó, and J. Stela, *Phys. Rev. D* **57**, 2397 (1998).

[157] A. Arbona, C. Bona, J. Massó, and J. Stela, *Phys. Rev. D* **60**, 104014 (1999).

[158] C. Bona, T. Ledvinka, C. Luque-Palenzuela, J. A. Pons, and M. Zajeck, Gauge pathologies in singularity-avoidant spacetime foliations, gr-qc/0410079, 2004.

[159] C. W. Misner, Magic Matter, the Computational Ether, and the Miner's Canary, URL https://drum.umd.edu/dspace/handle/1903/4361, 2001.

[160] D. Brown, O. Sarbach, E. Schnetter, M. Tiglio, P. Diener, I. Hawke, and D. Pollney, *Phys. Rev. D* **76**, 081503 (2007).

[161] H. Dimmelmeier, *PhD Thesis* Technische Universitat Munchen and Max-Planck-Institut fur Astrophysik, Germany, 2001.

[162] C. W. Shu and S. Osher, *J. Comput. Phys.* **77**, 439 (1988).

[163] S. Gottlieb and C. W. Shu, *Math. Comput.* **67**, 73 (1998).

[164] R. J. Spiteri and S. J. Ruuth, A new class of optimal high-order strong-stability-preserving time discretization methods, 2002.

[165] A. Savitzky and M. J. E. Golay, *Analytical Chemistry* **36**, 1627 (1964).

[166] H. O. Kreiss and J. Oliger, *Methods for the Approximate Solutions of Time Dependent Problems*, Global Atmospheric Research Programme Publications Series, 10, 1973.

[167] D. Alic, C. Bona, and C. Bona-Casas, Relativistic Astrophysics and Cosmology, in *Spanish Relativity Meeting, Encuentros Relativistas Españoles, ERE2007*, edited by A. Oscoz, E. Mediavilla, and M. Serra-Ricart, volume 30, pp. 213–217, EAS Publications Series, 2007.

[168] W. Kley and G. Schaefer, *Phys. Rev. D* **60**, 027501 (1999).

[169] P. Cerdá-Durán, G. Faye, H. Dimmelmeier, J. A. Font, J. M. Ibáñez, E. Mueller, and G. Schaefer, *Astron. Astrophys.* **439**, 1033 (2005).

[170] J. B. Hartle and K. S. Thorne, *Astrophys. J.* **153**, 807 (1968).

[171] R. Prix, J. Novak, and G. L. Comer, *Phys. Rev. D* **71**, 043005 (2005).